Gas Purification using Membrane Gas Absorption Processes

Promotion committee:

Prof.dr. T. Reith, voorzitter	Universiteit Twente
Prof. dr. ir. G.F. Versteeg, promotor	Universiteit Twente
Dr. ir. D.W.F. Brilman, assistent-promotor	Universiteit Twente
Dr. P.H.M. Feron, Referent	TNO-MEP, the Netherlands
Prof. dr. ir. J.A.M. Kuipers	Universiteit Twente
Prof. dr. Ing. M. Wesseling	Universiteit Twente
Prof. dr. V.G. Pangarkar	University of Mumbai, India
Prof. dr. H.F. Svendsen	Norwegian University of Science and Technology, Norway
Dr. F.H. Geuzebroek	Shell Global Solutions, the Netherlands

The research in this thesis was financially supported by the Centre for Separation Technology, a co-operation between the University of Twente and TNO, the Netherlands Organisation for Applied Scientific Research.

No part of this work may be reproduced by print, photocopy or any other means without the permission in writing from the author.

© V.Y. Dindore, Enschede, 2003.

Dindore, V.Y.

Gas Purification using Membrane Gas Absorption Processes

Thesis, University of Twente, the Netherlands

ISBN 90-365-1995-0

Print: PrintPartner Ipskamp, P.O. Box. 333, 7500 AH Enschede, the Netherlands, www.ppi.nl

GAS PURIFICATION USING MEMBRANE GAS ABSORPTION PROCESSES

PROEFSCHRIFT

ter verkrijging van
de graad van doctor aan de Universiteit Twente,
op gezag van de rector magnificus,
prof.dr. F.A. van Vught,
volgens besluit van het College voor Promoties,
in het openbaar te verdedigen,
op woensdag 19 november 2003 om 16.45 uur

door

Vishwas Yashwant Dindore
geboren op 2 april 1975
te Latur (India)

Dit proefschrift is goedgekeurd door de promotor,

Prof. dr. ir. G.F. Versteeg

en de assistent-promotor,

Dr. ir. D.W.F. Brilman

To my parents and family

Contents

Introduction

1.0 Gas purification

In general, gas purification refers to the removal of impurities from the gas stream. The processes which are used for this purpose vary from simple physical techniques to complex hybrid multi-step processes, depending on the nature and concentration of impurities as well as on the treated gas specifications. Usually the gas purification uses one of the following unit operations:

1. Absorption into liquids
2. Adsorption on solids
3. Separation by membrane
4. Condensation

Although various gas impurities such as H_2S, CO_2, SO_2, NO_x can be separated using these unit operations, the removal of carbon dioxide from the mixtures of gases is an important industrial process in several contexts and will be discussed in detail in the present work. The bulk carbon dioxide removal is carried out e.g. in the synthetic ammonia industry and gas based industries such as natural gas, refinery gas or coal gas purification, synthesis gas manufacture etc. The carbon dioxide separation is also important in the manufacture of synthetic gasoline, industrial organic chemicals such as salicylic acid, cracking of petroleum fractions and atmosphere control in submarines and space-crafts.

In recent years, the stringent environmental regulations towards the emissions of carbon dioxide have considerably changed economics of the fossil fuel fired power plants and energy industries due to the penalty caused by carbon dioxide emissions. On the other hand, the use of carbon dioxide has become important in enhanced oil recovery programs. In principle, various methods could be used for the removal of carbon dioxide. The selection of these methods depends on several parameters such as CO_2 concentration in the feed stream, nature of other components present in the feed stream and pressure and temperature at which the feed stream is available. Figure 1 shows the general guidelines for process selection of CO_2 removal technologies (Shaw & Hughes, 2001). It can be seen from this figure that absorption in a liquid is the most common process used in the industry for CO_2 removal. For economic reasons, the absorbent must have a large capacity for carbon dioxide and must be regenerable. Liquids used for the absorption of carbon dioxide may dissolve the gas physically (e.g. propylene carbonate, selexol, n-formyl morpholine etc.) or may contain a component which chemically reacts with dissolved gas (e.g. aqueous carbonate solutions, alkanol amines etc.). The specific rate of the absorption into physical solvents is in general much less compared to that into chemical absorbents. However, as the loading of physical solvents varies with partial pressure they can have a high loading capacity. The regeneration of a physical solvent is usually easy and less expensive. Owing to these properties, physical

solvents are mainly used when the concentration of carbon dioxide in the feed stream is very high and only bulk removal is required. On the other hand, it becomes necessary to employ chemical absorbents when it is desired to reduce the partial pressure of carbon dioxide to very low levels.

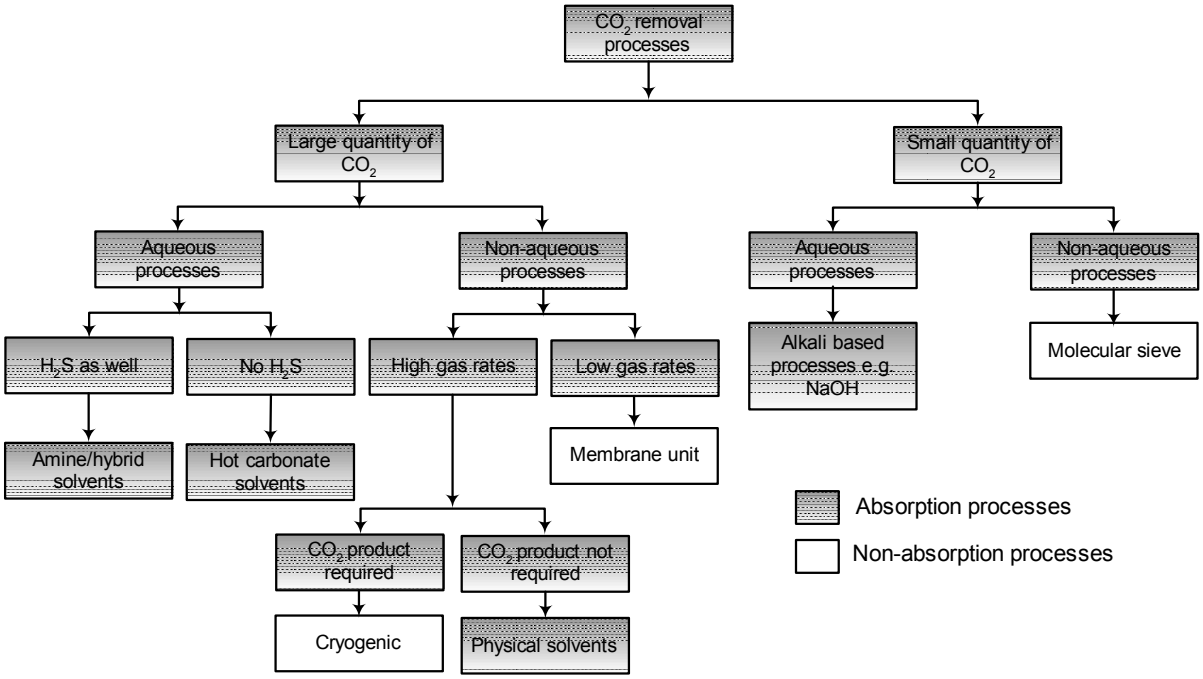

Figure 1: *Guidelines for selection of CO_2 removal processes (Shaw & Hughes; 2001).*

Generally these absorption processes are carried out using conventional gas-liquid industrial contactors. Most of the industrial contactors achieve the gas-liquid mass transfer by direct contact and with dispersion of one phase within another. These industrial contactors can be broadly classified into three categories depending on the dispersing and non-dispersing phase (Sharma & Doraiswamy, 1984).

1. Contactors in which the liquid flows as a thin film (e.g. packed column, disc contactors etc.).
2. Contactors where gas is dispersed into the liquid phase (plate column, bubble column, mechanically agitated contactors etc.).
3. Contactors where liquid is dispersed into the gas phase (spray column, venturi scrubbers etc.).

In any type of gas-liquid contactor, the rates at which components are being transferred from the gas phase to the liquid phase or vice versa depend on the individual mass transfer coefficients (k_L and k_G) and the gas-liquid interfacial area (a). Hence the design of gas-liquid contactors is aimed towards increasing the individual mass transfer coefficients and the interfacial area. Depending upon the gas-liquid contactor type and operating

conditions, there can be wide variation in k_L, k_G and the interfacial area. Table 1 (Sharma & Doraiswamy, 1984) shows the range of k_G, k_L and interfacial area for conventional gas-liquid contactors. In most of the dispersive type of contactors the mass transfer coefficients and the interfacial area cannot be varied independently since both depend on the process/operating conditions and are thus coupled. This interdependence of the mass transfer coefficient and the interfacial area can lead to unstable and inefficient operation of the dispersive type of gas-liquid contactors under certain operating conditions. For example under extreme gas and liquid-flow ratios conventional gas-liquid contactors suffer from flooding, weeping or foaming of the contactor. These disadvantages can be eliminated if the gas-liquid interface is immobilized.

Table 1: *Salient features of conventional Gas-Liquid contactors (Doraiswamy & Sharma, 1984)*

Type of contactor	**Liquid hold up**	**RTD**		**k_G ($m\ s^{-1}$)**	**k_L x 10^4 ($m\ s^{-1}$)**	**Interfacial area (m^{-1})**
		G	L			
Packed column	0.05-0.1	P	P	$1\text{-}5.10^{-2}$	0.3-2	20-350
Bubble column	0.6-0.8	P	M	$1\text{-}5.10^{-2}$	1-4	25-1000
MAC	0.5-0.8	PM	M	$1\text{-}5.10^{-2}$	1-5	200-1000
Spray column	0.05-0.1	PM	P	$1\text{-}5.10^{-2}$	0.5-1.5	20-150

Notation used in the table: G, gas; L, liquid; RTD, residence time distribution; P, plug flow; PM, partially mixed; M, mixed; MAC, mechanically agitated contactor.

2.0 Membrane gas-liquid contactors

In recent years, membranes have been frequently proposed for fixing gas-liquid interfacial areas. Such types of non-dispersive gas-liquid contactors are generally termed as membrane gas-liquid contactors. Unlike the dense membranes used in gas separation processes, the membranes used in these types of contactors are basically non-selective in nature and the selectivity aspect is primarily determined by the solvent used. In general, when microporous membranes are used in membrane contactors, the gas-liquid interface is immobilized at the opening of the pores of microporous membrane by careful control of the pressure difference between the two phases.

These membrane contactors offer numerous advantages over the conventional gas-liquid contactors. Some of the significant advantages are listed below.

1. The specific gas-liquid interfacial area (area per unit of contactor volume) offered by the membrane gas-liquid contactors is considerably higher, especially in the case of hollow fiber membrane contactors. For commercially available hollow fiber membrane modules, it varies between 1500-3000 m^2/m^3 of contactor volume, depending on the diameter and packing density of the hollow fiber. This value is much higher than the contact areas available in conventional contactors (20-1000 m^2/m^3) like stirred tanks, bubble columns, packed and plate columns (Sharma & Doraiswamy, 1984). In membrane contactors, the high interfacial area is obtained at the cost of the fiber side mass transfer coefficient, which is low due to the laminar flow of the fluids inside the fiber. Nevertheless, the overall volumetric mass transfer coefficient (k_La) is substantially higher, resulting in a considerable reduction in the size of the contactor.
2. The interfacial area for mass transfer in a membrane gas-liquid contactor equals the geometrical membrane surface area. Thus the interfacial area is constant and not influenced by orientation or change in flow rates. The feature of orientation free area is extremely useful for the offshore applications. In addition, the fixed interfacial area allows trouble free operation over a wide range of process conditions and easy estimation of the interfacial area. In the conventional gas liquid contactors, the interfacial area is strongly influenced by the process conditions and for reliable absorber design laborious experimental measurements of the interfacial area are required at different operating conditions.
3. For hollow fiber contactors, the flow within the fibers is usually laminar, thus the fiber side hydrodynamics are well known. This allows the accurate calculation of the fiber side mass transfer coefficient from first principles.
4. In these contactors, the mass transfer coefficient and the interfacial area can be varied independently. Thus the operating limitations such as flooding, loading, weeping etc. can be eliminated even at extreme gas and liquid flow ratio and at extreme hold up ratios.
5. The scale-up of the membrane contactor is straightforward and simple due to the modular nature of the contactor.
6. Since for membrane contactors, the direct contact of the two phases is prevented, the contamination due to the mixing of the phases is eliminated. Hence the requirement of equipments like ‘demister’ (mist-eliminator) used in conventional gas-liquid contactors can be omitted. This feature can be advantageous for the pharmaceutical and clinical applications where sterile process conditions are of high importance.

However, membrane contactors also suffer from following limitations;

1. The membrane adds an additional mass transfer resistance to the overall mass transfer process. The membrane mass transfer resistance is strongly influenced by the nature of

the phase that is present inside the pores of microporous membranes. This feature of the microporous membranes is a critical issue in the design of the membrane contactors.

2. An accurate control of transmembrane pressure is important in the case of microporous membrane contactors. The failure of efficient transmembrane pressure control may induce flow across the membrane (breakthrough), causing unwanted froth, foam and dispersion between the two phases.
3. Membrane contactors employ polymeric membranes and potting adhesive resins to bond the fiber bundle to the module casting. These materials may have limited compatibility with certain organic solvents. In such cases membrane contactors cannot be employed for the mass transfer operations.
4. Membrane life is considerably lower than that of the conventional gas-liquid contactors or their parts. The cost of periodic replacement of the membrane can be substantial, depending on the type of membrane material and size of membrane area to be replaced.
5. Membrane contactors may suffer from bypassing and dead zone formations on the shell side which results in loss in efficiency.
6. Microporous membrane contactors cannot be used in systems where in-situ formation of solids takes places. In such cases, depending on the size of the particle formed, complete blockage of the pores may occur resulting into complete loss of the operation.

3.0 Types of membrane contactors

Several membrane module configurations are available, both at commercial and laboratory scale respectively, for the conventional membrane applications such as filtration, gas separation etc. These module configurations can be conveniently adopted for the membrane gas-liquid contactors with relatively little modifications. Depending on the type of membranes used in the contactor, these devices can be broadly classified into two groups; the flat sheet membrane contactor and the hollow fiber membrane contactor. Flat sheet membranes are used in plate-and-frame or in spiral wound membrane contactors. Although equally efficient mass transfer operation can be carried out using flat sheet membrane contactors, hollow fiber membrane contactors are widely used due to the higher interfacial area.

Based on the flow directions of the gas and liquid phase, the hollow fiber membrane contactor can be used in two different modes of operation.

1. *Parallel flow mode*: The flow of the both phases is parallel to the axis of the fiber and both fluids flow either in same direction (co-current) or in opposite direction (counter current).

2. *Cross flow mode*: The flow of one of the fluid is perpendicular to the axis of fiber and other fluid flows parallel to the axis of fiber. Thus the two fluids flow at right angles to each other.

Parallel flow offers the highest average concentration driving force in the case of counter-current flow and is preferred in situations where membrane or fiber side mass transfer resistance controls (Wang & Cussler, 1993). The choice between the co-current and counter current operation is determined by the transmembrane pressure variation. In the case of counter current operation the variation in the transmembrane pressure is relatively high, which can interfere with the interface stability and can even lead to breakthrough of one phase into another. In the case of parallel flow, the overall mass transfer rate can be significantly reduced if the shell-side mass transfer resistance is significant. In such cases cross flow configurations are attractive as flow in the direction perpendicular to the fibers leads to higher shell-side mass transfer coefficients. This is mainly because of the concentration boundary layer break-up due to continuous splitting and remixing of the fluid flowing perpendicular to the fiber. However, the higher mass transfer coefficient is obtained at the cost of a reduced overall mass transfer driving force in comparison to counter current parallel flow.

The choice of the geometry of hollow fiber membrane contactors in early stages of developments was largely influenced by the simplicity of the module constructions. Conventionally, shell and tube geometry is preferred for membrane contactors due to the ease in the manufacturing of these modules. Later on, several investigators found that uneven packing and uneven flow distribution on the shell side of the shell and tube module resulted into reduced mass transfer rates. Hence considerable efforts have been made to explore the different module geometries in order to achieve uniform flow distribution on the shell side. In recent years, it has also been found that the use of fibers woven into fabric in the membrane module manufacture results in more uniform fiber spacing (Cussler, 1994). The fibers woven into a fabric have been successfully used for the manufacturing of module with different geometries such as rectangular module, helically wound fiber module, baffled shell and tube module and transverse flow module. Out of the various innovative geometries studied by several investigators, only rectangular module and shell and tube transverse flow module have been successfully commercialized. Hoechst Celanese provides shell and tube transverse flow Liqui-Cel® contactors for various gas-liquid contacting applications where as rectangular cross-flow module is commercialized by TNO Environmental Energy and Process Innovation (The Netherlands) and by Kvaerner Oil & Gas in co-operation with W. L. Gore & Associates GmbH.

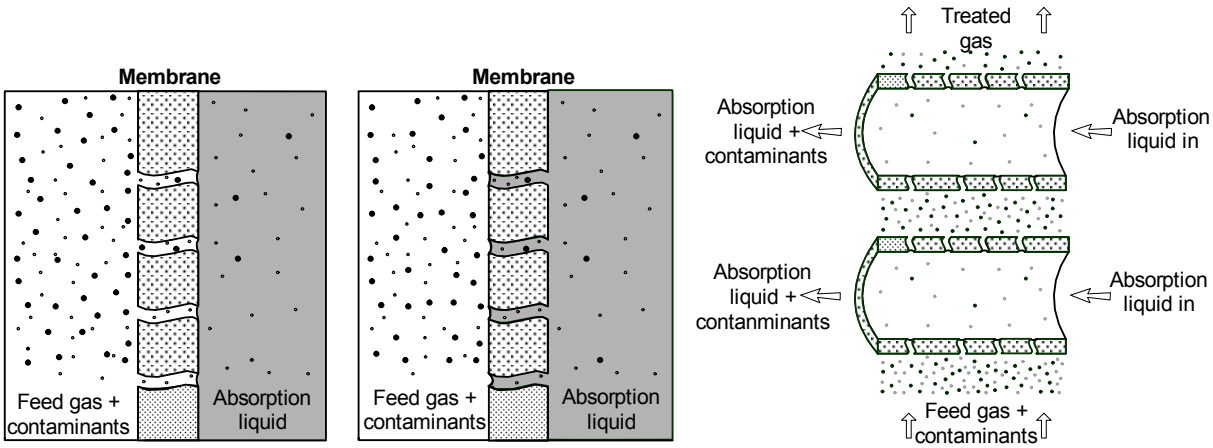

(a) (b) (c)

Figure 2: *(a) Non-wetted membrane gas-liquid contactor; (b) Wetted membrane gas-liquid contactor; (c) Cross flow hollow fiber membrane gas-liquid contactor;*

4.0 Design considerations for membrane gas-liquid contactors

The working principle of a microporous membrane contactor is shown in Figure 2. The mass transfer process in the membrane contactor consists of three steps in series, the transfer from gas phase to the membrane surface, transfer within membrane pores and transfer from liquid interface to the liquid bulk. The overall mass transfer coefficient in the case of membrane contactor is given by the 'resistance in series' model (Kreulen et al. 1993a).

$$\frac{1}{K_{ov}} = \frac{1}{k_G} + \frac{1}{k_m} + \frac{1}{mEk_L} \qquad (1)$$

Here, k_G, k_m, and k_L are individual mass transfer coefficients of the gas phase, membrane phase and the liquid phase respectively. 'm' is the physical solubility of the gaseous species into the liquid bulk and 'E' is the enhancement in mass transfer rate due to chemical reaction (if any). The mass transfer coefficient of membrane phase, k_m, depends on the type of phase present in the membrane pores. The mass transfer resistance of the gas filled (non-wetted) pores is usually very small and negligible. However, when the membrane pores are filled with the liquid (wetted), the mass transfer resistance of the membranes becomes significant (Kreulen et al. 1993a), resulting into economically unviable operation. The design strategy of the membrane gas-liquid contactors for CO_2 removal should be aimed at preventing the membrane wetting for long term application.

In general, the wetting of the membrane is decided by the membrane–liquid interactions. Hence, a suitable combination of the absorption liquid and the membrane material is critical for the stability of the membrane gas-liquid contactors. For porous membranes, a minimum pressure is required for the liquid to penetrate into the pores. This

minimum breakthrough pressure (ΔP) for ideal cylindrical pores is given by the Laplace equation.

$$\Delta P = -\frac{2\gamma_L \cos\theta}{r_{max}} \tag{2}$$

The higher breakthrough pressure is a key for the long term non-wetting application of gas-liquid membrane contactors. It can be seen from the Eq. (2) that this objective can be achieved by using solvents with high surface tension (γ_L), reducing the maximum pore size (r_{max}) and increasing the contact angle (θ). However, most of the physical solvents used for bulk CO_2 removal have low surface tensions and the reduction in the membrane pore size beyond certain limit results into reduced transport of the gas through the membrane owing to Knudsen flow. The higher contact angle for a given solvent is favored by the membrane material having low surface energies. Table 2 shows the membrane materials and their surface energies. It can be seen that the PTFE membrane material has a very low surface energy and this material is the most resistant for wetting. However, PTFE hollow fibers are very expensive as compared to the polyolefin fibers and very small diameter (<500 μm) fibers are not commercially available. On the other hand, the polypropylene membrane material has sufficiently low surface energy, is inexpensive, and commercially available in very small fiber diameters. Hence, the use of polypropylene membrane in combination with various CO_2 removal solvents is explored in the present work.

Table 2: *Surface energies of polymer materials (Mulder, 1991)*

Polymer	**Surface energy mN/m**
Polytetraflouroethylene (PTFE)	19.1
Polytriflouroethylene	23.9
Polypropylene	30.0
Polyvinylideneflouride	30.3
Polyethylene	33.2

As discussed earlier, cross flow modules have a higher shell side mass transfer coefficient and offer higher mass transfer rates at identical driving force. These modules can be arranged in serial or parallel cascades to give overall countercurrent flow, thereby increasing the overall driving force. In the case of CO_2 removal, using either reactive or non-reactive solvents, the overall mass transfer process is controlled by liquid side mass transfer resistance. It seems favorable to have the phase with controlling mass transfer resistance on the shell side of the cross flow membrane module. However the mechanical strength of the fibers is limited and the shear by the liquid flowing perpendicular to the fibers is likely to cause buckling and uneven distribution of fibers, resulting into eventual lowering of module

performance. In extreme cases of high liquid flow rates complete failure of the module is also possible as observed by Wang & Cussler (1993). Hence for practical reasons, it was decided to use the cross modules with liquid flowing through the fiber and gas flowing on the shell side. In addition, using this configuration the effect of variation of local concentration gradients in both directions, parallel and normal to flow, for both phases can be analyzed using first principles.

The primary focus of the present investigation is on the prevention of the membrane wetting for long term application and on the performance evaluation of the cross flow membrane module for CO_2 removal using non-reactive as well as reactive solvents. Single fiber studies, focusing on the prevention of wetting and on the liquid side mass transfer coefficient, with or with reaction, are part of the system development but also offer a nice opportunity as a gas-liquid research tool.

5.0 Previous work on CO_2 removal using membrane gas absorption

The application of hydrophobic microporous membrane as gas-liquid contactor was initially explored in the medical field for the oxygenation of blood as an artificial lung (Esato & Eiseman 1975, Tsuji et al. 1981). The absorption of a variety of gases in acidic or alkaline medium using membrane hollow fiber modules was initially studied by Cussler and his co-workers (Qi & Cussler, 1985a,b) for industrial applications. Since then, several investigators have studied the membrane based absorption and desorption method for removal of variety of solute such as CO_2, SO_2, NO_x, H_2S, VOC, NH_3 etc. using non-reactive as well as reactive solvents. Based on these studies several processes using membrane gas-liquid contactors are successfully commercialized. These industrial processes and the use of membrane gas-liquid contactors for possible applications are reviewed in detail by Ho & Sirkar (1997) and Gabelman & Hwang (1999). As it is not the intention to review all the applications of the membrane gas absorption process in this section only the studies related to CO_2 removal using this process are discussed.

A significant amount of the published research work on membrane gas-liquid contactors is related to CO_2 removal, due to the enormous scope for application in high volume gas treating processes (e.g. natural gas processing, flue gas processing) as well as low volume CO_2 removal processes (e.g. life support system, supply of CO_2 to green houses). In the initial work Qi & Cussler (1985a,b) studied the absorption of CO_2 into aqueous alkalis and alkanolamine solutions using polypropylene hollow fiber modules (pore-diameters 0.03 μm). These authors found that the membrane mass transfer resistance was negligible and the liquid-side mass transfer resistance controlled the CO_2 absorption in aqueous alkalis and alkanolamine solutions. However, later on Kreulen et al. (1993b) reported the wetting of the polypropylene membrane with somewhat larger pore diameter (0.2 μm) by aqueous methyl diethanolamine (MDEA) solutions. A similar observation of the wetting of polypropylene

membranes (pore diameter 0.03 μm) by aqueous diethanolamine (DEA) and NaOH solutions is also reported by Rangwala (1995), who attributed the wetting phenomena to the membrane surface modification by trace impurities.

Nii & Tekuchi (1994) showed that the more hydrophobic microporous polytetrafloroethylene (PTFE) hollow fibers (pore diameter 2 μm) can be used successfully without wetting problems in combination with various primary, secondary and tertiary aqueous alkanolamine solutions. Similarly, Kim & Yang (2000) used hydrophobic PTFE hollow fiber membranes at elevated temperatures for the removal of CO_2 using different aqueous alkanolamine (AMP, MDEA, MEA) solutions. These authors found that at high temperatures (≈ 60 ^oC) water evaporation resulted into membrane wetting and decrease in the absorption flux. In recent work, Hoff (2003) successfully used a cross flow PTFE hollow fiber membrane module for CO_2 removal from simulated exhaust gas using aqueous solutions of mono-ethanolamine (MEA) and methyl-di-ethanolamine (MDEA). Nishikawa et al. (1995) compared the performance of PTFE and polyethylene (PE) hollow fibers for CO_2 removal from the flue gas of thermal power plant using aqueous mono ethanaolamine (MEA) solution. These authors argued that PTFE owing to its more hydrophobic nature showed stable performance over 6600 hrs, however, the overall mass transfer coefficient for polyethylene membrane gradually decreased due to the capillary condensation which resulted into the wetting of the membrane. To improve on the performance of polyethylene (PE) fibers, the authors increased the hydrophobicity of PE membranes by pretreatment with fluorocarbonic material. However, the improvement turned out to be a temporary phenomenon only.

Another approach to eliminate the wetting problems with less hydrophobic microporous membranes is by applying a very thin coating of highly permeable dense membrane on the liquid side and thus physically preventing the liquid from entering into the membrane pores. Li & Teo (1996) compared the performance of an ultra thin skinned polyethersulfone (PESf) hollow fiber to the hydrophobic microporous polypropylene hollow fiber for removal of CO_2 using aqueous alkaline solutions. The authors found that the membrane mass transfer resistance of the dense membrane was much higher as compared to that of microporous membrane under non-wetted conditions and thus resulted into substantially lower mass transfer rates. However, the authors claimed that the reduction of the CO_2 transfer rate due to the high membrane resistance could easily be compensated by an elevation of feed gas pressure and thus increasing the driving force. Similar observations of reduction in mass transfer rates in the case of dense membranes are made by Al-Saffar et al. (1997), where the authors compared the performance of a non-porous silicon rubber membrane with a hydrophobic polypropylene fiber for removal of CO_2 using aqueous diethanolamine (DEA) solutions. The strategy of coating the microporous membrane with a thin, dense membrane layer on the liquid side is advantageous if the resistance of mass transfer through the dense membrane is much lower than the mass transfer resistance of the

liquid filled pores. This also necessitates an ability to create an ultra thin coating of a dense membrane on the desired side of the microporous membrane, which can become a challenging and expensive task if this is to be done on the inner side of the hollow fiber.

The wetting can also be avoided by carefully controlling the transmembrane pressure which was reported by Karoor & Sirkar (1991). However, no detailed investigation was carried out using this technique.

The commercial scale testing of membrane gas-liquid contactors for CO_2 removal is carried out by only a few research groups. Kvaerner Oil & Gas in collaboration with W. L. Gore & Associates GmbH are developing membrane gas-liquid contactors with PTFE hollow fiber membranes for CO_2 removal from natural gas as well as flue gas, using commercial reactive (alkanolamines) or non-reactive (Morphysorb®) solvents (Hoff, 2003). TNO Environment and Process Innovation (the Netherlands) has also worked on larger scale for the development of a membrane gas absorption process for CO_2 removal using less expensive polypropylene hollow fiber modules in combination with newly developed and patented CO_2 aqueous absorption liquids (Feron & Jansen, 1995). However, these newly developed absorption liquids may suffer from crystallization at higher loadings of CO_2 (Kumar, 2002).

The literature survey shows that most of the published work on CO_2 removal using membrane gas absorption process is related to the use of liquids with high surface tension such as water, aqueous alkali or alkaline salt solutions in combination with hydrophobic membrane to avoid the wetting of membrane pores. The use of absorption liquids having a low surface tension such as aqueous alkanolamine solutions or the use of physical organic solvents suffered from drawbacks due to the wetting of less hydrophobic (e.g. polypropylene) membranes.

Cross flow membrane contactors have been applied for gas absorption by few research groups (e.g. Feron & Jansen, 1995; Wickramasinghe et al., 1992). However, the effects of changes in concentration difference and changes in flow rates have not been considered in detail. These changes can have significant effect on the overall performance of the membrane gas-liquid contactor when the solute concentration in the feed stream is considerable and a high degree of removal of the solute is desired.

In addition, most of research is carried out at atmospheric pressures where as for natural gas processing, depending on the reservoir the system, pressures up to 70 bars and CO_2 partial pressures up to 20 bars are reported (Kohl & Nielson, 1997). At such high pressures the performance and stability of the membrane gas absorption needs to be investigated.

6.0 Structure of this thesis

This thesis titled "Gas Purification using Membrane Gas Absorption" is focused on the development of the membrane gas absorption for CO_2 removal from natural gas using non-reactive (low surface tension) as well as reactive solvent (high surface tension) in combination with the relatively less expensive polypropylene microporous membranes. In the case of physical organic solvents, the technique of carefully controlling the transmembrane pressure in order to avoid the wetting microporous membranes is explored.

As discussed in Section 4, proper selection of the membrane-solvent combination is an important step in the development of a membrane gas absorption process. In **Chapter 1** theoretical considerations on the wetting of the microporous membrane are presented and important criteria for the selection of membrane-solvent combinations are developed. Using these criteria, the membrane-solvent selection is carried out for the case of bulk CO_2 removal from natural gas by absorption in a physical organic solvent.

The information on the application of membrane gas absorption at elevated pressure is limited. **Chapter 2** is devoted to investigate the membrane gas absorption at elevated pressures. CO_2 removal experiments using a physical, organic solvent (propylene carbonate) are carried out at pressures up to 20 bars using a micro-contactor consisting of a single hollow fiber. The long term application of the membrane gas-liquid contactor is also tested and a simple method to avoid the wetting of the microporous hollow fiber membrane by the absorption liquid via carefully controlling the transmembrane pressure is explored.

The shell-side mass transfer performance of the membrane modules strongly depends on the shell-side mixing and the shell geometry. However, limited information is available in literature on the shell-side mixing of hollow fiber membrane modules. In the **Chapter 3** shell-side mixing of a rectangular cross-flow hollow fiber membrane contactor is investigated using gas-phase RTD measurements. A novel ultrasound based measurement technique is used to characterize the system. The response of the system to an idealized step input is used to estimate the axial dispersion coefficient by fitting the axial dispersion model with the proper boundary conditions. The transversal dispersion coefficients are estimated by measuring steady state exit concentration profiles of a tracer point source and by fitting the general dispersion model. Thus the shell-side mixing of the cross-flow rectangular module is determined in terms of dispersion coefficients in all three directions.

Cross-flow operation of the gas-liquid membrane contactors offers several advantages compared to the parallel flow contactors. **Chapter 4** deals with the use of rectangular cross flow hollow fiber membrane modules for CO_2 removal using water as a ('green') solvent. However, in the case of cross flow contactors the concentrations of both fluids and volumetric flow rates of compressible fluids vary in both directions i.e. parallel and perpendicular to the flow direction. In this case, a simple logarithmic average of concentration driving force cannot be used to predict the performance of the contactor.

Hence, a detailed mathematical model which takes into account changes in concentrations as well as changes in flow rates in both directions is developed. The possibility of application of analytical solutions that were developed for cross-flow heat exchangers is also explored. Experimental studies were carried out to validate the modeling results.

In **Chapter 5** the performance of rectangular cross flow hollow fiber membrane gas-liquid contactors for CO_2 and H_2S removal using aqueous carbonate solutions is investigated. To describe the effect of the chemical reaction on the absorption in a cross-flow hollow fiber membrane gas-liquid contactor, a detailed mathematical model with multiple chemical reactions occurring in the liquid phase is developed using first principles. A complete scheme of the reversible, ionic reactions and equilibria involved in the absorption of CO_2 and H_2S using aqueous carbonate solutions was implemented in the model to describe the solute uptake. The model was validated using experimental studies in a laboratory and in a commercial contactor, respectively.

An innovative application of a (single) hollow fiber membrane contactor for the determination of the physical and kinetic properties of a gas-liquid system is explored in **Chapter 6**. This novel model contactor offers numerous advantages over conventional gas-liquid model contactors like stirred cell, laminar jet etc.. The main features of this novel contactor such as known and orientation-independent mass transfer area, well-defined hydrodynamics, a wide rang of exposure time etc. make this contactor a handy tool for gas-liquid research. The applicability and the limitations of this model contactor for the determination of diffusivities, solubility and reaction kinetics are explored using absorption of CO_2 in water and in aqueous NaOH solution as model systems.

References

Al-Saffar, H.B., Ozturk, B., & Hughes, R. (1997). A comparison of porous and non-porous gas-liquid membrane contactors for gas separation. *Chemical Engineering Research and Design,* **A75**, 685-692.

Cussler, E.L. (1994). Hollow fiber contactors in *Membrane Processes in Separation and Purification* (Edited by J.G. Crespo and K.W. Boddeker). Dordrecht: Kluwer Academic.

Doraiswamy, L.K., & Sharma, M.M. (1984). *Heterogeneous Reactions: Analysis, Examples, and Reactor Design. Volume 2: Fluid-Fluid-Solid Reactions.* Singapore: John Wiley.

Esato, K., & Eiseman, B. (1975). Experimental evaluation of Gore-Tex membrane oxygenator. *Journal of Thoracic and Cardiovascular Surgery*, **69(5)**, 690-697.

Feron, P.H.M., & Jansen, A.E. (1995). Capture of carbon dioxide using membrane gas absorption and reuse in the horticultural industry. *Energy Conversion & Management*, **36(6-9)**, 411-414.

Gabelman, A., & Hwang, S.T. (1999). Hollow fiber membrane contactors. *Journal of Membrane Science*, **159**, 61-106.

Hoff, A. K. (2003). *Modeling and experimental study of carbon dioxide absorption in a membrane contactor*. Ph.D. Thesis, NTNU, Norway.

Karoor, S., & Sirkar, K. K. (1991). Microporous hollow fiber gas absorption in reactive and non-reactive systems. *Paper presented at 4th National meeting of NAMS*, San Diego, CA.

Kim, Y., & Yang, S. (2000). Absorption of carbon dioxide through hollow fiber membranes using various aqueous absorbents. *Separation and Purification Technology*, **21**, 101-109.

Kohl, A. L., & Nielsen, R.B. (1997). *Gas Purification*: 5th ed., Houston: Gulf Publishing Company.

Kreulen, H., Versteeg, G.F., Smolders, C.A., & van Swaaij, W.P.M. (1993a). Microporous hollow fiber membrane modules as gas-liquid contactors I: Physical mass transfer processes - A specific application – Mass transfer in highly viscous liquids. *Journal of Membrane Science*, **78(3)**, 197-216.

Kreulen, H., Versteeg, G.F., Smolders, C.A. and van Swaaij, W.P.M. (1993b). Microporous hollow fiber membrane modules as gas-liquid contactors II: Mass transfer with chemical reaction. *Journal of Membrane Science*, **78(3)**, 217-238.

Kumar, P. S. (2002). *Development and design of membrane gas absorption processes*. Ph.D. Thesis, University of Twente, the Netherlands.

Li, K., & Teo, W.K. (1996). An ultra thin skinned hollow fiber module for gas absorption at elevated pressures. *Chemical Engineering Research and Design,* **A74**, 856-862.

Mulder, M. (1996). *Basic Principles of Membrane Technology.* 2nd Ed., Dordrecht: Kluwer Academic.

Nii, S., & Takeuchi, H. (1994). Removal of CO_2 and SO_2 from gas streams by a membrane absorption method. *Gas Separation and Purification*, **8(2)**, 107-114.

Nishikawa, H., Ishibashi, M., Ohta, H., Akutsu, N., Matsumoto, H., Kamata, T., & Kitamura, H. (1995). CO_2 removal by hollow fiber gas-liquid contactors. *Energy Conversion & Management*, **36(6-9)**, 415-418.

Qi, Z., & Cussler, E.L. (1985a). Microporous hollow fibers for gas absorption I. Mass transfer in the liquid. *Journal of Membrane Science*, **23**, 321-333.

Qi, Z., & Cussler, E.L. (1985b). Microporous hollow fibers for gas absorption II. Mass transfer across the membrane. *Journal of Membrane Science*, **23**, 333-345.

Rangwala, H.A. (1996). Absorption of carbon dioxide into aqueous solution using hollow fiber membrane contactors. *Journal of Membrane Science*, **112**, 229-240.

Shaw, T.P., & Hughes P.W. (2001). Optimize CO_2 removal, *Hydrocarbon Processing*. **May**, 53-58.

Sirkar, K.K. (1992). Other New Membrane Processes *in Membrane Handbook* (Edited by W.S. Winston Ho and K.K. Sirkar). New York: Chapman and Hall.

Sirkar, K.K. (1997). Membrane separation technologies: Current developments, *Chemical Engineering Communications*, **157**, 145-184.

Tsuji, T., Suma, K., Tanishita, K., Fukazawa, Z., Kanno, M., Hasegawa, H., & Takashi, A. (1981). Development and clinical evaluation of hollow fiber membrane oxygenator. *Transactions of American Society of Artificial Internal Organs*, **27**, 280-284.

Wang, K.L., & Cussler, E.L., (1993). Baffled membrane modules made with hollow fiber fabric. *Journal of Membrane Science,* **85,** 265-278.

Wickramasinghe, S.R., Semmens, M.J., & Cussler, E.L., (1992). Mass transfer in various hollow fiber geometries. *Journal of Membrane Science,* **69**, 235-250.

Chapter 1

Membrane-Solvent Selection for Membrane Gas-Liquid Contactors

Abstract:

Membrane contactors can provide very high interfacial area per unit volume, independent regulation of gas and liquid flows and are insensitive to module-orientation, which make them very attractive in comparison with conventional equipments for offshore application. However, the membrane adds additional to the resistance in the process of mass transfer. The mass transfer resistance of the membrane is affected by the presence of liquid inside the membrane pores. This wetting of the membrane is determined by the properties and mutual interactions of the membrane and the liquid. Hence, a proper choice of the membrane-solvent combination is a critical and determining step in developing membrane gas absorption processes.

Important criteria for the selection of the membrane-solvent combination for membrane gas-liquid contactors, such as the critical entry pressure, contact angle and critical solvent surface tension are evaluated in this chapter. These characterizing properties of membranes and solvents are experimentally measured for various membrane and solvent combinations for the case of carbon dioxide removal from natural gas. For selected combinations the actual gas-liquid mass transfer process for carbon dioxide absorption is explored experimentally in flat sheet as well as for hollow fiber membrane configuration. The experimental results were compared to the theoretical calculations, to determine possible mass transfer limitations due to wetting effects. The polypropylene membrane in combination with propylene carbonate as absorption liquid was found to be a suitable combination.

1.0 Introduction

The membrane gas absorption technology is an emerging technology for selective separation of gaseous components. The microporous membrane used in this process acts as a fixed interface between the gas and the liquid phase without dispersing one phase into another. Unlike dense membranes used for gas separation, the microporous membranes used in this process do not impart any selectivity towards the solute and just act as a physical barrier between the two phases. These membrane gas–liquid contactors offer numerous advantages over conventional mass transfer equipments. The noticeable advantages of the membrane contactors are operational flexibility, higher mass transfer rates and easy linear scale up. The operational flexibility is due to the absence of interpenetration of the phases in the contactor and hence the liquid and gas phase flow rates can be manipulated independently of each other, without any consequences like flooding, entrainment and weeping, as encountered in column type contactors.

The absorption rate depends on the interfacial area for gas-liquid contact ($\underline{a}$) and the mass transfer coefficient (k_L). The interfacial area for mass transfer in a membrane gas-liquid contactor equals the geometrical membrane surface area. For commercially available hollow fiber membrane modules, it varies between 1500-3000 m^2/m^3 of contactor volume, depending on the diameter and packing density of the hollow fiber. This value is much higher than the contact areas available in conventional contactors (100-800 m^2/m^3) like stirred tanks, bubble columns, packed and plate columns (Westerterp et al., 1984). In the membrane contactors, the high interfacial area is obtained at the cost of the fiber side mass transfer coefficient, which is low due to the laminar flow of fluids inside the fiber. Nevertheless, the volumetric mass transfer coefficient ($k_L\underline{a}$) is several times higher, resulting in a considerable reduction in the size of the contactor. The structuring of the gas-liquid interface by a membrane makes this interfacial area independent to the orientation of the module. Especially for off-shore applications the compactness and independence of orientation offers tremendous advantages. The modular design also allows easy scale up or scale down of the gas membrane absorption plant by simply adding or removing membrane modules.

The presence of a membrane adds additional resistance to the overall mass transfer process. In the ideal case, the membrane pores are filled with the gaseous component resulting into negligible mass transfer resistance. However, when the membrane pores are filled with the liquid (wetted), the mass transfer resistance of the membranes becomes significant (Kreulen et al. 1993a), resulting into economically unviable operation. Thus long-term stable operation of the membrane contactor requires that the pores of the membrane remain completely gas filled (non-wetted) over prolonged periods of operational time. The wetting tendency of a membrane solvent combination is mainly determined by properties of the membrane (e.g. pore size), properties of the liquid (e.g. surface tension) and their mutual

interactions (e.g. contact angle). In general, liquids with low surface tensions tend to wet the surface more easily as compared to solvents having higher surface tensions.

Most of the physical solvents used in the bulk removal of carbon dioxide such as methanol (Rectisol process), propylene carbonate (Fluor solvent), selexol, n-formyl morpholine etc. are organic in nature and have low surface tension. The 'green' solvent water, on the other hand, has relatively low carbon dioxide solubility. Hence, there is need for reliable guidelines to select the suitable membrane-solvent combination for bulk removal of carbon dioxide. Therefore the governing and important criteria for the selection of a membrane-solvent combination for bulk carbon dioxide removal using a membrane G-L contactor are evaluated. These characterizing properties of membranes and solvents are experimentally measured for various membrane-solvent combinations. For selected membrane-solvent combinations the actual gas-liquid mass transfer process for carbon dioxide absorption is explored experimentally in flat sheet as well as for hollow fiber membrane configuration.

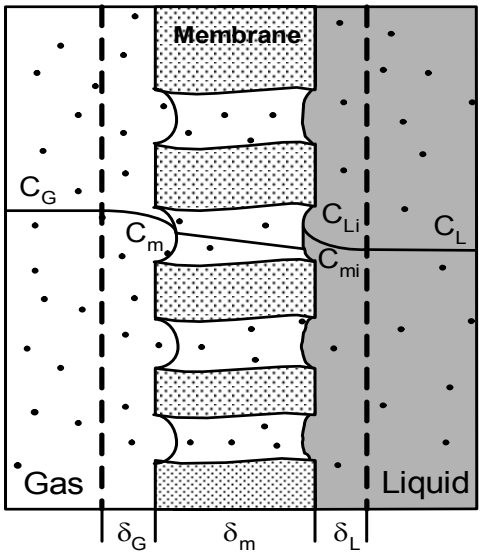

Figure 1: *Mass transfer process in membrane G-L contactor.*

2.0 Theory

2.1 Mass transfer in the membrane contactor

The mass transfer process in the membrane contactor can be more easily visualized and interpreted using the film theory approach. Figure 1 depicts schematically the mass transfer process in a membrane-gas liquid contactor and the concentration profile. Here the membrane pores are filled with gas. In the transfer of gaseous solute to the liquid bulk the following steps are involved;

1. Transfer of solute from the bulk gas phase to the membrane surface.

2. Transfer of gas through membrane pores to the liquid interface.
3. Transfer of gas from liquid interface into the liquid bulk.

The overall mass transfer process consists of three resistances in series: the gaseous phase boundary layer, the membrane and liquid phase boundary layer. The mass transfer in the gas-liquid membrane contactor can be described with the resistance-in-series model. The overall mass transfer coefficient can be obtained by summing the partial resistances in series i.e. in the gas phase, in the membrane and in the liquid phase respectively. The concentration profile is discontinuous at the gas-liquid interface, where the equilibrium relationship holds:

$$C_{li} = mC_{mi} \tag{1}$$

Here C_{li} and C_{gi} are liquid side and gas side solute concentration at the interface and m is the distribution coefficient. The overall resistance of the mass transfer process, $(1/K_o)$, can be obtained by taking steady state flux balance across the membrane

$$\begin{aligned} N_A &= k_g(C_G - C_m) \\ &= k_m(C_m - C_{mi}) \\ &= k_l(C_{Li} - C_L) \\ &= K_o(mC_G - C_L) \end{aligned} \tag{2}$$

Thus,
$$\frac{1}{K_o} = \frac{1}{k_G} + \frac{1}{k_m} + \frac{1}{mk_L} \tag{3a}$$

When the membrane pores are filled with liquid, the overall mass transfer resistance is given by Eq. (3b)

$$\frac{1}{K_o} = \frac{1}{k_G} + \frac{1}{mk_m} + \frac{1}{mk_L} \tag{3b}$$

The Eqs. (3a) and (3b) assume that pore size and membrane wetting characteristics are uniform throughout the membrane and there is no solute transport through the non-porous part of the membrane. The individual mass transfer coefficients, k_g and k_l, are mainly determined by the geometry of the membrane contactor and hydrodynamic conditions. Various correlations are available to determine these mass transfer coefficients depending on the flow geometry. An overview of the fiber side mass transfer coefficient correlations is presented in Table 1.

The membrane mass transfer resistance is an extra resistance in the mass transfer process in the membrane gas-liquid contactors as compared to the conventional gas-liquid contactors. Since convection in the membrane pores can be neglected, the mass transfer resistance of membrane is entirely determined by diffusion of the solute in the membrane

pores. The membrane mass transfer resistance can be estimated from Eq. (4) (Kreulen et.al., 1993a).

$$\frac{1}{k_m} = \frac{\delta}{D_i}\frac{\tau}{\varepsilon} \tag{4}$$

Table 1: *Summary of equations predicting mass transfer coefficient for fiber side flow.*

Author	Equation	Comment
Leveque (1928)	$Sh = 1.62(Gz)^{0.33}$ Gz > 20 $Sh = 3.67$ Gz < 10	Analogy of theoretical laminar heat transfer flux
Sieder & Tate (1936)	$Sh = 1.86(Gz)^{0.33}$ Gz > 100	Analogy of empirical laminar heat transfer flux
Yang & Cussler (1986)	$Sh = 1.64(Gz)^{0.33}$ 30 < Gz < 2000	Empirical equation for gas-liquid absorption in hollow fiber module.
Dahuron & Cussler (1988)	$Sh = 1.5(Gz)^{0.33}$	Empirical equation for liquid-liquid extraction in hollow fiber module.
Takeuchi et al (1990)	$Sh = 1.4(Gz)^{0.33}$ 50 < Gz < 1000	Empirical equation for liquid-liquid extraction in hollow fiber.
Viegas et. al. (1998)	$Sh = 0.2\,\mathrm{Re}\left(Sc\frac{d_i}{L}\right)^{0.33}$ Gz < 65	Empirical equation for liquid-liquid extraction in hollow fiber module.

In porous structures two types of diffusion can be distinguished: the continuum or molecular diffusion and Knudsen diffusion. The molecular diffusion is determined by the interactions between the different molecules. The corresponding diffusion coefficient can be calculated from the kinetic gas theory. However, if the pores are smaller and/or when the pressure of the gas is reduced, the mean free path of the diffusing molecules becomes comparable or larger than the pore size of the membrane. In this case the interactions of the molecules with the pore wall become dominating and Knudsen diffusion is important. The Knudson diffusion coefficient can be estimated by Eq. (5) (Mason & Malinauskas, 1983).

$$D_{Ki} = k_d\sqrt{\frac{8RT}{\pi M}} \tag{5}$$

The constant k_d depends on the membrane pore geometry and the interactions between membrane and molecule. In the intermediate region where both types of diffusion play a role, in this region the overall diffusion coefficient is given by Eq. (6).

$$\frac{1}{D_i} = \frac{1}{D_{ij}} + \frac{1}{D_{Ki}} \tag{6}$$

When the membrane pores are filled with the liquid phase, the Knudson diffusion can be ignored owing to the higher molecular density. In this case the membrane mass transfer resistance is given by Eq. (7) (Cussler et. al. 1995).

$$\frac{1}{k_m} = \frac{\delta}{mD_L}\frac{\tau}{\varepsilon} \tag{7}$$

where, $D_{L,}$ is the diffusion coefficient of the solute in the liquid phase. The presence of liquid phase in the membrane pore results in very low membrane mass transfer coefficient and the application of the membrane gas-liquid contactor becomes economically unviable. Hence, care must be taken to avoid the filling of membrane pores with liquid phase.

2.2 Wetting characteristics of membrane-solvent combination

The membrane is wetted when the pores of the membrane are filled with liquid. In this mode of operation, the gas has to diffuse through the liquid filled pores. Since the diffusion coefficient of gaseous components in liquids is several orders of magnitude lower than that in the gas phase, the mass transfer coefficient of the membrane in the wetting mode is also very small. The tendency of the liquid to wet the surface is determined by the surface morphology and properties of the liquid. When a drop of a liquid is brought into contact with a flat polymer surface, the final shape taken by the drop and the partial wetting of surface depends on the relative magnitudes of the molecular forces that exist within the liquid (cohesive) and between the liquid and the surface (adhesive). The surface wetting can be predicted from the contact angle made by a liquid drop with the polymer surface (Figure 2).

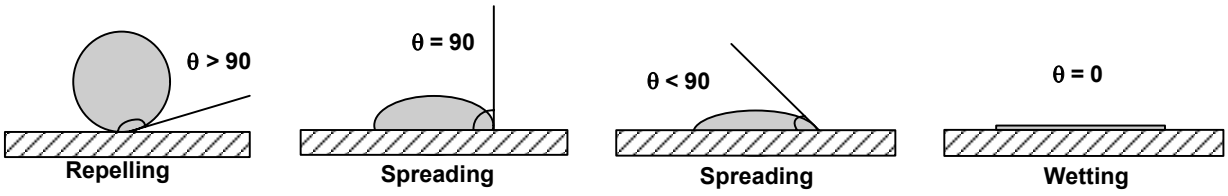

Figure 2: *Contact angle and wetting of surfaces.*

A contact angle of zero results in complete wetting of the porous or non-porous surface, while an angle between 0^o and 90^o results in spreading of the drop (due to molecular attraction) on a non-porous surface and the wetting of pores on a porous surface. An angle

greater than 90° indicates that the liquid tends to shrink away from the solid surface and thus exhibit non-wetting tendencies. The liquids having low surface tension usually wet most polymer surfaces, giving a zero contact angle. However, for the low energy surfaces like polytetraflouroethylene (PTFE) and polypropylene (PP) many of the organic liquids having low surface tension found to exhibit non-wetting characteristics. Thus interactions of the liquid with the membrane control the wetting phenomenon; therefore in addition to the contact angle made by the liquid with the membrane surface, pore size and the surface tension of the liquid are important parameters. For instance, hydrophobic porous membranes do not permit the aqueous liquid to enter into the pores until a certain critical liquid-side overpressure is exerted. This critical entry pressure (CEP) is defined as the trans-membrane pressure difference at which liquid penetrates into the pores of the membrane. The critical entry pressure is correlated to the surface tension of liquid, the contact angle of the liquid on the membrane surface and the size and shape of membrane pores and is given by Laplace-Young equation (Eq. 8).

$$\Delta P_c = -\frac{2\gamma_L \cos\theta}{r_p} \tag{8}$$

In this equation, the membrane pores are assumed to be uniform, cylindrical and sufficiently small so that the curvature radius can be assumed to be constant. However, most of the membranes do not have cylindrical pores. Some membranes have a fibrous structure and the pores are irregular spaces that remain between adjacent fibers. In other membranes, the pores are holes in a spongy structure and they tend to suffer directional changes and cross linking between them. To take into account such irregular pore structures Franken et al. (1987) introduced a geometric coefficient of the pore, *B,* in the R.H.S. of the Laplace-Young equation; $B = 1$ for cylindrical pores and $0 < B < 1$ for non cylindrical pores. Kim & Harriott (1987) studied the critical entry pressure for liquids in hydrophobic membrane with non cylindrical pores. They assumed a doughnut type of pore structure and derived an equation similar to the Laplace-Young equation. In which the contact angle θ is replaced by the effective contact angle θ_{eff} . Using this effective contact angle, the mechanical equilibrium state of a membrane-liquid-vapor system (as shown in Figure 3) can be described by the Young equation as follows;

$$\gamma_L \cos\theta_{eff} = \gamma_S - \gamma_{SL} \tag{9}$$

where γ is the surface tension, and subscripts L, S, and SL refer to liquid-vapor, solid-vapor and solid-liquid interfaces respectively. For polar or hydrogen bonding liquids on non-polar low energy surfaces, it can be assumed that only Van der Waals dispersion forces act between the liquid and solid phase. The interfacial tension between the solid and liquid phase is given approximately by Eq. (10) (Bargeman & van Voorst Vader, 1973)

$$\gamma_{SL} = \gamma_S + \gamma_L - 2\sqrt{\gamma_S^d \gamma_L^d} \tag{10}$$

where γ_S^d and γ_L^d are the dispersion components of surface tension of solid and liquid respectively. The term $2\sqrt{\gamma_S^d \gamma_L^d}$ accounts for the dispersion component of the work of adhesion of a liquid to a solid surface.

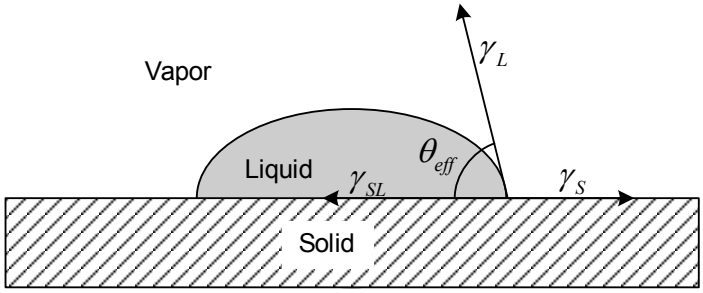

Figure 3: *Contact angle and force balance in wetting of surfaces.*

Substitution of γ_{SL} according to Eq. (10) into Eq. (9);

$$\gamma_L \cos\theta_{eff} = -\gamma_L + 2\sqrt{\gamma_S^d \gamma_L^d} \tag{11}$$

Eq. (8) and Eq. (11) can be used to relate the liquid critical entry pressure with the liquid surface tension.

$$\Delta P_c = \frac{2\left(\gamma_L - 2\sqrt{\gamma_S^d \gamma_L^d}\right)}{r_p} \tag{12}$$

The quantity $\sqrt{\gamma_S^d \gamma_L^d}$ is constant for low surface tension liquids such as high alcohol concentration aqueous solution. When $\gamma_L = 2\sqrt{\gamma_S^d \gamma_L^d}$, the RHS term in the Eq. (12) becomes zero and no over pressure is required for wetting of the membrane pores. This value of surface tension is known as the critical surface tension γ_L^C. Thus the critical surface tension is the value of surface tension when critical entry pressure is zero, and can be obtained by the x-axis intercept of the critical entry pressure versus surface tension plot. Any solution having a surface tension lower than γ_L^C, will therefore spontaneously wet the membrane surface.

In the present study the critical entry pressure and contact angle measurements are carried out for the selected membranes using aqueous ethanol solutions to determine the critical surface tension. The critical entry pressure and contact angle are also measured for selected membrane-solvent combinations to study the wetting characteristics of the membrane-solvent combinations.

Table 2: *Physical solvents for CO_2 absorption (data for 298 K).*

	Solvent	CO_2 solubility m#	Surface Tension mN/m	Viscosity cP	Selectivity CO_2/CH_4	Vapor Pressure Pa
1	Propylene Carbonate	3.50	41.5	2.5	26.31	11.33
2	Selexol	3.60	33.5	5.8	14.92	0.097
3	N-methyl pyrrodilone	4.56	34.4	1.7	13.88	53.33
4	Dimethyl formamide	4.86	30.2	0.8	-	-
5	Tributyl phosphate	2.50	27.5	3.4	25.00	-
6	Glycerol triacetate	3.70	35.8	3.5	20.55	0.13
7	n-Formyl morpholine	3.15	49.1	6.7	-	869.31
8	water	0.82	72.3	1.0	23.5	3167.20

$m = (C_L / C_G)_{equilibrium}$

3.0 Screening of membrane –solvent combinations

Considering the wetting phenomenon as described in Section 2, the selection of a membrane-solvent combination is a very critical step in developing a membrane gas absorption process. A key parameter in the screening of potential solvents is the solubility of CO_2. Table 2 shows the equilibrium CO_2 solubility in terms of the distribution coefficient for the various commercially available physical solvents and their properties. Apart from the solubility, the solvent should be non-toxic, thermally stable, easily regenerable and commercially available at low cost and should have a low vapor pressure to minimize the losses. The solvent should have a low viscosity to avoid high pressure drop over the fiber length. A high viscosity also reduces the mass transfer rates thereby increasing the requirement of membrane area. This effect becomes especially noticeable at reduced temperatures. The solvents in Table 2 are commercially available and have proven plant performance for CO_2 absorption processes in conventional contactors and are therefore selected for the initial screening of solvent-membrane combinations. The most important requirement is that the long term application should not damage the membrane either

physically or chemically and that the solvent–membrane combination should have sufficiently high critical entry pressure to avoid wetting.

Table 3: *Membrane-solvent compatibility.*

Solvent	PTFE	PP	PVDF	PES	PS
Water	√	√	√	√	√
Propylene Carbonate	√	√	x	x	x
Selexol	√	x	x	x	x
N-methylpyrrodilone	x	x	x	x	x
Dimethyl formamide	x	x	x	x	x
Tributyl phosphate	x	x	x	x	x
Glycerol triacetate	√	x	x	x	x
n-Formyl morpholine	√	√	x	x	x

√ = compatible combination x = incompatible combination

The solvents (Table 2) were tested with commercially available membranes for mutual compatibility of the membrane-solvent combination. The initial screening of the membrane materials is based on the hydrophobicity of the membrane. Membranes having a high hydrophobicity and low surface energies such as PTFE, polypropylene, PVDF, polysulfone and polyethersulfone are selected. The selected membranes were kept in contact with the solvents over a period of time. These membranes are then carefully investigated for immediate spreading of solvent and/or for damage caused by the solvent to the membrane. Table 3 shows the compatibility of the solvents with the membranes in terms of immediate spreading of the solvent and/or surface damage of the membrane. As indicated in Table 3 only PTFE and polypropylene membranes were found to be compatible with some of the selected organic solvents. The rest of the membranes showed incompatibility with the selected solvents in terms of morphological damage, swelling, shrinkages, color change or dissolution. Hence it is therefore decided to use PTFE and polypropylene membranes for further experimental work.

4.0 Experimental

4.1.1 Measurement of Critical Entry Pressure and Contact Angle

As explained previously, the critical entry pressure is of great importance for characterizing the compatibility of a membrane-solvent combination in a membrane gas absorption process. As indicated in the Eqs. 8 and 12, the wetting tendency of the membrane and thus the operating trans-membrane pressure depends on the liquid surface tension,

membrane pore size and the contact angle between the two phases. The Eqs. (8) and (12) are indirectly related to the operating temperature since the surface tension of the liquid depends on the temperature. Hence for the liquids having low surface tension a small change in the operating trans-membrane pressure or temperature can cause spontaneous wetting of the membrane. The range of operating trans-membrane pressure, minimum allowable surface tension and hence the operating temperature can be determined from the critical entry pressure and contact angle measurements. In these critical entry pressure measurements only active pores (pores open at both ends of membrane) are taken into account. Since mass transfer in membrane gas absorption takes place through active pores, the critical entry pressure measurement is a good characterization method for the wetting tendency of the membrane solvent combination in comparison to other methods.

4.1.2 Materials and Methods

Two different experimental techniques were used to measure the wetting characteristics of membrane solvent combinations. The critical entry pressure was measured for different membranes and solutions and additionally contact angle measurements were also carried out for the same membrane-solvent combinations.

Two commercial types of flat sheet hydrophobic membranes were used; polypropylene (PP) and polytetraflouroethylene (PTFE). The maximum pore size of membranes used was 0.45 μm and 0.36 μm for the PTFE and PP membrane respectively. The details of the membranes used in this study are listed in Table 4. Membranes were tested as received without any pretreatment. All solvents used in the study were of analytical grade. Double distilled water is used to prepare the aqueous ethanol solutions with different concentrations.

Table 4: *Membrane Characteristics.*

Membrane	Maximum pore size	Thick-ness	Porosity	Inner diameter	Trade name	Manufacturer
PTFE Flat sheet	0.45 μm	158 μm	-	-	TE 36	Schleicher & Schuell
PP Flat sheet	0.36 μm	92.5 μm	69 %	-	PP 1E	Membrana-Accurel
PTFE Hollow fiber	1.00 μm	500 μm	50 %	1000 μm	Perflon	Sumitomo
PP Hollow fiber	0.64 μm	200 μm	~ 80 %	600 μm	Q3/2	Membrana-Accurel

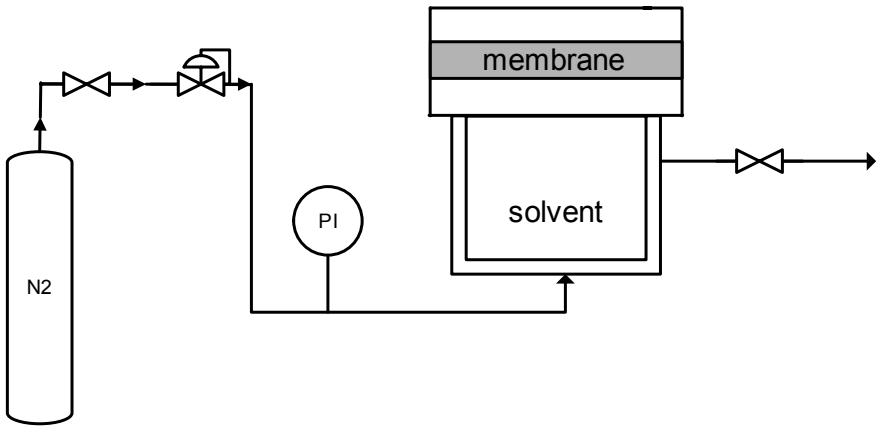

Figure 4: *Experimental set-up to measure critical entry pressure.*

The experimental set-up for critical entry pressure measurement is shown in Figure 4. It mainly consists of a small stainless steel vessel for holding the membrane and the solvent. A dry membrane is placed in the vessel with support of Teflon gaskets. The solvent is filled into the solvent chamber and then the solvent is pressed into the membrane pores by applying pressure. The pressure is applied with the help of high-pressure compressed nitrogen fed from a cylinder. The applied pressure was measured with the help of digital pressure transducer. The pressure is gradually increased with the help of precision pressure regulator till the first drop of the solvent appeared on the membrane surface. This pressure is then defined as the critical entry pressure for the particular membrane–solvent combination.

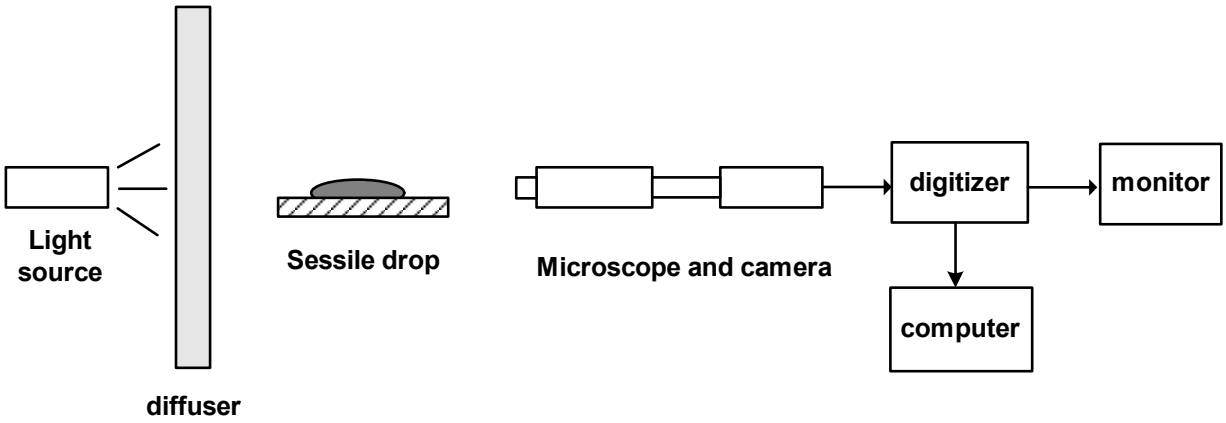

Figure 5: *Experimental set-up to measure contact angle.*

The contact angles were measured with the sessile drop method using aqueous solutions of ethanol and pure solvents on PTFE and PP membranes. Figure 5 shows the schematic block diagram of the contact angle measuring instrument (Data Physics, OCA). Experiments were carried out at room temperature. A piece of membrane material (dimensions: 5 cm x 5 cm) was placed on a measuring platform of the above mentioned device and a 3 µl drop of the solvent was placed on the membrane surface using a micro

syringe. The contact angle is calculated using a digital image processor. The average of 4-6 readings was taken for each individual measurement.

4.2 Measurement of Mass Transfer Characteristics

Experiments are carried out to study the CO_2 absorption using the selected membrane-solvent combinations as determined in Section 3. Since the mass transfer coefficient is also dependent on the configuration of the contactor, separate experiments are carried out in the flat sheet as well as in the hollow fiber membrane configuration. The experiments are useful to determine the effect of membrane resistance on the overall performance of the process and can indicate the wetting/partial wetting of the membrane.

4.2.1 Experiments with Flat-sheet Membrane Configuration

Carbon dioxide absorption is carried out in the flat sheet membrane contactor for the selected solvent and membrane combinations. The experimental set-up is shown in Figure 6. The membrane gas-liquid contactor is a bi-chambered glass vessel with an internal diameter of 8 cm. A flat sheet membrane, which is to be tested, separates the two chambers. The height of each compartment is 7.5 cm. To minimize gas and liquid side mass transfer resistances, each compartment is equipped with two pitched blade stirrers. The stirrers could be stirred independently. The speed of gas phase stirrers could be varied from 5 to 35 rps. The liquid phase stirrers' speed could be varied from 0.25 to 2 rps. The stirrers in both phases were magnetically driven to avoid the leakage from the contactor. The membranes were glued between metal rings to give an interfacial area of 2.64×10^{-3} m^2. Both compartments were jacketed. To maintain the same temperature on the gas and the liquid side, a thermostat water-bath supplies water at constant temperature through the double walls of the contactor. A thermocouple is immersed in the water bath to measure the temperature. Both compartments are provided with an inlet and outlet, to fill and to discharge the fluid. Considering the importance of the trans-membrane pressure on the possible wetting of membrane pores, it is necessary to monitor the pressure of both compartments closely and hence each compartment was equipped with a digital pressure indicator. The maximum pressure in both compartments is 1 atm for the glass membrane gas contactor. All the experiments were carried out in batch mode. Before starting the experiment the liquid is thoroughly degassed by applying vacuum. To start the experiments the gas chamber is filled with pure carbon dioxide and the pressure decrease was measured as a function of time. As the carbon dioxide starts absorbing into the solvent, the partial pressure of carbon dioxide on gas side starts decreasing steadily with time. This drop in the gas side pressure is then noted as a function of time to calculate the absorption flux. The mass balance for carbon dioxide absorption yields following equation.

$$ln\left\{\frac{P_{CO_2}-P_{CO_2,\infty}}{P_{CO_2,0}-P_{CO_2,\infty}}\right\}=-\frac{mV_L+V_G}{V_LV_G}K_oAt \tag{13}$$

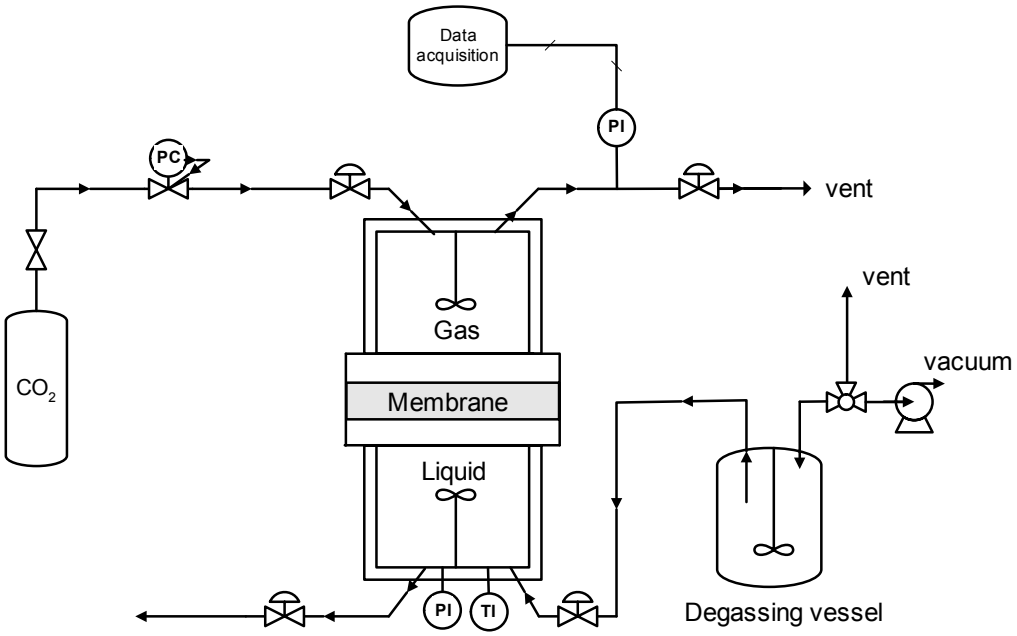

Figure 6: *Measurement of mass transfer flux in flat sheet membrane contactor.*

The slope in a plot of LHS term of Eq. (13) versus time yields the overall mass transfer coefficient, K_o. The experiments are carried out with and without membrane respectively to analyze the effect of the membrane on the overall mass transfer rate.

4.2.2 Experiments with Hollow Fiber Membrane Configuration

Absorption experiments were carried out in a single hollow fiber membrane contactor, with absorption liquid flowing through the fiber. Figure 7 shows schematically the experimental setup used for the absorption experiments. The single hollow fiber membrane contactor used in the experiments was made of glass. The contactor consisted of a jacketed, cylindrical tube with threaded ends. The two ends of a membrane hollow fiber were passed through two small stainless steel (SS) tubes whose inside diameter was slightly larger than the outside diameter of the hollow fiber. The length of the fiber exposed to the gas during the measurements was the distance between these two SS tubes. The distance between the SS tubes was carefully adjusted and the fiber was potted using epoxy resin to the SS tubes on both the ends of the two tubes. The length of the fiber inside the SS tube (> 0.07 m), on the liquid entry side provides sufficient distance (> $10d_{in}$) for the laminar liquid flow profile inside the fiber to be fully developed, before it contacts the gas. The hollow fiber between the SS tubes was placed coaxial to the jacketed tube and the two SS tubes were fixed to the ends

of the threaded tube without stretching or putting slack in the fiber. The liquid feed line was connected to the SS tube on the feed side of the contactor. Two vertical glass tubes ('Bubble Indicators') were attached in the upstream and down stream of the liquid feed line so that in the event of gas bubble formation in the liquid stream, the bubbles could be observed.

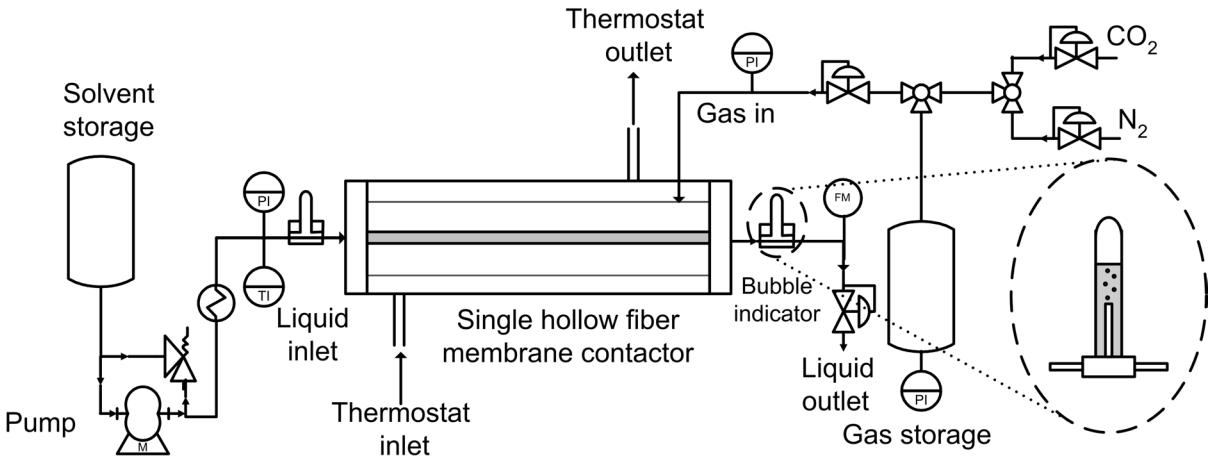

Figure 7: *Measurement of mass transfer flux in hollow fiber membrane contactor.*

A semi-batch mode of the gas-liquid contacting operation was used during the experiments. The liquid flow through the fiber was continuous. The solvent was fed from a gear pump via a flow controller. The solvent used in the experiments was degassed before usage by applying vacuum in a separate apparatus. The solvent is passed through the heat exchanger to maintain the desired temperature before passing to the single hollow fiber module. The upstream solvent pressure is controlled using a high precision back pressure controller valve. During the experiments sufficient high pressure on the liquid side is maintained to avoid the bubble formation. The CO_2 partial pressure outside the hollow fiber in the contactor was maintained constant by feeding pure CO_2 from a gas supply vessel, through a pressure regulator. From the drop in the pressure of CO_2 in the gas supply vessel, the absorption rate and hence the average CO_2 flux across the membrane was calculated:

$$< J >= \left(\frac{V}{RT} \right) \left(\frac{1}{\pi d_i l} \right) \left(\frac{P_1 - P(t)}{t} \right) \tag{14}$$

The theoretical average flux can be calculated by a simple mass balance of CO_2 over the length of fiber:

$$\langle J \rangle = \frac{Q_L m C_g \left(1 - \exp\left(\frac{-K_O \pi d_i l}{Q_L} \right) \right)}{\pi d_i l} \tag{15}$$

The measured flux is then equated to the Eq. (15) to calculate the overall mass transfer coefficient K_o.

5.0 Results and Discussion

5.1 Measurement of Critical Entry Pressure

To study the effect of surface tension the critical entry pressure experiments were carried out for flat sheet membranes. Figure 8 shows the critical entry pressure for the flat sheet membranes for various concentrations of aqueous ethanol. This set of experiments was carried out with PP (0.36 μm) and PTFE (0.45 μm) membranes at ambient temperature (≈ 20 ^{o}C). Only four points could be measured with PP (0.36 μm) membrane because of the lower mechanical strength and low burst pressure (0.9 bar) of the membrane. Hence it was not possible to measure the critical entry pressure for lower concentrations of ethanol. Moreover at higher ethanol concentrations the membrane wetted spontaneously. The effect of the surface tension on the critical entry pressure is shown in Figure 9. The critical entry pressure shows linear dependence, as given in Eq. (12) on, the surface tension at relatively low surface tension values (i.e. at high ethanol concentration). However, for the higher surface tension liquids, the experimental data recede below the linear dependency in the case of PTFE membrane. This is because at lower concentrations of the ethanol, the dispersion component of the surface tension, $\sqrt{\gamma_S^d \gamma_L^d}$, is not constant and depends on the ethanol concentration. In this case, the linear dependence of critical entry pressure on surface tension is no longer valid.

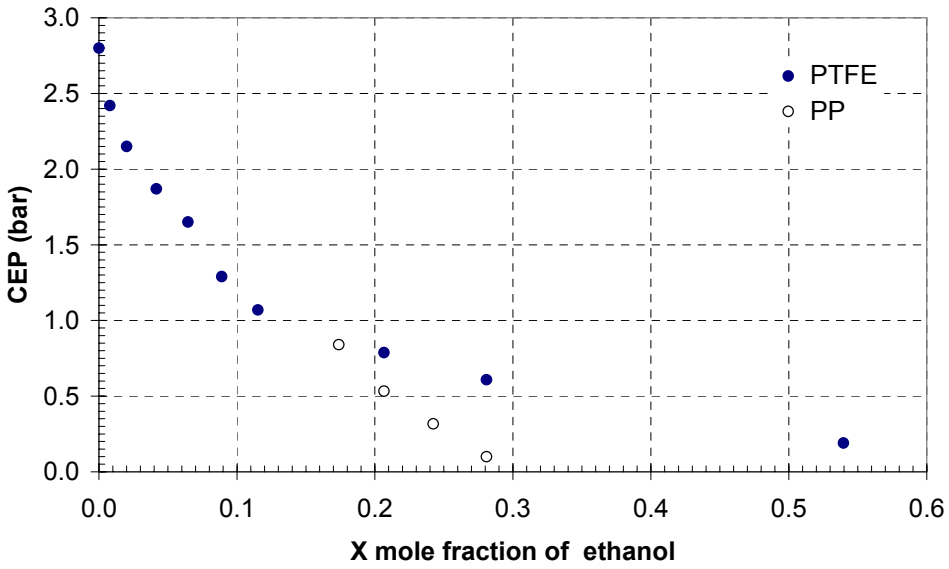

Figure 8: *Critical entry pressure for aqueous ethanol solutions.*

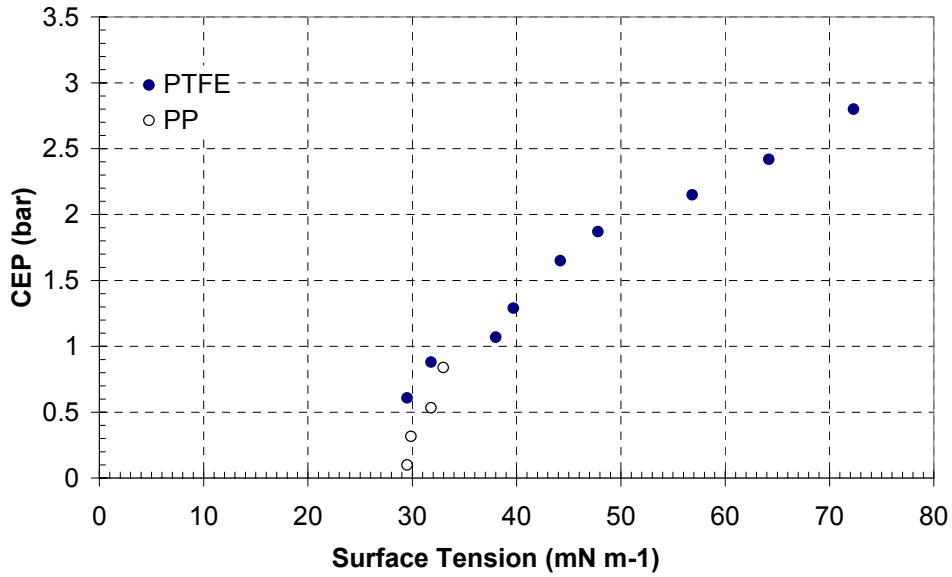

Figure 9: *Effect of surface tension on entry pressure.*

The critical surface tension (γ_L^C) for the given membrane can be calculated from the x-intercept of the plot. Experimentally determined and literature values (Franken et al. 1987; Zisman, 1964) are given in Table 5. There is good agreement between the experimentally determined values and these from literature data. Since any liquid having a surface tension lower than the critical surface tension wets the membrane spontaneously, the solvents to be used must have a substantially higher surface tension than the critical surface tension values given in Table 5.

Table 5: *Critical surface tension of membrane.*

Membrane	**Experimental γ_L^C mN/m**	**Literature γ_L^C mN/m**
PTFE	20	18
PP	29	29

Besides water, of the selected solvents only propylene carbonate, n-formyl morpholine and glycerol triacetate have sufficiently high surface tensions and are compatible with both PTFE and PP membranes. The critical entry pressure values for these solvents are determined using flat sheet membranes. The results are presented in Table 6. The critical entry pressure for the water-polypropylene and n-formyl morpholine-polypropylene combinations could not be determined because of the lower burst pressure of the PP membrane.

Table 6: *Critical entry pressure for selected solvents.*

Solvent	Critical entry pressure, kPa	
	PTFE	PP
water	310	>90
Propylene carbonate	110	78
n-formyl morpholine	130	>90
Glycerol triacetate	53	7.5

Table 7: *Contact angle for various membrane-solvent combinations (293 K).*

Membrane	Liquid	Ethanol concentration (vol %)	γ mN/m	θ°
Polypropylene	Distilled water	-	72.30	117.70
	Ethanol-water	2	64.18	106.88
		5	56.84	103.80
		10	47.80	94.49
		20	39.70	81.60
		30	34.33	71.15
		40	31.80	60.53
	Propylene carbonate	-	42.00	90.83
	n-FM	-	48.14	94.56
PTFE	Distilled water	-	72.30	127.42
	Ethanol-water	2	64.18	122.10
		5	56.84	115.11
		10	47.80	110.39
		20	39.70	103.79
		30	34.33	98.01
		40	31.80	95.90
	Propylene carbonate	-	42.00	106.40
	n-FM	-	48.14	110.80

5.2 Measurement of Contact Angle

Contact angles of distilled water and aqueous solutions of the ethanol on PTFE and PP membranes were measured at ambient conditions. The measured contact angles are summarized in Table 7. The results indicate that the contact angle θ decreases with increasing ethanol concentration. To analyze the effect of ethanol concentration on the contact angle, cosine of angle θ is plotted as a function of ethanol mole fraction in Figure 10. The plots of the contact angle versus ethanol mole fraction are fitted to best fit empirical equation of type:

$$\cos\theta = \cos\theta_w + \frac{ax}{1+bx} \tag{17}$$

where, a and b are fitting parameters. $\cos\theta_w$ represents the contact angle of pure water on the membrane and x is alcohol concentration in mole fraction. As seen in Figure 10, excellent fits were achieved, with correlation coefficients greater than 0.995. The values of experimentally obtained $\cos\theta_w$ and empirically fitted $\cos\theta_w$ demonstrate a good agreement.

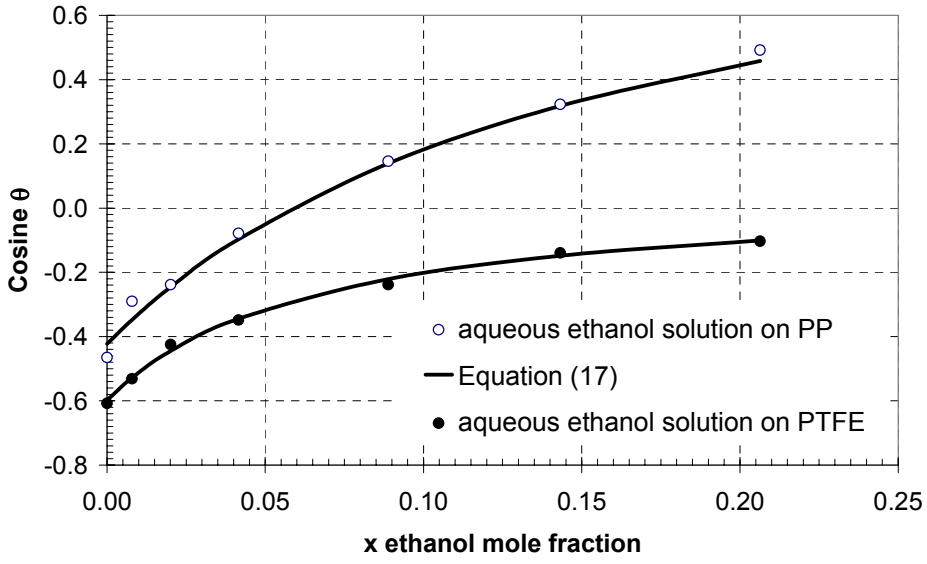

Figure 10: *Contact angle measurements for aqueous ethanol solutions.*

Figure 11 shows the plot of the cosine of the contact angle θ and the surface tension. From this figure, a rectilinear relation can be seen between $\cos\theta$ and surface tension for PTFE membrane. A similar trend is reported in the literature (Zisman, 1964) for various liquids and hydrophobic surfaces. For PP membrane two distinct trend lines can be observed. The points below cosineθ = 0.0 falls on a line, which has approximately the same slope as that of the PTFE line. However, the points above cosineθ = 0.0 can be correlated with a different line that has steeper slope, indicating that a small decrease in the surface tension results in a more substantial decrease in the contact angle. This can be attributed to the porous

structure of the membrane. The membranes used in this work do not have ideally smooth surfaces. The roughness is caused by the presence of the pores, so the liquid droplets are in contact with both the rough polymer surface and the air cavities respectively. For such system, the apparent effective contact angle is always higher than the true intrinsic contact angle on the clean polished surface in the case when the latter is greater than 90^o. However, the apparent effective contact angle is always smaller than the true contact angle on the clean polished surface if the true contact angle is lower than 90^o. (Zisman, 1964). Thus apparent contact angle in case of PP membrane decreases sharply below cosine$\theta = 0.0$ or $\theta = 90^o$. On the other hand, the contact angle of pure water on a smooth PTFE surface reported in the literature varied from 108^o to 112^o (Drelich et al. 1996), whereas in this work the contact angle reached a value of 127^o, indicating that surface roughness resulted into increased apparent contact angle. It is interesting to note that the contact angles for propylene carbonate and n-formyl morpholine also fall close to the straight line determined for both membranes using the aqueous ethanol solutions.

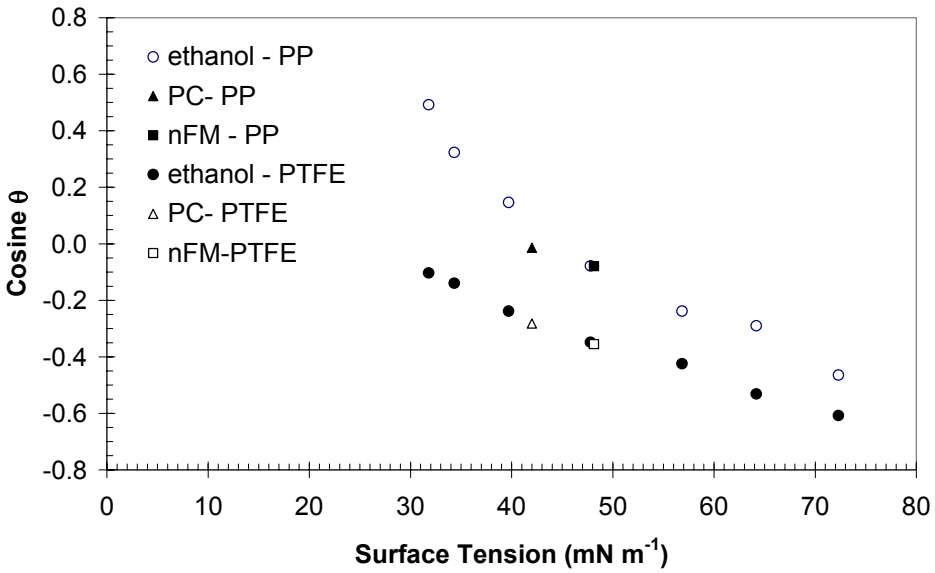

Figure 11: *Effect of surface tension on contact angle.*

5.3 Measurement of mass transfer flux using flat sheet membranes

To study whether the mass transfer resistance in the liquid phase was influencing the absorption process, the mass transfer resistance in the liquid phase was measured with absorption of carbon dioxide in the various solvents. Pure carbon dioxide and a high stirrer speed on the gas side is used in the absorption experiments in order to eliminate the gas side mass transfer resistance. The experiments are carried out with and without membrane to analyze the effect of the membrane on the overall mass transfer rate. The results are presented in Figure 12. From Figure 12 it can be concluded that the presence of the membrane does not

influence the overall mass transfer coefficient, although in the presence of a membrane the gas-liquid interface is fixed ('no-slip' boundary) whereas in the absence of a membrane the gas-liquid interface can be freely moving ('free-slip' boundary). It can also be concluded that the membranes used in these experiments are not wetted by the solvents. Moreover, it appears that the active mass transfer area in both cases is the same and the non-porous part of the membrane doesn't affect the overall mass transfer process. In the experiments without membrane, the liquid stirrer speed could not be chosen above 90 rpm because the flat interface was then disturbed by the stirrer movement. A flat, smooth, horizontal G-L interface is essential to calculate the exact G-L interfacial area and absorption flux. On the other hand, the presence of membrane offers the possibility to increase the stirrer speed, thus higher K_L, without disturbing the interfacial area. This can be useful if higher mass transfer coefficients are required e.g. in the determination of kinetic data. Figure 12 also indicates that, the overall mass transfer coefficient is a strong function of the liquid side stirrer speed. This indicates that the liquid side mass transfer resistance is the controlling parameter in the overall mass transfer process. The overall mass transfer obtained for the different solvents is in line with the viscosity of the solvents i.e. a solvent having a higher viscosity (i.e. nFM) shows a lower mass transfer coefficient and vice versa.

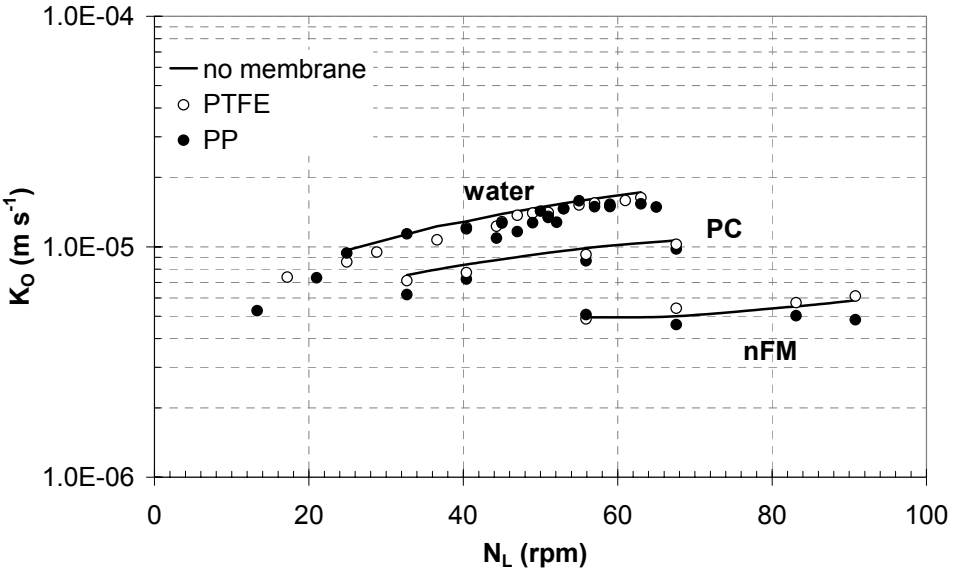

Figure 12: *Mass transfer coefficient in flat sheet membrane contactor.*

Figure 13 shows the measured carbon dioxide flux as a function of the liquid stirrer speed. Note that the flux obtained for the water is lower as compared to propylene carbonate and n-formyl morpholine solvents, due to the lower solubility of carbon dioxide in water. Amongst the solvents used in the experiments, propylene carbonate seems to have the highest mass transfer flux (Figure 13) at a moderate overall mass transfer coefficient (Figure 12).

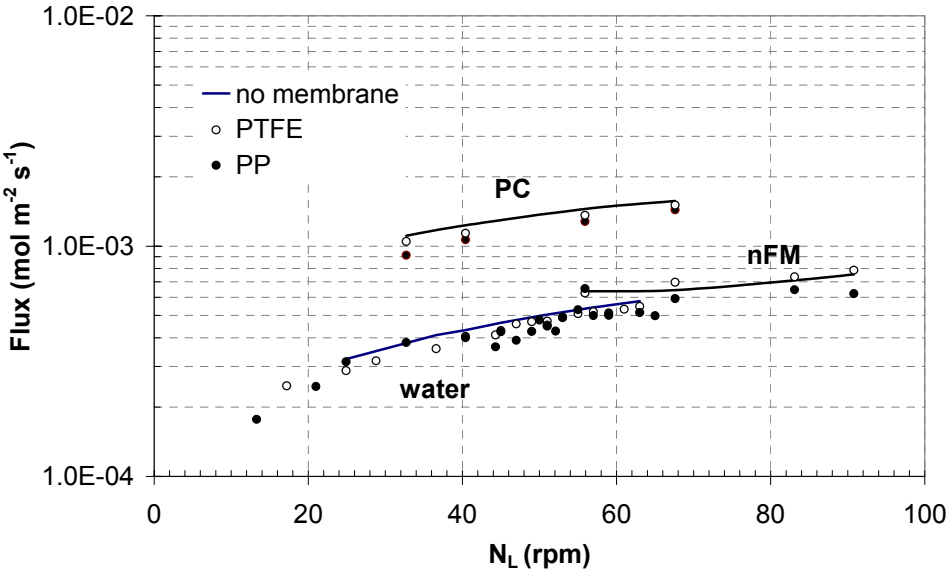

Figure 13: *Mass transfer flux in flat sheet membrane contactor.*

5.4 Measurement of mass transfer flux in single hollow fiber membrane module

Carbon dioxide absorption is carried out in a single hollow fiber membrane module using two different hollow fibers (PTFE and PP) and three different solvents. The details of the hollow fiber membranes used in the experiments are given in Table 4. All experiments are carried out using pure carbon dioxide on the shell side, in order to minimize the gas side mass transfer resistance. The details of the experimental conditions are given in Table 8.

Table 8: *Operating conditions for experiments.*

Configuration	System	Operating pressure, bar	Temperature ^{o}K	Length/Diameter m
Flat sheet membrane	PP-water-CO_2	1	298	0.058
	PP-PC-CO_2	1	298	0.058
	PP-nFM-CO_2	1	298	0.058
	PTFE-water-CO_2	1	298	0.058
	PTFE--PC-CO_2	1	298	0.058
	PTFE--nFM-CO_2	1	298	0.058
Hollow fiber membrane contactor	PP-water-CO_2	1	293	0.27
	PP-PC-CO_2	1	293	0.27
	PP-nFM-CO_2	1	293	0.27
	PTFE-water-CO_2	1	293	0.12
	PTFE--PC-CO_2	1	293	0.12

Several correlations have been developed by many investigators to predict the mass transfer coefficient in a hollow fiber membrane contactor for both fiber and shell side flow. Table 1 gives a summary of the various correlations used to calculate the fiber side mass transfer coefficient in the membrane gas liquid contactors. However, in all the work published the data is limited to aqueous solvents in case of gas-liquid applications. Two asymptotic correlations based on the heat transfer analogy of Graetz-Leveque equations are widely used (Yang & Cussler, 1986; Kreulen et. al. 1993b) to predict the mass transfer coefficient on the fiber side.

$$Sh = 1.62(Gz)^{1/3} \qquad \text{Gz} > 20 \qquad (18a)$$

$$Sh = 3.67 \qquad \text{Gz} < 10 \qquad (18b)$$

Eq. (18a) is the well-known Leveque solution, a limiting case of the more general Graetz solution. Eq. (18a) is valid for the entrance region where the concentration profile has to build up, Gz>20, whereas Eq. (18b) is applicable for long fibers where the concentration profile is completely developed, Gz <10.

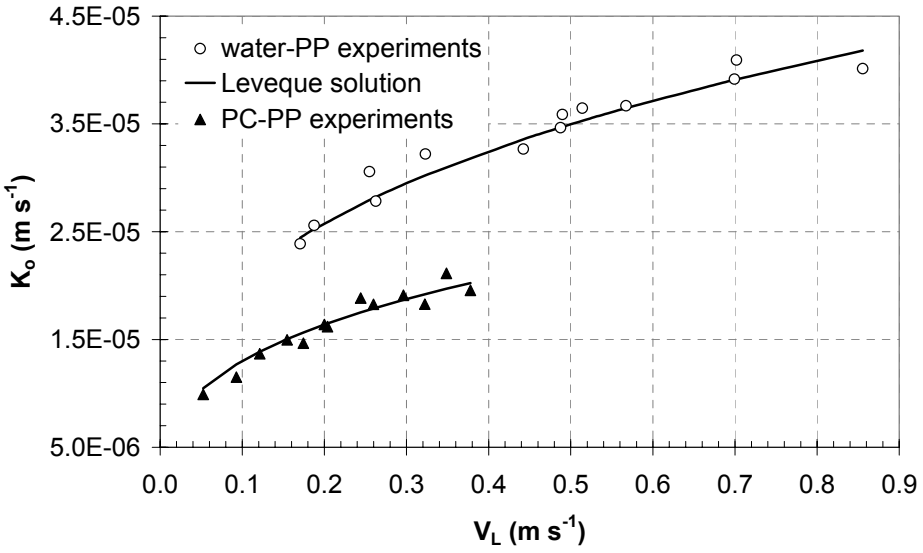

Figure 14a: *Mass transfer coefficient in PP hollow fiber membrane contactor.*

Figures 14a and 14b show the effect of the liquid velocity on the overall mass transfer coefficient for different PP and PTFE membranes with water and propylene carbonate respectively. It is clear from these figures that the fiber mass transfer coefficient can be described well with Eq. (18a) and that therefore the controlling resistance to mass transfer process is indeed in the liquid phase. Moreover the Leveque equation can also be used to predict the fiber side mass transfer coefficient in case of organic solvents.

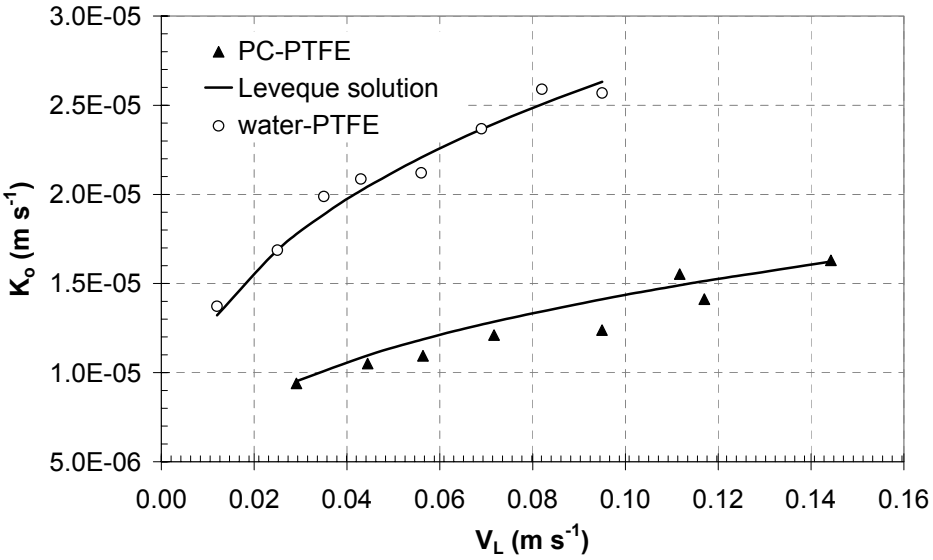

Figure 14b: *Mass transfer coefficient in PTFE hollow fiber membrane contactor.*

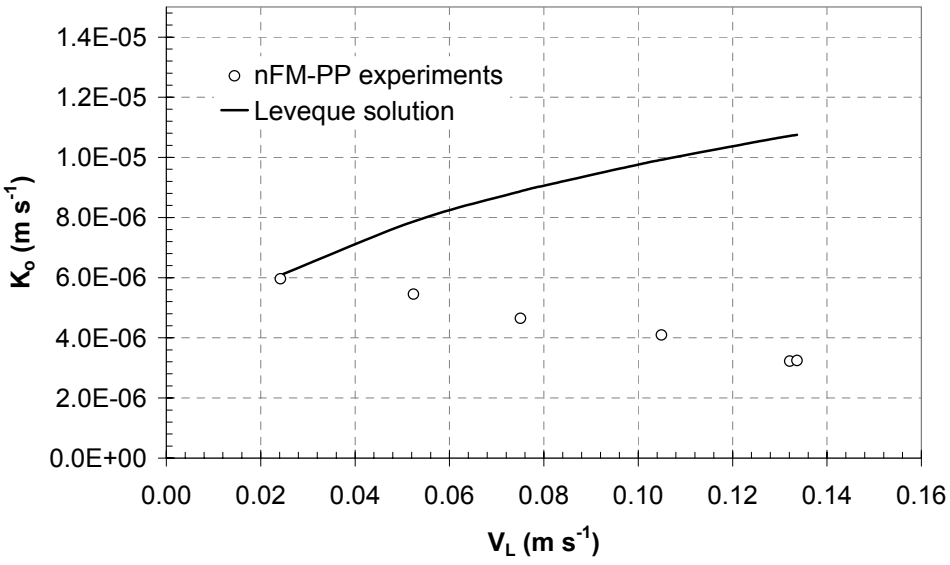

Figure 14c: *Mass transfer coefficient in PP hollow fiber membrane contactor using n-FM as an absorption liquid.*

Experiments were also carried out using polypropylene- nFM as a solvent–membrane combination. The results are given in Figure 14c. As shown in this figure, the mass transfer coefficient obtained in this case is very low. Now, the overall mass transfer coefficient even decreases with increasing the liquid velocity. These results can be explained by partial wetting of the membrane. This phenomenon, of the wetting of membrane was indeed observed during the experimentation. Because of the small diameter of the fiber, the pressure drop of the liquid inside the fiber lumen will be inevitably increased with the liquid velocity and the fiber length according to the Hagen-Poiseuille law. Since n-FM has a high viscosity

as compared to water and propylene carbonate, this pressure drop over the fiber in the case of nFM is significant, leading to membrane wetting in the initial part of the fiber due to higher pressure gradient over the fiber. This phenomenon can be observed visually by the presence of liquid droplets at the outer surface of the membrane, especially near the inlet of the fiber. As the length of the wetted portion increases with increase in the liquid velocity, hence the average mass transfer coefficient over the length of fiber decreases with the liquid velocity. Thus a pressure drop over the membrane fiber is also a critical parameter for non-wetted mode of operation. Similar results were obtained for the n-FM and PTFE combination.

6.0 Conclusion

Important criteria, such as critical entry pressure, critical surface tension of the membrane and contact angle, in the selection of the membrane-solvent combination for the development of membrane gas absorption have been investigated. These criteria are evaluated for the case of carbon dioxide absorption in physical organic solvents. Using these criteria a selection of mutually compatible membrane-solvent combinations for this application has been performed using commercially available organic solvents and organic membranes. The measurement of 'critical entry pressure' and 'critical surface tension' is a simple experimental method to select a suitable membrane–solvent combination for a membrane gas absorption process. The critical entry pressure and critical surface tension are also useful in determining the operating conditions such as allowable solvent surface tension, temperature and trans-membrane pressure. The experimentally determined values of critical surface tension for PTFE and PP micro-porous membrane match well with literature values of homogeneous non-porous PTFE and PP materials, indicating that critical surface tension is independent of the porous or non-porous structure of the material.

The measurement of the contact angle indicates that contact angles decrease with alcohol concentration and hence with the surface tension of the liquid. In general, straight line relation between the cosine of angle, θ, and liquid surface tension is observed even for the liquids having different chemical structure. The porous structure of the membrane causes an increase in the apparent contact angle when the intrinsic true contact angle on non-porous cleaned polish surface is more than 90^{o}.

For the selected membrane-solvent combinations, membrane mass transfer resistance is found to be negligible in the non-wetted mode of operation. The fiber side mass transfer coefficient in the case of organic solvent can be predicted using Leveque equation. A high pressure drop over the fiber length may lead to (partial) wetting in the initial part of the fiber and hence in such cases low mass transfer rates are observed.

PTFE and polypropylene membranes in combination with propylene carbonate seem to be promising candidates for the absorption of carbon dioxide in a membrane gas absorption process. Looking at the cost and the manufacturing difficulties in PTFE micro-

hollow fibers, a polypropylene membrane in combination with propylene carbonate as CO_2 absorption liquid seems to be the best choice among the tested membrane and solvent combinations and will therefore be used in further studies.

Acknowledgement

This research is part of the research program performed within the Centre for Separation Technology (CST), which is a co-operation between the Netherlands Organization for Applied Scientific Research (TNO) and the University of Twente. We acknowledge Herman Bruns for his assistance to the experimental work and Wim Leppink and Benno Knakan for the construction of the experimental set up.

Nomenclature

A	Area	[m^2]
C	Concentration	[mol m^{-3}]
d	Diameter	[m]
D	Diffusivity	[m^2 s^{-1}]
Gz	Graetz number , $\frac{vd^2}{Dz}$,	[-]
J	Flux	[mol m^{-2} s^{-1}]
k	Mass transfer coefficient	[m s^{-1}]
L	Length	[m]
m	Distribution coefficient	[-]
N	Flux	[mol m^{-2} s^{-1}]
P	Pressure	[pa]
Q	Flow rate	[m^3 s^{-1}]
R	Gas constant	
r	Pore radius	[m]
Sh	Sherwood number, $\frac{k_l d}{D}$,	[-]
T	Temperature	[K]
t	Time	[s]
V	Volume	[m^3]
v	Velocity	[m s^{-1}]
x	Mole fraction	[-]
z	Length	[m]

Greek letters

δ	Thickness	[m]
ε	Porosity	[-]

τ	Tortuosity	[-]
γ	Surface tension	[mN m^{-1}]
θ	Contact angle	

Subscripts

A	Average
c	Critical
d	Dispersion
eff	Effective
g	Gas
i	Interface/inside
k	Knudson
l	Liquid
m	Membrane
o	Overall/outside
p	Pore
s	Solid
z	Local value
w	Water
0	Initial
∞	Final

Superscripts

d	Dispersion
C	Critical

Abbreviation

PS	polysulfone
PP	polypropylene
PTFE	polytetraflouroethylene
PES	polyethersulfone

References

Bargeman, D., & van Voorst Vader, F. (1973). Effect of surfactants on contact angles at non-polar solids. *Journal of Colloid Interface Science*, **42**, 467-472.

Cussler, E.L., Reed, B.W., & Semmens, M.J., (1995). Membrane Contactors *in Membrane Separation Technology: Principles and Applications* (Edited by R.D. Noble and S.A. Stern). Amsterdam: Elsevier.

Dahuron, L., & Cussler, E.L. (1988). Protein extraction with hollow fibers. *A.I.Ch.E. Journal,* **34**, 130-141.

Drelich, J., Miller, J., & Good, R.J. (1996). The effect of drop (bubble) size on advancing and receding contact angles for heterogeneous and rough solid surfaces as observed with sessile-drop and captive-bubble techniques. *Journal of Colloid Interface Science*, **179(1)**, 37-50.

Franken, A.C.M., Nolten, J.A.M., Mulder, M.H.V., Bargeman, D., & Smolders, C.A. (1987). Wetting criteria for the application of membrane distillation. *Journal of Membrane Science,* **33**, 315-328.

Garcia-Payo, M.C., Izquierdo-Gil, M.A., & Fernandez-Pineda, C. (2000). Wetting study of hydrophobic membrane via liquid entry pressure measurement with aqueous alcohol solutions. *Journal of Colloid Interface Science,* **230**, 420-431.

Kim, B., & Harriott, P. (1987). Critical entry pressure for liquids in hydrophobic membranes. *Journal of Colloid Interface Science*, **115(1)**, 1-8.

Kreulen, H., Smolders, C.A., Versteeg, G.F., & van Swaaij, W.P.M. (1993a). Determination of mass transfer rates in wetted and non-wetted microporous membranes. *Chemical Engineering Science,* **48**, 2093-2102.

Kreulen, H., Smolders, C.A., Versteeg, G.F., & van Swaaij, W.P.M. (1993b). Microporous hollow fiber membrane modules a gas-liquid contactor. Part 1. Physical mass transfer processes. *Journal of Membrane Science*, **78**, 197-216.

Lawson, K.W., & Lioyd, D.R. (1997). Membrane distillation. *Journal of Membrane Science,* **124**, 1-25.

Leveque, M.C. (1928). Les lois de transmission de chaleur par convection. *Annal. Mines.,* **13,** 201-299.

Mason, E.A., & Malinauskas, A. P. (1983). *Gas transport in porous media: the dusty gas model. Chem. Eng. Monograph 17*, Amsterdam: Elsevier.

Mulder, M. (1996), *Basic Principles of Membrane Technology*, Dordrecht: Kluwer Academic Publishers.

Sieder, E.N., & Tate, G.E. (1936). Heat transfer and pressure drop of liquids in tubes. *Industrial & Engineering Chemistry,* **28**, 1429-1439.

Sirkar, K.K. (1992). Other New Membrane Processes *in Membrane Handbook* (Edited by W.S. Winston Ho and K.K. Sirkar). New York: Chapman and Hall.

Sweny, J. W. (1985). Gas treating with physical solvents *in Acid and sour gas treating processes* (Edited by S. A. Newman). Houston: Gulf Publishing Company.

Takeuchi, H., Tahamashi, K., & Nanako, E.M. (1990). Mass transfer in single oil containing micro-porous hollow fiber contactors. *Industrial & Engineering Chemistry Research,* **29**, 1471-1477.

Viegas, R.M.C., Rodriguez, M., Luque, S., Alvarez, J.R., Coelhoso, I.M., & Crespo, J.P.S.G. (1998). Mass transfer correlation in membrane extraction: Analysis of Wilson plot methodology. *Journal of Membrane Science,* **145**, 129-135.

Westerterp, K.R., Van Swaaij, W.P.M., & Beenackers, A.A.C.M. (1984). *Chemical reactor design and operation*. New York: John Wiley & Sons.

Yang, M.C., & Cussler, E.L. (1986). Designing hollow-fiber contactors. *A.I.Ch.E. Journal*, **32**, 1910-1915.

Zisman, W. A. (1964). Relation of the equilibrium contact angle to liquid solid constitution, *in Contact Angle Wettability and Adhesion* (Edited by R.F.Gould), Washington: American Chemical Society.

Chapter 2

CO_2 Absorption at Elevated Pressures using Hollow Fiber Membrane Contactor

Abstract:

Recently, hollow fiber membrane based gas absorption processes have gained an increasing attention. However, the research done so far is mainly limited to atmospheric pressures applications using aqueous absorption solvents. In this study, the use of hollow fiber membrane contactor for gas absorption at elevated pressure is investigated. CO_2 absorption in propylene carbonate solvent is used as a model system. The absorption is carried out in a single hollow fiber membrane contactor at elevated pressures up to 20 bars. The hollow fiber membrane used was made of polypropylene (PP). The experiments were carried out in a semi-batch mode with solvent continuously flowing through the fiber. The long time duration experiments at atmospheric pressure suggest that Accurel PP Q3/2 hollow fiber membrane was subject to morphological changes when used with propylene carbonate as an absorbing solvent. These changes resulted possibly in the wetting of the fiber. It was found that by applying higher pressure on the gas side, the long term wetting of the fiber could be avoided and stability of the operation over the long period of application can be obtained. The higher operating pressure results in the increase of the driving force and thus enable higher rates of removal. The study shows that the decrease in the binary gas phase diffusivity and hence the membrane mass transfer coefficient due to increase in the gas pressures, does not have a significant effect on the overall mass transfer coefficient. Thus the overall mass transfer coefficient K_o is controlled by the liquid film resistance even at elevated pressures. The overall fiber side mass transfer coefficients, at all pressures investigated, can be given the Graetz-Leveque solution.

1.0 Introduction

In recent years, gas treating constraints have become more stringent because of higher fuel cost, environmental protection and appearance of carbon dioxide as a large volume product needed in the enhanced oil recovery. The feed gas is usually obtained directly from natural gas wells with wide range of pressures (normally 2-7 MPa). Depending on the quality of natural gas, it contains varying quantities of carbon dioxide (2-50 %). The product of such treating process is an enriched methane product stream containing less than 2% of carbon dioxide and sold as a pipeline fuel. The product stream is produced with essentially no pressure loss. A large number of natural gas treating plants around the world are operated with processes based on aqueous solutions of amines and alkali-metal salts. These solvents chemically react with carbon dioxide. The regeneration of these chemical solvents require large amount of heat supply usually in combination with pressure reduction. These processes become economically unattractive when the carbon dioxide content in the feed gas is high. In the latter cases, usually physical solvents such as propylene carbonate are used for the removal of carbon dioxide (Kohl & Nielsen, 1985). These physical solvents can be regenerated by just pressure reduction method without excessive heat inputs and thus considerable energy savings can be obtained. These physical solvents are especially useful when the partial pressure of carbon dioxide exceeds 1 MPa (Sweny J.W., 1985).

Membrane based gas separation process using dense membrane permeation method are known for their modular design and energy efficiency. The dense membrane permeation methods have been successfully used for the CO_2 removal for enhanced oil recovery at relatively high pressures (Kohl & Nielsen, 1985). However, at low CO_2 concentrations, the CO_2 partial pressure driving force is reduced and significant amount of hydrocarbon (primarily methane) is lost with CO_2 rich permeate. The problem becomes even more severe when other impurities such as H_2S need to be removed as well. The heavy methane loss makes the membrane permeation process economically unattractive in comparison with conventional absorption processes where the selectivity is primarily determined by the absorption liquid. In addition, at high partial pressure of CO_2 the dense membranes used in this process are seriously affected by CO_2 plasticization phenomenon which results in the reduction of selectivity of the process (Kapantaidakis et al. 2003).

High separation selectivity (even at low driving force) of the traditional absorption process can be combined with the flexibility, modularity and compactness of membrane process to give a membrane gas absorption process. The contactor used in this membrane gas absorption process to carry out mass transfer operation is generally termed as membrane gas-liquid contactors. This relatively new hybrid process offer several advantages over the conventional absorption and membrane permeation processes. The advantages and limitation offered by the membrane gas absorption process over the conventional separation processes are discussed in details in Introduction of this thesis.

In recent years, significant amount of research is carried out to use the membrane gas absorption process for removal of CO_2 from various feed streams. However, most of published work is related to use of the aqueous solvents such as aqueous alkali or alkaline salt solutions which have limited loading of CO_2 due to the chemical nature of these solvents (Gableman & Hwang, 1999). In addition, the work done with these membrane gas-liquid contactors is limited to low pressure applications. Hence, there is a need of detailed investigation for the use of membrane gas liquid contactors at elevated pressure and using physical organic solvents for bulk CO_2 removal.

The membrane contactors have been successfully applied at high pressures (> 5 M Pa) for dense gas extraction and compressed solvent extraction (Brunner, 1994; Bothun et al., 2003). The key aspect to operate at high pressures using hollow fibers having burst strength of < 500 K Pa is the careful control of the pressure on either side of membrane such that although the system pressure is quite high, the pressure drop across the membrane (transmembrane pressure) is low.

In the present study, application of gas-liquid membrane contactors for the removal of carbon dioxide from natural gas at elevated pressures is investigated. It was shown earlier that commercial organic solvent propylene carbonate can successfully be used in combination with polypropylene hollow fiber for CO_2 removal (Chapter 1). Thus the absorption of CO_2 in propylene carbonate at elevated pressure is used as model system in present work. The effects of operating conditions such as pressure, liquid velocity and long term application are analyzed. The measured mass transfer rates are compared with correlations reported in the literature.

2. 0 Theory

In order to describe the mass transfer process involved in the membrane gas-liquid contactor, the resistance in series model can be used. Figure 1 depicts the mass transfer process in the hollow fiber membrane gas-liquid contactor. The overall process consists of three steps. First, the transfer of solute gas from bulk gas phase to the membrane surface. Second, transfer through the membrane pores and last, the transfer from the membrane-liquid interface into the bulk of the liquid. In the last step, the combined solving of the momentum and diffusion equations is necessary to understand the laminar mass transfer process inside the fiber. The concentration profile in the liquid and the mass transfer rate can be calculated from the differential mass balance equation. An analytical solution for these mass balance equations can be obtained when the external mass transfer resistance is very small and can be neglected and if equilibrium exists at the gas liquid interface. The solution can be derived using the method suggested by Leveque and Graetz (Skelland, 1974). The local value of Sherwood number in terms of Graetz solution is given by Eq. (1) and average Sherwood number is given by Eq. (2).

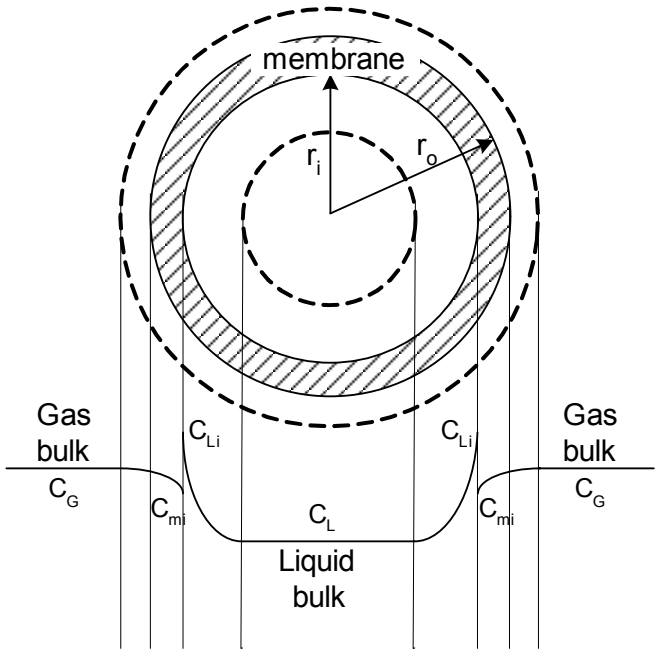

Figure 1: *Mass transfer process in membrane G-L contactor.*

$$Sh_z = \frac{\sum_{j=1}^{\infty} \frac{B_j}{2}\left(\frac{d\phi_j}{dr^*}\right)_{r^*=1} exp\left(\frac{-2\beta_j^2}{Gz_z}\right)}{2\sum_{j=1}^{\infty} \frac{B_j}{2\beta_j^2}\left(\frac{d\phi_j}{dr^*}\right)_{r^*=1} exp\left(\frac{-2\beta_j^2}{Gz_z}\right)} \tag{1}$$

$$Sh = 0.5Gz\theta \tag{2}$$

where

$$\theta = \frac{1 - \sum_{j=1}^{\infty} \frac{-4B_j}{\beta_j^2}\left(\frac{d\phi_j}{dr^*}\right)_{r^*=1} exp\left(\frac{-2\beta_j^2}{Gz}\right)}{1 + \sum_{j=1}^{\infty} \frac{-4B_j}{\beta_j^2}\left(\frac{d\phi_j}{dr^*}\right)_{r^*=1} exp\left(\frac{-2\beta_j^2}{Gz}\right)}$$

$$B_j = 4(j-1) + 8/3; (j = 1,2,3.....)$$

$$r^* = r / r_i$$

$$\frac{B_j}{2}\left(\frac{d\phi_j}{dr^*}\right)_{r^*=1} = 1.01276\, B_j^{-1/3}$$

The series in the equation for local Sherwood number converges rapidly for small values of *Gz,* so that only first term is significant. Under these asymptotic conditions the average and the local Sherwood number is given by Eq. (3).

$$Sh = 3.67 \qquad \text{Gz} < 10 \tag{3}$$

Another asymptotic solution is given by the Leveque equation. Leveque's approximate solution to the Eq. (1) is of simpler form and obtained by assuming that the concentration boundary layer is confined to a thin zone near the wall of the fiber. This approximation is valid in cases of high mass velocities through relatively short fibers in laminar flow. One important consequence of this assumption is that the Leveque solution is only applicable for *Gz* numbers exceeding 20. The Leveque solution is given as

$$Sh = 1.62(Gz)^{1/3} \qquad \text{Gz} > 20 \tag{4}$$

It has been shown by many researchers that for systems using aqueous solutions at atmospheric pressures, the Graetz-Leveque solution can be used to predict the fiber-side mass transfer coefficient. Kreulen et al (1993) gave the generalized solution of Graetz-Leveque equation by curve fitting of Eqs. (3) and (4), which is also valid for the transition region not covered by Eqs. (3) and (4).

$$Sh = \sqrt[3]{3.67^3 + 1.62^3 Gz} \qquad 10 < \text{Gz} < 20 \tag{5}$$

However, membrane contactors for gas absorption in which organic solvents are applied were reported as unstable systems (Reed et al. 1995) owing to excessive wetting tendencies of the organic solvent. This results in the liquid-filled pores and substantial increase in the mass transfer resistance. In this present study, the absorption of carbon dioxide in a commercially applied organic physical solvent for carbon dioxide removal (propylene carbonate) in single hollow fiber membrane module at elevated pressure is investigated. The gas-liquid interface is stabilized at the liquid side by putting higher pressure on the gas side of the fiber. It was found that the wetting of the membrane can be effectively prevented by trans-membrane pressure balancing.

3.0 Experimental

3.1 Materials

Double distilled water and propylene carbonate were used as the carbon dioxide absorption solvents. The propylene carbonate obtained was 99.7 % pure and carbon dioxide and nitrogen had 99.99% of purity. Owing to highly hydrophobic nature of polypropylene as a membrane material in combination with commercial availability, it was decided to use a Accurel Q3/2 polypropylene hollow fiber in all experiments. The Q3/2 fiber has an outside

diameter meter of 1000 μm and inside diameter of 600 μm. The maximum pore size of the Q3/2 fiber is 0.64 μm.

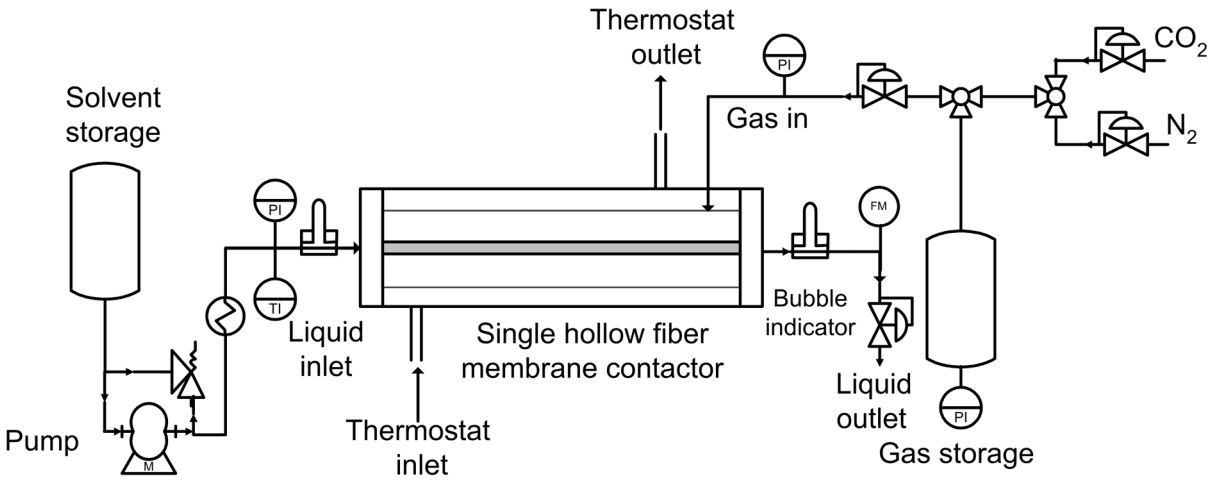

Figure 2: *Experimental set up.*

3.2 Method

Absorption experiments were carried out in a single hollow fiber membrane contactor. Figure 2 shows schematically the experimental setup used for the absorption experiments. Two single hollow fiber membrane contactors were used in the experiments. A glass contactor is used for the pressures up to 10 bars and a stainless steel (SS) contactor for higher pressures. Both contactors consisted of a jacketed, cylindrical tube with threaded ends as shown in Figure 3a and 3b. The two ends of a membrane hollow fiber were passed through two small stainless steel (SS) tubes whose inside diameter was slightly larger than the outside diameter of the hollow fiber. The length of the fiber exposed to the gas during the measurements was the distance between these two SS tubes. The distance between the SS tubes was carefully adjusted and the fiber was potted using epoxy resin to the SS tubes on both the ends of the two tubes. The length of the fiber inside the SS tube (> 0.07 m), on the liquid entry side provides sufficient distance (> $10d_{in}$) for the laminar liquid flow profile inside the fiber to be fully developed, before it contacts the gas. The hollow fiber between the SS tubes was placed coaxial to the jacketed tube and the two SS tubes were fastened to the ends of the threaded tube without stretching or putting slack in the fiber. The liquid feed line was connected to the SS tube on the feed side of the contactor. Two vertical glass tubes were attached in the upstream and down stream of the liquid feed line so that the gas bubble formation in the liquid stream could be observed.

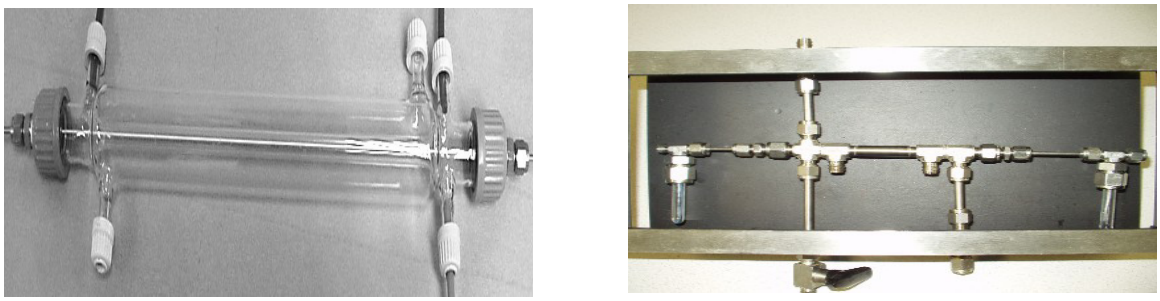

(a) (b)

Figure 3: *Single fiber membrane gas-liquid contactor (a) glass; (b) steel.*

Table 1: *Operating conditions for experiments.*

No.	System	Operating pressure, bar	Temperature ^{o}K	Fiber length m
1	PP-water-CO_2	1	293.16	0.27
2	PP-PC-CO_2	1	293.16	0.27
3	PP-PC-CO_2	1.7	293.16	0.15
4	PP-PC-CO_2	2	293.16	0.15
5	PP-PC-CO_2	4.2	298.16	0.13
6	PP-PC-CO_2	8	298.16	0.13
7	PP-PC-CO_2	10	298.16	0.115
8	PP-PC-CO_2	15	298.16	0.135
9	PP-PC-CO_2	20	298.16	0.135
10	PP-PC-CO_2-N_2	8	298.16	0.13
11	PP-PC-CO_2-N_2	4	298.16	0.13
12	PP-PC-CO_2-N_2	4	298.16	0.13

PP = polypropylene hollow fiber

PC= propylene carbonate

A semi-batch mode of gas-liquid contacting operation was used during the experiments. The liquid flow through the fiber was continuous. The solvent was fed from a high pressure pump via a flow controller. The solvent used in the experiments was degassed before usage by applying vacuum in a separate apparatus. The solvent is passed through the heat exchanger to maintain the desired temperature before passing to the single hollow fiber module. The upstream solvent pressure is controlled using a high precision back pressure controller valve. In all experiments, sufficient gas pressure is maintained in the contactor before starting the liquid flow. The absence of the gas pressure results in the wetting of the fiber. The carbon dioxide partial pressure outside the hollow fiber in the contactor was maintained constant by feeding pure carbon dioxide from a gas supply vessel, through a pressure regulator. From the drop in the pressure of carbon dioxide in the gas supply vessel,

the absorption rate and hence average carbon dioxide flux across the membrane was calculated:

$$< J >= \left(\frac{V}{RT} \right) \left(\frac{1}{\pi d_i l} \right) \left(\frac{P_1 - P(t)}{t} \right) \tag{6}$$

The theoretical average flux can be calculated by a simple mass balance of carbon dioxide over the length of fiber:

$$\langle J \rangle = \frac{Q_L m C_G \left(1 - exp\left(\frac{-K_O \pi d_i l}{Q_L} \right) \right)}{\pi d_i l} \tag{7}$$

The measured flux is then equated to the Eq. (7) to calculate the overall mass transfer coefficient K_o. The derivation of the Eq. (7) is given in Appendix A.

4.0 Results and Discussions

4.1 Absorption in water at atmospheric pressure

Absorption of pure carbon dioxide in degassed water was carried out in semi-batch mode at atmospheric pressure to test the setup. Pure carbon dioxide is used to minimize the gas side resistance to mass transfer. In these initial test experiments the liquid-side pressure is maintained higher than that of gas-side pressure in order to avoid the bubble formation in the fiber. The results are shown in Figure 4. The overall mass transfer coefficient is given as a function of liquid velocity through the fiber. This figure indicates that the absorption rate of carbon dioxide in water using hollow fiber membrane contactors can be estimated satisfactorily by the Graetz-Leveque equation. In case of physical absorption in hollow fiber membrane contactors, the controlling resistance for the mass transfer usually is concentrated in the liquid phase. Hence by increasing the liquid velocity, the overall mass transfer coefficient increases. To check effect of the long term application, water was allowed to run through the fiber for two weeks. At the end of two weeks the single hollow fiber contactor showed no decrease in the performance.

4.2 Absorption in propylene carbonate at atmospheric pressure

Initial absorption tests with carbon dioxide and propylene carbonate were carried out at atmospheric pressure. As recommended in the literature a slight over-pressure was maintained on the liquid side to avoid the bubble formation. The initial results with virgin membrane are shown in Figure 5. The overall mass transfer coefficient in this case also can be estimated perfectly with the Graetz-Leveque equation.

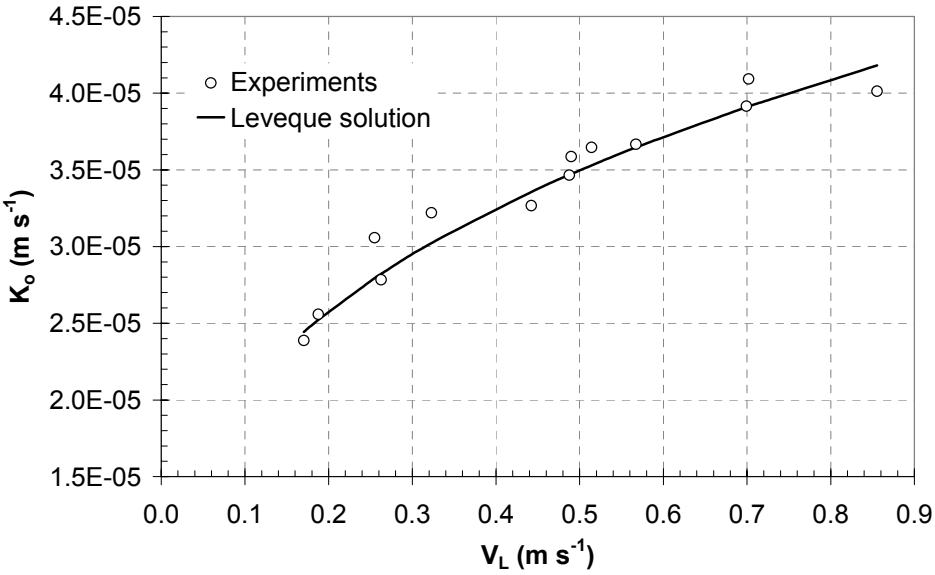

Figure 4: *Effect of liquid velocity on overall mass transfer coefficient for the absorption of CO_2 in water at atmospheric pressure.*

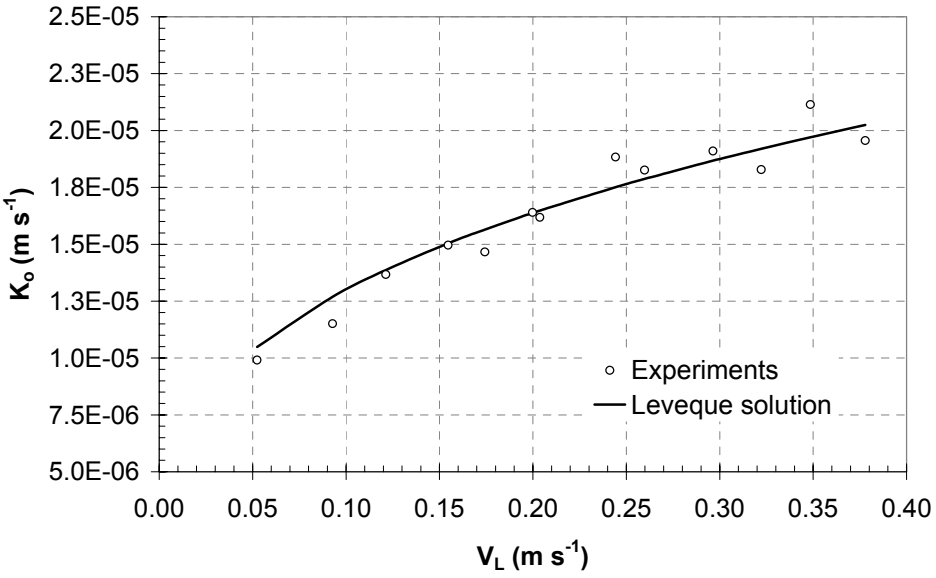

Figure 5: *Effect of liquid velocity on overall mass transfer coefficient for the absorption of CO_2 in propylene carbonate at atmospheric pressure using new fiber.*

It is known that the long term application of the membrane contactor can affect the morphological characteristics of polymeric membranes i.e. hydrophobic nature of polymer surface. Therefore the critical time duration for which membrane contactor can be used without significant decrease in the mass transfer strongly depends on the properties of the liquid phase in the contact with the membrane and the wetting characteristics of the membrane-solvent combination. The operating conditions such as gas side and liquid side pressure also affect the mass transfer performance of the membrane contactor. Li & Teo

(1996) observed that long term operation of high pressure on the liquid side resulted into the wetting or partially wetting of the membrane pores with the liquid absorbent. To analyze this effect and also to check the long term application, propylene carbonate was allowed to run through the fiber for two weeks continuously. The absorption experiments were carried out at the end of two weeks to check the performance of the membrane contactor. The results are shown in Figure 6.

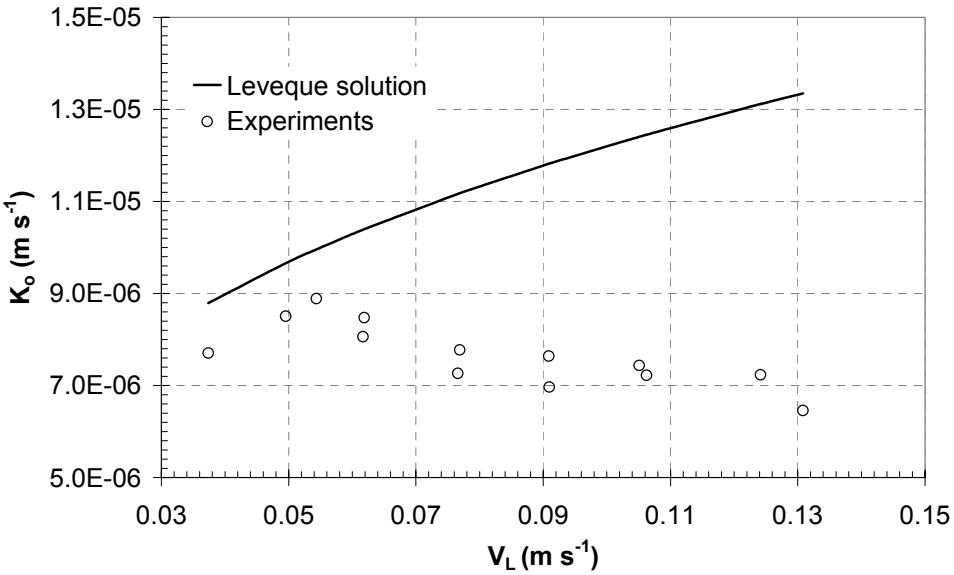

Figure 6: *Overall mass transfer coefficient for the absorption of CO_2 in propylene carbonate at atmospheric pressure after two weeks of operation.*

It is clear from the figure that the performance of the membrane contactor had decreased substantially, most likely owing to the wetting of fiber. As a result the overall mass transfer coefficient obtained is very low. The overall mass transfer coefficient even decreased slightly with an increase in the liquid velocity. This result can be explained by partial wetting of the membrane and indeed the wetting of the membrane was observed during the experimentation and also reported in the literature (Malek et. al, 1997). Because of the small diameter of the fiber, pressure drop of the liquid inside the fiber lumen will be inevitably increased with increasing liquid velocity and the fiber length according to the Hagen-Poiseuille equation. Since propylene carbonate has a high viscosity compared to water, the pressure drop over the fiber in the case of propylene carbonate is significant, leading to membrane wetting in the initial part of the fiber due to higher pressure gradient over the fiber. This phenomenon can be observed visually by the presence of liquid droplets at the outer surface of the membrane, especially near the inlet of the fiber. The length of the wetted part increases with liquid velocity and thus the average mass transfer coefficient over the length of fiber decreases with the liquid velocity.

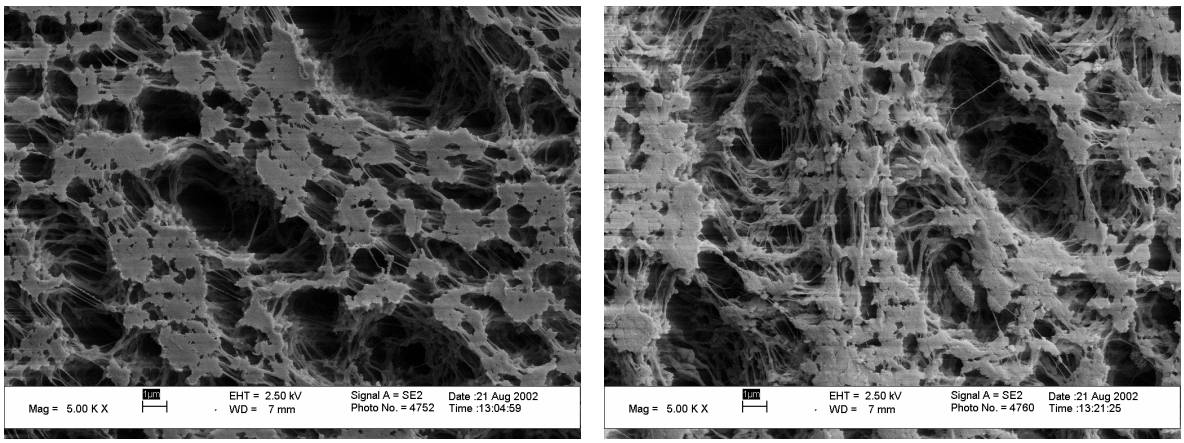

(a) **(b)**

Figure 7: *Scanning electron micrograph of Accurel PP Q3/2 fiber (a) before use; (b) after use.*

To study any changes in the morphology of fiber due to wetting by propylene carbonate, SEM analyses were carried out. Figures 7a and 7b show the SEM micrographs of the inner surface of the hollow fiber membrane before and after the use respectively. Although, the detailed morphological changes are difficult to perceive visually in the micrographs, Figure 7b shows the general roughing of membrane surface after the use. It also can be seen that the number of smaller pores present in the membrane are reduced significantly after the use, while the larger pores seemed to have increased in size slightly. Two possible reasons for these observations could be considered. The first is the intrusion of solvent into larger pores and subsequent enlargement of larger pores. The intrusion into the larger pores is easier than that into the smaller pores. Once larger pores are wetted by the solvent, the additional intrusion into the larger pores exerts lateral force on the pore walls causing the displacement of these walls. This displacement of the pore walls of larger pores results in the decrease in the size of smaller pores and possibly blocking of these pores. Similar observations are made by Barbe et al (2000) in their recent study about the surface morphological changes induced in microporous membranes due to intrusion of liquid in membrane pores. Another reason could be the contraction of microfibrils due to wetting and subsequent drying of the fiber. An effect due to liquid contact was observed by Kamo et al. (1992) on wetted-out polyethylene membranes after the contact with various organic solvents. The pore size was found to increase by an amount that was a function of surface tension of the solvent. It was suggested that the solvent formed a liquid bridge between the microfibrils and that subsequent drying of the solvent then drew the microfibrils sufficiently close together for van der Waals forces to maintain a more open structure.

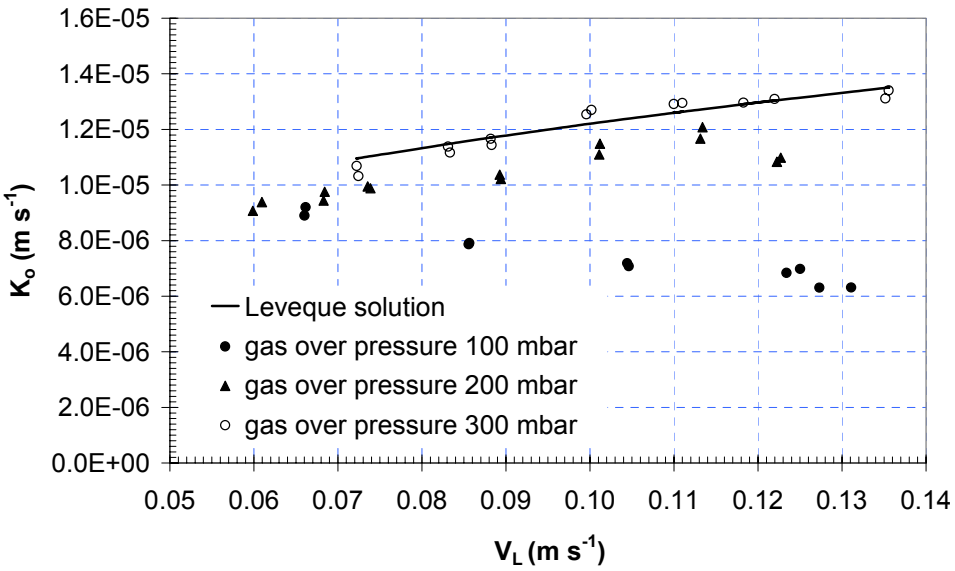

Figure 8: *Effect of gas side over pressure on CO_2 absorption flux through the hollow fiber in propylene carbonate.*

Now it seems that the long term application of high pressure on the liquid side results in changes in the membrane surface morphology and consequently wetting behavior of the fiber. Li and Teo (1996) applied a thin dense layer on the liquid side to avoid wetting. However, they found that membrane resistance was considerably increased resulting into a low absorption flux. Another possible option to reduce the wetting is to 'push back' the liquid from gas side to liquid side by applying high pressure on the gas side. To verify this idea, experiments were performed using same hollow fiber contactor and gradually increasing the pressure on the gas side. The results are shown in the Figure 8. This figure shows the experimentally measured absorption flux at various liquid velocities through the fiber. It is clear from the results that with increasing gas side pressure, the experimental data becomes more in line with the results represented by the Greatz-Leveque equation. At 300 mbar gas side over-pressure, the experimental values and theoretical values are in good agreement. During these experiments no bubble formation is observed on the liquid side. Thus over-pressure on the gas side can be used to prevent the wetting of the fiber. However, it is important to note that in case of a virgin fiber, over-pressure on the gas side resulted in the bubble formation. Hence, remaining high pressure experiments were carried out with pre-used fiber and applying a slight over-pressure on the gas side. It seems that the wetting effects can be eliminated by applying an over-pressure on the gas side, however, the controllability and the degree of operational freedom is significantly limited.

Three different operating conditions can exists depending on the pressure difference between the gas and liquid side and the critical wetting and/or bubbling pressure. These three difference cases are shown in Figures 9a, 9b and 9c. The first case (9a) is mostly applicable for the aqueous systems where high pressure is applied on the liquid side to prevent the

bubbling. In this case, too high pressure on the liquid side could result into wetting of initial part of fiber in long term application. Hence care should be taken that the L-G trans-membrane pressure (P_L- P_G) should not exceed the critical pressure of wetting (ΔP_w) at the liquid inlet.

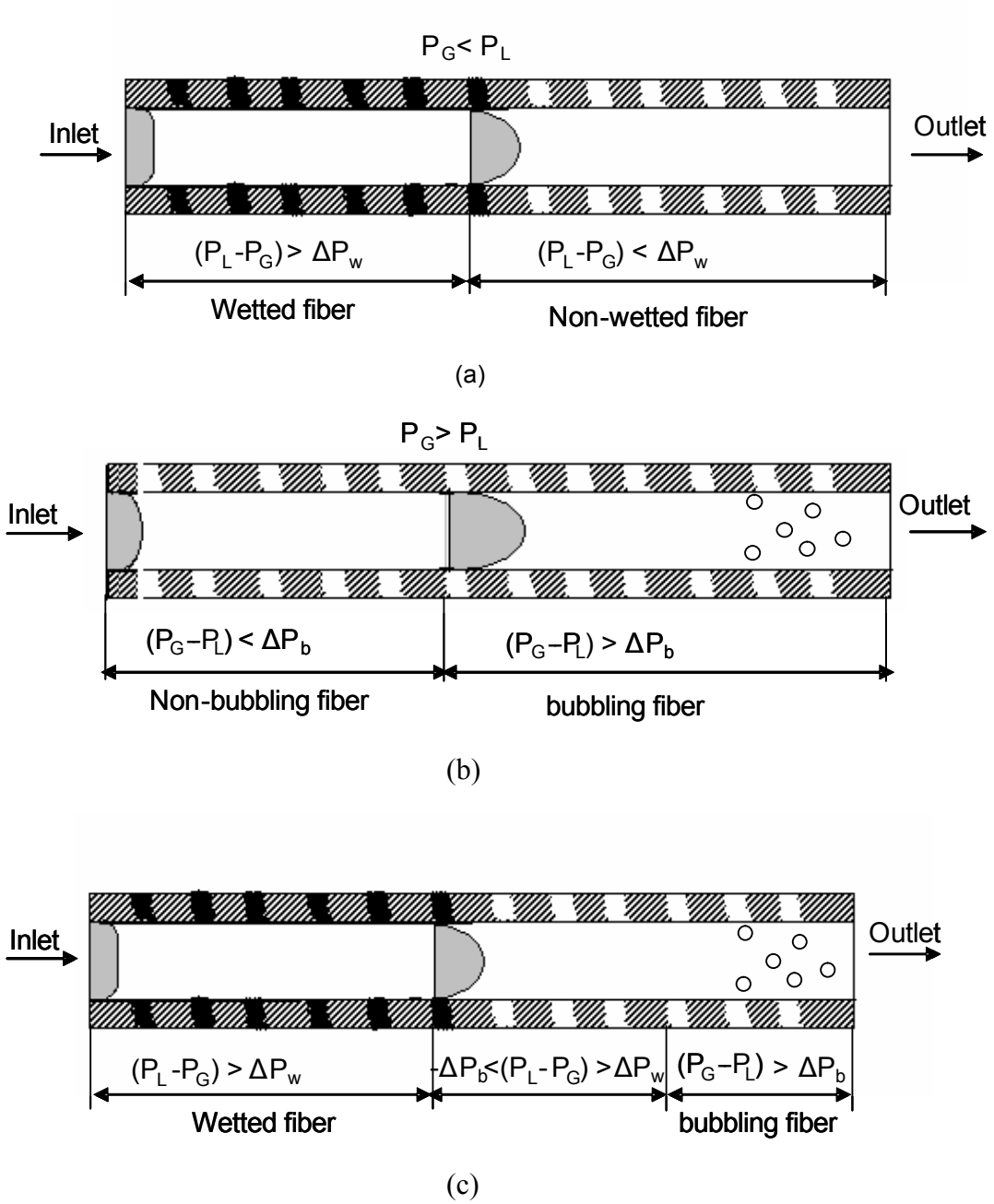

Figure 9: *Microporous hollow fiber membrane operated under (a) partially wetted mode; (b) partially bubbling mode; (c) partially wetted as well as bubbling mode.*

Second case is explained in the Figure 9b, applicable for the non-aqueous system where high pressure is applied on the gas side to prevent the wetting of fiber. In this case, the liquid pressure drop over the fiber leads to bubbling of gas in the liquid stream at the liquid

outlet. Hence care should be taken that the G-L trans-membrane pressure (P_G- P_L) should not exceed the critical pressure of bubbling (ΔP_b) at the liquid outlet.

In third case, both phenomena can occur simultaneously i.e. wetting in the initial part of the fiber and bubbling of gas in the end part of the fiber. This situation is illustrated in Figure 9c. Such case is observed when liquid has intermediate surface tension as compared to aqueous and organic solvents. To avoid these conditions, the L-G trans-membrane pressure (P_L- P_G) in the initial part of the fiber should be lower than the critical pressure of wetting (ΔP_w), where as G-L trans-membrane pressure (P_G- P_L) should not exceed the critical pressure of bubbling (ΔP_b) in the end part of the fiber.

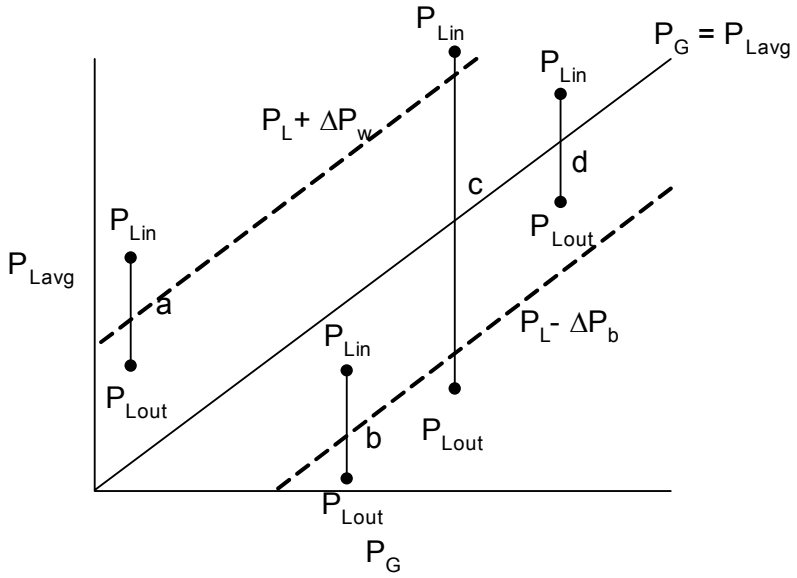

Figure 10: *Operating limitations for membrane G-L contactor.*

These limitations of the operating conditions are illustrated Figure 10, which gives the qualitative indication of pressure drop control over the fiber. In the figure, solid straight line indicates the $P_G = P_{L\ avg}$ line and two dotted lines indicates the two limiting cases of wetting ($P_{L\ avg} + \Delta P_W$) and bubbling ($P_{L\ avg} - \Delta P_b$) of the fiber, respectively. The four operating lines (case a, case b, case c and case d) show the pressure drop over the fiber, with inlet pressure P_{Lin} being higher than the outlet pressure P_{Lout}. In case (a) (applicable for aqueous system), the high pressure drop over the fiber results into higher inlet pressure and P_{Lin} crosses the wetting line causing wetting in the initial part of the fiber. Hence, when high pressure on the liquid side is applied by controlling liquid outlet pressure, the pressure drop over the fiber should be lower than the critical pressure of wetting (ΔP_W). In case (b) (applicable for the organic systems), the high pressure drop over the fiber results into lower outlet pressure and P_{Lout} crosses the bubbling line causing bubbling in the end part of the fiber. Hence, when high pressure on the gas side is applied by controlling liquid inlet pressure, the pressure drop over

the fiber should be lower than the critical pressure of bubbling (ΔP_b). In case (c) (applicable liquid having intermediate surface tensions), the high pressure drop over the fiber results into a higher inlet pressure as well as a lower outlet pressure. P_{Lin} crosses the wetting line causing wetting in the initial part of the fiber and P_{Lout} crosses the bubbling line causing bubbling in the end part of the fiber. Case (d) shows the optimum control of the pressure over the fiber. In general, the pressure drop over the fiber should be always lower then ($\Delta P_{W+} \Delta P_b$). Thus the degree of freedom in the operational conditions becomes limited in such cases and process control turns out to be important.

4.3 Absorption in propylene carbonate at elevated pressure

Carbon dioxide absorption experiments were carried out at elevated partial pressures of carbon dioxide up to 20 bars with slight over-pressure on the gas side. The experiments up to 10 bar were carried out in a glass container whereas experiments at high pressure were carried out in a stainless steel container. The results are shown in the Figure 11. Measured flux and theoretically calculated flux match very well. The flux at a given liquid velocity increases with pressure. This increase in the flux is due to the increased concentration of carbon dioxide in the gas phase.

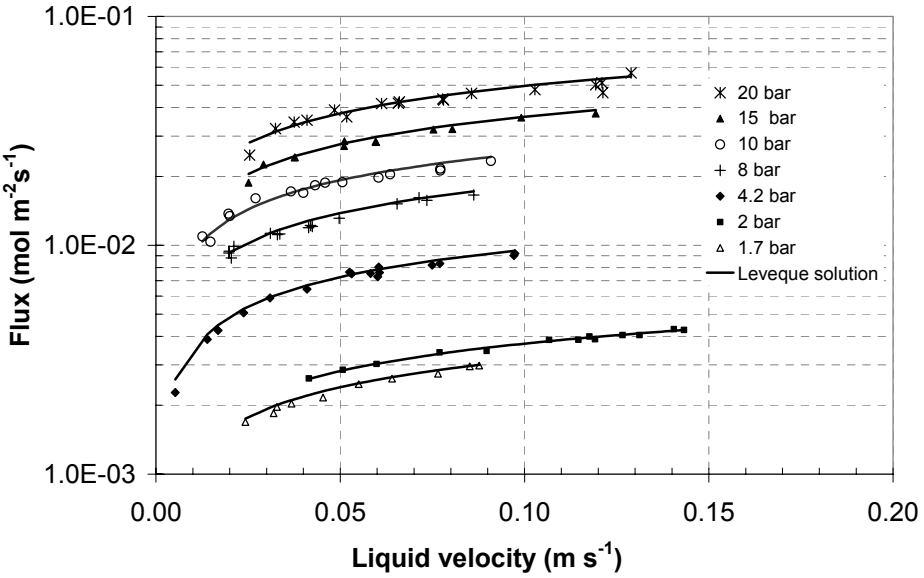

Figure 11: *Measurement of CO_2 absorption flux through the hollow fiber in propylene carbonate at elevated CO_2 partial pressures.*

Figure 12 shows the measured mass transfer coefficient (in terms of dimensionless Sh number) as function of liquid velocity (in terms of dimensionless Gz number) for experiments at all pressures. It is clear the measured mass transfer coefficient can be predicted using the Graetz-Leveque equation, even at elevated pressures. It can be concluded from these figures that there is no effect of pressure on the overall mass transfer coefficient.

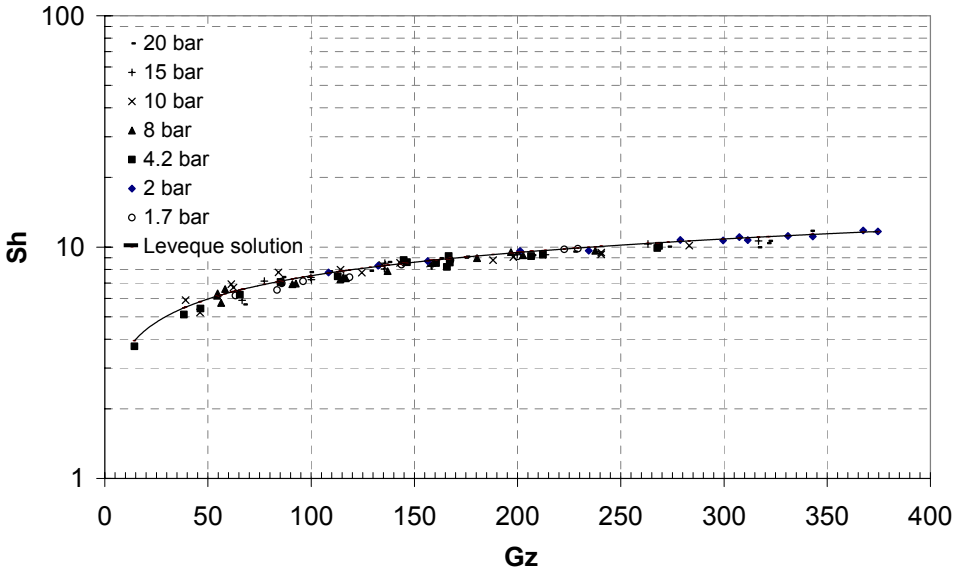

Figure 12: *Measurement of overall mass transfer coefficient for the hollow fiber at elevated pressures.*

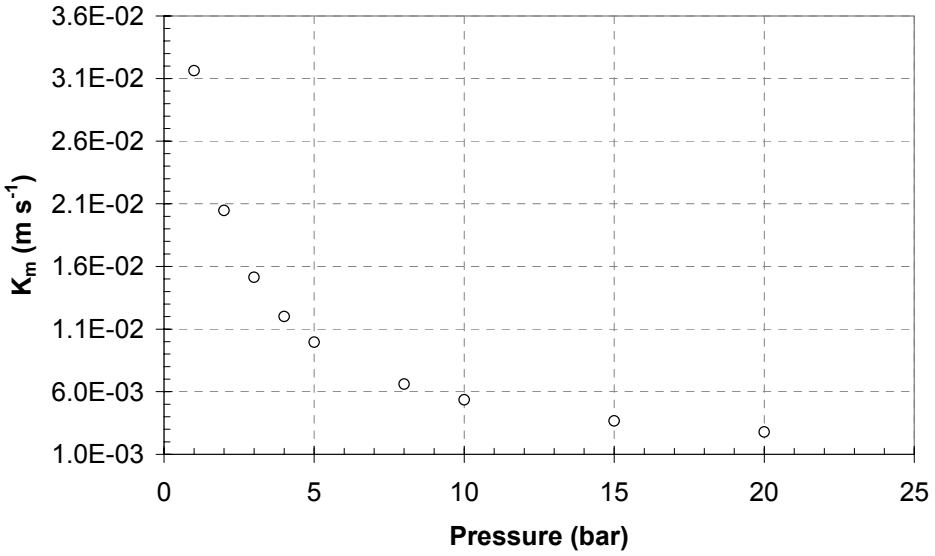

Figure 13: *Effect of system pressure on the membrane mass transfer coefficient of Q3/2 fiber.*

At low to moderate pressures, binary gas diffusion coefficients vary inversely with pressure or density of gas mixture. Thus in case of a binary gas mixture the increase in the pressure results into a decrease in the gas phase diffusivity and hence a decrease in the gas-side and membrane mass transfer coefficient. Figure 13 shows the effect of pressure on the membrane mass transfer coefficient (calculated) of the Q3/2 fiber for CO_2–N_2 binary

mixtures. It is clear that with an increase in the system pressure there is a significant decrease in the membrane mass transfer coefficient. To check this effect of decrease in the membrane mass transfer coefficient on the mass transfer performance of the fiber, experiments were carried out using carbon dioxide and nitrogen binary mixture. The results are shown in the Figure 14. It can be seen that there is no influence of the decrease in the membrane mass transfer coefficient on the overall mass transfer performance. This is because in case of physical absorption, the liquid side mass transfer resistance is higher as compared to the membrane mass transfer resistance. The percentage contribution of membrane and gas phase mass transfer resistances together to the overall mass transfer resistance is very low (< 0.5 %), even at the higher pressures. Hence the controlling mass transfer resistance still lies in the gas diffusion through liquid phase and since the pressure has no effect on this, the overall mass transfer coefficient is independent of the total system pressure. It should be noted that in case of mass transfer with chemical reaction, with a lower liquid side mass transfer resistance due to the chemical enhancement, increase in the gas and membrane mass transfer resistances at high pressures may significantly affect the results.

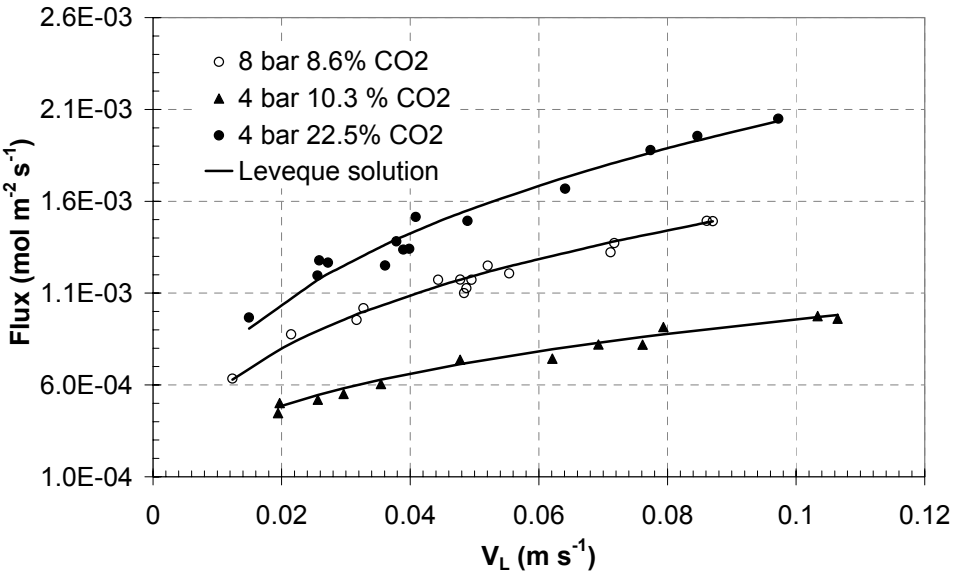

Figure 14: *Measurement of CO_2 absorption flux through the hollow fiber in propylene carbonate at elevated pressures for CO_2-N_2 binary gas mixtures.*

5.0 Conclusion

Absorption of carbon dioxide in propylene carbonate, a commercial physical organic solvent used in the carbon dioxide removal process, is studied in a hollow fiber membrane contactor. The experimental study shows that in the case of physical absorption the overall mass transfer is controlled by the liquid side mass transfer resistance. Duration experiments at atmospheric pressure suggest that the Accurel PP Q3/2 hollow fiber membrane seems to be

subjected to morphological changes when used with propylene carbonate as an absorbing solvent. These changes eventually result in the wetting of the fiber. The wetting problem in long term application can be avoided by applying over-pressure on the gas side. The pressure drops over the fiber length now becomes a critical design parameter to ensure a non-wetted mode of operation. Higher pressure drop over the fiber may lead to wetting in the initial part of the fiber. Too high gas-side pressure may result in to the bubble formation in the liquid phase. The experiments carried out at elevated pressure suggest that membrane gas-liquid contactors can be applied for high pressure applications. The overall mass transfer coefficient is found to be independent of the system pressure. The Graetz-Leveque equation can be used to predict the mass transfer coefficient in a single fiber even at elevated pressures.

Acknowledgement

This research is part of the research program performed within the Centre for Separation Technology (CST), which is a co-operation between the Netherlands Organization for Applied Scientific Research (TNO) and the University of Twente. We acknowledge Herman Bruns for his assistance to the experimental work and Wim Leppink for the construction of the experimental set up.

Nomenclature

A	Area	[m^2]
C	Concentration	[mol m^{-3}]
d	Diameter	[m]
D	Diffusivity	[m^2 s^{-1}]
Gz	Graetz number , $\frac{vd^2}{Dz}$,	[-]
J	Flux	[mols m^{-2} s^{-1}]
K	Mass transfer coefficient	[m s^{-1}]
L	Length	[m]
m	Distribution coefficient	[-]
P	Pressure	[Pa]
Q	Flow rate	[m^3 s^{-1}]
r	Radius	[m]
R	Gas constant	
Sh	Sherwood number, $\frac{k_l d}{D}$,	[-]
T	Temperature	[K]
t	Time	[s]
V	Volume	[m^3]

v	Velocity	[m s^{-1}]
z	Length	[m]

Subscripts

b	Bubbling
G	Gas
i	Interface/inside
L	Liquid
m	Membrane
o	Overall/outside
w	Wetting/Water
z	Local value

References

Barbe, A.M., Hogan, P.A., & Johson, R.A. (2000). Surface morphology changes during initial usage of hydrophobic, micro-porous polypropylene membranes. *Journal of Membrane Science,* **172**, 197-216.

Bothun, G.D., Knutson, B.L., Strobel, H.J., Nokes, S.E., Brignole, E.A., & Diaz, S. (2003). Compressed solvents for the extraction of fermentation products within a hollow fiber membrane contactor. *Journal of Supercritical Fluids,* **25**, 119-134.

Brunner, G. (1994). *Gas extraction*, New York: Springer.

Diaz, M., Vega, A., & Coca, J. (1987). Correlation for the estimation of the gas-liquid diffusivity. *Chemical Engineering Communications,* **52**, 271-281.

Doraiswamy, L.K., & Sharma, M.M. (1983). *Heterogeneous reactions: analysis, examples and reactor design (Vol. II Fluid-fluid-solid reactions)*, New York: John Wiley & Sons.

Gabelman, A., & Hwang, S. (1999). Hollow fiber membrane contactors. *Journal of Membrane Science,* **159**, 61-106.

Kapataidakis, G.C., Koops, G.H., Wessling, M., Kaldis, S.P., & Sakellaropoulos (2003). CO_2 plasticization of polyethersulfone/polyimide gas-separation membranes. *A.I.Ch.E. Journal,* **49(7)**, 1702-1711.

Kamo, J., Hirai, T., & Kamada, K. (1992). Solvent induced morphological change of microporous hollow fiber membranes. *Journal of Membrane Science,* **70**, 217-224.

Kohl, A. L., & Nielsen, R.B. (1997). *Gas Purification*: 5th ed., Houston: Gulf Publishing Company.

Kreulen, H., Smolders, C.A., Versteeg, G.F., & van Swaaij, W.P.M. (1993). Microporous hollow fiber membrane modules as gas-liquid contactor Part 1. Physical mass transfer processes. *Journal of Membrane Science,* **78,** 197-216.

Li, K., & Teo, W.K. (1996). An ultra thin skinned hollow fiber module for gas absorption at elevated pressures. *Chemical Engineering Research and Design,* **A74**, 856-862.

Malek, A., Li, K., & Teo, W. K. (1997). Modeling of microporous hollow fiber membrane modules operated under partially wetted conditions. *Industrial Engineering Chemistry Research,* **36 No.3**, 784-793.

Mason, E.A., & Malinauskas, A.P. (1983). *Gas transport in porous media: the dusty gas model. Chem. Eng. Monograph 17*, Amsterdam: Elsevier.

Matson, S.L., Lopez, J., & Quinn, J.A. (1983). Separation of gases with synthetic membranes. *Chemical Engineering Science,* **38,** 503-524.

Reed, B.W., Semmens, M.I., & Cussler, E.L., (1995). Membrane Contactors *in Membrane separation Technology, principles and applications* (Edited by R.D. Noble and S.A. Stern). Amsterdam: Elsevier.

Reid, R.C., Prausnitz, J.M., & Poling, B. E. (1987). *The properties of gases and liquids.* New York: McGraw-Hill.

Skelland, A.H P. (1974). *Diffusional Mass Transfer.* New York: John Wiley & Sons.

Sweny, J. W. (1985). Gas treating with physical solvents *in Acid and sour gas treating processes* (Edited by S. A. Newman). Houston: Gulf Publishing Company.

Versteeg, G.F., & van Swaaij, W.P.M. (1988). Solubility and diffusivity of acid gases in aqueous alkanolamine solutions. *Journal of Chemical Engineering Data,* **33**, 29-34.

Appendix A: Derivation of flux across the fiber

Since the liquid is continuously flowing through the membrane, the driving force for mass transfer varies with the position in the module. The concentration of carbon dioxide in the inlet of liquid stream is zero. The concentration of carbon dioxide in the gas phase is maintained constant by applying constant pressure on the gas side. As the liquid flows through the fiber, carbon dioxide is absorbed into the liquid and liquid gets saturated. Thus the driving force for the gas absorption drops with the length of the fiber. An expression for overall flux of the carbon dioxide absorption can be derived by mass balance across a small length of the fiber 'dz':

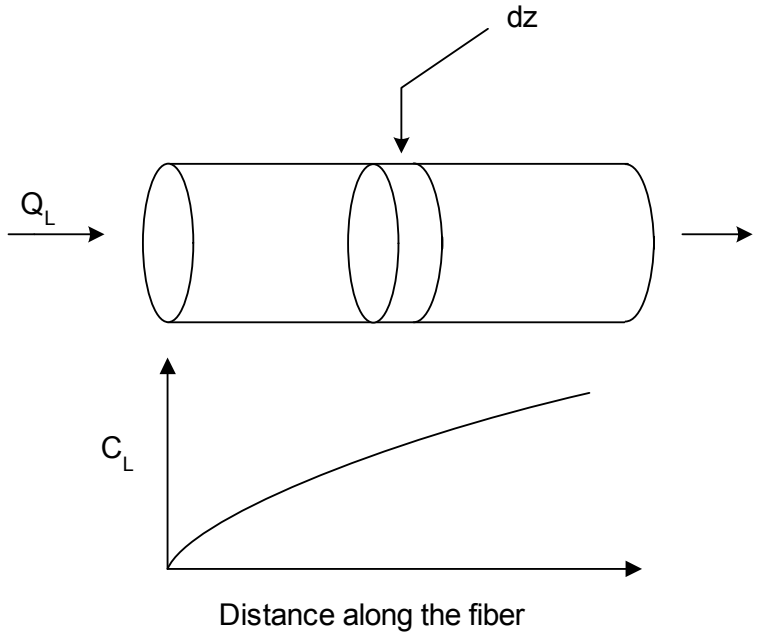

Figure A1: *Mass balance across the small fiber element*

$$0 = Q_L\, C\big|_z - Q_L\, C\big|_{z+dz} + J\,\pi\, d_i\, dz \qquad \text{(A1)}$$

where $$J = k_z\left[mC_G - C_L\right]$$

The mass transfer coefficient 'k_z' is a clubbed local mass transfer coefficient, taking into account the contribution of the gas-side, liquid-side and membrane mass transfer coefficients.

$$0 = -Q_L \frac{dC}{dz} + k_z\left(mC_G - C\right)\pi\, d \qquad \text{(A2)}$$

$$\frac{dC}{dz} = \frac{k_z \pi\, d}{Q_L}\left(mC_G - C\right) \qquad \text{(A3)}$$

$$\frac{1}{(mC_G - C)} dC = \frac{k_z \pi d}{Q_L} dz \tag{A4}$$

$$\frac{1}{(mC_G - C)} \cdot \int_0^L dC = \frac{\pi d}{Q_L} \int_0^L k_z dz \tag{A5}$$

Integrating equation A5 over the entire length of fiber outlet concentration in the liquid stream can be determined.

$$ln\left(\frac{mC_G - C_{Lo}}{mC_G} \right) = -\frac{k_L \pi d_i}{Q_L} L \tag{A6}$$

$$C_{Lo} = mC_G \left(1 - e^{-\frac{k_L \pi \cdot d_i}{Q_L} \cdot L} \right) \tag{A7}$$

The mass transfer coefficient 'k_l' is the average clubbed mass transfer coefficient over the entire length of the fiber. With the equation for the concentration on position L, the average flux can be determined:

$$\langle J_{av} \rangle = \frac{(Q_L C_L)_{z=L}}{A} \tag{A8}$$

$$\langle J_{av} \rangle = \frac{Q_L m C_G \left(1 - e^{-\frac{k_L \cdot \pi \cdot d_i}{Q_L} \cdot L} \right)}{\pi d_i L} \tag{A9}$$

Appendix B: Physical Parameters

B.1 Solubility

The solubility of carbon dioxide in terms of distribution coefficient in pure water, m_w, is taken from Versteeg and Swaaij (1988).

$$m_w = 3.59X10^{-7}\, RT\, exp\left(\frac{2044}{T}\right) \tag{B1}$$

where R is universal gas constant (mol.m^{-3}K^{-1}) and T is in Kelvin.

The solubility of carbon dioxide in terms of mole fraction in pure propylene carbonate, x, is taken from Solubility Data Series.

$$ln\, x = -36.218 + \frac{2856.7}{T} + 3.9003 ln(T) \tag{B2}$$

where T is in Kelvin.

B.2 Diffusivity

The diffusivity of the carbon dioxide and nitrogen in water and propylene carbonate is calculated using correlation proposed by Diaz et al. (1987).

$$D_{12} = 6.02X10^{-5}\left(\frac{V_2^{0.36}}{\mu_2^{0.61} V_1^{0.64}}\right) \tag{B3}$$

where, V_1 and V_2 are molar volume at normal boiling point temperature for gas solute and liquid solvent respectively. μ is the viscosity of the solvent in cP and D_{12} is the diffusivity of solute '1' in solvent '2' in cm^2/s.

The binary diffusion coefficient D_{AB} (cm^2/s) for the CO_2-N_2 mixture is calculated using Fuller equation (Reid et al. 1987).

$$D_{AB} = \frac{0.00143T^{1.75}}{PM_{AB}^{1/2}\left[\left(\sum_v\right)_A^{1/3} + \left(\sum_v\right)_B^{1/3}\right]^2} \tag{B4}$$

where, M_A, M_B are molecular weights of A and B; P is pressure (bars); T is temperature (K)

$M_{AB} = 2[(1/M_A) + (1/M_B)]^{-1}$

$\sum_v$ = summation of atomic diffusion volumes

Chapter 3

Shell-side Dispersion Coefficients in Rectangular Cross-flow Hollow Fiber Membrane Module

Abstract:

Membrane processes utilizing hollow fiber membrane modules are gaining increased interest in many industrial applications. The shell-side mass transfer performance of these membrane modules strongly depends on the shell-side mixing and the shell geometry. However, in literature limited information is available on the shell-side mixing of hollow fiber membrane modules. In the present work, shell-side mixing of a rectangular cross-flow hollow fiber membrane contactor is investigated using gas-phase RTD measurements. A novel ultrasound based measurement technique is used to characterize the system. The shell-side mixing of the module is determined in terms of dispersion coefficients in three directions. The axial dispersion coefficient is found to have values between those applicable to pipe flow and packed bed correlations. This can be attributed to the intermediate packing density of the membrane module. The dispersion in transversal directions, along and across the fibers, is significantly lower. The transversal dispersion coefficient across the fiber is higher and more sensitive to the shell side velocity than the dispersion coefficient along the fiber due to the continuous splitting and remixing of shell side flow across the fibers.

1.0 Introduction

Polymeric hollow fiber membrane modules have gained widespread use in industry for various purification and recovery processes and in medicinal field as artificial kidneys and lungs. Common modules consist of hair-like hollow fibers potted at both ends and installed in various shell geometries. The module performance is often characterized by how efficiently a module separates the components from a mixture. Prediction of the performance for design purpose requires knowledge of the mixing patterns and mass transfer characteristics on the shell-side, lumen-side and of the membrane. The membrane mass transfer properties (Mulder, 1996) and the lumen side flow pattern and mass transfer (Skelland, 1974) are generally well described. However, scarce information is available for predicting shell-side mixing patterns and mass transfer characteristics. Moreover, the shell geometry strongly influences the shell-side mass transfer performance and different shell geometries are used depending on various factors such as process requirements, availability of membrane materials etc. The use of cross-flow membrane contactors is favored because a considerable enhancement in the shell side mass transfer coefficient can be obtained by positioning the membrane fibers perpendicular to the flow direction (Wickramasinghe et al. 1992, Feron et al. 1994).

Typical approaches for predicting shell-side mixing behavior either require solving continuum mass and momentum balances based on first principles or assume simplified flow patterns. The first approach would require the descretization of the complex three dimensional (3-D) regions and solving large sets of computationally demanding equations. The second approach is possible in more simple geometries like e.g. parallel flow in shell and tube geometry without baffles and many researchers have assumed a simplified geometry of flow around a single fiber in this case (Chun & Lee, 1997 and Karoor & Sirkar, 1993). Often these simplifications do not match with the real module performance due to uneven distribution and bending of fibers. Such simplifications are however not possible in the case of the cross-flow contactor due to the continuous splitting and remixing of the shell side phase.

Another approach to obtain valuable information on the macroscopic mixing behavior of the phase flowing through a reactor without knowing the exact flow patterns is by measuring the deviation of the flow from the two ideal flow patterns; namely ideally mixed and completely plug flow. Generally, this information is deduced from the measurement of the residence time distribution (RTD) and fitting a model to represent a real process which has the same or a similar type of the residence time distribution. In the present work, shell-side hydrodynamics of the cross flow hollow fiber membrane contactor is investigated using RTD measurements.

Various RTD measurement techniques are reported in literature. For accurate measurements the technique needs to be non-intrusive, causing minimum flow disturbances

and, for the present case, should be capable of measuring residence times in the range of 0.1 s. In this study, a novel gas-phase RTD measurement technique based on the dependence of the ultrasonic velocity on the gas-phase composition is used (Cents et al. 2003). The method meets all the requirements and, in addition, offers the opportunity to measure through non-transparent reactor walls.

In the first section, the principle of the measurement technique will be explained in short and the method will be validated for a single phase ideal plug flow reactor for short holding times. Subsequently, the analysis of the RTD measurements for the cross-flow hollow fiber membrane contactor using this novel method will be presented.

2.0 Ultrasonic RTD measurement technique

2.1 Measurement principle

The measurement principle of this novel method makes use of the dependence of the speed of sound in a material on the bulk modulus (of elasticity) and density of this medium. This dependence for a pure component or for a mixture is given for a fluid by Eq. (1) (Povey, 1997).

$$v = \sqrt{\frac{dp}{d\rho}} = \sqrt{\frac{E_v}{\rho}} \tag{1}$$

Both the density and the bulk modulus of the pure components used in this study (Helium and Nitrogen) are well tabulated or can be calculated. The average density and bulk modulus of a binary mixture of ideal gases are given by:

$$\rho = (1-\varphi)\rho_1 + \varphi\rho_2 \tag{2}$$

$$\frac{1}{E_v} = (1-\varphi)\frac{1}{E_{v,1}} + \varphi\frac{1}{E_{v,2}} \tag{3}$$

Thus using Eqs. (1), (2) and (3) the composition of the binary mixture can be expressed as function of the measured velocity of sound in the mixture and the known ρ and υ of the pure components:

$$\varphi = \frac{-B \pm \sqrt{B^2 - 4AC}}{2A} \tag{4}$$

where:

$$A = v_1^2\left(1 - \frac{\rho_1}{\rho_2}\right) + v_2^2\left(1 - \frac{\rho_2}{\rho_1}\right) \tag{4a}$$

$$B = v_2^2\left(\frac{\rho_2}{\rho_1} - 2\right) + v_1^2\frac{\rho_1}{\rho_2} \tag{4b}$$

$$C = v_2^2\left(1 - \frac{v_1^2}{v^2}\right) \tag{4c}$$

Eq. (4) was used to convert the experimentally determined sound velocity values into the mixture's composition. Note that, in the above analysis, the term binary is not restricted to two pure components. The relation also holds when a component, the tracer-gas, is considered next to a mixture of components (e.g. air) of which the relative composition does not change during the measurement. This concentration measurement technique can be used to determine the system's response to a step-function or to measure steady state concentration gradients.

2.2 Determination of the velocity of sound

The velocity of sound is determined using a tone-burst technique. A tone-burst is a narrow banded signal consisting of a certain number of periods of a single frequency. The velocity of this signal is measured as the path length divided by the time of flight (TOF) of the signal from the transmitting transducer to the receiver one. The TOF is difficult to determine directly, because the transfer function of the complete measurement system is not known. For this reason the time difference (Δt) is determined between the signal in the mixture and a reference signal in which the velocity of sound is known accurately (e.g. in air). The velocity of sound in air (v_r) is taken from CRC's Handbook of Chemistry and Physics. From these values the velocity of sound in an unknown medium can be calculated as:

$$v = \frac{x}{t} = \frac{x}{\frac{x}{v_r} + \Delta t} \tag{5}$$

The path length (x) in the measurement cell can be determined with an accurate caliper or by the measurement of the time difference (Δt in Eq. 5) between a reference signal in air (which has traveled once the path length) and its first reflection (which has traveled three times the path length).

3.0 Experimental

The experimental set-up consists of an arbitrary waveform generator (AWG), which sends any desired electric signal to a piezo-electric transducer (T) with a center frequency of 800 kHz. The signal is amplified with a maximum of 44 dB with a variable power amplifier. The transmitting transducer converts the electric signal to a pressure wave that is received in another transducer (R). The converted electric signal is, after 31 dB amplification, acquired with a maximum sampling rate of 2 GS/s ($2 \cdot 10^9$ samples per second) and with 8-bits resolution in a digital oscilloscope. At the same time the AWG sends the electric signal, a trigger signal is transmitted both to the oscilloscope and to an electrically controlled valve to start tracer injection. In this way in every measurement the starting point, t = 0, is well defined. Data from the oscilloscope is transferred to the computer using a GPIB interface bus. The overall sampling frequency in this experimental set-up is limited by the data transfer rate and is 33 Hz. Of course, this problem could be overcome, which means that the theoretical maximum sampling frequency is in the order of 10,000 Hz. The complete set-up is schematically represented in Figure 1. The two transducers are placed in a measurement cell, which can be placed at several locations in the used reactors. Both the input step function as well as the response leaving the reactor could be measured in this way. The path length applied in the measurement was 18 mm, and the cell was designed to minimize the disturbance of the flow in the employed reactors. Helium was selected as the tracer-gas because of its pronounced difference in sound velocity compared to N_2 (983 m/s vs. 345 m/s at 23°C). N_2 was introduced in the reactors through a mass flow controller and the total outgoing flow rate was derived from the N_2 flow-rate and the total helium fraction.

To measure the accuracy of the technique at low residence times, two stainless steel tubular reactors with inner diameters of 19.0 and 18.4 mm and lengths of 1635 and 815 mm respectively were used to approximate plug-flow (PFR) behavior (Pe > 50). To study the shell-side mixing behavior of the cross flow hollow fiber membrane contactor, experiments were carried out using a commercial module provided by TNO-MEP, Apeldoorn. The module is made up of microporous polypropylene hollow fibers (Accurel PP: Type Q3/2; inside diameter 600 μm; wall thickness 200 μm). The module is 0.1m x 0.1m x 0.1m (H x W x L) in dimensions and contains around 4900 fibers arranged in in-line square pitch (pitch = 1.45).

Two different sets of experiments were carried out to study the mixing in all three directions i.e. in the direction of the gas flow, in the directions perpendicular to the gas flow (along and across the fibers) respectively. Initial experiments were performed to determine the axial mixing (in the direction of the gas flow) in terms of an axial dispersion coefficient. To determine the axial dispersion coefficient, a step input of the tracer is given and its response at the exit of the module is measured as function of time. The measurement cells

were located 11 cm after module outlet and 35 cm before the module inlet. The dead time due these measuring tubes was taken into account in the calculations.

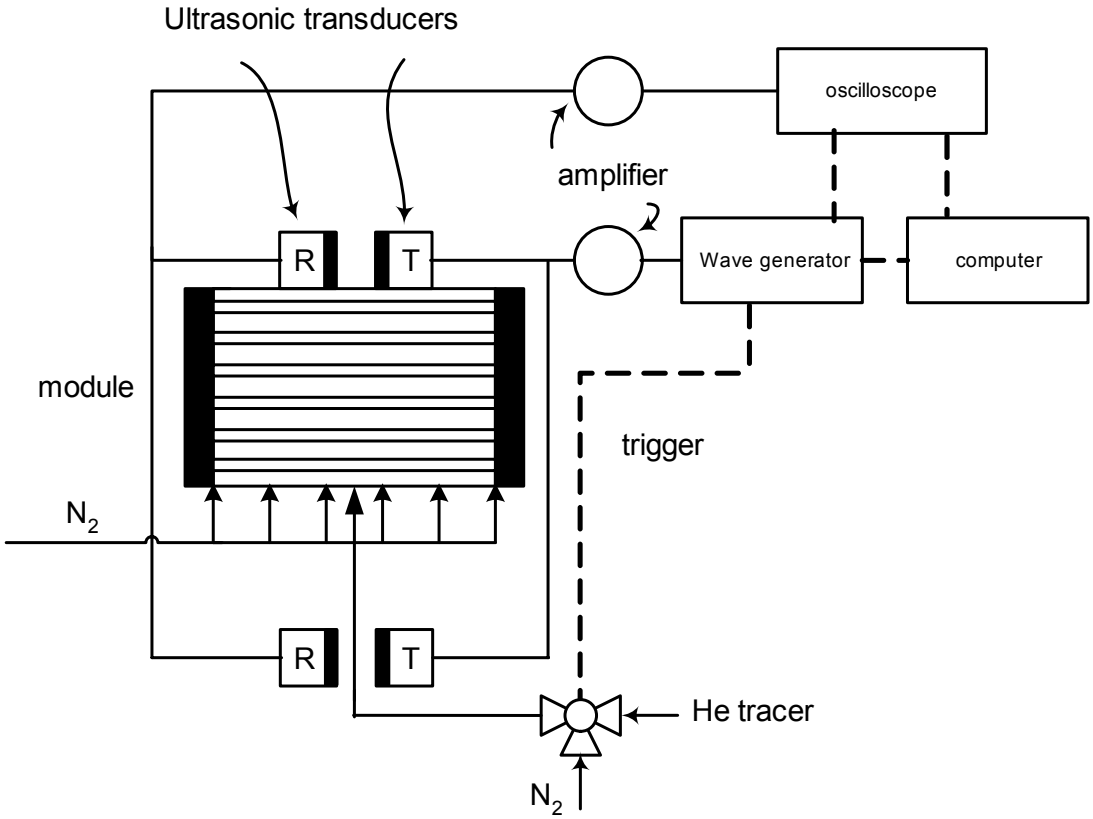

Figure 1: *Experimental set-up RTD analysis of membrane module.*

The next set of experiments was aimed at the determination of dispersion coefficients in the transversal or normal to the flow direction. In this case, the tracer is introduced as point source at a known inlet location into the module. The velocity of the tracer was kept same as the velocity of nitrogen flow in the rest of the module. The concentration profile of the tracer is determined at the exit of the module by measuring the concentration of the tracer at various positions in the 'x' and 'y' direction. A perforated plate with 8 x 8 grid holes is used to change the position of the measuring cell in the top x-y plane of the module.

Since the fibers used in the module are microporous, accumulation of the tracer gas inside the fibers might occur. To avoid this trace gas accumulation, the fibers in the module were filled with the water during all experiments.

4.0 Interpretation of RTD measurements

4.1 Axial dispersion coefficient

This section focuses on the employed methods/models for the interpretation of the concentration response curves to estimate the axial dispersion coefficient. The residence time distribution, which is essentially a statistic description of the fluid flow, expresses the probability of an entering fluid element to leave the reactor after a certain time. It is common practice to use the probability function, E, to describe the distribution of residence times:

$$\int_0^\infty E(t)\,dt = 1 \tag{6}$$

The cumulative function, F, is also frequently used for the representation of the RTD:

$$F(t) = \int_0^t E(t)\,dt \tag{7}$$

The mean residence time (first moment) can be calculated on basis of the E- and F-curve as follows:

$$\bar{t} = \int_0^\infty tE(t)\,dt = \int_0^1 t\,dF(t) \tag{8}$$

This equation provides the most direct method for the calculation of the mean residence time. It is interesting to compare the mean residence time derived from the RTD experiments with the residence time (τ) calculated by dividing shell-side volume by the shell-side volumetric flow rate. This comparison will yield information regarding the presence of dead-zones and/or short-cut streams with hardly any exchange to the main flow field.

Normally the F-curve is presented using a reduced time, where 'τ' is the residence time.

$$\theta = \frac{t}{\tau} \tag{9}$$

The spread in residence time is characterized by the variance:

$$\sigma^2 = MO_2 - \left(\bar{t}\right)^2, \quad \sigma_\theta^2 = \frac{\sigma^2}{\tau^2} \tag{10}$$

In this work a step function was used as input function, which yields the F-curve as a response curse. The RTD-curves obtained were interpreted using the axially dispersed plug flow model using Danckwerts (closed-closed) boundary conditions at inlet and outlet respectively. The analytical F-curve for this case is given by Eq. (11) (Danckwerts, 1953).

$$F = 0.5\left\{1 - erf\left(0.5\sqrt{Pe}\,\frac{(1-\theta)}{\sqrt{\theta}}\right)\right\} \tag{11}$$

A numerical fit-procedure was used to minimize the deviation between the measured F-curve and the model. The resulting fit parameters are the mean residence time and the axial dispersion coefficient.

4.2 Transversal dispersion coefficients

When the information necessary to describe the flow pattern in a reactor is not known, a model which contains empirical parameters and approximates the actual flow behavior is used to describe the mixing in the reactor. One of the most widely used models is the dispersion model. The general mathematical expression for this model is given by Eq. (12) for the case of a rectangular module with flow in z-direction.

$$\frac{\partial C}{\partial t} = E_x \frac{\partial^2 C}{\partial x^2} + E_y \frac{\partial^2 C}{\partial y^2} + E_z \frac{\partial^2 C}{\partial z^2} \quad - < v > \frac{\partial C}{\partial z} \tag{12}$$

where, 'E_z' is the axial dispersion coefficient in the direction of flow, 'E_x' and 'E_y' are transversal (normal to the direction of flow) dispersion coefficients in x and y directions and <v> is the average fluid velocity through the module. The difference between 'E_x' and 'E_y' can be identified as one along the length of fiber and one normal to the fiber respectively. These coefficients are assumed to be independent of concentration and position. The equation can be solved numerically as well as analytically for various boundary conditions at steady state. However, the analytical solution using three dispersion coefficients in three directions is rather complex, hence it was decided to solve the model using a numerical technique under steady state conditions. The following boundary and initial conditions are used to solve the model using an implicit numerical method.

$$C = 0 \text{ at } t = 0 \text{ for any } x, y, z \tag{13a}$$

At the walls of module the flux of tracer is assumed to be zero.

$$\frac{\partial C}{\partial x} = 0 \text{ at } x = 0 \;\&\; x = X \text{ for any } y,z,t \tag{13b}$$

$$\frac{\partial C}{\partial y} = 0 \text{ at } y = 0 \;\&\; y = Y \text{ for any } x,z,t \tag{13c}$$

$$C = C_{ini} \text{ at } z = 0 \text{ for known } x, y \;\&\; t > 0 \tag{13d}$$

$$\frac{\partial C}{\partial z} = 0 \text{ at } z = Z \text{ for any } x,y,t \tag{13c}$$

The exit concentration profile of the tracer is computed under steady state conditions using guessed values of the transversal dispersion coefficients. The computed concentration is then compared with the experimental concentration profile and the guess value is changed if necessary to minimize the deviation between the experimental and computed concentration profile.

5.0 Results and Discussion

5.1 *Validation of the method*

To validate the ultrasonic technique regarding the ability to determine the composition of a binary gas mixture, the helium fraction in air calculated from the measured ultrasonic velocity of the mixture using Eq. 4 was compared with the helium fraction of a known mixture. The latter was based on the readings of the mass flow controllers placed in the air and He supply lines. The results are shown in Figure 2, from which it can be concluded that the ultrasound technique can be used to determine the composition of a binary gas mixture. Obviously, the nature of the components has to be known (ρ_i & υ_i in Eq. 4).

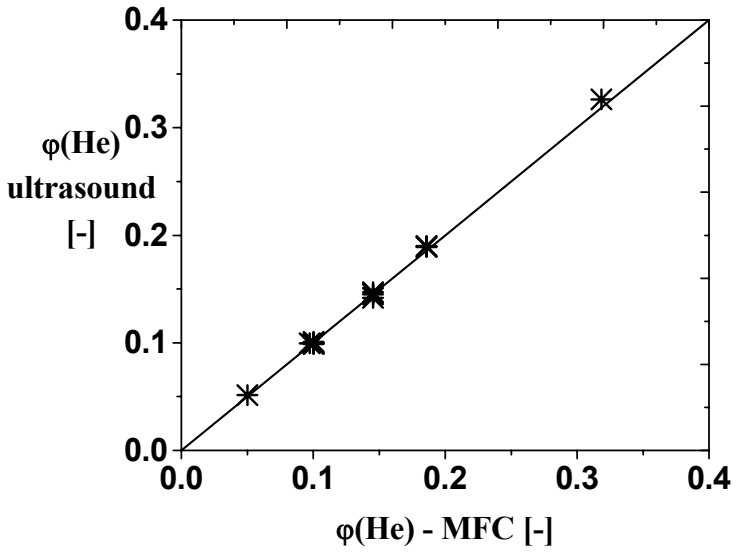

Figure 2: *Parity plot of the volume fraction of helium calculated using Eq. 4 and according to mass flow controller readings.*

To measure the applicability of the measurement technique at low residence times, RTD analysis of tubular plug flow reactors with different low residence times (τ) is carried out. Figure 3 clearly shows that the measurement system is already able to determine the gas-phase RTD of reactors with a residence time down to 0.08 seconds. Since in principle with the current measurement cell the theoretical maximum sampling frequency is 10,000 Hz,

even systems with much smaller residence times can be analyzed provided that data transfer rate is equally fast. In general, a higher sampling frequency will improve the accuracy of the RTD-curve analysis, because more data are available on the slopes of the curves.

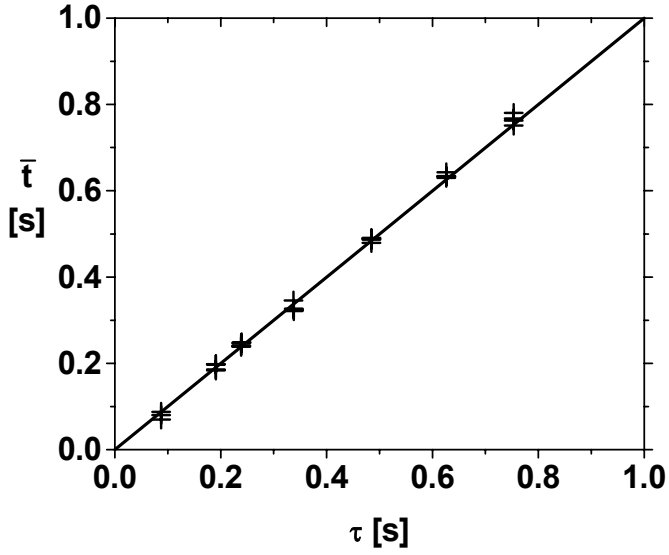

Figure 3: *Parity plot of the mean residence time (calculated by interpretation of measured F-cured with axial dispersion model) and residence time of the PFRs.*

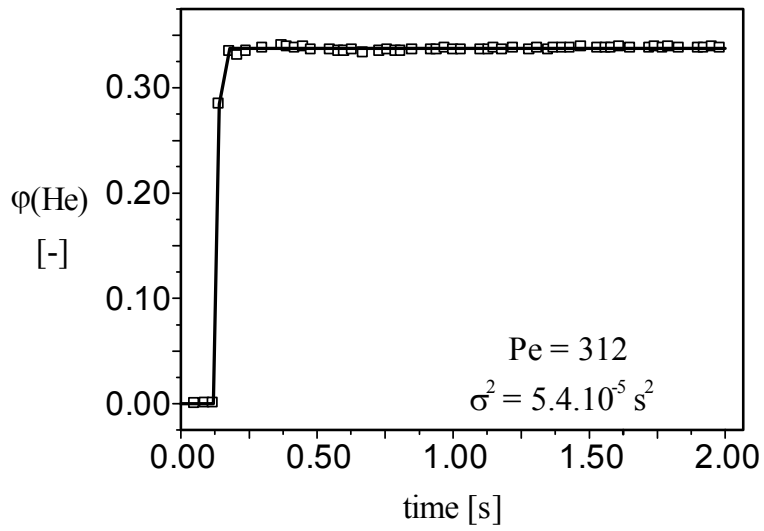

Figure 4: *Response of the tracer injection valve.*

For very short residence times (say $\tau < 0.05$ s) the dynamic behavior of the tracer-gas injection valve may become dominant, and the input step must be determined in all cases. An example of this input step function (with 10 cm tubing after the valve) is presented in Figure 4, from which can be seen that the valve opens very fast. However, the actual profile is

difficult to determine, at least within the current maximum sampling frequency of 33 Hz. Although exact values for the variance of the valve opening (σ^2_v) cannot be determined, the variance that can be determined from this curve is maximally $5{\cdot}10^{-5}$ s^2 ($\sigma^2_\theta = 5.10^{-3}$). Thus the assumption of an ideal input step function is still justified.

5.2 Analysis of the cross-flow hollow fiber membrane contactor

A typical F-curve in the RTD analysis of the rectangular membrane module is shown in Figure 5. It can be seen that the shell-side flow is neither ideal plug flow nor resembles completely stirred tank flow. Similar F-curves are obtained for different velocities to study the effect of shell-side velocity on the dispersion coefficient. The axial dispersion coefficient can be obtained using Eq. (11) by fitting the experimentally obtained concentration versus time profiles.

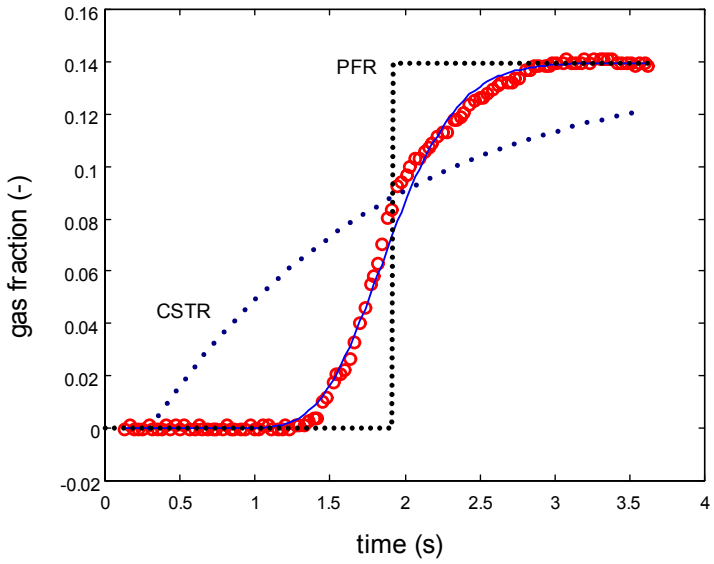

Figure 5: *Typical response F-curve of rectangular hollow fiber membrane module (Line indicates the axial dispersion model fit).*

Figure 6 shows the variation of the thus obtained axial dispersion coefficient with the shell side velocity. The axial dispersion coefficient increases with the shell side velocity. The axial dispersion coefficient 'E_z' obtained in the membrane module has intermediate values as compared to the pipe flow and to the packed bed correlations (Wen & Fan, 1975). The presence of fibers in the module reduces the axial mixing and thus axial dispersion coefficient for membrane module is lower as compared to the pipe flow correlation. Higher values of the axial dispersion coefficient for the membrane module as compared to packed bed correlation could possibly be explained by the fact that the membrane module contains two dead zones at the inlet and the outlet of the module which contributes to the mixing of the shell-side fluid.

In addition, the packing density of the fibers in the membrane module considered (around 20%) is much lower as compared to the packing density in packed beds (40-60%).

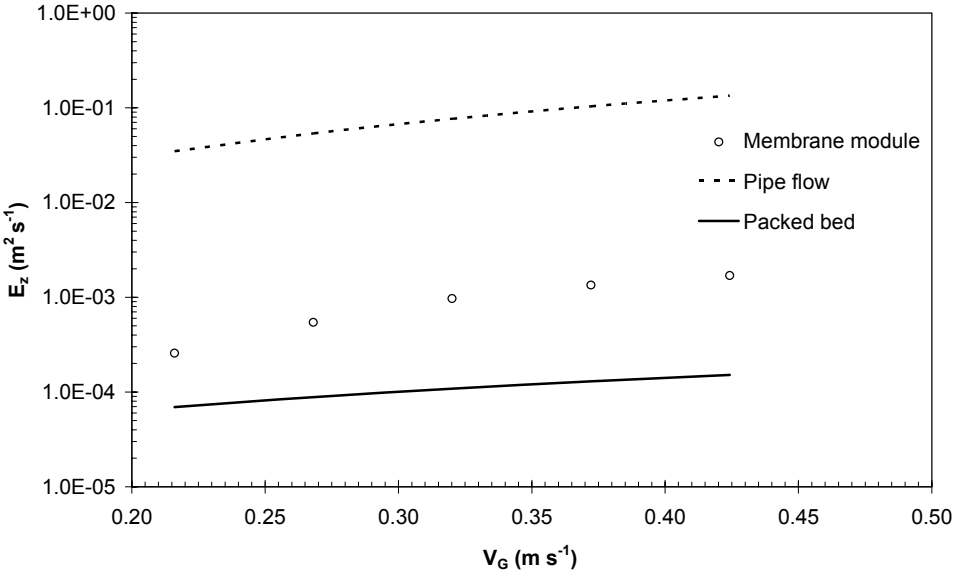

Figure 6: *Effect of shell side velocity on axial dispersion coefficient.*

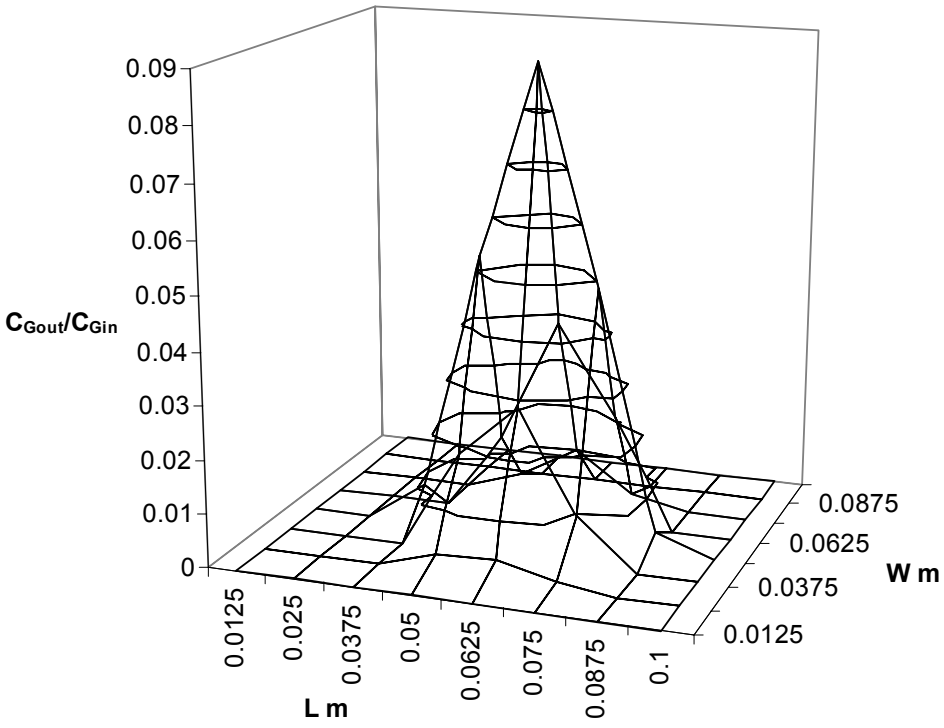

Figure 7: *Measured concentration profile of the tracer at the exit of the module.*

A typical concentration profile of the tracer at the module exit, using a single point source at the inlet is shown in the Figure 7 and the corresponding computed concentration profile is shown in Figure 8. The difference in the axes scale is due to the conversion of the module dimensions into cells and the conversion of the dimensionless outlet concentration into absolute values. Experiments are carried out at different shell side velocities to study the effect of the shell-side velocity on the transversal dispersion coefficients.

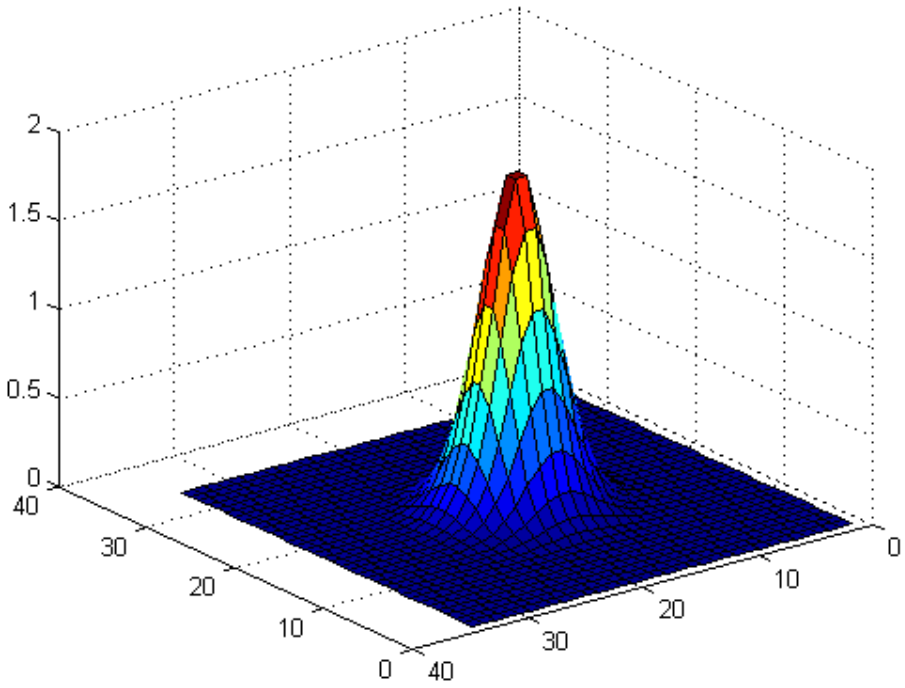

Figure 8: *Computed concentration profile of the tracer at the exit of the module.*

The variations of the obtained transversal dispersion coefficients with the shell side velocity are given in Figure 9 and Figure 10. In general, the transversal dispersion coefficients increase with the shell side velocity. The transversal dispersion coefficient across the fiber length has a higher value and increases much steeper with velocity when compared to the transversal dispersion coefficient along the length of fiber. This higher value and greater dependence of transversal dispersion coefficient across the fiber on the shell side velocity can be attributed to the splitting and remixing of the shell side stream across each fiber. The axial dispersion coefficient 'E_z' is much higher as compared to the transversal diffusion coefficients 'E_x' and 'E_y'. Similar observations were made for the packed bed and the pipe flow dispersion coefficients (Westerterp et al. 1984). This can be attributed to the increased residence time distribution due to wall effects, especially at low L/D ratio.

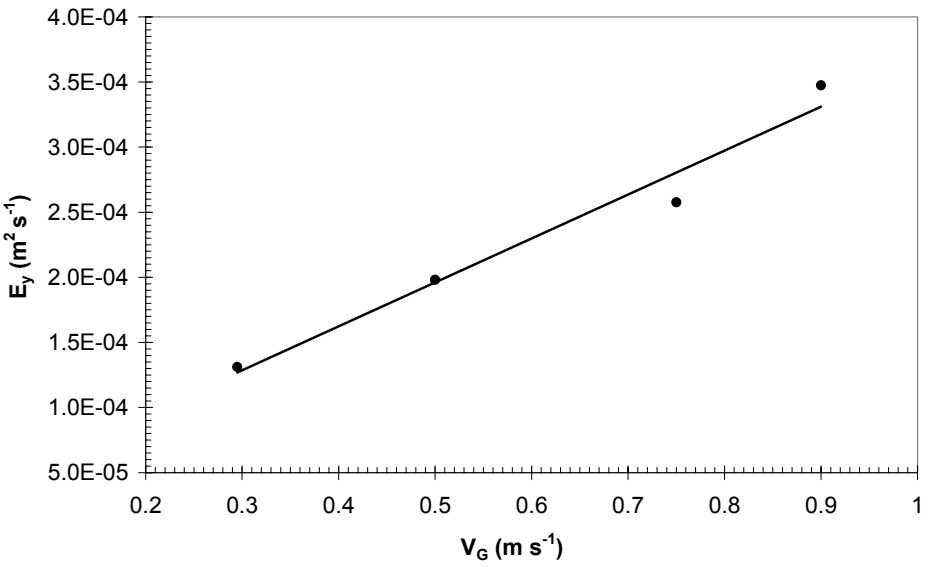

Figure 9: *Transversal dispersion coefficient across the length of fiber.*

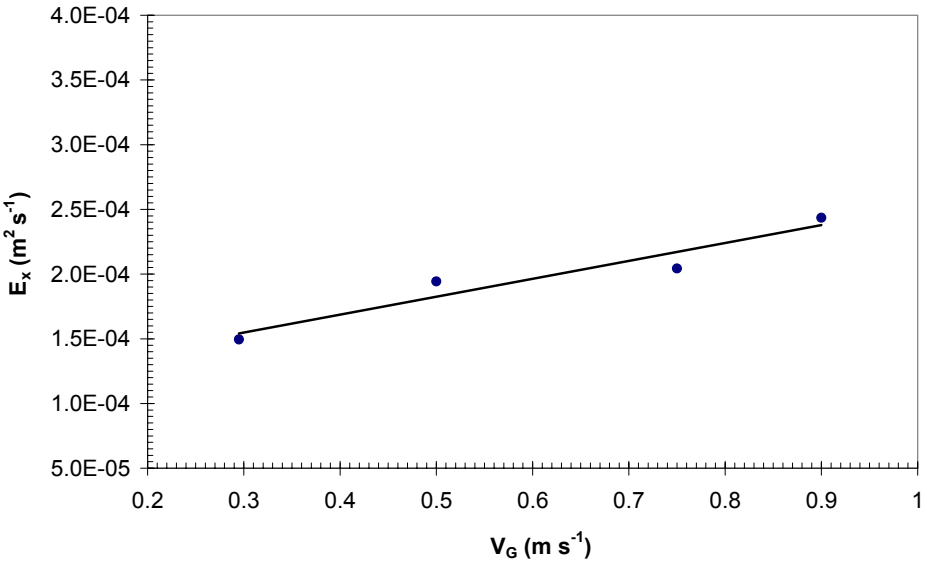

Figure 10: *Transversal dispersion coefficient along the length of fiber.*

6.0 Conclusion

In this work a novel ultrasonic technique is used to study the shell-side mixing behavior of the cross-flow hollow fiber membrane contactor. The technique can be successfully used to characterize the system with low residence times typically in the range of 0.1 seconds. In addition, the technique can be also used to measure the gas-phase concentrations without disturbing the flow.

The shell-side mixing behavior of a cross-flow hollow fiber membrane contactor is characterized in terms of dispersion coefficients in axial and transversal directions. The fibers used in the contactor act as a kind of packing and thus thereby reduce the mixing in axial

direction. The axial dispersion coefficient is found to be in between the values obtained for pipe flow and packed beds. The axial dispersion coefficient is found to be higher than the transversal dispersion coefficients. The transversal dispersion coefficient across the fiber length has a stronger dependence on the shell side velocity as compared to transversal dispersion coefficient along the fiber length due to the splitting and remixing action of the stream.

Acknowledgement

This research is part of the research program performed within the Centre for Separation Technology (CST), which is a co-operation between the Netherlands Organization for Applied Scientific Research (TNO) and the University of Twente. We acknowledge Toine Cents for his help in the RTD analysis. We also thank Benno Knaken for the construction of the experimental set up.

Nomenclature

C	Concentration	[mol m^{-3}]
D	Diameter	[m]
E(t)	E-function defined in Eq. (6)	[s^{-1}]
F(t)	F-function defined in Eq. (7)	[-]
E_v	Bulk modulus of elasticity	[Pa]
E	Dispersion coefficient	[m^2 s-1]
L	Length	[m]
MO_2	Second moment	[s^2]
P	Pressure	[pa]
Pe	Péclet number (Pe=UL/D)	[-]
t	Time	[s]
$\bar{t}$	Mean residence time	[s]
<v>	Average velocity	[m s^{-1}]
ν	Sound velocity	[m s^{-1}]
w	Width	[m]
x	Distance	[m]
z	Length	[m]

Greek letters

φ	Tracer-gas volume fraction	[-]
ρ	Density	[kg m^{-3}]
θ	Reduced time defined in Eq. (9)	[-]
τ	Residence time	[s]

σ^2	Variance defined in Eq. (10)	[s^2]
σ_θ^2	Normalized variance defined in Eq. (10)	[-]

Subscripts

ini	Initial condition
r	Reference component
v	Valve
x	x-directional
y	y-directional
z	z-directional

References

Cents, A.H.G., Kersten, S.R.A., & Brilman, D.W.F. (2003). Gas-phase RTD measurement in gas and gas-solids reactors using ultrasound. *Industrial Engineering Chemistry Research, **42**, 5506-5515.*

Chun, M., & Lee, K. (1997). Analysis on a hydrophobic hollow fiber membrane absorber and experimental observations of CO_2 removal by enhanced absorption. *Separation Science and Technology,* **32(15)**, 2445-2466.

Danckwerts, P.V. (1953). Continuous flow systems: distribution of residence time. *Chemical Engineering Science*, **2**, 1-13.

Feron, P.H.M., Jansen, A.E., Klaassen, R., Hanemaaijer, J.H., & ter Meulen, B.Ph. (1994). Membrane gas absorption processes in environmental applications *in Membrane Processes in Separation and Purification* (Edited by J.G. Crespo and K.W. Boddeker). Dordrecht: Kluwer Academic.

Karoor, S., & Sirkar, K.K. (1993). Gas absorption studies in microporous hollow fiber membrane modules. *Industrial Engineering Chemistry Research,* 32, 674-684.

Mulder, M. (1996). *Basic Principles of Membrane Technology*. Dordrecht: Kluwer Academic Publishers.

Povey, M.J.W. (1997). *Ultrasonic Techniques for fluids Characterization.* Amsterdam: Academic Press.

Skelland, A.H P. (1974). *Diffusional Mass Transfer.* New York: John Wiley & Sons.

Wen, C.Y., & Fan, L.T. (1975). *Models for flow systems and chemical reactors.* New York: Marcel Dekker.

Westerterp, K.R., Van Swaaij, W.P.M., & Beenackers, A.A.C.M. (1984). *Chemical reactor design and operation*. New York: John Wiley & Sons.

Wickramasinghe, S.R., Semmens, M.J., & Cussler, E.L., (1992). Mass transfer in various hollow fiber geometries. *Journal of Membrane Science,* **69**, 235-250.

Chapter 4

Cross Flow Membrane Contactors: Physical Mass Transfer Processes

Abstract:

Traditionally, membrane contactors used for gas-liquid contacting were designed in a shell and tube configuration with shell side fluid flowing parallel to the fiber side fluid, either in co-current or counter-current pattern. The primary limitations of these so-called 'parallel flow' contactors are the shell side flow channeling or mal-distribution due to non-uniform packing of the hollow fibers, higher shell side pressure drop and relatively lower mass transfer coefficients. These limitations can be eliminated or reduced by using cross flow membrane contactors. In the case of cross flow membrane contactors the concentrations of both fluids vary in both directions i.e. in the direction of the flow and in the direction perpendicular to the flow. Hence unlike parallel flow contactors, simple logarithmic averaging of the concentration driving force cannot be used to predict performance of the cross flow contactors. Similar changes in the driving force are also found in the cross flow heat exchanger. The possibility of application of cross-flow heat exchanger analytical solutions to describe the mass transfer in cross flow membrane gas-liquid contactor is explored. At low removal rate and low solute concentration in feed stream the experimental results match very well with the predictions by analytical solution derived on the basis of heat transfer analogies. However, when the change in the volumetric flow is significant, heat transfer analogies cannot be used to predict the performance of the cross flow gas-liquid membrane contactor. Therefore, a detailed numerical model is developed to predict the performance of the cross flow membrane contactor in such cases. To validate the model and heat transfer analogy carbon dioxide absorption experiments are carried out in cross flow membrane contactor using water as a solvent. The predictions of the developed numerical model are found to be in good agreement with the experimental results.

1.0 Introduction

The use of micro-porous membranes for direct contacting of two immiscible phases, such as gas and liquid, without dispersing one phase into another is a relatively new concept. Such devices are typically referred to as 'membrane contactors'. The main function of the membranes in these contactors is the immobilization of the gas-liquid interface at the membrane pore by a combination of surface tension and pressure difference effects. In this way a large interfacial area for efficient mass transfer can be created.

Cross-flow operation of gas-liquid membrane contactors offers several advantages when compared to the parallel flow contactors. Main advantages are relatively high mass transfer coefficients and lower shell side pressure drop. In general, the mass transfer coefficient on the shell side of hollow fiber modules is described by various empirical correlations developed for the different geometries and fiber packings. Correlations obtained for the shell side mass transfer coefficient from the literature are summarized in Table 1. In all the cases higher values of mass transfer coefficient are reported for the cross flow module than for the parallel flow modules. Wickramasinghe et al. (1992) evaluated the performance of different parallel and cross flow gas-liquid membrane contactors based on the equal flow per membrane area and equal flow per module volume. They found that in both cases cross-flow membrane modules are more effective as compared to parallel flow modules. Feron et al. (1994) used the cross flow membrane module made up of polypropylene hollow fibers for the absorption of SO_2 and extraction of hydrocarbon from waste water. They found that mass transfer coefficient for the cross flow modules are typically one order of magnitude higher than for conventional parallel flow modules. In addition, the shell side pressure drop was also considerably lower than that for the conventional parallel flow modules. This difference in the module performance is mainly due to the flow path taken by the shell side fluid. The differences in shell side fluid paths affect module performance in two ways. First, the extent of mass transfer varies from streamline to streamline due to the residence time distribution of the shell side fluid. Thus largest concentration difference occurs in a fluid element having longest residence time. Secondly, the local mass transfer resistance is a function of local velocity and turbulence. In case of cross-flow contactors the concentration boundary layer break-up occurs due to splitting and remixing of the shell-side fluid. Hence the mass transfer coefficient obtained in the cross-flow contactors turns out to be higher as compared to the parallel flow contactors.

In case of the cross flow membrane contactors the concentrations of both fluids vary in both directions i.e. in the direction of the flow and in the direction perpendicular to the flow. Hence, unlike parallel flow contactors, simple logarithmic averaging of the concentration driving force therefore cannot be used to predict the performance of the cross flow contactors. Similar local variations in the driving force with position are also found in the cross flow heat exchanger. Detailed analysis of the cross flow heat exchanger and

analytical solutions to predict the performance of the cross flow heat exchanger have been presented by many investigators (Nusselt, 1911; Smith, 1934; Hofmann, 2000). However, in the case of cross flow membrane gas-liquid contactors along with the change in the concentrations, the volumetric flow of the gas phase can also change significantly over the volume of the module. In such cases direct application of the heat transfer analogy may lead to erroneous results. The performance of these types of contactors will therefore be analyzed by detailed mathematical modeling to study the impact of this phenomenon.

Table 1: *Summary of equations predicting mass transfer coefficient for shell side flow.*

A. *Shell side flow parallel to the fibers.*

Author	Equation	Comment
Wickramasinghe et al. (1992)	$Sh = 0.019Gz$ Gz < 60; Φ = 0.7	Developed with closely packed fibers for gas-liquid contactor.
Yang & Cussler (1986)	$Sh = 1.25\left(\mathrm{Re}\frac{d_e}{L}\right)^{0.93} Sc^{0.33}$ 0.5 < Re < 500 ; Φ = 0.03	Developed with loosely packed fibers for gas-liquid contactor.
Prasad & Sirkar (1988)	$Sh = \beta\left[d_e\frac{(1-\phi)}{L}\right]\mathrm{Re}^{0.6} Sc^{0.33}$ 0 < Re < 500 ; 0.04 < Φ < 0.4	Developed for liquid –liquid contactor. β=5.8 for hydrophobic fiber and β = 6.1 for hydrophilic fibers
Dahuron & Cussler (1988)	$Sh = 8.8\,\mathrm{Re}\frac{d_e}{L} Sc^{0.33}$ Re < 100; Φ = 0.15	Developed for liquid-liquid extraction.
Wu & Chen (2000)	$Sh = \left(0.31\phi^2 - 0.34\phi + 0.001\right)\mathrm{Re}^{0.9} Sc^{0.33}$ Re < 100; 0.25 < Φ < 0.92	Reflects the effect of random fiber packing for gas-liquid contactor.
Viegas et al. (1998)	$Sh = 8.71\frac{d_e}{L}\mathrm{Re}^{0.74} Sc^{0.33}$ 0.16< Re < 7.30; Φ = 0.30	Developed for liquid-liquid extraction.
Costello et. al. (1993)	$Sh = \left(0.53 - 0.58\phi\right)\mathrm{Re}^{0.53} Sc^{0.33}$ 21 < Re < 324 ; 0.32 < Φ < 0.76	Reflects the effect of shell side hydrodynamics using gas-liquid contactor.

B. *Shell side flow across the fibers.*

Author	Equation	Comment
Yang & Cussler (1986)	$Sh = 0.9\,\mathrm{Re}^{0.4}\,Sc^{0.33}$ 1 < Re < 25; Φ = 0.07	Developed for loosely packed fibers using gas-liquid contactor.
	$Sh = 1.38\,\mathrm{Re}^{0.4}\,Sc^{0.33}$ 1 < Re < 25; Φ = 0.7	Developed for closely packed fibers using gas-liquid contactor.
Feron et al. (1994)	$Sh = 0.9\,\mathrm{Re}^{0.5}\,Sc^{0.33}$ 1 < Re < 1000; Φ = 0.2	Proposed for rectangular module.
Wickramasinghe et al. (1992)	$Sh = 0.15\,\mathrm{Re}^{0.8}\,Sc^{0.33}$ 2.5 < Re; Φ = 0.2	Independent of geometry (helically wound, shell and tube, rectangular).
	$Sh = 0.12\,\mathrm{Re}\,Sc^{0.33}$ 2.5 < Re; Φ = 0.2	Independent of geometry and considering polydispersity of fibers.
Schoner et al. (1998)	$Sh = 1.76\,\mathrm{Re}^{0.82}\,Sc^{0.33}$ 0.01 < Re < 10	Developed for the liquid-liquid extraction.
Ahmed & Semmens (1996)	$Sh = 1.45\,\mathrm{Re}^{0.32}\,Sc^{0.33}$	Developed for transverse flow G-L membrane contactors.
Bhaumik et al. (1998)	$Sh = 0.57\,\mathrm{Re}^{0.31}\,Sc^{0.33}$ 0.01 < Re < 10	Developed for transverse flow G-L membrane contactors.
Wang & Cussler (1993)	$Sh = 0.18\,\mathrm{Re}^{0.86}\,Sc^{0.33}$	Developed for baffled G-L cross flow contactor.
Cote et. al. (1989)	$Sh = 0.61\,\mathrm{Re}^{0.363}\,Sc^{0.33}$ 0.6 < Re < 49; Φ = 0.003	Developed for G-L cross flow contactor.

In the present work a numerical model is developed to describe and estimate the performance of cross flow membrane contactors. Attempts have been made to use and compare the analytic solutions developed for the cross flow heat exchangers in limiting cases. To experimentally validate the numerical model and derived analytical expressions from heat transfer analogy, carbon dioxide absorption is carried out in cross flow membrane contactors using water as a solvent. The main aim of the study was to study the performance of cross flow membrane contactors using a numerical model based on first principles; the experiments were performed with water on the fiber side and gas on the shell side. The liquid on the fiber side also helps in the visual inspection fiber to check if any wetting is occurring. However, it should be noted that passing the phase with the controlling mass transfer resistance on the shell side gives a better overall performance.

2.0 Theory

Due to the inherent variation of the mass transfer rate with position within the cross flow module, detailed modeling of the mass transfer process seems necessary. Nevertheless, first analytical expressions will be derived for the asymptotic cases, similar to the derivation made for the cross flow heat exchangers.

2.1 Application of heat transfer analogy

The literature on the mathematical analysis of cross flow heat exchangers is mainly focused on the calculation of mean temperature difference in single-pass and multi-pass heat exchangers (Nusselt 1911, Smith 1934). In case of cross flow membrane modules both fluids flow at right-angles to each other. Thus the concentration of the fluids may vary in a direction normal to its flow as well as in the direction of flow. At the outlet, all infinitesimal sections of a stream may be at different concentrations as each was subjected to a different driving force for mass transfer. The final outlet concentration is obtained by the complete mixing of all infinitesimal sections. By making following assumptions the heat transfer analysis can be used to describe the mass transfer in cross flow gas-liquid membrane contactors.

1. Steady state and isothermal operation.
2. No chemical reaction.
3. The changes in flow rates are very small and can be neglected.
4. Overall mass transfer coefficient and distribution coefficient are constant over the module.
5. The pitch and placing of the membrane fibers are similar to that of the heat transfer equipments.

The cross flow membrane contactor is shown schematically in Figure 1. One of the fluids is arranged to pass through the membrane fibers, while other fluid passes perpendicular to the fibers. Figure 1 also serves to explain the nomenclature used in the analysis. Taking a mass balance over a small rectangular element of area *dxdy, two* partial differential equations can be obtained.

$$\frac{\partial C_1}{\partial y} = -\frac{KX}{Q_1}\left(mC_1 - C_2\right) \tag{1}$$

$$\frac{\partial C_2}{\partial x} = \frac{KY}{Q_2}\left(mC_1 - C_2\right) \tag{2}$$

where ‘m’ is the distribution coefficient and ‘K’ is the overall mass transfer coefficient. Once the module outlet concentrations ‘$C_{1,e}$’ and ‘$C_{2,e}$’ are determined, the overall mass transfer rates can be obtained by

$$W = Q_1\left(C_{1i} - C_{1e}\right) \tag{3}$$

$$W = Q_2\left(C_{2e} - C_{2i}\right) \tag{4}$$

$$W = KA(\Delta C)_m \tag{5}$$

where is 'A' is the overall mass transfer area and $(\Delta C)_m$ is the mean effective concentration difference. The problem is analyzed in two asymptotic cases namely unmixed shell side fluid and completely mixed shell side fluid. For both cases analytic solutions can be derived. It should be noted that 'Unmixed' and 'Mixed' shell side fluid refers to the mixing in the direction normal to the shell side flow.

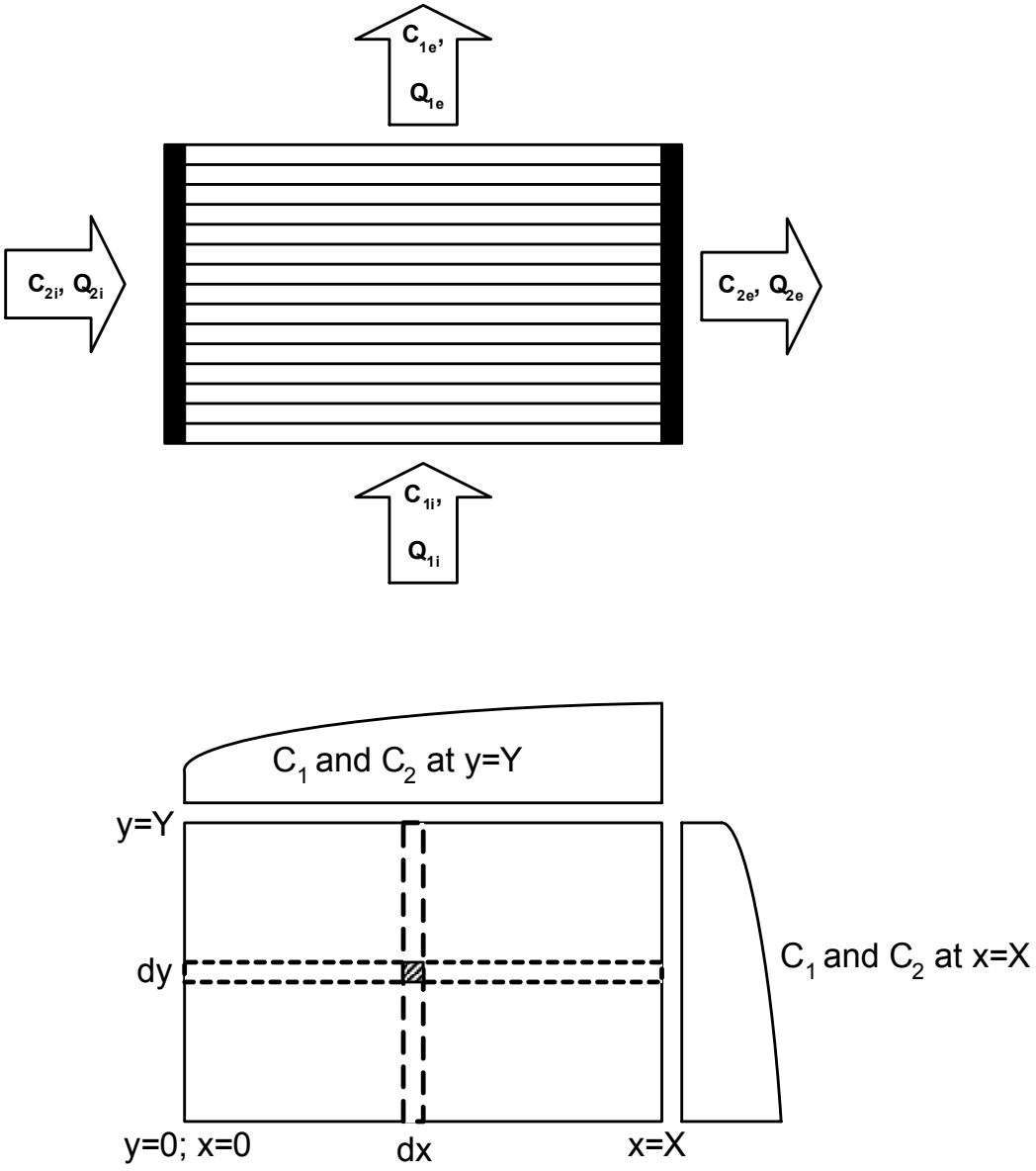

Figure 1: *Cross flow membrane contactor.*

2.1.1 Both Fluids Unmixed

In this case both fluids passes in the series of independent infinitesimal streams. There is no mixing between the streams either in the direction of flow or in the direction normal to the flow until the outlet is reached. Since each streamline is subject to a different range of concentration of the other fluid, the streams will have different outlet concentrations. The final outlet concentration is the result of mixing of all streams. This situation is nearly approached when one fluid flows through many fibers and the other fluid is divided into number of streams e.g. by baffles. The exact solution in this case requires simultaneous solution of the differential Eqs. (1) and (2). The mathematical derivation is given in Appendix C. The final solutions to calculate the average dimensionless outlet concentrations are given below.

$$\Theta_{1xm} = \frac{1}{a^*}\sum_{N=0}^{\infty}\left(1 - e^{-a^*}\sum_{N=0}^{N}\frac{(a^*)^N}{N!}\right)\left(1 - e^{-mb^*}\sum_{N=0}^{N}\frac{(mb^*)^N}{N!}\right) \tag{6}$$

$$\Theta_{2xm} = 1 - \frac{1}{mb^*}\sum_{N=0}^{\infty}\left(1 - e^{-mb^*}\sum_{N=0}^{N}\frac{(mb^*)^N}{N!}\right)\left(1 - e^{-a^*}\sum_{N=0}^{N}\frac{(a^*)^N}{N!}\right) \tag{7}$$

where Θ_{1xm} and Θ_{2xm} are the average dimensionless outlet concentrations of fluid 1 and fluid 2, a and b are dimensionless x and y coordinates, see Eqs. (C3) and (C4).

2.1.2 One Fluid Mixed, Other unmixed

In this case, one fluid (shell side fluid) is completely mixed normal to its flow. Hence there is no concentration gradient normal to the flow of fluid. The second fluid is assumed to consist of independent streams between which there is no mixing. This case is approached by passing one fluid across the fibers in absence baffles to allow complete mixing in the direction normal to flow and passing a second fluid through the fibers. The average concentration of both fluids can be obtained by solving Eqs. (1) to (5) by selecting proper boundary conditions. The average outlet concentration of the shell side mixed fluid 1 is given by the Eq. (8). The derivation of the outlet concentration of the shell side fluid is given in Appendix C. The average outlet concentration of the unmixed fluid 2 can be calculated from the overall mass balance Eqs. (3) and (4).

$$\Theta_{1xm} = 1 - \exp\left[\frac{mQ_2}{Q_1}\left(\exp\left(\frac{-KA}{Q_2}\right) - 1\right)\right] \tag{8}$$

2.2 Numerical Model

In membrane gas-liquid contactors, the gas phase flow can change considerably due to absorption. This is especially true when the gas stream contains a considerable amount of

the solute gas which is absorbed and particularly for highly soluble compounds. In such cases, the higher absorption of one component results in an increase in the partial pressure of the slower absorbing component resulting into increased the driving force for slower absorbing component. This inverse coupling of the concentration differences leads to complex situation where the direct application of the cross flow heat exchanger analogy can no longer be applied. Moreover, when the absorption of (one or more) the gaseous component is enhanced by a chemical reaction, the heat transfer analogy is no longer valid. Hence it is necessary to develop a numerical model that takes into account the changes in the gas flow rate as well as variations in the concentration driving force. Following assumptions are made in the numerical model

1. Steady state and isothermal operation.
2. Laminar flow within the fiber.
3. The membrane pores are gas filled.
4. The shell side flow can be described by a number of ideally mixed cells in both directions.
5. Pitch and placing of the fibers are well defined and not a function of position in the contactor.

Using above assumptions, the steady state mass balance in the fiber for the transport of component ‘j’can be written as:

$$2\bar{v}\left[1-\left(\frac{r}{r_i}\right)^2\right]\frac{\partial C_j}{\partial z}=D_j\left[\frac{1}{r}\frac{\partial}{\partial r}\left(r\frac{\partial C_j}{\partial r}\right)\right] \tag{9}$$

where ‘v’ is average flow velocity through the fiber. Boundary and initial conditions are given below

$$C_j|_{z=0}=C_{ji} \tag{10}$$

At the centre of the fiber the concentration profile is symmetric which results in the boundary condition (11)

$$\left(\frac{\partial C_j}{\partial r}\right)_{r=0}=0 \qquad (0\le z\le L) \tag{11}$$

At the gas-liquid interface i.e. the membrane or fiber wall mass transfer from the gas phase to the liquid phase occurs, which is described by the Eq. (12)

$$D_j\left(\frac{\partial C_j}{\partial r}\right)_{r=r_i}=K_{ex}\left(\bar{C}_{j,S}-\frac{C_j}{m}\right) \qquad (0\le z\le L) \tag{12}$$

where 'K_{ex}' is the overall mass transfer coefficient obtained by combining membrane wall and gas phase transport resistance respectively. For a non-volatile liquid phase component flowing through the fiber, the boundary condition at the gas-liquid interface is given by the Eq. (13).

$$D_j\left(\frac{\partial C_j}{\partial r}\right)_{r=r_i} = 0 \tag{13}$$

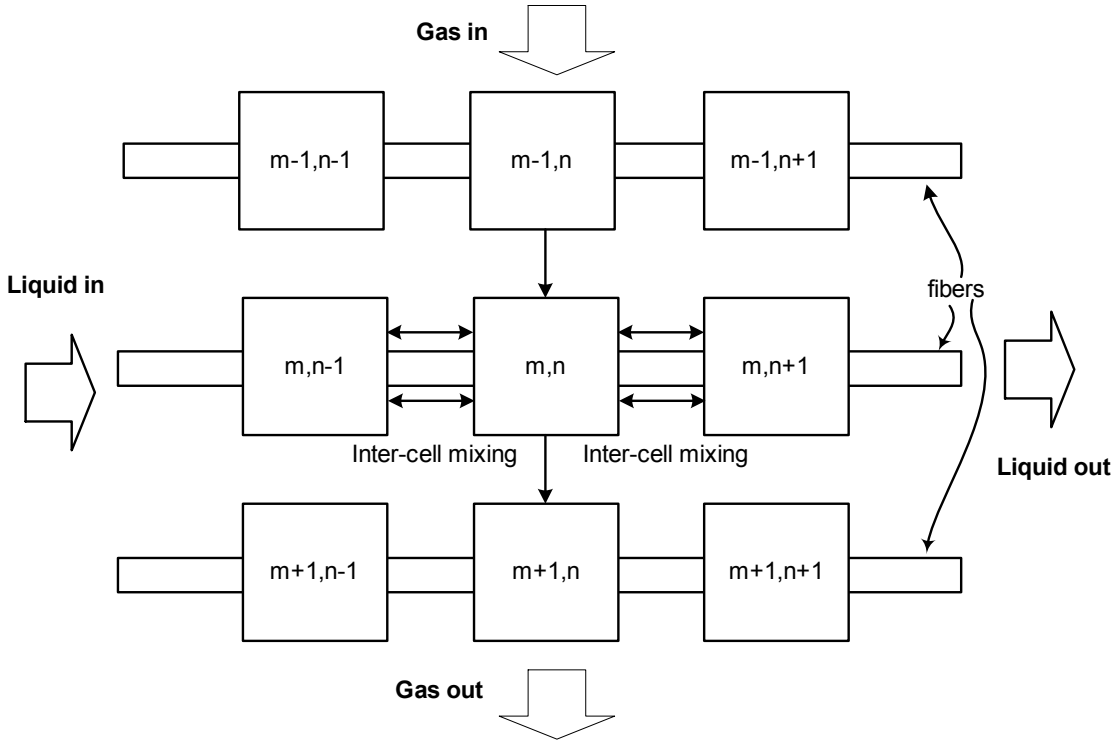

Figure 2: *Cell arrangement for shell side flow.*

The liquid can either be new, unloaded solution or partially saturated with the solute at the liquid entrance of the cross flow membrane contactor, whereas at the outlet of the liquid stream, the solvent has increased loading. Thus there is a gradual decrease in the driving force along the length of fiber. This results into higher absorption rates at the liquid entrance side as compared to the liquid outlet side. As a consequence the drop in shell side concentration of the solute in the direction of gas flow is more near the liquid entrance as compared to the drop in the shell side concentration of the solute in the direction of gas flow near the liquid exit. This effect is significant when the concentration of the solute in the gas stream is high and/or the solubility is high, thus resulting into the higher removal rates in the membrane contactor. To take this effect into account the shell side stream, in this study the gas phase, is divided into a number of unit cells. This method preserves the concentration gradients of the gas and liquid phase in both directions. The applied cell arrangement is

shown in Figure 2. Each cell is completely, ideally mixed and there is no back mixing in the direction of the flow. The number of cells in the direction of the flow represents the well known CSTR in series model. Note that in the direction perpendicular to the flow mixing takes place between the adjacent cells. A solute balance over a single cell gives following equation.

$$Q_{Gm-1,n}C_{Gm-1,n} - Q_{Gm,n}C_{Gm,n} = Q_{Lm,n}\left(C_{Lm,n} - C_{Lm,n-1}\right) \qquad (14)$$

$$= A_{m,n}J_{m,n}$$

where '$A_{m,n}$' and '$J_{m,n}$' are mass transfer area and the mass transfer flux (from shell-side to fiber-side) within the cell (m,n), respectively.

Based on this mass balance for a single cell the solute outlet concentration and the gas outlet flow rate are calculated for every cell by an iterative method. The gas concentration, gas flow rate and liquid concentration are assumed to be uniform over the inlet of the module. The composition and gas flow rate leaving the row of cells are stored and used as inputs for the corresponding cells in next row. At the last row, the average outlet concentration is calculated by mixing cup concentration method.

Three different stages of mixing can be defined and used for the mixing between the cells in this model. First option assumes no mixing between the adjacent cells, so the entire row of the gas moves up to the next segment. This rule results into maximum concentration gradient on the shell side. This case is similar to the earlier described heat transfer analogy with unmixed shell side flow. The second option is that the gas leaving one segment is completely mixed before entering next segment. This case is similar to the heat transfer analogy with completely mixed shell-side flow. The third option is an intermediate case with respect to the first two alternatives. In this case, the mixing between the cells perpendicular to the flow direction is calculated using Fick's law (see Figure 2).

$$J_{inter-cell\ mixing}(m,n) = -E\left(\frac{\partial C_{j,S}}{\partial z}\right) \qquad (15)$$

where, 'E' is the dispersion coefficient between the cells in the direction normal to the flow. To get an impression of actual shell side dispersion coefficients, in the direction of flow and in the direction normal to the flow, these parameters are determined in separate experiments using RTD analysis. The details of these RTD experiments and results are presented elsewhere (Dindore et. al. 2003) and are used in this study.

The complete solution of the model is obtained by solving Eqs. (9)-(13) simultaneously, along with the shell side mass balance. These equations were solved numerically using the discretisation scheme introduced by Baker and Oliphant.

3.0 Experimental

3.1 Material

Double distilled water was used as an absorption solvent. Carbon dioxide and nitrogen used in the experiments were of 99.99% purity. Owing to high hydrophobic nature of polypropylene as a membrane material and the commercial availability, it was decided to use an Accurel Q3/2 polypropylene hollow fiber for module construction. The Q3/2 fiber has an outside diameter meter of 1000 μm and inside diameter of 600 μm. The maximum pore size of the Q3/2 fiber is 0.64 μm. Two modules were used in the experiments. The details of the modules are given in Table 2.

Table 2: *Module specifications.*

Module	Fiber type	Length (m)	Width (m)	Height (m)	Nr. of fibers	Voidage	Pitch	A in m^2
I	PP	0.1	0.1	0.1	4900	0.615	1.45	0.924
II	PP	0.1	0.04	0.04	400	0.8	2.0	0.074

Module I was provided by TNO-MEP, Apeldoorn, and module II was specifically constructed for present work. The details of the modules are shown in Figure 3a and 3b. Both modules had PVC shell housing. Fibers in both modules were arranged in the square pitch. For construction simplicity reason, the shell housing of module II was kept circular with an internal diameter of 5 cm. To make the shell side flow area rectangular in cross section, a rectangular opening was cut from the circular shell and the concave volume of the shell was filled with the epoxy resin. To arrange the fibers uniformly the tube-sheet of the module II were drilled with 1.2 mm precision drill with square pitch. The fibers were then woven through the tube sheets. Once all fibers were woven, a liquid epoxy resin (slow setting) was poured on the tube sheet so that the gaps between the fibers are filled. Sufficient time (12 hours) is allowed to cure the epoxy. The procedure is repeated until the desired length of the epoxy glue is obtained. The same procedure is used to pot the other end of the module. In both modules the length of the potting was more than 5 cm. This ensures that the potting length on the liquid entry side provides sufficient distance ($> 10d_{in}$) for the laminar liquid flow profile inside the fiber to be fully developed, before it contacts the gas. Uniform flow distribution on the shell side is important to prevent the maldistribution and dead zones formation. To achieve uniform flow distribution on the shell-side, fluid is passed through an area-reducer filled with glass wool.

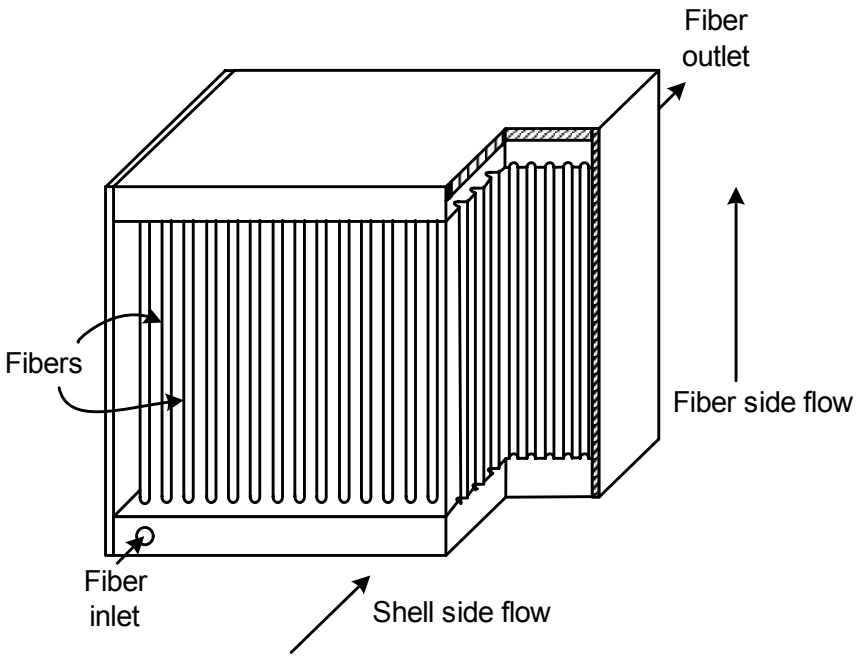

Figure 3a: *Cross flow membrane module I.*

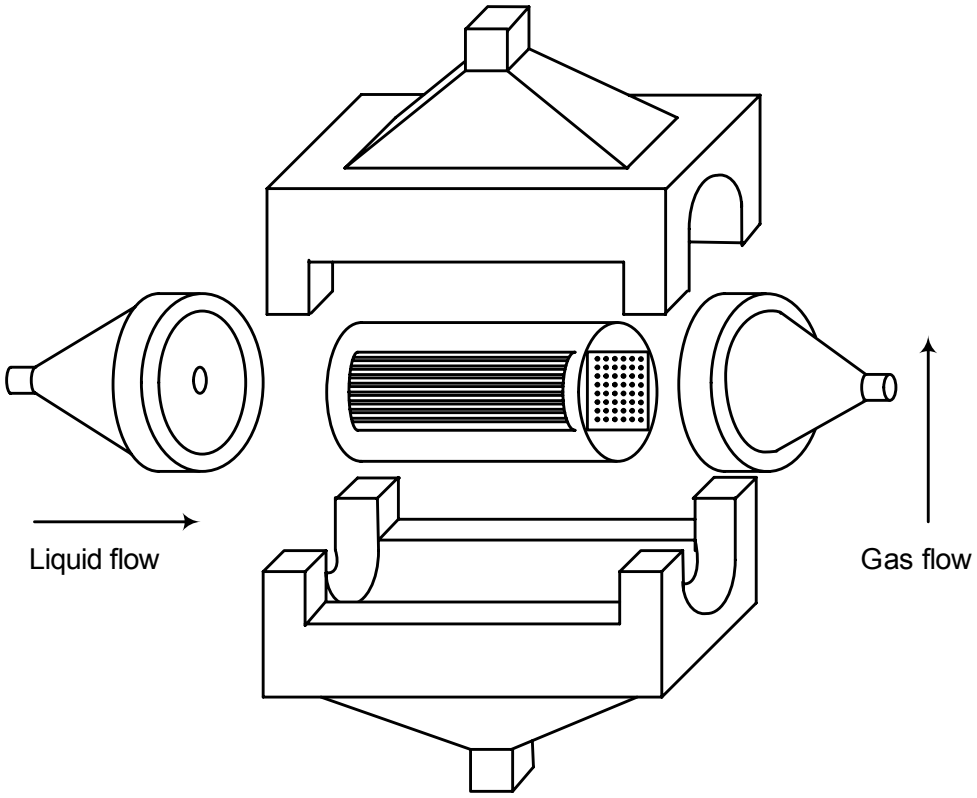

Figure 3b: *Cross flow membrane module II.*

3.2 Method

The experimental set-up to study the physical absorption of carbon dioxide in the cross flow membrane modules is shown in Figure 4. A continuous mode of gas-liquid contacting operation was used during the experiments. The liquid was passed through the fibers and gas was passed through shell side. The solvent was fed from a gear pressure pump via a flow controller. The solvent used in the experiments was degassed before usage by nitrogen bubbling in a separate apparatus. This is also useful to minimize the absorption of the nitrogen into the solvent. The solvent is passed through the heat exchanger to maintain the desired temperature before passing to the hollow fiber membrane module. The upstream solvent pressure was controlled using a high-precision back-pressure controller valve. In all experiments, sufficient gas pressure is maintained in the contactor before starting the liquid flow. The absence of the gas pressure may result in the wetting of the fiber. The liquid inlet and liquid outlet pressures were measured separately using digital pressure indicators. The liquid inlet was also fitted with a digital thermometer to monitor the liquid inlet temperature. The average velocity of the liquid through the fibers is measured by collecting a calibrated amount of sample in a fixed period of time.

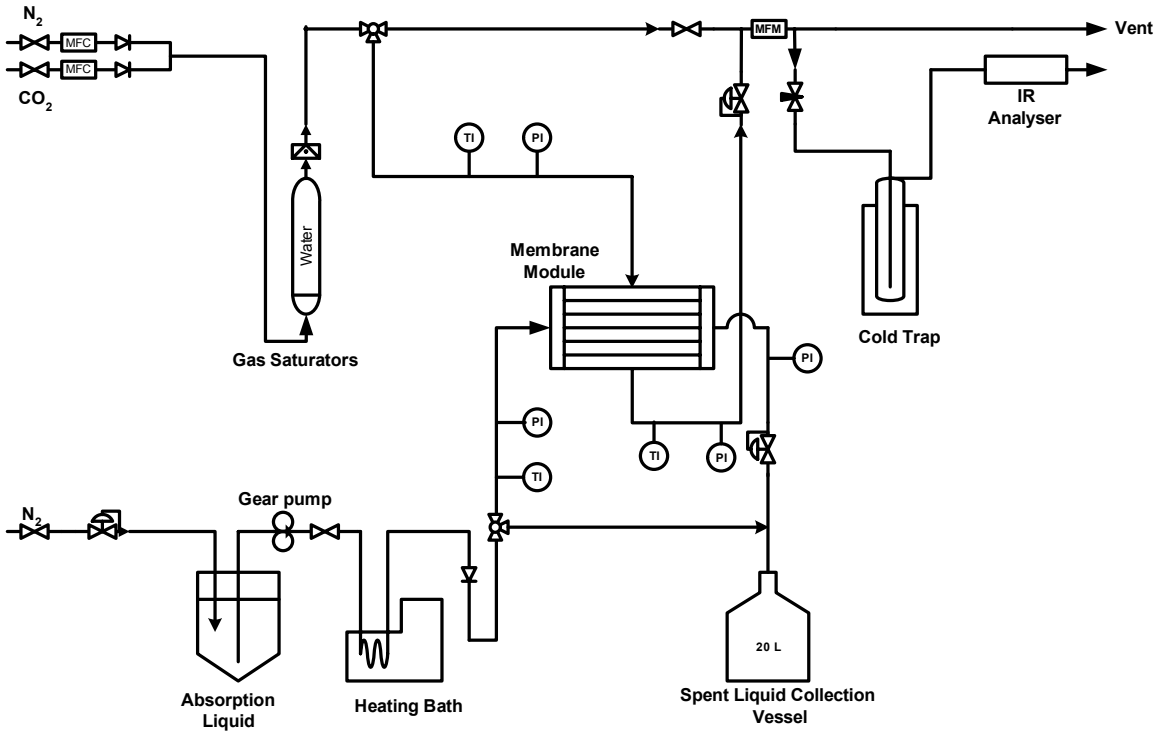

Figure 4: *Cross flow membrane module experimental set up.*

The shell-side gas flow was adjusted using mass-flow controllers. All mass flow controllers were calibrated by means of a gas flow meter and/or soap film meter. Nitrogen and carbon dioxide were premixed to a desired concentration using mass flow controllers and

fed to the contactor after saturating the gas stream with water vapor. The shell side pressure was controlled using a 5866-Brooks digital pressure controller. During all the experiments the liquid-side pressure was kept higher than the shell-side gas pressure to avoid the bubbling of gas. The gas inlet and gas outlet pressure were measured separately using digital pressure indicators. The gas inlet and gas outlet were also equipped with digital thermometers to monitor the temperatures. It is important to know both inlet and outlet temperatures of the gas stream in order to check any cooling effect which might result into a change in the volumetric gas flow rate. The carbon dioxide concentration in the feed and outlet gas streams of the contactor was measured using Maihak Infrared carbon dioxide analyzers of different ranges depending on gas composition (0-5 %, 0-15 %). The experiments are carried out using either pure carbon dioxide or mixed streams of nitrogen and carbon dioxide. The samples of the gas stream were adjusted by dilution with calibrated amounts of nitrogen in order to adjust the concentration range of Infrared analyzer. The carbon dioxide absorption flux and liquid average outlet concentration was estimated by making an overall mass balance on the reactor.

$$\left\langle J_{CO_2} \right\rangle = \frac{Q_{G,i}C_{G,i} - Q_{G,e}C_{G,e}}{A} \tag{16}$$

$$C_{Lout} = \frac{Q_{G,i}C_{G,i} - Q_{G,e}C_{G,e}}{Q_L} \tag{17}$$

Since the Infrared analyzer gives carbon dioxide concentration in terms of volume percentage, it is possible to calculate both the volumetric gas flow rate and the molar concentration of carbon dioxide by mass balance. In all experiments the gas flow rate was kept sufficiently low so that the outlet gas flow rate and molar concentration of the carbon dioxide was significantly lower than the inlet conditions. All the experiments are carried out at atmospheric pressure and 297 K.

4.0 Results and Discussions

4.1 Absorption experiments with single module

Experiments were carried out in module II to study the influence of various operating parameters such as gas-velocity, liquid-velocity and CO_2 partial pressure on the module performance. In all experiments the gas residence time in the membrane module was kept considerably high to get a significant change in the gas phase concentration. Initial experiments were carried out using very low percentage of the carbon dioxide in the inlet gas stream and low rates of removals in order to avoid large changes in the volumetric gas flow rate due to absorption. Figure 5 shows liquid phase and gas phase outlet concentrations of carbon dioxide for the absorption of carbon dioxide into water as a function of the liquid velocity through the fiber. The experiments were carried out using 2.5 % carbon dioxide in

the inlet gas stream at flowing at constant flow rate of 0.65 lit/min. As indicated in the figure both liquid and gas outlet concentration are functions of the liquid velocity through the fiber. As the liquid velocity through the fiber is increased, both gas and liquid outlet concentration are decreased. Both heat transfer analogies (with mixed and unmixed shell side flow) and the numerical model predictions of outlet gas and liquid concentrations using third mixing option are in good agreement with experimental results. However, the effect of mixing option in the numerical model is found to be negligible due to the flat shell side concentration gradients. It is important to note that in this case the CO_2 removal was always less than 15 %. Moreover, the change in volumetric flow rate of the gas was very small (less than 0.5 %) and was allowed to be neglected. Thus for these process conditions it is allowed to apply both heat transfer analogies to estimate the performance of the module.

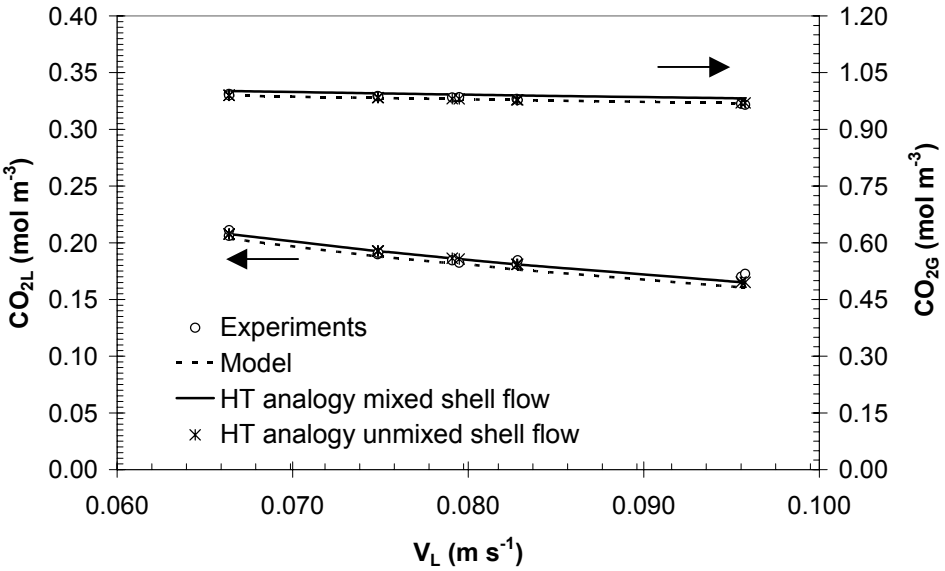

Figure 5: *Carbon dioxide (2.5 %) absorption in module II.*

To analyze the effect of a change in the volumetric flow rate of the gas stream, experiments were carried out at relatively high removal rates and using a gas stream containing a high percentage of carbon dioxide. Figures 6 and 7 show the gas and liquid outlet concentrations for the absorption of 30% and 87.5% carbon dioxide in module II, respectively. The experiments were carried out at constant flow rate of 0.39 lit/min. It can be seen from the graphs that as the liquid velocity is increased, both gas phase and liquid phase outlet concentration are decreased. Both liquid and gas phase outlet concentrations as predicted by the numerical model are in good agreement with experimental results. However, the gas phase concentrations predicted by heat transfer analogies are lower from the experimental results and this deviation increases with the liquid velocity. As a result of the lower gas phase concentration and hence lower mass transfer driving force, the liquid outlet

concentrations predicted by heat transfer analogy are also lower as compared to the numerical model. The transfer of moles from gas phase to the liquid phase results into a decrease in the gas phase volumetric flow rate as well as the gas phase solute concentration. However, the heat transfer analogy is derived for the constant volumetric flow rate and only takes into account the change in the solute concentration. As the solute concentration in the gas-phase and the removal rate increases, the decrease in the volumetric flow rate is more pronounced than the decrease in the solute concentration. In the present case the percentage removal increases with the liquid velocity and hence the deviation in the prediction of gas phase outlet concentration by heat transfer analogies increases also with the liquid velocity.

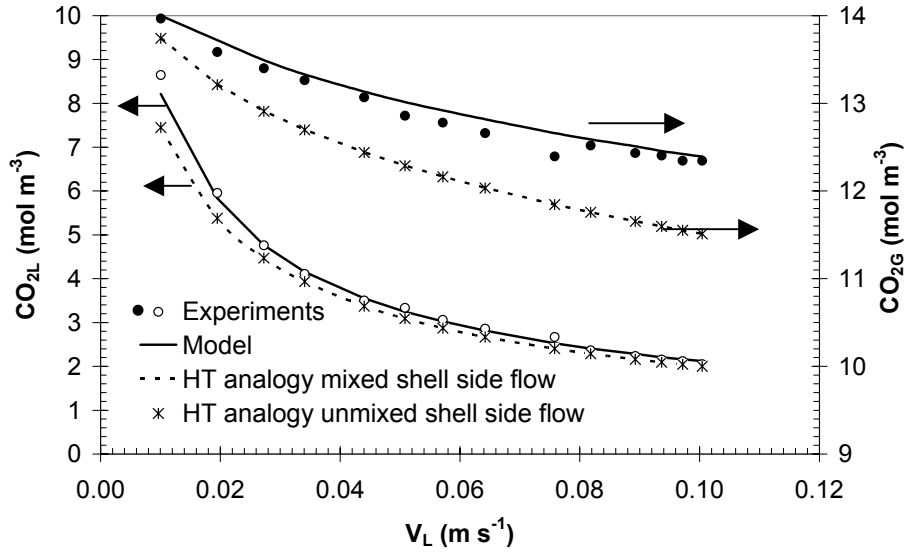

Figure 6: *Carbon dioxide (30 %) absorption in module II.*

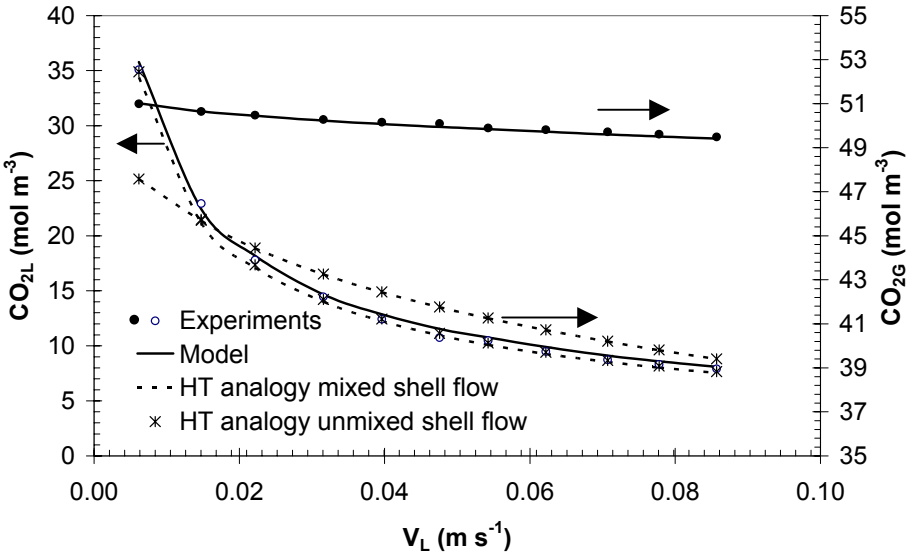

Figure 7: *Carbon dioxide (87.5 %) absorption in module II.*

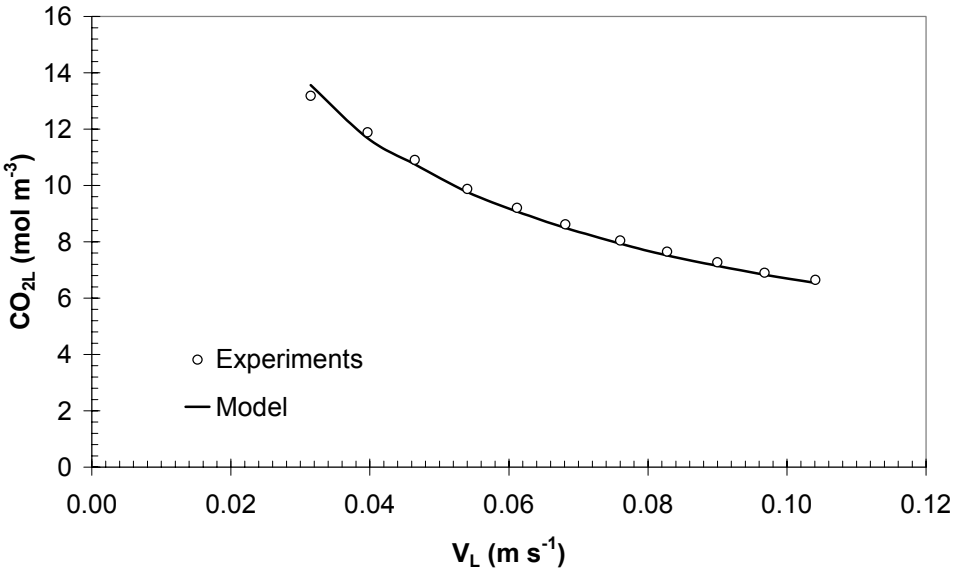

Figure 8: *Absorption of pure carbon dioxide in module II.*

In the asymptotic case of a pure gas only the volumetric flow rate will change. Figure 8 shows the absorption of pure carbon dioxide in module II. Thus when solute gas phase concentration is relatively high and removal rate is significant, heat transfer analogies cannot be used to estimate the module performance.

Figure 9 and 10 shows the absorption flux as a function of the liquid and gas velocity. The absorption flux is a strong function of the liquid velocity whereas the gas velocity has almost a negligible influence on the absorption flux. This confirms the fact that in the case of physical absorption of a sparingly soluble gas, the controlling mass transfer resistance lies on the liquid side.

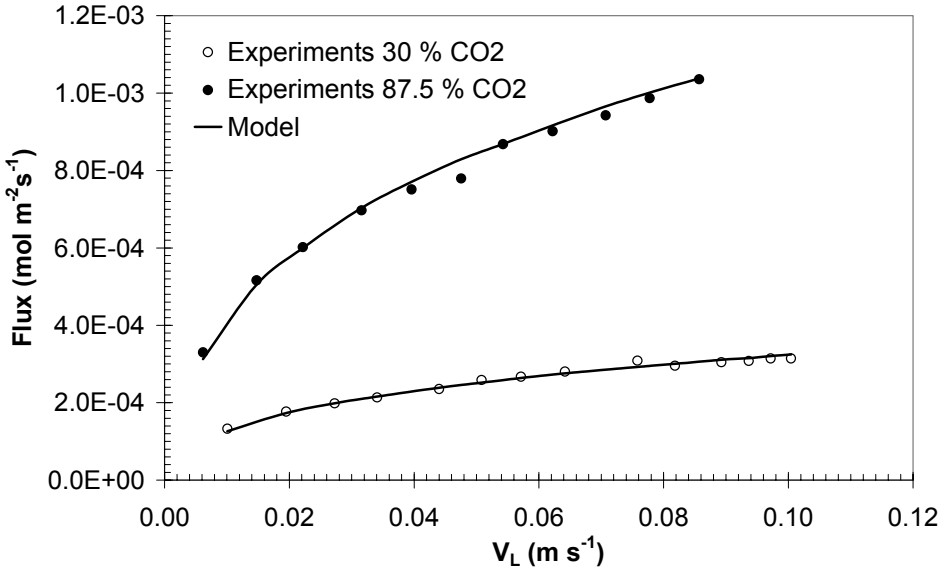

Figure 9: *Effect of liquid velocity on the absorption flux (module II).*

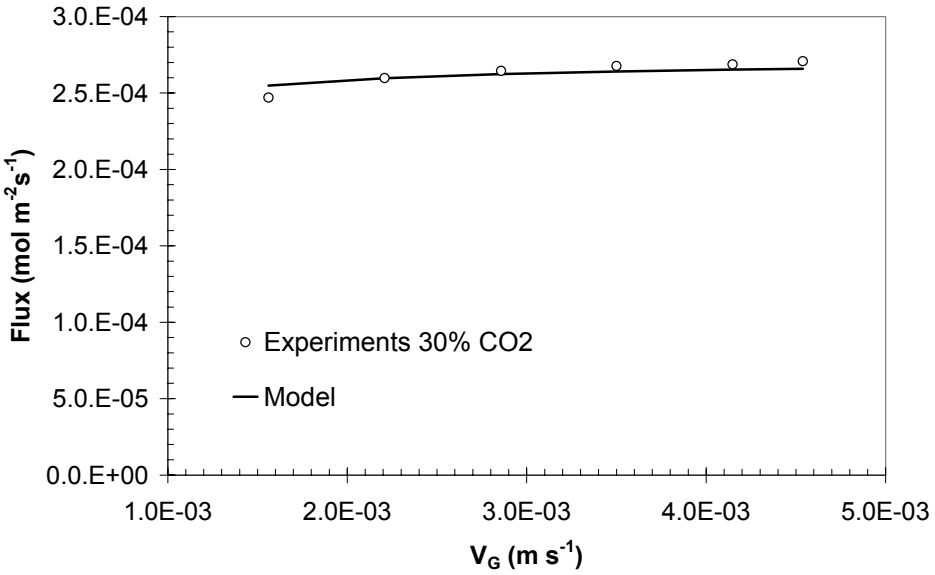

Figure 10: *Effect of gas velocity on the absorption flux (module II).*

Similar results are obtained for absorption of carbon dioxide using the larger module I. The results are presented in the Figure 11 and 12. The gas flow rate during the experiment was kept constant at 16.1 lit/min for the absorption of 70 %-30 % carbon dioxide-nitrogen mixture and at 13.3 lit/min for the absorption of 30 %-70 % carbon dioxide-nitrogen mixture. The percentage removal of carbon dioxide in both experiments was very low due to the low gas residence time, typically below 8 %. Hence the heat transfer analogies prediction about gas outlet concentration is in good agreement with the experiments.

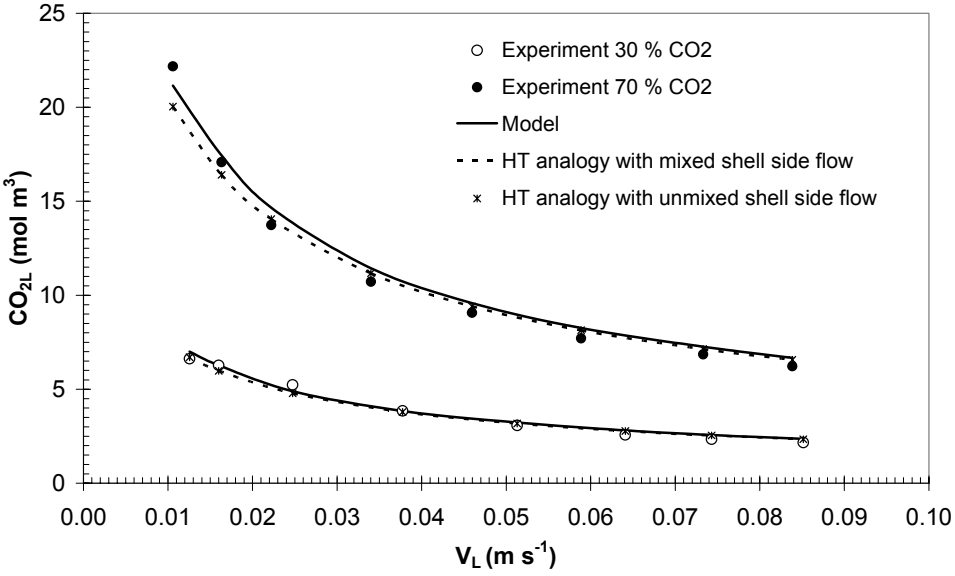

Figure 11: *Effect of liquid velocity on the liquid outlet concentration for absorption in module I.*

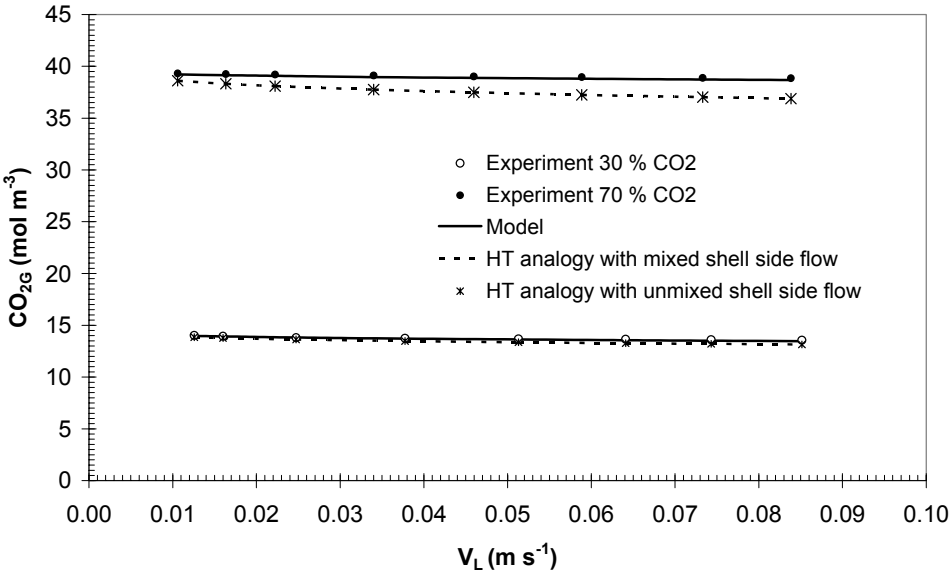

Figure 12: *Effect of liquid velocity on the gas outlet concentration for absorption in module I.*

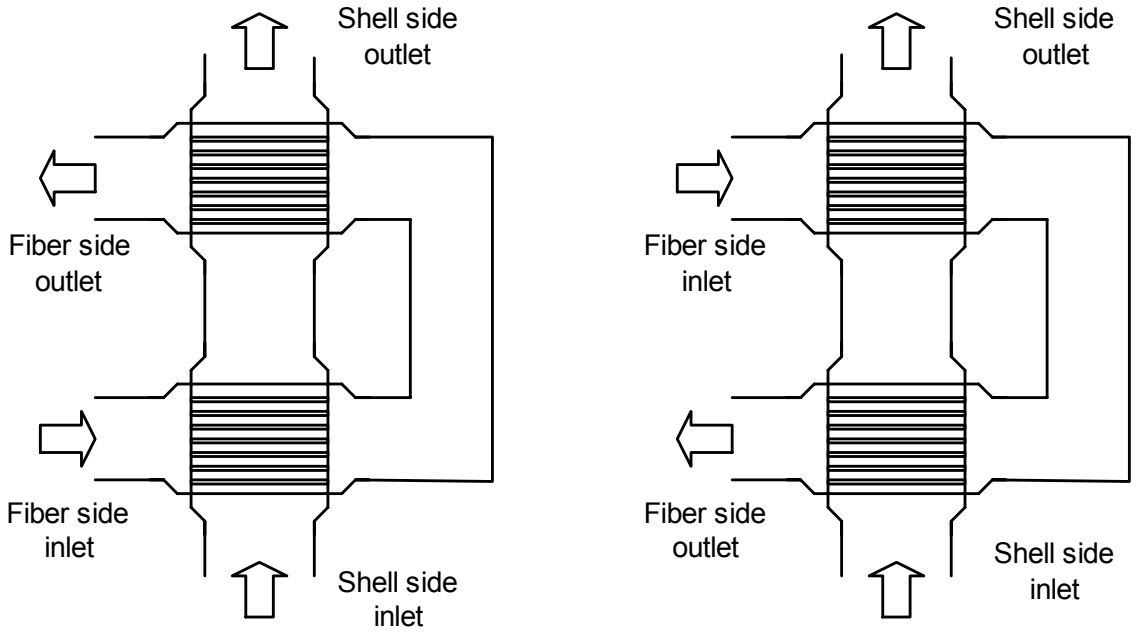

Figure 13: *Co-current and counter-current arrangement of two modules in series.*

4.2 Absorption experiments with two modules in series

Cascading of two or more membrane contactors can be applied to affect the overall contact pattern of the process. In a single module both fluids are in cross-current contact via this cascading an overall counter-current and/or a co-current pattern can be realized while maintaining the advantages if cross flow operation at each stage. The co-current and counter current flow arrangement is shown in Figure 13. For any set of concentrations, the average

concentration difference for counter-current operation is higher compared to the co-current. Therefore the performance of the counter-current flow arrangement is generally assumed to be better as compared to the co-current flow arrangement for the process involving equilibria.

Absorption of carbon dioxide from 70 %-30 % carbon dioxide-nitrogen mixture is carried out to study the effect of flow arrangement. The results are shown in Figure 14. The figure shows the effect of the liquid velocity on the absorption flux for a cascade of two modules. Hardly any difference is obtained between these two cases. This can be attributed to the relatively small percentage removal (less than 20%) which is in line with the observations are made by Wang & Cussler (1993). The numerical model also gives similar results indicating no significant difference in the co-current or counter current flow. However, the numerical model indicates that, as expected, at higher velocities the flux obtained in the counter current flow is slightly higher than in the co-current flow arrangement. It should be noted that in the case of counter-current operation for the model, the exit gas concentration and the gas flow rate must be guessed to start the calculations. In actual model, the uniform feed concentration would result in a concentration and flow gradient in the gas leaving the final segment. Thus in principle gas outlet concentration and flow gradient must be guessed to start the calculation, which results into complex and tedious calculation. To make the calculation routine easy, the uniform gas outlet concentration and uniform gas flow for each module were guessed. Thus the calculations result into concentration and flow gradient in the incoming feed even though the actual feed has no gradient. The mixing cup concentration of the incoming feed is then compared with the known feed concentration and guess of exit concentration could be adjusted if necessary.

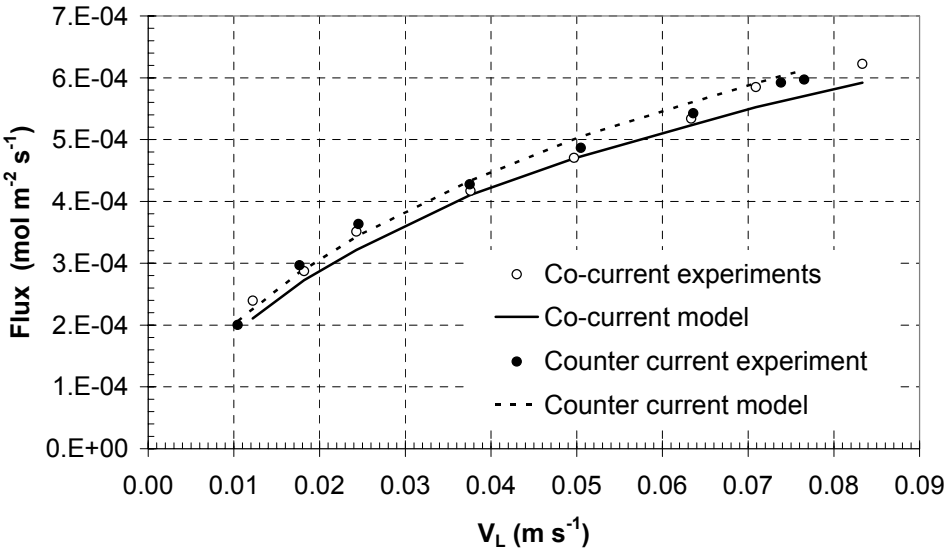

Figure 14: *Effect of module arrangement on the absorption flux.*

4.3 Performance analysis of cross flow membrane module with the numerical model

The numerical model is useful for calculating the two dimensional concentration profiles on the shell and fiber side and thus calculating the local driving force. The understanding of the driving force and concentration profiles within the modules is useful to optimize the flux in the module and thus selecting the ideal operating conditions. Numerical simulations are carried out for the absorption of carbon dioxide into fresh unloaded water using TNO modules (module type I) to study the effect of operating conditions on the shell side concentration profiles. The shell side flow is divided into 20 cells along the length of the fiber and 70 cells (equal to the number of fibers) in the direction of gas flow and no mixing (in the direction normal to the gas flow) between the cells is assumed. In this way maximum variation in the shell side gas concentration over the module is obtained. Figure 15 shows the shell side gas concentration for three different values of percentage removals.

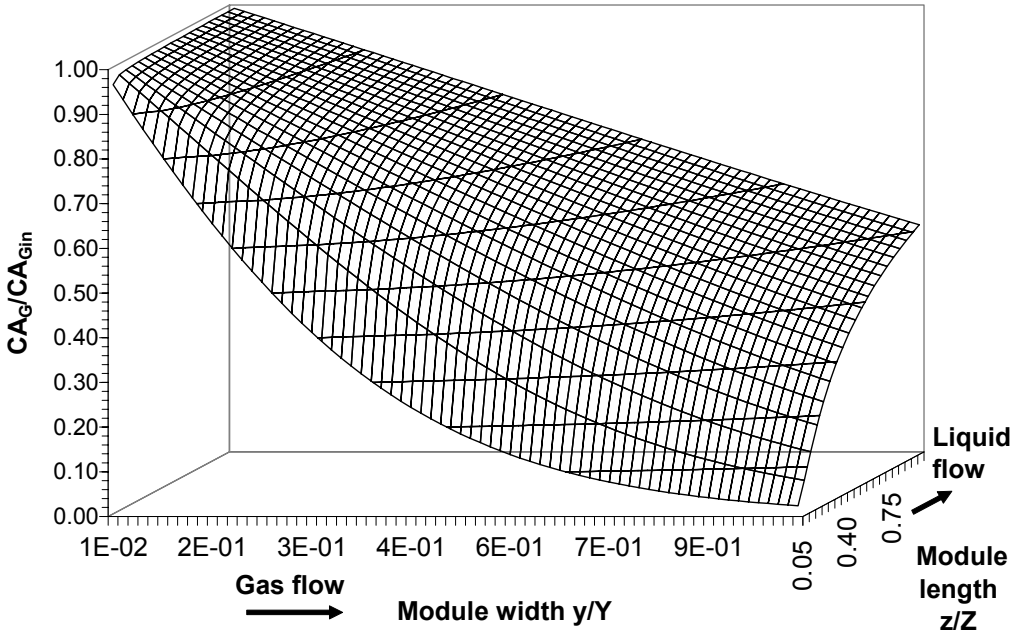

Figure 15a: *Shell side concentration profile at 70 % removal.*

When percentage removal is 70 %, most of the solute is removed from the gas phase. It can be seen from the figure that drop in the shell side solute concentration in the direction of gas flow is very sharp at the liquid entrance as compared to the liquid exit. This is because the driving force is largest in the module where gas first meets the clean unloaded liquid. However, at the liquid exit, the liquid is partially loaded with the solute and hence the decrease in the shell side solute concentration near the liquid exit is smaller. The combination of these effects results into reversal of the concentration driving force gradient along the length of fiber near the gas exit. The shell side concentration profile is also useful in identifying less efficient/dead zone for mass transfer. The region near the liquid entrance and

the gas exit has very low gas concentration and therefore is less efficient in the mass transfer process. In such case, the installation of baffles perpendicular to gas flow will improve on the mixing or reversal of the liquid flow direction will improve the overall driving force.

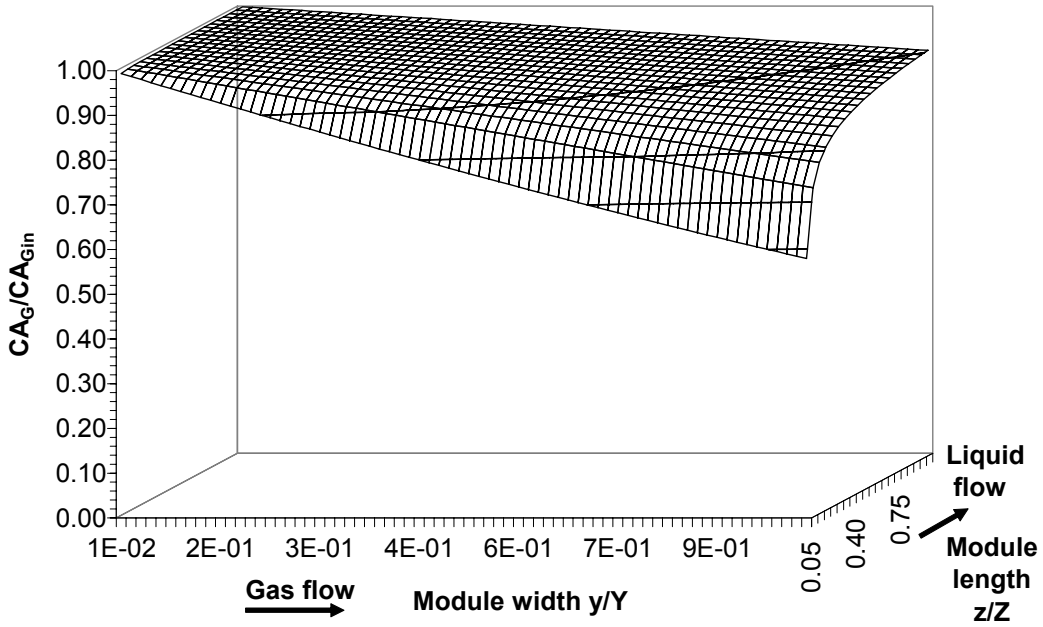

Figure 15b: *Shell side concentration profile at 20 % removal.*

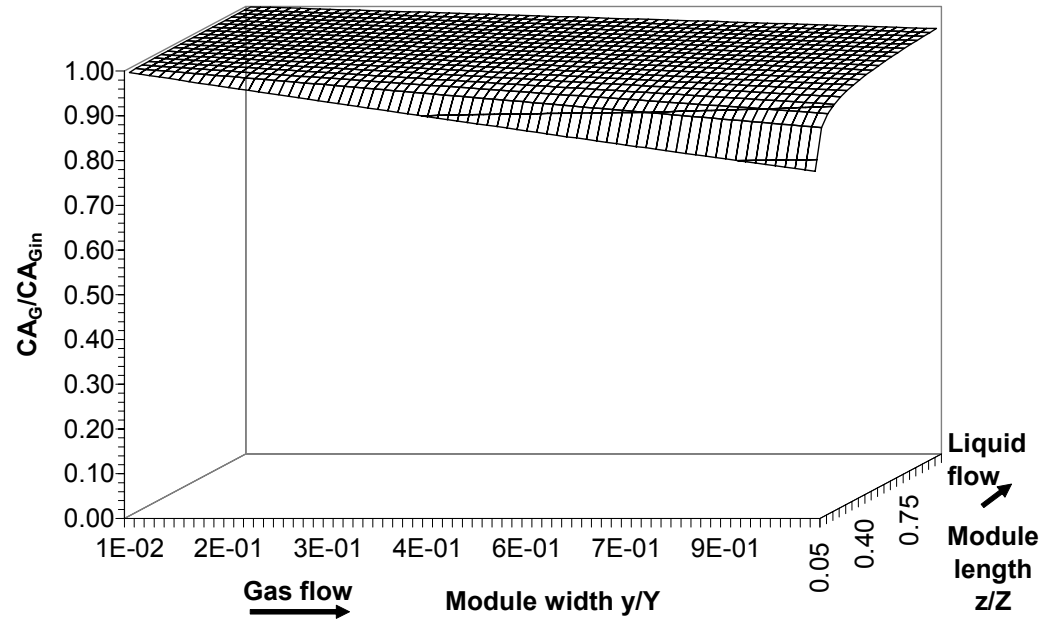

Figure 15c: *Shell side concentration profile at 10 % removal.*

By increasing the gas flow rate, the percentage removal as well as the shell side gas concentration decreases as shown in the case percentage removal 20% and 10 % (refer Figure 15b and 15c). At very high gas flow rates, there would be hardly a gradient in the shell side gas concentration. In this case, the liquid outlet concentration and the mass transfer flux can be calculated by a simple mass balance across the whole module.

The sensitivity of the numerical model with respect to the shell side mixing rules is also analyzed. Numerical simulations are carried out for the absorption of 30-70 % carbon dioxide-nitrogen mixture into fresh unloaded water using TNO module at different operating conditions to get different removal rates. Figure 16 shows the percentage deviation in the outlet gas concentration obtained between compete mixing on shell side and no mixing on the shell side as a function of removal percentage. The percentage error is defined as the relative difference between the outlet concentrations obtained with complete mixing on shell side i.e. using single cell and the outlet concentration obtained using multi-cells on shell side with no mixing among the cells. It can be seen from the figure that at low percentage of removal both mixing patterns give the same outlet concentrations. However, at higher percentages of removal the deviation in outlet concentration increases substantially. This is because at a higher percentage of removal, the concentration gradient on shell side is steep. Hence the number of cells and mixing pattern has a significant effect on the performance of the module. At low percentage of removal the shell side concentration profile is flat and the mixing between the cells becomes unimportant.

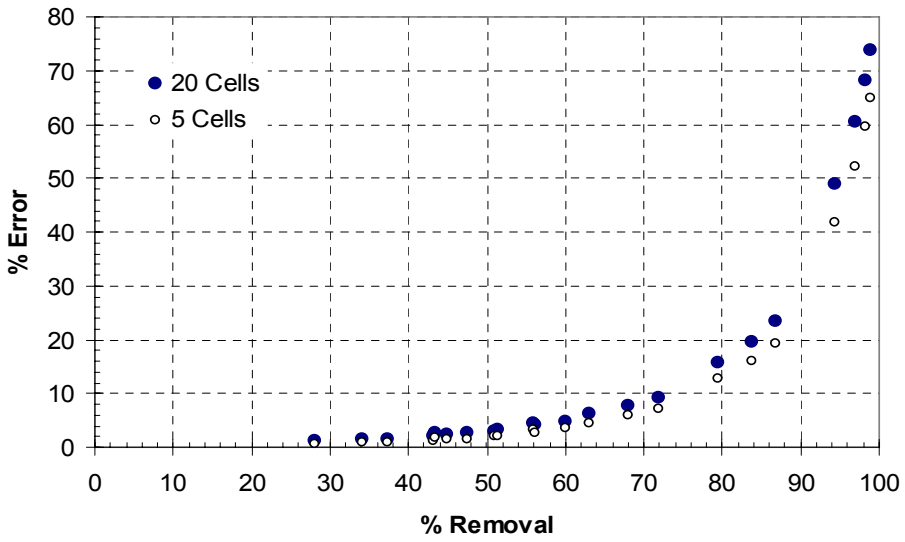

Figure 16: *Effect of shell side mixing on the gas outlet concentration.*

4.4 Heat transfer analogies predictions

As discussed in Section 4.1, the heat transfer analogies can be used to predict the outlet concentrations of the cross flow module when the change in the volumetric flow rate of the gas is very small and can be neglected. This necessary condition is achieved at low percentage removal and/or low solute gas concentrations. The heat transfer analogies with no mixing on the shell side can also be used to predict local concentration profiles and average outlet concentration of the module within the limiting conditions. Figures 17a, b, and c indicate the local concentration on the shell side, local concentration on the fiber side and local driving force within the membrane gas liquid contactor respectively. Eqs. (C30), (C40) and (C41) from Appendix 'C' are used to calculate local concentration driving force, local liquid concentration and local gas concentration respectively. The concentrations and driving force are plotted as a function of normalized x and y dimensions as 'a' and 'b'. The liquid flows in the direction of 'x' or 'a' through the fiber and gas flows on the shell side in the direction of 'y' or 'b' (refer Figure 1). Thus the fresh liquid meets feed gas at a=0 and b=0.

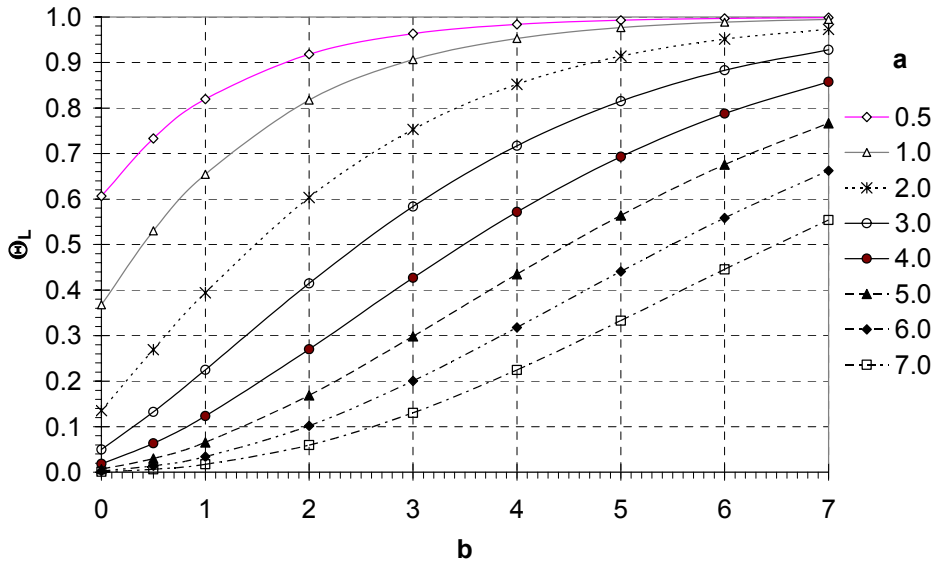

Figure 17a: *Local fiber side concentration within the membrane contactor.*

As can be seen from the Figure 17a, when 'b' increases the dimensionless liquid concentration Θ_L increases i.e. local liquid concentration decreases (see the definition of dimensionless liquid concentration) in the direction of the gas flow. This is obvious since the gas concentration decreases in the direction of the gas flow. The dimensionless liquid concentration Θ_L decreases in the direction of the liquid flow i.e. liquid local concentration increases in the direction of liquid flow due to liquid saturation.

Figure 17b indicates the shell side gas concentration profile of the module. The shell side solute dimensionless concentration Θ_G decreases with 'a', i.e. local shell side

concentration increases with 'a'. This is due to saturation of the liquid increases with 'a' and hence amount of gas absorbed decreases with 'a' thus increasing the local shell side concentration. As expected Θ_G increases with 'b', i.e. local shell side concentration decreases in direction of the gas flow.

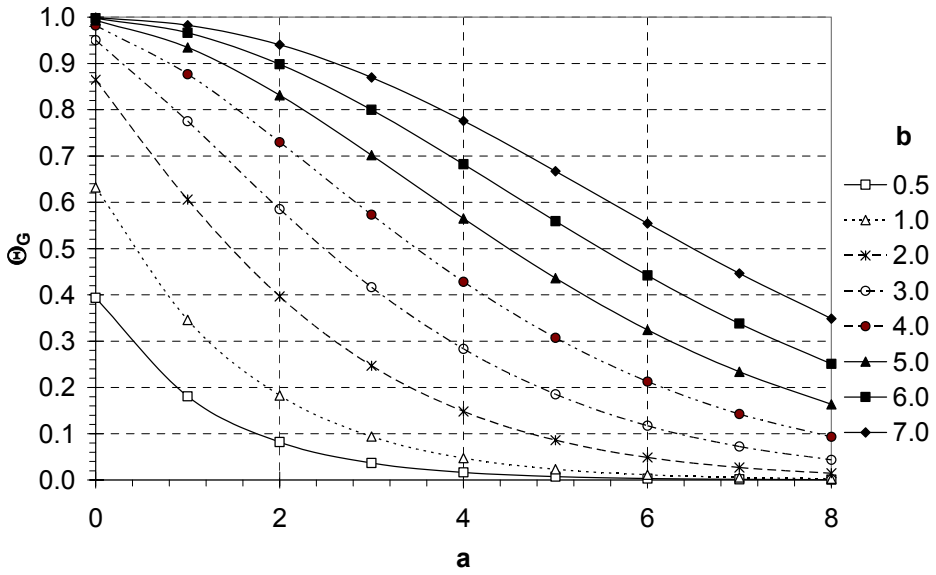

Figure 17b: *Local shell side concentration within the membrane contactor.*

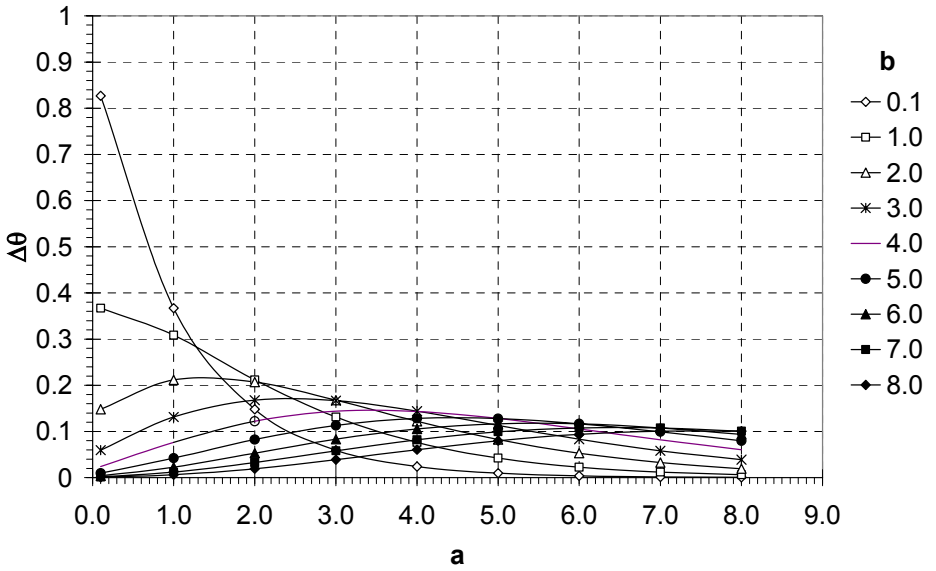

Figure 17c: *Local concentration driving force within the membrane contactor.*

Figure 17c shows the dimensionless driving force as a function of the normalized module dimensions. The local concentration driving force goes through maxima. This driving force is greatest at the corner of the module where the gas first meets unloaded solvent. Due to this maximum the gas leaving that region will be depleted much faster in the solute

concentration and thus driving force is decreases sharply along the edge of gas entrance. As liquid flows past this maximum driving force corner, its increased solute concentration and decreased solute concentration in the gas phase reduces the driving force. Hence, less solute is absorbed by the liquid flowing through the fibers and eventually increasing again the driving force and shifting its position towards the opposite corner.

5.0 Conclusion

In the present study, physical gas absorption in a rectangular cross flow membrane gas liquid contactor is discussed in details. Experiments are carried out to study the effect of various parameters such as gas and liquid flow rates, solute concentration in the feed stream on the performance of the rectangular cross flow membrane gas-liquid contactors. The possibility of application of the cross flow heat exchanger analogy in the limiting cases to the cross flow membrane gas-liquid contactor is also explored. At low removal rates and/or low solute concentrations in the feed stream the experimental results match very well with the predictions of heat transfer analogies. Thus the cross-flow heat exchanger analogy can be used to predict concentration profiles and local driving force when percentage removals and solute concentrations in the feed stream are low. However, at the higher percentage of removals and at higher solute concentrations the change in the volumetric flow is significant and heat transfer analogies can no longer be used to predict the performance of the cross flow gas-liquid membrane contactor. In the case of absorption of the pure gas in the membrane contactor the absorption results into decrease in the volumetric flow rate. To predict the performance of the cross flow membrane contactor in such cases a more detailed mathematical model is developed. The predictions of the developed numerical model are in good agreement with the experimental results. Three different mixing patterns namely; complete mixing, no mixing and dispersive mixing on the shell side are considered. The numerical simulations show that the type of shell side mixing is important at high percentages of solute removal. At low percentage of removal all mixing rules give same results. At higher percentage of removal no mixing on the shell side gives better performance.

The strong dependence of the absorption flux on the liquid velocity confirms the observation that in the case of physical absorption controlling mass transfer resistance lies on the liquid side. The experimental study of co-current and counter-current arrangements for small stack of two modules showed no significant difference in the performance of the module. This, however, can be attributed to the small percentage of removal obtained in the lab scale modules. Nonetheless, at higher rate of removal overall counter current arrangement gives better performance.

Acknowledgement

This research is part of the research program performed within the Centre for Separation Technology (CST), which is a co-operation between the Netherlands Organization for Applied Scientific Research (TNO) and the University of Twente. We acknowledge Benno Knaken and Wim Leppink for the construction of the experimental set-ups.

Nomenclature

a	Dimensionless x-coordinate	[-]
A	Area	[m^2]
b	Dimensionless y-coordinate	[-]
C	Concentration	[mol m^{-3}]
D	Diffusivity	[m^2 s^{-1}]
d	Diameter	[m]
E	Dispersion coefficient	[m^2 s^{-1}]
J	Flux	[mol m^{-2} s^{-1}]
K	Mass transfer coefficient	[m s^{-1}]
L	Length	[m]
m	Distribution coefficient	[-]
Q	Flow rate	[m^3 s^{-1}]
R	Radius	[m]
Re	Reynolds number	[-]
Sc	Schmidt number	[-]
Sh	Sherwood number	[-]
t	Time	[s]
v	Velocity	[m s^{-1}]
W	Mass transfer rate	[mol s^{-1}]
X	x-dimension of module	[-]
Y	y-dimension of module	[-]
z	Length	[m]

Greek letters

Θ	Dimensionless concentration
θ	Dimensionless time
Φ	Fiber packing density

Subscript

1	Fluid 1
2	Fluid 2
e	Exit/equivalent

G	Gas
i	Inlet
j	Component ‘j’
L	Liquid
t	Tube side
s	Shell side
xm	Average value
z	Local value

References

Ahmed, T., & Semmens, M.J. (1996). Use of transverse flow hollow fibers for bubbleless membrane aeration. *Water Research,* **30**, 440-446.

Bhaumik, D., Majumdar, S., & Sirkar, K.K. (1998). Absorption of CO_2 in a transverse flow hollow fiber membrane module having a few wraps of the fiber mat. *Journal of Membrane Science,* **138,** 77-82.

Costello, M.J., Fan, A.G. P., Hogan, A., & Schofield, R.W. (1993). The effect of shell side hydrodynamics on the performance of the axial flow hollow fiber modules. *Journal of Membrane Science,* **80**, 1-11.

Cote, P., Bersillon, J., & Huyard, A. (1989). Bubble free aeration using membranes: mass transfer analysis. *Journal of Membrane Science,* 47, 91-106.

Duhuron, L. & Cussler, E.L. (1988). Protein extractions with hollow fibers. *A.I.Ch.E. Journal,* **34(1)**, 130-136.

Dindore, V.Y., Brilman, D.W.F., Feron P.H.M., Geuzebroek, F.H., & Versteeg G.F. (2003). Shell side dispersion coefficients of rectangular cross flow hollow fiber membrane module. (To be published, Chapter 3 of this thesis).

Feron, P.H.M. Jansen, A.E., & Klassen, R. (1992). Membrane technology in carbon dioxide removal. Energy *Conservation and Management,* **33**, 5-8:421-428.

Feron, P.H.M., Jansen, A.E., Klaassen, R., Hanemaaijer, J.H., & ter Meulen, B.Ph. (1994). Membrane gas absorption processes in environmental applications *in Membrane Processes in Separation and Purification* (Edited by J.G. Crespo and K.W. Boddeker). Dordrecht: Kluwer Academic.

Hoffman, A. (2000). Theoretical solution for cross flow heat exchanger. *Heat and Mass Transfer*, **36,** 127-133.

Nusselt, W. (1911). Der warmeubergang im kreuzstorm. *Zeitschrift des Vereines deutscher Ingenieur,* **55,** 2021-2024.

Prasad, R., & Sirkar, K.K. (1988). Dispersion free solvent extraction with microporous hollow fiber modules. *A.I.Ch.E. Journal,* **34(2),** 177-188.

Schoner, P., Plucinski, P., Nitsch, W., & Daiminger, U. (1998). Mass transfer in the shell side of cross flow hollow fiber modules. *Chemical Engineering Science*, **53 (13),** 2319-2326.

Smith, D. M. (1934). Mean temperature difference in cross flow. *Engineering,* **138,** 479-482 & 606-607.

Viegas, R.M.C., Rodriguez, M., Luque, S., Alvarez, J.R., Coelhoso, I.M., & Crespo, J.P.S.G., (1998). Mass transfer correlations in membrane extraction: analysis of Wilson-Plot methodology. *Journal of Membrane Science,* **145**, 129-142.

Wang, K.L., & Cussler, E.L. (1993). Baffled membrane modules made with hollow fiber fabric. *Journal of Membrane Science,* **85,** 265-278.

Westerterp, K.R., Van Swaaij, W.P.M., & Beenackers, A.A.C.M. (1984). *Chemical reactor design and operation*. New York: John Wiley & Sons.

Wickramasinghe, S.R., Semmens, M.J., & Cussler, E.L. (1992). Mass transfer in various hollow fiber geometries. *Journal of Membrane Science,* **69**, 235-250.

Wu, J., & Chen, V. (2000). Shell-side mass transfer performance of randomly packed hollow fiber modules. *Journal of Membrane Science,* **172**, 59-74.

Yang, M.C., & Cussler, E.L. (1986). Designing hollow fiber contactors. *A.I.Ch.E. Journal,* **32(11),** 1910-1916.

Appendix C

Analytical solutions for gas and liquid concentrations in cross flow hollow fiber membrane contactors

C 1: Both fluids unmixed

Taking a mass balance across a small rectangular element of area *dxdy* (see Figure 1 of Chapter 4), two partial differential equations can be obtained.

$$\frac{\partial C_1}{\partial y} = -\frac{KX}{Q_1}\left(mC_1 - C_2\right) \tag{C1}$$

$$\frac{\partial C_2}{\partial x} = \frac{KY}{Q_2}\left(mC_1 - C_2\right) \tag{C2}$$

Using new variables to make these equations dimensionless

$$a = \frac{KY}{Q_2}x \tag{C3}$$

$$b = \frac{KX}{Q_1}y \tag{C4}$$

Using Eqs. (C3) and (C4) in Eqs. (C1) and (C2)

$$\frac{\partial C_1}{\partial b} = -\left(mC_1 - C_2\right) \tag{C5}$$

$$\frac{\partial C_2}{\partial a} = \left(mC_1 - C_2\right) \tag{C6}$$

Differentiating Eq. (C6) with 'b' and using Eq. (C5)

$$\frac{\partial^2 C_2}{\partial a \partial b} + m\frac{\partial C_2}{\partial a} + \frac{\partial C_2}{\partial b} = 0 \tag{C7}$$

Similarly equation for C_1 can be obtained by differential Eq. (C5) with 'a' and using Eq. (C6)

$$\frac{\partial^2 C_1}{\partial a \partial b} + m\frac{\partial C_1}{\partial a} + \frac{\partial C_1}{\partial b} = 0 \tag{C8}$$

The equation of the local concentration gradient can be obtained and written as follows

$$\frac{\partial^2 (mC_1 - C_2)}{\partial a \partial b} + m\frac{\partial (mC_1 - C_2)}{\partial a} + \frac{\partial (mC_1 - C_2)}{\partial b} = 0 \tag{C9}$$

In order to find a solution of Eq. (C9) we follow the procedure given by Hoffman (2000). For the local concentration difference of the two fluids following assumption of the solution is made.

$$\left(mC_1 - C_2\right) = e^{-(a+mb)}.\Delta(a;b) \tag{C10}$$

where $\Delta(a;b)$ is an unknown function of 'a' and 'b' which has to be determined. Now we separate $\Delta(a;b)$ from Eq. (C10) and differentiate w.r.t. 'a' and then w.r.t. 'b'.

$$\Delta(a;b) = \left(mC_1 - C_2\right)e^{(a+mb)} \tag{C11}$$

$$\frac{\partial^2 \Delta(a;b)}{\partial a \partial b} = e^{(a+mb)}\left[\frac{\partial^2 (mC_1 - C_2)}{\partial a \partial b} + m\frac{\partial (mC_1 - C_2)}{\partial a} + \frac{\partial (mC_1 - C_2)}{\partial b}\right] + e^{(a+mb)}(mC_1 - C_2) \tag{C12}$$

As the value in bracket is zero from Eq. (C9), we obtain the condition for the unknown function.

$$\frac{\partial^2 \Delta(a;b)}{\partial a \partial b} = m\Delta(a;b) \tag{C13}$$

For the function $\Delta(a;b)$, the following polynomial can be introduced.

$$\Delta(a;b) = A_0(ab)^0 + A_1(ab)^1 + A_2(ab)^2 + \ldots\ldots + A_N(ab)^N \tag{C14}$$

Substituting Eq. (C14) in Eq. (C13)

$$\frac{\partial^2 \Delta(a;b)}{\partial a \partial b} = 0 + A_1(ab)^0 + A_2 4(ab)^1 + A_3 9(ab)^2 \ldots\ldots + A_N N^2 (ab)^{N-1} \tag{C15}$$

From Eq. (C13), (C14) and (C15) we obtain

$$A_1(ab)^0 + A_2 4(ab)^1 + A_3 9(ab)^2 \ldots\ldots + A_N N^2 (ab)^{N-1} = m\left[A_0(ab)^0 + A_1(ab)^1 + A_2(ab)^2 + \ldots\ldots + A_N(ab)^N\right] \tag{C16}$$

The comparison of coefficient leads to,

$$(ab)^0 : A_1 = mA_0 \rightarrow A_1 = \frac{mA_0}{1^2} \tag{C17}$$

$$(ab)^1 : 4A_2 = mA_1 \rightarrow A_2 = \frac{mA_1}{2^2} = \frac{m^2 A_0}{1^2.2^2} \tag{C18}$$

$$(ab)^2 : 9A_3 = mA_2 \rightarrow A_3 = \frac{mA_2}{3^2} = \frac{m^3 A_0}{1^2.2^2.3^2} \tag{C19}$$

From Eqs. (C17) to (C19) we can see that the coefficient can be expressed in the form

$$A_N = \frac{m^N A_0}{(N!)^2} \tag{C20}$$

Eq. (14) can be rewritten using Eq. (20) as

$$\Delta(a;b) = \frac{m^0 A_0}{(0!)^2}(ab)^0 + \frac{m^1 A_0}{(1!)^2}(ab)^1 + \frac{m^2 A_0}{(2!)^2}(ab)^2 + \ldots\ldots + \frac{m^N A_0}{(N!)^2}(ab)^N \tag{C21}$$

$$\Delta(a;b) = A_0 \sum_{N=0}^{\infty} \frac{(mab)^N}{(N!)^2} \tag{C22}$$

From Eq. (C10) and substituting the function $\Delta(a;b)$ from Eq. (C22), we obtain local concentration difference of the two fluids.

$$\left(mC_1 - C_2\right) = e^{-(a+mb)} A_0 \sum_{N=0}^{\infty} \frac{(mab)^N}{(N!)^2} \tag{C23}$$

The constant A_0 has to be determined from the boundary conditions.

$$x = 0; \rightarrow a = 0; \rightarrow C_1 = C_{1,i} \tag{C24}$$

$$y = 0; \rightarrow b = 0; \rightarrow C_2 = C_{2,i} \tag{C25}$$

From Eqs. (C24), (C25) and (C23) we obtain:

$$\left(mC_{1,i} - C_{2,i}\right) = A_0 \tag{C26}$$

Eq. (C23) can be rewritten by using Eq. (26)

$$\frac{\left(mC_1 - C_2\right)}{\left(mC_{1,i} - C_{2,i}\right)} = e^{-(a+mb)} \sum_{N=0}^{\infty} \frac{(mab)^N}{(N!)^2} \tag{C27}$$

With Eq. (C27) the local concentration difference of the two fluids at any point of the contactor can be calculated. The Eq. (C27) also represents the ratio of local driving force to the maximum driving force. It is only a function of the dimensionless variables ‘a’ and ‘b’. For variable ‘a’ all values from a = 0 for x = 0 to a = a_{max} for x = X are possible and also for variable ‘b’ all values from b = 0 for y = 0 to b = b_{max} for y = Y are possible.

The local dimensionless concentrations are defined as follows:

Local dimensionless concentration of fluid 1:

$$\Theta_1 = \frac{\left(mC_{1,i} - mC_1\right)}{\left(mC_{1,i} - C_{2,i}\right)} \tag{C28}$$

Local dimensionless concentration of fluid 2:

$$\Theta_2 = \frac{\left(mC_{1,i} - C_2\right)}{\left(mC_{1,i} - C_{2,i}\right)} \tag{C29}$$

Local concentration difference at any point of the contactor

$$\Delta\Theta = \Theta_2 - \Theta_1 = \frac{\left(mC_1 - C_2\right)}{\left(mC_{1,i} - C_{2,i}\right)} = e^{-(a+mb)} \sum_{N=0}^{\infty} \frac{(mab)^N}{(N!)^2} \tag{C30}$$

The next step is to find out the local concentration of the fluid 1 'C_1' or corresponding dimensionless concentrations 'Θ_1'. Substituting Eq. (C27) in Eq. (C5) and integrating the equation along the constant 'a' line. Let this constant 'a' line has upper limit 'b^*'.

$$\frac{\partial C_1}{\partial b} = -\left(mC_{1,i} - C_{2,i}\right) e^{-(a+mb)} \sum_{N=0}^{\infty} \frac{(mab)^N}{(N!)^2} \tag{C31}$$

$$\int_{C_{1,i}}^{C_1} \partial C_1 = -\left(mC_{1,i} - C_{2,i}\right) \int_0^{b^*} e^{-(a+mb)} \sum_{N=0}^{\infty} \frac{(mab)^N}{(N!)^2} \partial b \tag{C32}$$

$$\frac{\left(C_1 - C_{1,i}\right)}{\left(mC_{1,i} - C_{2,i}\right)} = -\int_0^{b^*} e^{-(a+mb)} \sum_{N=0}^{\infty} \frac{(mab)^N}{(N!)^2} \partial b \tag{C33}$$

Eq. (C33) can be rearranged to get following equation

$$\Theta_1 = m \int_0^{b^*} e^{-(a+mb)} \sum_{N=0}^{\infty} \frac{(mab)^N}{(N!)^2} \partial b \tag{C34}$$

Similarly the equation for the local concentration of fluid 2 'C_2' or the corresponding dimensionless concentration 'Θ_2' can be obtained by substituting Eq. (C27) in Eq. (C6) and integrating the equation along the constant 'b' line. Let this constant 'b' line has upper limit 'a^*'.

$$\frac{\partial C_2}{\partial a} = \left(mC_{1,i} - C_{2,i}\right) e^{-(a+mb)} \sum_{N=0}^{\infty} \frac{(mab)^N}{(N!)^2} \tag{C35}$$

$$\int_{C_{2,i}}^{C_2} \partial C_2 = \left(mC_{1,i} - C_{2,i}\right) \int_0^{a^*} e^{-(a+mb)} \sum_{N=0}^{\infty} \frac{(mab)^N}{(N!)^2} \partial a \tag{C36}$$

$$\frac{\left(C_2 - C_{2,i}\right)}{\left(mC_{1,i} - C_{2,i}\right)} = \int_0^{a^*} e^{-(a+mb)} \sum_{N=0}^{\infty} \frac{(mab)^N}{(N!)^2} \partial a \tag{C37}$$

Eq. (C37) can be rearranged as follows

$$\frac{\left(mC_{1,i} - C_{2,i}\right)}{\left(mC_{1,i} - C_{2,i}\right)} - \frac{\left(mC_{1,i} - C_2\right)}{\left(mC_{1,i} - C_{2,i}\right)} = 1 - \Theta_2 = \int_0^{a^*} e^{-(a+mb)} \sum_{N=0}^{\infty} \frac{(mab)^N}{(N!)^2} \partial a \tag{C38}$$

$$\Theta_2 = 1 - \int_0^{a^*} e^{-(a+mb)} \sum_{N=0}^{\infty} \frac{(mab)^N}{(N!)^2} \partial a \tag{C39}$$

Thus the local concentration of the fluid 1 and fluid 2 is given by Eq. (C34) and (C39) respectively. The solution of the integral can be found easily. The final equations for the local concentrations are summarized below.

$$\Theta_1 = me^{-a} \sum_{N=0}^{\infty} \frac{a^N}{N!m} \left(1 - e^{-mb^*} \sum_{N=0}^{N} \frac{(mb^*)^N}{N!}\right) \tag{C40}$$

$$\Theta_2 = 1 - e^{-mb} \sum_{N=0}^{\infty} \frac{(mb)^N}{N!} \left(1 - e^{-a^*} \sum_{N=0}^{N} \frac{(a^*)^N}{N!}\right) \tag{C41}$$

At the outlet of the fluid 2, where x= X or $a^* = a^*_{\max}$, the local concentration 'C_2' or corresponding dimensionless concentration 'Θ_2' is only function of 'b'. Since all concentration mix at outlet, the mean outlet concentration is given by

$$\Theta_{2xm} = \frac{\left(mC_{1,i} - C_{2xm}\right)}{\left(mC_{1,i} - C_{2,i}\right)} \tag{C42}$$

$$\Theta_{2xm} = \frac{1}{b^*} \int_0^{b^*} \Theta_2 \partial b \tag{C43}$$

Using Eq. (C40) one can obtain the final solution.

$$\Theta_{2xm} = 1 - \frac{1}{mb^*} \sum_{N=0}^{\infty} \left(1 - e^{-mb^*} \sum_{N=0}^{N} \frac{(mb^*)^N}{N!}\right) \left(1 - e^{-a^*} \sum_{N=0}^{N} \frac{(a^*)^N}{N!}\right) \tag{C44}$$

Similarly at the outlet of the fluid 1, where y= Y or $b^* = b^*_{\max}$, the local concentration 'C_1' or corresponding dimensionless concentration 'Θ_1' is only function of 'a'. Since all concentration mix at outlet, the mean outlet concentration for fluid 1 is given by

$$\Theta_{1xm} = \frac{\left(mC_{1,i} - mC_{1xm}\right)}{\left(mC_{1,i} - C_{2,i}\right)} \tag{C45}$$

$$\Theta_{1xm} = \frac{1}{a^*}\int_0^{a^*} \Theta_1 \partial a \tag{C46}$$

The final equation is given by

$$\Theta_{1xm} = \frac{1}{a^*}\sum_{N=0}^{\infty}\left(1 - e^{-a^*}\sum_{N=0}^{N}\frac{(a^*)^N}{N!}\right)\left(1 - e^{-mb^*}\sum_{N=0}^{N}\frac{(mb^*)^N}{N!}\right) \tag{C47}$$

The mean effective concentration difference $(\Delta C)_m$ can be obtained by integrating the local concentration difference over the entire area of module. The total molar flux in the module is given by

$$W = KA(\Delta C)_m \tag{C48}$$

The dimensionless mean concentration is defined as follows

$$\Delta\Theta_m = \frac{(\Delta C)_m}{\left(mC_{1,i} - C_{2,i}\right)} \tag{C49}$$

$$\Delta\Theta_m = \frac{1}{a^* b^*}\int_0^{a^*}\int_0^{b^*} \Delta\Theta \partial a \partial b \tag{C50}$$

From Eq. (30)

$$\Delta\Theta_m = \frac{1}{a^* b^*}\int_0^{a^*}\int_0^{b^*} e^{-(a+mb)}\sum_{N=0}^{\infty}\frac{(mab)^N}{(N!)^2}\partial a \partial b \tag{C51}$$

The final solution is given by

$$\Delta\Theta_m = \frac{1}{a^* mb^*}\sum_{N=0}^{\infty}\left(1 - e^{-a^*}\sum_{N=0}^{N}\frac{(a^*)^N}{N!}\right)\left(1 - e^{-mb^*}\sum_{N=0}^{N}\frac{(mb^*)^N}{N!}\right) \tag{C52}$$

C 2: One Fluid Mixed, Other unmixed

Let the shell side fluid Q_1 is flowing in y-direction and is completely mixed (refer Figure 1 of Chapter 4). The fiber side fluid Q_2 is unmixed and flowing in x-direction. Since the mixing on the shell side is assumed to be complete, C_1 is a function of y only and C_2 is function of both x and y. Consider the strip of width '*dy'* at y. The fluid flowing across this strip is having a constant concentration C_1, while the fluid flowing along the strip is unmixed and its varying concentration C_2 is determined by

$$\frac{\partial C_2}{\partial x} = \frac{KY}{Q_2}\left(mC_1 - C_2\right) \tag{C53}$$

subject to boundary condition

$$C_2 = C_{2,i} \text{ at } y = 0 \tag{C54}$$

The outlet concentration from the strip is given by

$$\frac{\left(mC_1 - C_{2x,y}\right)}{\left(mC_1 - C_{2,i}\right)} = \exp\left(\frac{-KXY}{Q_2}\right) \tag{C55}$$

The total mass transfer in the strip to the mixed shell side fluid is

$$Q_2\left(C_{2,i} - C_{2x,y}\right)\frac{dy}{Y} = Q_1 dC_1 \tag{C56}$$

Using Eq. (C55) in Eq. (C56)

$$Q_2\left(mC_1 - C_{2,i}\right)\left(exp\left(\frac{-KXY}{Q_2}\right) - 1\right)\frac{dy}{Y} = Q_1 dC_1 \tag{C57}$$

The product 'XY' is the total mass transfer area of the module. Rearranging and integrating Eq. (C57) from 0 to X and using boundary conditions at x=0; $C_1=C_{1,i}$ and at x=X, $C_1=C_{1,xm}$, the final outlet concentration of the shell side fluid can be given by

$$\Theta_{1xm} = \frac{\left(mC_{1,i} - mC_{1,xm}\right)}{\left(mC_{1,i} - C_{2,i}\right)} = 1 - \exp\left[\frac{mQ_2}{Q_1}\left(\exp\left(\frac{-KA}{Q_2}\right) - 1\right)\right] \tag{C58}$$

Chapter 5

Cross Flow Membrane Contactors: Mass Transfer with Chemical Reactions

Abstract:

Conventionally, carbon dioxide and hydrogen sulphide are absorbed using aqueous alkanolamines or carbonate solution in column type of equipment. However, in view of the unparallel advantages offered, the use of microporous hollow fiber membrane modules is an attractive alternative. In the present study application of cross-flow membrane contactor for absorption of these gases using aqueous potassium carbonate as a solvent is explored. The carbon dioxide and hydrogen sulphide absorption into aqueous solutions carbonate involves complex chemical reactions. The effect of these chemical reactions on the absorption rate into a liquid flowing though a hollow fiber membrane may not be described using mass transfer models like e.g. the penetration or surface renewal theory because of the lack of a well defined liquid phase bulk and the presence of a laminar velocity profile in the mass transfer zone. Moreover, in the case of cross flow membrane contactors, the concentrations of both fluids, inside and outside the fibers, vary in both directions i.e. in the direction of flow and in the direction normal to the flow. Hence the theoretical analysis of the cross flow membrane contactor is more complicated. To describe the effect of the chemical reaction on the absorption rate in the cross flow hollow fiber contactor, a detailed mathematical model is developed using first principles. A complete scheme of the reversible, ionic reactions and equilibria involved was implemented in the model to describe the solute uptake. The experiments are carried out study the effects various parameters such as gas and liquid velocities, bulk concentrations of solute gas and liquid phase reactant. The theoretical predictions were compared with experimental results. An excellent match between experimental results and model predictions is obtained.

1.0 Introduction

Natural gas, refinery gas contains hydrogen sulphide as a major impurity. Hydrogen sulphide is a highly toxic and corrosive gas and is one of the major sources for the environmental problems such as acid rains. Therefore, in order to utilize these fuels for chemical processing or energy generation, the concentrations of hydrogen sulphide concentration must be reduced to very low levels; less than 0.0115 g/m^3 is required for some specific applications (Strauss, 1975).

Increasing demand of energy has given more attention to the low quality natural gas containing high percentages of carbon dioxide (up to 30%). In view of high transportation cost and corrosive effects caused by carbon dioxide it is necessary to reduce the concentration of carbon dioxide to acceptable levels. Carbon dioxide is also produced whenever fossil fuels such as natural gas or coal are burned for energy generation. A typical quantity of carbon dioxide generation rate from a thermal power plant is $5x10^6$ kg/hr in the case of 600-MW coal fired plant. Emission of carbon dioxide is regarded as a serious potential cause of environmental problems such as global warming. Hence, carbon dioxide removal from these sources is important if the green house effect is to be reduced.

Both hydrogen sulphide and carbon dioxide are acidic in nature and are similar in many physical and chemical aspects. Hence the solvents used for the removal of hydrogen sulfide in gas treating process also absorb carbon dioxide. Traditionally, there has been great deal of effort in applying aqueous solutions of alkanolamines and aqueous carbonate solutions as absorbing solvents. Compared to physical solvents, enhanced absorption incorporating chemical reaction results into high selectivity and reduced solvent circulation. The most common process for removal of these gases is gas absorption using conventional absorption column such as packed or plate column. In addition to these conventional absorption processes, the use of microporous hollow fiber membrane modules is an attractive alternative. In view of the unparallel advantages offered by these hollow fiber membrane contactors, considerable academic and industrial work has been done to develop these contactors for natural gas treating (Gabelman & Hwang, 1999). However, up to now only very few of these processes have been successfully tested on a larger scale. Kvaerner Oil & Gas and W.L. Gore & Associates GmbH have been developing a membrane gas absorption process for the removal of acid gases from natural gas and exhausts of the offshore gas turbines (Hanisch, 1999). In this process, PTFE hollow fiber membranes are used in combination with physical (Morphysorb®) or chemical (alkanolamines) solvents. However, PTFE hollow fibers are not available in small diameters (few hundred microns) and are more expensive, making natural gas treating using membrane gas absorption not so attractive as compared to the conventional absorption process. TNO Environment Energy and Process Innovation (The Netherlands) have been developing a membrane gas absorption process for the removal of CO_2 from flue gases using commercially available and cheaper polypropylene

hollow fiber membranes. However, the conventional alkanolamine solutions are found to wet the polypropylene membranes. To avoid these wetting problems, TNO has developed a range of new reactive absorption liquids based on the amino acid salt solutions (Feron & Jansen, 1995). Nevertheless, these newly developed reactive solvent may suffer from the problem of precipitation of reaction products at high amine concentration and high amine loading (Kumar, 2002). The precipitation of the reaction products may result into a significant increase in the overall mass transfer resistance due to blockage of the membrane pores.

On the other hand, absorption of carbon dioxide and hydrogen sulphide into aqueous carbonate solutions using polyolefin membranes contactors has been studied experimentally by Nii et al (1993) and Chun & Lee (1997), who found that membrane modules made up of polyolefin are ideally suitable for this system. The theoretical analysis of this system is more difficult due to complex reactions involved in the system. The investigators used an overall mass transfer coefficient or simple kinetics to describe the system. The more detailed theoretical analysis of carbon dioxide absorption into potassium carbonate system using membrane contactors by Lee et al. (2001) lacks experimental validation of the system. It is important to note that all the work was carried out using parallel-flow modules, where the change is concentration of both fluids is unidirectional (i.e. in the direction of flow). In case of cross flow membrane contactors the concentrations of both fluids vary in both directions i.e. in the direction of flow and in the direction normal to the flow. Hence the theoretical analysis of cross flow membrane contactor is more difficult.

In this work, a detailed theoretical analysis is carried out for the removal of carbon dioxide and hydrogen sulphide by absorption into aqueous potassium carbonate solutions using cross flow hollow fiber membrane contactors. Complete reversible reactions scheme was included in the microscopic theoretical model equations as opposed to the use of overall mass transfer coefficient to describe solute uptake. The theoretical predictions were validated by the experimental analysis carried out using cross flow membrane contactors.

2. 0 Theory: Mass transfer with chemical reactions

2.1 Reactive absorption of carbon dioxide in aqueous carbonate solutions

Absorption of carbon dioxide into the aqueous carbonate solutions has been studied by many investigators (Roberts & Danckwerts, 1962, Hikita et al. 1976). In these studies most of the work has been carried out using high bicarbonate to the carbonate ratios. In such cases the carbon dioxide into the aqueous carbonate buffer solutions can be treated as absorption accompanied by an irreversible pseudo-first order reaction. The chemical absorption mechanism under the conditions of low or negligible bicarbonate to carbonate ratio is, however, more complex and contains two step reversible reactions (Vas Bhat et al. 1998).

When the potassium carbonate is dissolved in water it is ionized into the potassium ion (K^+) and carbonate ion (CO_3^{-2}). The bicarbonate ion (HCO_3^-) and hydroxyl ion (OH^-) are then generated by the hydrolysis of carbonate ion (inverse of reaction 2 in following reaction scheme). In the potassium carbonate aqueous solution, the various reactions taking place are given below (Hikita et al. 1976).

$$CO_2 + OH^- \underset{k_{1,2}}{\overset{k_{1,1}}{\leftrightarrow}} HCO_3^- \tag{1}$$

$$HCO_3^- + OH^- \underset{k_{2,2}}{\overset{k_{2,1}}{\leftrightarrow}} CO_3^{2-} + H_2O \tag{2}$$

$$2H_2O \underset{k_{3,2}}{\overset{k_{3,1}}{\leftrightarrow}} H_3O^+ + OH^- \tag{3}$$

$$CO_2 + 2H_2O \underset{k_{4,2}}{\overset{k_{4,1}}{\leftrightarrow}} HCO_3^- + H_3O^+ \tag{4}$$

$$CO_2 + CO_3^{2-} + H_2O \leftrightarrow 2HCO_3^- \tag{5}$$

Reactions (1) and (4) are rate controlling reactions. Reaction (1) is practically irreversible for the pH values greater than 10. Reaction (4) is much slower and only of importance in solutions with pH values less than 8 (Nijsing et al., 1959). The reactions (2) and (3) involve only proton transfer and can be considered as instantaneous so that they are assumed to be at equilibrium. Reaction (5) is the overall reaction of carbon dioxide absorption in aqueous carbonate solution. The corresponding equilibrium constants of the reactions are defined as follows:

$$K_1 = \frac{[HCO_3^-]}{[CO_2][OH^-]} \tag{6}$$

$$K_2 = \frac{[CO_3^{2-}]}{[HCO_3^-][OH^-]} \tag{7}$$

$$K_w = [H_3O^+][OH^-] \tag{8}$$

$$K_4 = \frac{[HCO_3^-][H_3O^+]}{[CO_2]} \tag{9}$$

All the kinetic parameters have been obtained from the literature and are given in the Appendix D. The initial bulk concentration of each species is determined by simultaneously solving the equilibrium equations along with a mass balance for the carbon species and an electro-neutrality balance.

$$K_1 A_0 B_0 - C_0 = 0 \tag{10a}$$

$$K_2 B_0 C_0 - E_0 = 0 \tag{10b}$$

$$E_{ini} - A_0 - C_0 - E_0 = 0 \tag{10c}$$

$$H_3O^+ - \frac{K_w}{B_0} = 0 \tag{10d}$$

$$K^+ + H_3O^+ = B_0 + C_0 + 2E_0 \tag{10e}$$

where A = CO_2, B = OH^-, C = HCO_3^- and E = CO_3^{2-} . E_{ini} refers to the initial concentration of the K_2CO_3. In the implementation of the complete numerical model, the initial concentrations are calculated using Newton's method. However, these solutions are reported to be non-ideal solutions, the effect of non-ideality is taken into account in the form of ionic strength and its effect on various kinetic and equilibrium constants (refer Appendix D).

2.2 Reactive absorption of hydrogen sulphide in aqueous carbonate solutions

Once the hydrogen sulphide is physically absorbed into the aqueous carbonate solution following reactions take place along with reactions (2) and (3).

$$H_2S + OH^- \underset{k_{5,2}}{\overset{k_{5,1}}{\leftrightarrow}} HS^- + H_2O \tag{11}$$

$$HS^- + OH^- \underset{k_{6,2}}{\overset{k_{6,1}}{\leftrightarrow}} S^{2-} + H_2O \tag{12}$$

$$H_2S + HCO_3^- \underset{k_{7,2}}{\overset{k_{7,1}}{\leftrightarrow}} HS^- + H_2O + CO_2 \tag{13}$$

$$H_2S + CO_3^{2-} \leftrightarrow HS^- + HCO_3^- \tag{14}$$

Reaction (11) is extremely fast and is very much favored to the right. The reaction (12) has an equilibrium constant of 0.12 m^3 $kmol^{-1}$ at 25 ^{o} C at infinite dilution (Astarita, 1967), hence reaction (12) is of minor importance in the strongly alkaline solutions and can be entirely neglected in the weakly alkaline solutions such as aqueous carbonate solution. The

final result of the reaction (13) is the production of carbon dioxide, which should desorb to the gaseous phase if no carbon dioxide is present in the gas. Reaction (13) is made up of two steps; reaction (11) followed by inverse of reaction (1). The second step of reaction (13) is non-ionic and rate determining and has a very low kinetic rate constant (Astarita & Gioia, 1964). Hence rate reaction (13) can be neglected in comparison with overall reaction. Equation (14) gives the overall reaction of hydrogen sulphide in aqueous carbonate solution with above assumptions and equilibrium for this reaction is favored to the right (equilibrium constant of 2 x 10^3 at 25 ^oC). Initial bulk concentrations of carbonate, bicarbonate and hydroxyl ions can be calculated by simultaneously solving the set of equations (10). All the kinetic parameters have been obtained from the literature and are given in Appendix D.

3.0 Model development

Numerous mass transfer models such as film, penetration and surface renewal models are available in literature to describe the reactive absorption of a gas in a liquid (Westerterp et al., 1984). The basic and common assumption of all these models is the presence of a well-mixed bulk phase adjacent to the gas-liquid interface. For the present case of the reactive absorption of a gas in the liquid flowing through a hollow fiber, this well-mixed liquid bulk, however, is absent. Due to the laminar flow of liquid through the hollow fiber, there is a velocity profile in the liquid phase, which extends from the gas-liquid interface to the axis of the fiber. Hence, the mathematical treatment of the present problem to predict the enhancement factor for the effect of chemical reaction on absorption is not straightforward. However, for physical absorption and constant gas-liquid interface conditions, Kreulen et al. (1993a) proposed an approximate solution for the mass transfer coefficient analogous to the heat transfer coefficient in the constant wall temperature heat transfer problem of Graetz (1885) and Leveque (1928).

For Gz < 10, $Sh = 3.67$ (15a)

For Gz > 20, $Sh = 1.62\ (Gz)^{1/3}$ (15b)

For 10< Gz< 20 $Sh = \sqrt[3]{3.67^3 + 1.62^3\, Gz}$ (15c)

The above equation was found applicable for the complete range of Graetz numbers in the laminar flow regime. Due to the limitations mentioned above, the mass transfer process involving chemical reaction in the liquid flowing inside the hollow fiber has to be described by a model based on first principles. The fiber side mass balance for a species ‘i’ is given by,

$$V_z \frac{\partial C_i}{\partial z} = D_i \left[\frac{1}{r} \frac{\partial}{\partial r} \left(r \frac{\partial C_i}{\partial r} \right) \right] - R_i \qquad (16)$$

where ‘R’ is the source term due to the chemical reaction. The adiabatic temperature rise during the absorption process was considered to be negligible. The assumption is valid in

the present case, since the absorption flux in a fiber is very low. In addition the length of fiber used in the module is considerably small. The change in the interface temperature due to the absorption can also be neglected since the solubility of the gas is low (Doraiswamy & Sharma, 1983). As the liquid flow inside the fiber is laminar, the velocity profile in the radial direction is given by,

$$V_z = 2\bar{v}\left[1 - \left(\frac{r}{r_i}\right)^2\right] \tag{17}$$

The entrance effects had been neglected as the liquid flows through the hollow fiber for a considerable distance (> $10d_{in}$, required for the velocity profile to be fully developed, see e.g. Perry & Green, 1984) before it contacts the gas phase. A generalized reversible reaction scheme to take into account the multiple reactions, as described in Section 2.1 and 2.2, was incorporated in the model. The partial differential equation (16) requires one initial condition and two boundary conditions in the axial and radial directions respectively. For the axial direction, the inlet conditions/properties of the liquid are specified.

$$\text{At } z = 0, \qquad C_i = C_{i,o} \tag{18}$$

In the radial direction, symmetry was assumed at the axis of the cylindrical fiber,

$$\text{At } r = 0, \qquad \left(\frac{\partial C_i}{\partial r}\right) = 0 \tag{19}$$

At the gas-liquid interface, the conservation of mass with respect to the component 'A' that is absorbed from the gas phase was enforced.

$$\text{At } r = r_i \qquad D_A\left(\frac{\partial C_i}{\partial r}\right) = k_{ext}\left(C_{i,g} - C_{i,g,i}\right) \tag{20}$$

All components other than the gas species absorbed are assumed to be non-volatile.

$$\text{At } r = r_i \qquad \left(\frac{\partial C_i}{\partial r}\right) = 0 \tag{21}$$

In case of the cross flow membrane contactors, the shell side concentration of the solute as well as the volumetric flow rate of the gas changes in both directions. This effect is significant when the concentration of the solute in the gas stream is high and the fraction removed in the membrane contactor is relatively high. To take this effect into account the shell side is flow is divided into number of cells. The details of the cell arrangement are presented elsewhere (Dindore et al. 2003). This method preserves concentration gradient of gas and liquid phase in all directions. A solute balance over a single cell gives following equation.

$$Q_{Gm-1,n}C_{Gm-1,n} - Q_{Gm,n}C_{Gm,n} = A_{m,n}J_{m,n} \quad (22)$$

Based on this mass balance for a single cell the solute outlet concentration and the gas outlet flow rate are calculated for every cell by an iterative method. The gas concentration, gas flow rate and liquid concentration are assumed to be uniform at the inlet of the module. The composition and gas flow rate leaving the last row of cells are stored and used as inputs for the corresponding cells in the next row.

The set of equations (the number depending on the number of chemical species involved in the reaction scheme) on the fiber side and on the shell side was solved simultaneously using a numerical technique. The details of the numerical treatment are given in the Section 4. From the concentration profile of the solute in the liquid phase obtained from the solution of mass balance equations, the local absorption flux of the solute along the length of the fiber was calculated using Fick's law for each cell. The average solute absorption flux over the entire module was obtained from integration of the local fluxes over the complete module. The change in the driving force in the cross flow contactors results into the concentration profile on shell side as well as on fiber side outlets. The final outlet concentrations are computed by mixing the different outlet streams and taking the mixing cup concentration.

4.0 Numerical treatment

In the case of gas absorption in a liquid flowing through a hollow fiber, the mass transfer rate is calculated from the concentration profiles of species along the radius and length of the fiber. The concentration profiles are obtained as a solution of a system of non-linear parabolic partial differential equations subjected to specified initial and boundary conditions. These concentration profiles are steep near the gas-liquid interface when absorption is follow by a chemical reaction. In order to have a finer grid near the gas-liquid interface, the distribution of spatial grid points in the r-z plane is transformed. The final set of the partial differential equation was discretised using the implicit second order scheme based on the Baker & Oliphant method (1960). The reaction terms were linearised using the Newton-Raphson method. The discretization for 'np' grid point in radial direction gives a set of np+1 equation for each component at each z-directional grid point. These equations are solved simultaneously using LU decomposition method according to Crout algorithm. This solution is used to calculate the set of equations at the next z-directional coordinate.

5.0 Experimental

5.1 Materials

The potassium carbonate salt, carbon dioxide, hydrogen sulphide and nitrogen used in the experiments had 99.99% of purity. Owing to the high hydrophobic nature of

polypropylene as a membrane material and its commercial availability, it was decided to use an Accurel Q3/2 polypropylene hollow fiber for module construction. The Q3/2 fiber has an outside diameter meter of 1000 μm and inside diameter of 600 μm. The maximum pore size of the Q3/2 fiber is 0.64 μm. Two modules were used in the experiments. The details of the modules are given in Table 1.

Table 1: *Module specifications.*

Module	Fiber type	Length (m)	Width (m)	Height (m)	Nr. of fibers	Voidage	Pitch	A_{in} m^2
I	PP	0.05	0.05	0.05	729	0.77	1.85	0.069
II	PP	0.1	0.04	0.04	400	0.80	2.0	0.074

Module I was obtained from TNO-MEP, Apeldoorn and module II was constructed in our laboratory. The details of construction of module II is given elsewhere (Dindore et al., 2003). Figures 1a and 1b show the cross flow modules I and II. In both modules the length of the potting was more than 5 cm. This ensures that the potting length on the liquid entry side provides sufficient distance (> $10d_{in}$) for the laminar liquid flow profile inside the fiber to be fully developed, before it contacts the gas. Uniform flow distribution on the shell side is important to prevent maldistribution and dead zone formation. To achieve the uniform flow distribution on the shell, the shell side fluid is passed through an area reducer filled with glass wool.

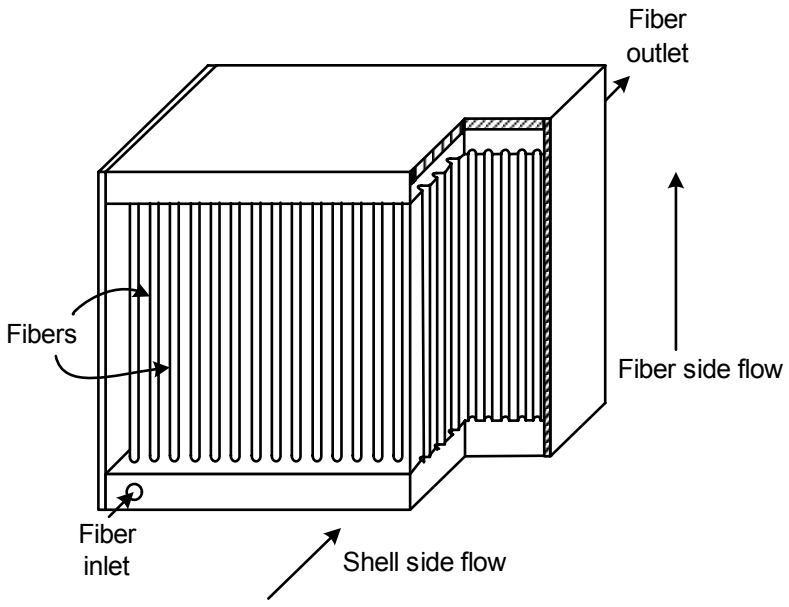

Figure 1a: *Cross flow membrane module I.*

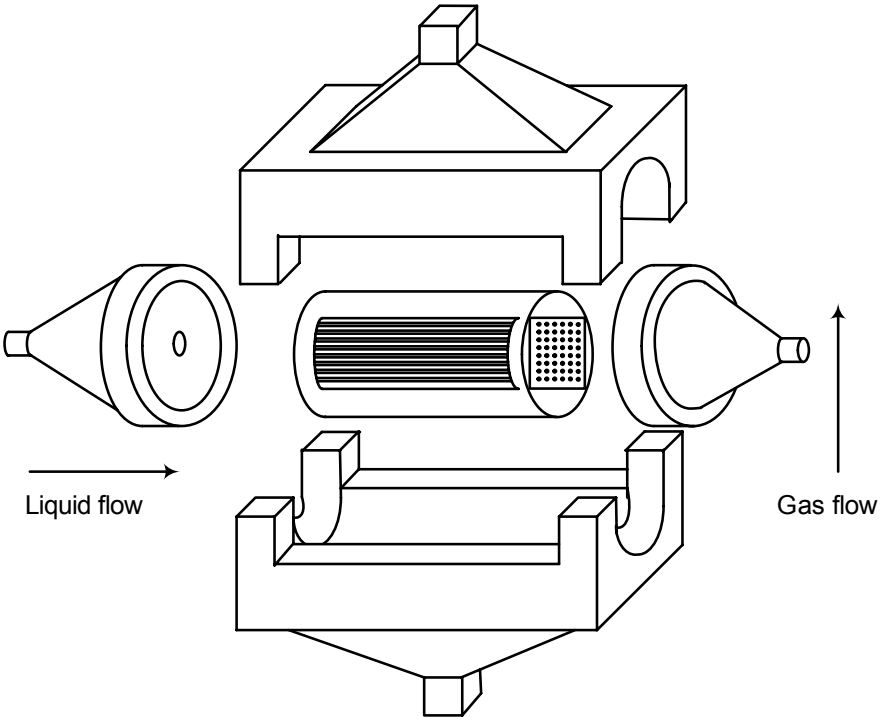

Figure 1b: *Cross flow membrane module II.*

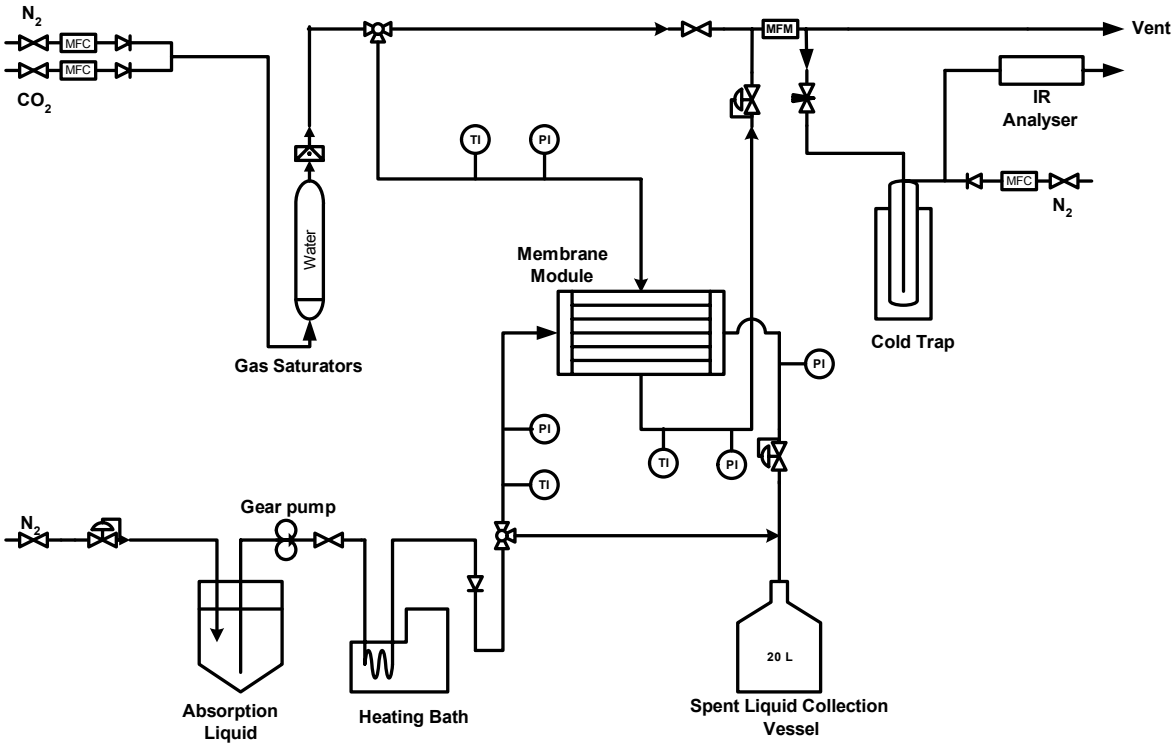

Figure 2: *Experimental set up for absorption of CO_2 in K_2CO_3.*

5.2 Method

Absorption of carbon dioxide in aqueous potassium carbonate is carried out in module II. The experimental set-up for the carbon dioxide absorption is shown in Figure 2. A continuous mode of gas-liquid contacting operation was used during the experiments. Aqueous potassium carbonate solutions were prepared by dissolving a known amount potassium carbonate salt into the degassed and deionized water. The carbonate solution was passed through the fibers and gas was passed through the shell-side. The carbonate solution was fed using a gear-pressure pump through the heat exchanger to maintain the desired temperature before passing to the hollow fiber membrane module. The upstream liquid pressure was controlled using a high precision back-pressure controller valve. In all experiments, sufficient gas pressure is maintained in the contactor before starting the liquid flow. The absence of the gas pressure may result in the wetting of the fiber. The liquid inlet and liquid outlet pressures were measured separately using digital pressure indicators. The liquid inlet was also fitted with a digital thermometer to monitor the liquid inlet temperature. The average velocity of the liquid through the fibers is measured by collecting and weighing a sample in a known amount of time.

The shell-side gas flow was adjusted using mass flow controllers. All mass flow controllers were calibrated using a gas flow meter or soap film meter. Nitrogen and carbon dioxide were premixed to a desired concentration using mass flow controllers and fed to the contactor after saturating the gas stream with water vapor. The shell-side pressure was controlled using a 5866-Brooks digital pressure controller. During all the experiments the liquid side pressure was kept sufficiently higher than the shell side gas pressure to avoid bubbling of gas. The gas inlet and gas outlet pressure were measured separately using digital pressure indicators. The gas inlet and gas outlet were also equipped with digital thermometers to monitor the temperatures. It is important to know both inlet and outlet temperatures of the gas stream in order to check any cooling effect which might result into a change in the volumetric gas flow rate. The carbon dioxide concentration in the feed and outlet gas streams of the contactor was measured using Maihak Infrared carbon dioxide analyzers of different ranges depending on gas composition (0-5 %, 0-15 %). The concentrations of the gas samples to the infrared (IR) analyzer were adjusted within the range of the IR analyzer by diluting the gas stream with nitrogen. The carbon dioxide absorption flux and liquid average outlet concentration was estimated by making a mass balance over the reactor.

$$\left\langle J_{CO_2} \right\rangle = \frac{Q_{G,i}C_{G,i} - Q_{G,e}C_{G,e}}{A} \tag{23}$$

$$C_{L,e} = \frac{Q_{G,i}C_{G,i} - Q_{G,e}C_{G,e}}{Q_L} \tag{24}$$

Since the IR analyzer gives carbon dioxide concentrations in terms of volume percentage, it is possible to calculate both the volumetric gas flow rate and the molar concentration of carbon dioxide using the overall mass balance. In all experiments the gas flow rate was kept sufficiently low so that the outlet gas flow rate and molar concentration of the carbon dioxide was significantly lower than the inlet conditions. All the experiments are carried out at atmospheric pressure and 24.0 ^{o}C.

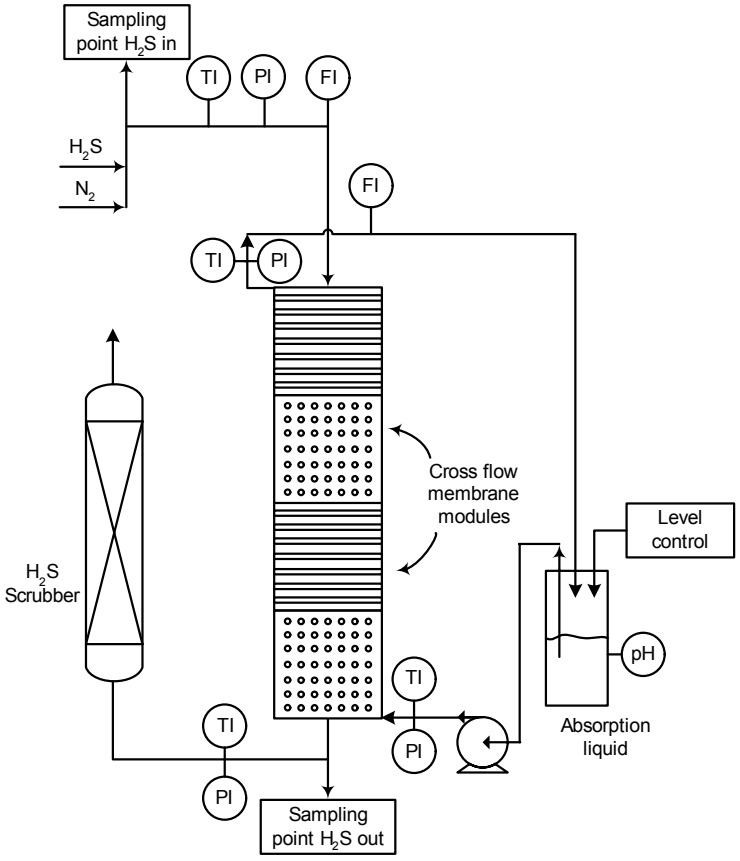

Figure 3: *Experimental set up for absorption of H_2S in K_2CO_3.*

Absorption of hydrogen sulphide into potassium carbonate solution was carried out in a separate experimental set-up at TNO-MEP laboratory. The details of the experimental set-up are given in Figure 3. The experiments are carried out using a stack of four modules (type I) arranged to realise an overall counter-current operation. The carbonate solution was recirculated over the membrane absorber through the fiber. The water loss due to the evaporation was made up in the storage vessel. The liquid-circulation loop is equipped with temperature and pressure indicators at the inlet and the outlet of the stream. The pH of the solution was continuously monitored using a pH-meter. The liquid velocity through the hollow fiber was calculated by measuring the total liquid flow fed to the membrane absorber.

Hydrogen sulphide is premixed with nitrogen to obtain a gas stream with the desired hydrogen sulphide concentration. This gas stream was fed continuously through the

membrane absorber. For safety reasons, a hydrogen sulphide scrubber was installed after the membrane gas absorption unit to remove completely the traces of hydrogen sulphide before it is passed to the vent. The gas-circulation loop is also equipped with temperature and pressure indicators to measure the inlet and outlet temperatures and pressures. The concentration of hydrogen sulphide in the inlet and outlet stream was measured using a Galvanic H_2S analyzer. As the liquid is continuously recirculated over the module, the liquid will get continuously loaded with hydrogen sulphide till it gets saturated. At this point there will be no absorption of hydrogen sulphide because the composition of the gas and liquid streams are at equilibrium and inlet and outlet concentration of the gas-stream will be the same. To simulate the once through experiments for both gas as well as liquid, the outlet concentration at t = 0 is taken as outlet concentration at zero loading of hydrogen sulphide.

6.0 Results and Discussions

In case of mass transfer with chemical reaction in membrane gas liquid contactors, the overall mass transfer resistance can be controlled by either of gas film resistance, membrane resistance or liquid side resistance depending on the enhancement due to chemical reaction. Hence information on the gas (shell side in present case) side mass transfer coefficient and membrane mass transfer coefficient is necessary. Feron et al. (1994) studied the shell side mass transfer performance of the cross flow rectangular module similar to those used in this study. The shell side mass transfer coefficient for these modules is given by the following equation.

$$Sh = 0.9\, Re^{0.5}\, Sc^{0.33} \tag{25}$$

The membrane mass transfer coefficient becomes a key factor for the gas film controlled systems such as absorption of H_2S into alkalis and carbonate solutions. Qi & Cussler (1985) reported an overall gas phase and membrane mass transfer coefficient of 0.0073 m/s for the absorption of H_2S into NaOH, which is mentioned to be considerably lower than that for the conventional gas-liquid contactors. In these situations the absorption of such system is strongly influenced by the membrane mass transfer coefficient. The membrane mass transfer coefficient depends on the structural properties of the membrane such as porosity to tortuosity ratio (ε/τ), Knudsen diffusion parameter (K_d) and viscous flow parameter (B_o). To determine these parameters separate gas permeation experiments were carried out. The details of these experiments and results are given in Appendix E. The membrane mass transfer coefficient is calculated by the method described in Chapter 1 (Section 2.1). The estimated value of the membrane mass transfer coefficient is 1.9×10^{-2} m s^{-1}. The combined mass transfer coefficient of the gas phase and the membrane phase can be calculated by the resistance in series model.

The diffusivity of carbon dioxide in water is obtained from literature (Versteeg and van Swaaij, 1988) and diffusivity of hydrogen sulphide in water is estimated using the correlation given by Diaz et al. (1987). Ion diffusivities of the simple ions in water at infinite dilution are estimated using the Nerst equation. These diffusivities were corrected using the Stokes-Einstein relation for the viscosity changes of the solutions. Electro-neutrality in the liquid phase was maintained by using mean ion diffusion coefficients for the ionic species in the liquid phase. Solubilities of carbon dioxide and hydrogen sulfide in water as a function of temperature are obtained from literature and these data are corrected for the ionic strength of the solution using the method given by Weisenberger & Schumpe (1996). All the parameters used in the model simulation are given in Appendix D.

6.1 Absorption of carbon dioxide in aqueous carbonate solutions

Absorption of carbon dioxide in 0.25M and 0.5M aqueous carbonate solutions is carried out using Module II. The experiments were carried out to study the effects of various operating parameters such as liquid velocity, gas velocity and concentration of the aqueous carbonate solution. In all experiments the gas residence time in the membrane module was kept high enough to assure a significant change in the gas phase concentration. All the experiments were carried out using 30-70 % binary mixture of carbon dioxide and nitrogen.

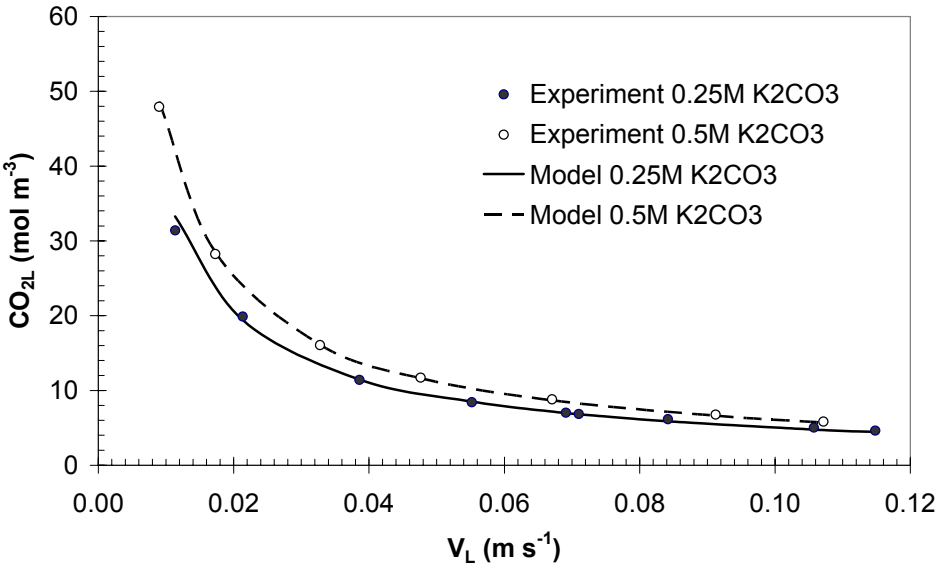

Figure 4: *Effect liquid velocity on the liquid outlet concentration for the absorption of carbon dioxide in module II.*

Figure 4 shows the carbon dioxide concentration in the liquid outlet stream as a function of the liquid velocity through the fibers and subsequent comparison with the numerical model predictions. No fit parameters are used in the numerical simulations. Note that the carbon dioxide concentration is given as total carbon dioxide present in the form of

physically dissolved carbon dioxide and reaction products. It can be seen from the figure that the numerical predictions are in good agreement with the experimental results. As expected, the carbon dioxide concentration decreased as the liquid flow rate increased. The effect of the concentration of carbonate solution is also shown in the figure. As the concentration of the carbonate solution is increased, the concentration of the absorbed carbon dioxide is also increased.

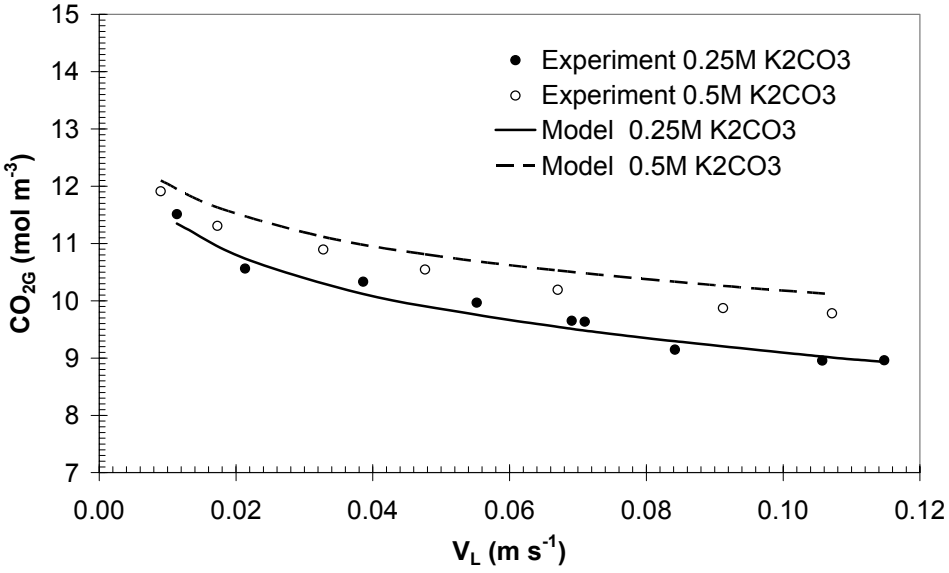

Figure 5: *Effect liquid velocity on the gas outlet concentration for the absorption of carbon dioxide in module II.*

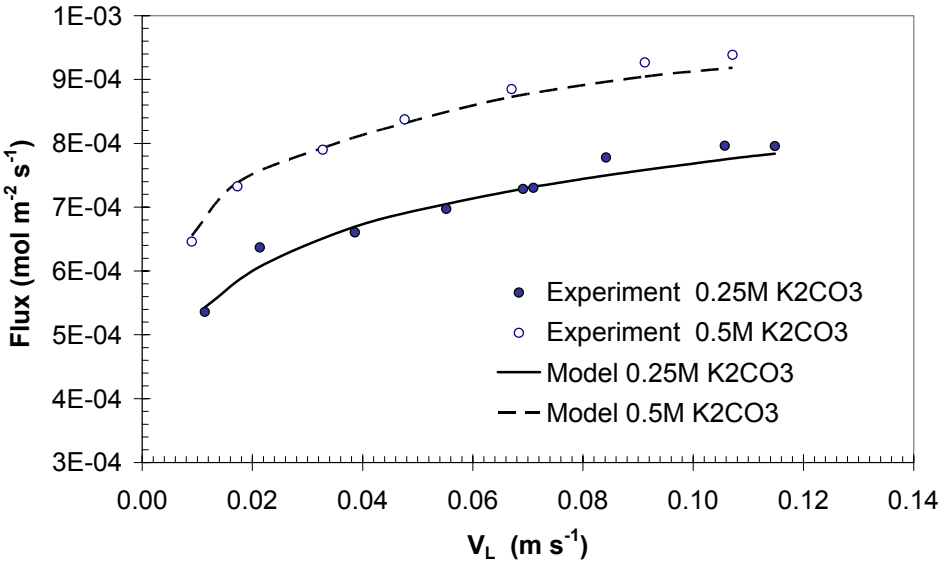

Figure 6: *Effect Liquid velocity on the average absorption flux in module II.*

Figure 5 shows the gas outlet concentration as a function of liquid velocity through the fibers for constant gas flow rate of 0.42 l/min and 0.55 l/min for 0.25 M and 0.5 M K_2CO_3 solutions respectively. It can be seen from the figure that as the liquid velocity increases, the gas outlet concentration decreases and thus the removal rate of the carbon dioxide increases.

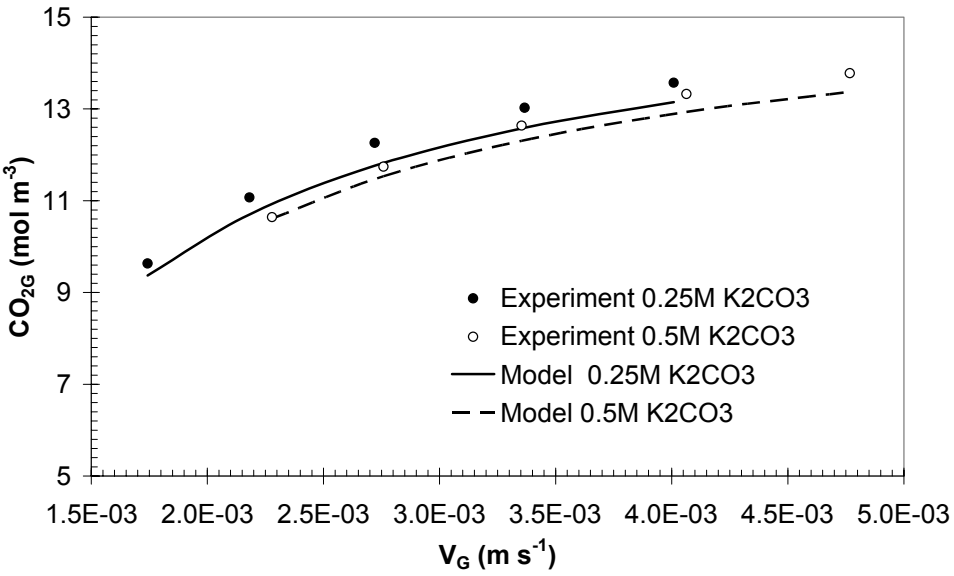

Figure 7: *Effect gas velocity on the gas outlet concentration for the absorption of carbon dioxide in module II.*

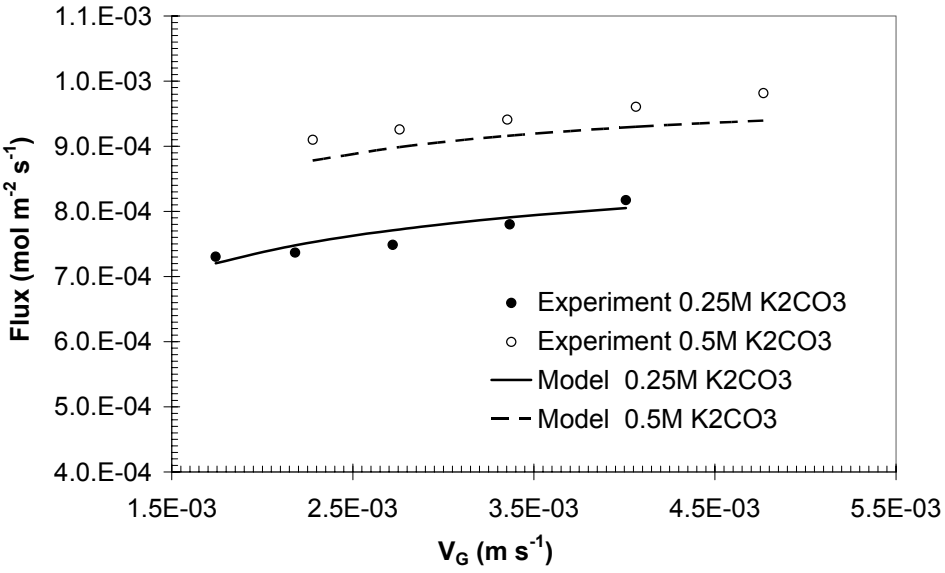

Figure 8: *Effect gas velocity on the absorption flux for the absorption of carbon dioxide in module II.*

The effect of the liquid velocity on the average absorption flux is shown in the Figure 6. The average absorption flux in the module is calculated by integrating the local absorption

flux over the entire volume of the module. It can be seen from the figure that the absorption flux is a strong function of the liquid velocity when the liquid velocity is relatively low. However, at higher velocities the average absorption flux is less dependent on the liquid velocity. It is known from the theory of mass transfer with chemical reaction that in the case of fast reaction regime, the absorption flux is independent of the mass transfer coefficient whereas in the case of instantaneous reaction regime, the absorption flux depends on the mass transfer coefficient. At high velocities there is relatively less depletion of the reactive species at the gas-liquid interface. As the absorption rate is influenced by the chemical reaction rate, the liquid velocity has less influence on the average absorption flux. However, at lower velocities the depletion of the reactive species may occur depending on the reaction regime. For extreme case of the complete depletion of the reactive species at the interface and the reaction regime may change from fast reaction regime at the liquid inlet to instantaneous reaction regime at liquid exit. In such cases the absorption flux is strongly influenced by the mass transfer coefficient and hence by the liquid velocity. The solute gas concentration on the shell side also decreases in the direction of the gas flow. Higher depletion of the solute gas in the direction of the gas flow results into change in reaction regime in the direction of gas flow as well. Thus in the case of cross flow membrane contactor, the reaction regime changes along length of fiber as well as in the direction of the gas flow. Therefore the application of conventional mass transfer models for complete module becomes difficult and detailed mathematical modeling of the contactor is necessary.

The effect of gas velocity on the gas outlet concentration and average absorption flux in module is shown in the Figures 7 and 8 respectively. The experiments were carried out at constant liquid velocity at 0.06 m/s. As can be seen from Figure 7, the gas outlet concentration predicted by the simulation is in good agreement with the experiment results. The figure 8 indicates that average absorption flux in the module is less dependent on the gas velocity. It can be concluded that the overall mass transfer process is still controlled by the liquid side mass transfer resistance even after enhancement due to chemical reaction.

6.2 Absorption of hydrogen sulphide in aqueous carbonate solutions

The absorption of hydrogen sulphide is carried out using a stack of four modules of type I in TNO-MEP laboratories. The experiments were carried out in such a mode that overall counter current flow is realised. Experiments were carried out for two different gas velocities, 0.556 m/s and 1.11 m/s. The liquid velocity through the fiber was kept constant for all the experiments ($2.69.10^{-3}$ m/s). The experimental conditions are given in Table 2.

Table 2: *Experimental conditions for H_2S absorption.*

Variable	Value
Temperature	20 ^oC
Pressure	1 bar
Inlet H_2S concentration	93-2071 ppm
K_2CO_3 concentration	0.2-2 kmol m^{-3}
Liquid velocity	$2.69x10^{-3}$ m s^{-1}
Gas velocity	0.556 -1.11 m s^{-1}

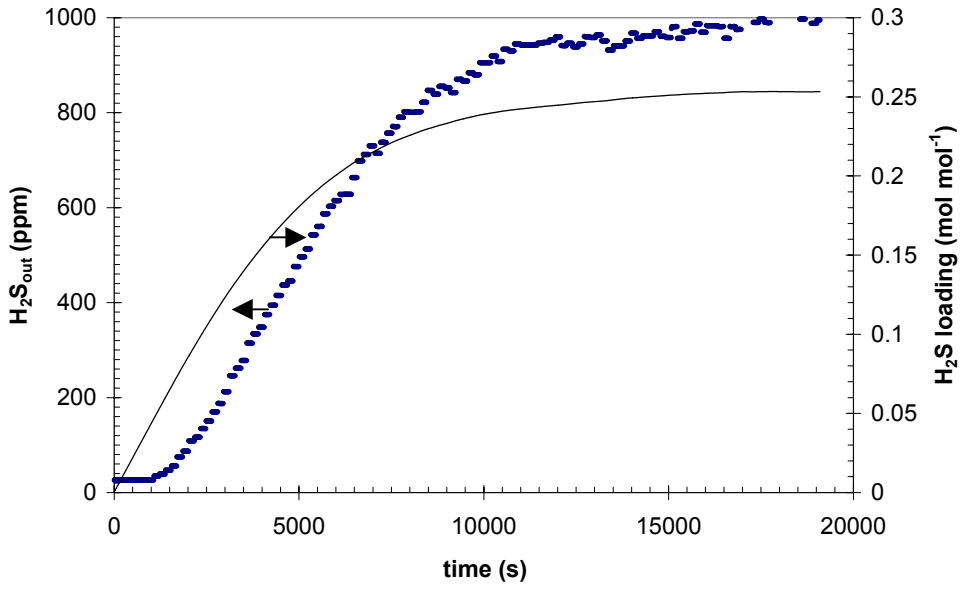

Figure 9: *H_2S concentration at the gas outlet and H_2S loading as a function of time (Inlet concentration = 1000 ppm, gas velocity =0.556 m/s, $[K_2CO_3]$ = 2 kmol m^{-3}).*

Throughout an experiment the carbonate solution gets loaded with the hydrogen sulphide from the feed gas and thus hydrogen sulphide loading of carbonate solution steadily increases with time. The absorption flux of the hydrogen sulphide drops steadily due to increase in the back-pressure of the hydrogen sulphide. As a consequence, the outlet concentration of the hydrogen sulphide increases steadily with time.

The temporal variation of hydrogen sulphide loading of carbonate solution and the outlet concentration of the hydrogen sulphide for a typical case is shown in Figure 9. It can be seen from the figure that after a certain period of time, the outlet concentration becomes identical to the inlet concentration. The summary of the experimental results is given in Table 3.

Table 3: *Experimental results for H_2S absorption*.

Inlet H_2S concentration (ppm)	**Gas velocity m s^{-1}**	**[K_2CO_3] kmol m^{-3}**	**Outlet H_2S concentration (ppm) at t =0**
1000	0.556	2.0	25.98
2071	0.556	2.0	43.00
1010	0.556	2.0	26.00
93	0.556	0.2	2.55
561	0.556	1.0	9.85
530	1.111	1.0	50.00
1000	1.111	2.0	100.00
2030	1.111	2.0	300.00
105	1.111	0.2	8.00

The numerical simulations are carried out for the stack of modules using the experimental data. In all the experiments the outlet concentration of the hydrogen sulphide is measured as function of time. However, the model simulations are carried out for steady state operation for once through experiments. Hence to compare the results of the simulations and experiments, the outlet concentration measured at time t=0 is taken as the result for a once through experiment. The outlet of one module is passed as an inlet for the next module in the stack. The outlet streams are assumed to be completely mixed. In actual model, a uniform concentration in the inlet stream would result in a concentration gradient (and flow gradient as well for the gas stream) in the stream leaving the final segment of a module in stack. However, during the experiment the liquid outlets of the each fiber are collected and sent as a single inlet for next module, giving uniform concentrations at the inlet of all fibers. To get the similar effect in the simulation a hypothetical liquid mixing chamber is assumed at the outlet of each module. Similarly for the gas phase, in the actual module configuration a sufficient space is provided on the inlet and outlet of a module. This void space acts a mixing chamber for the gas stream. Moreover, the modules were arranged in such a way that the fibers of the two consecutive modules were at right angles to each other. In such arrangements any concentration profile developed at the outlet of the shell side is vanished at the inlet of next module. Hence a complete mixing of the shell side flow at the outlet of each module is also assumed. In the simulation, the combined mass transfer coefficient of the gas and the membrane phase is used as a fitting parameter. The estimated values of these combined mass transfer coefficient and the values used in the simulation are given in the Table 4. It can be seen from Table 4 that both estimated and used values of the clubbed mass transfer coefficient match excellently.

Table 4: *Combined mass transfer coefficients.*

Gas velocity m s^{-1}	Estimated k_{ext} m s^{-1}	Used in simulation k_{ext} m s^{-1}
0.556	1.62×10^{-2}	1.58×10^{-2}
1.111	1.70×10^{-2}	1.73×10^{-2}

The comparison of the experimental results and the simulation results are given in the form of parity plot in Figure 10. It can be seen from this figure that there is a good match between the experimental results and numerical simulations.

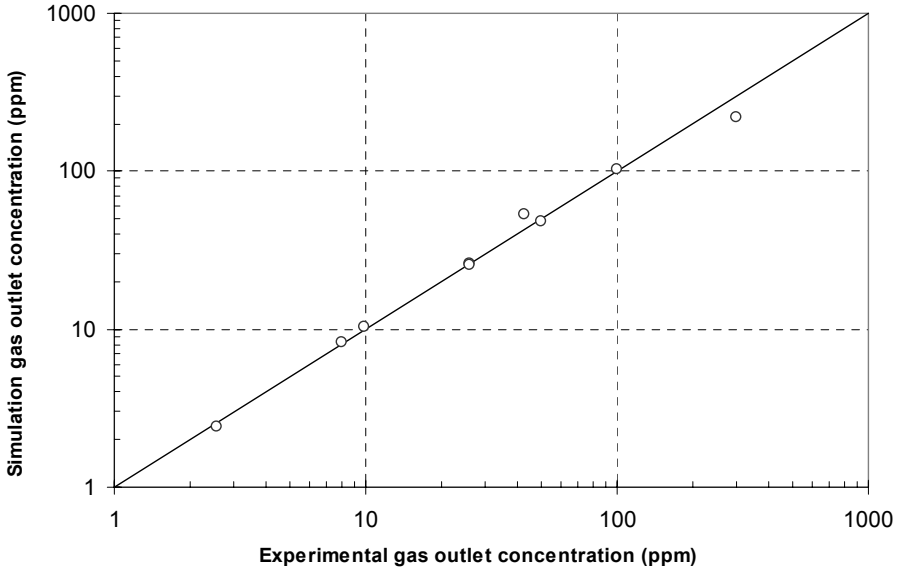

Figure 10: *Parity plot of predicted and experimental H_2S gas outlet concentration.*

7.0 Conclusion

In the present study, mass transfer with chemical reaction in a rectangular cross flow membrane gas liquid contactor is studied. Two different experimental systems namely absorption carbon dioxide in aqueous carbonate solution and absorption of hydrogen sulphide in aqueous carbonate solution are used in the study. Experiments are carried out to study the effect of various operating parameters such as gas and liquid flow rates, concentrations of the feed streams and enhancement due to chemical reaction on the performance of the rectangular cross flow membrane gas-liquid contactors.

Simple single gas permeation experiments were carried out to determine the membrane properties. The estimated value of ε/τ (=0.42) from these experiments for polypropylene Accurel Q3/2 hollow fibers is in good agreement with the value calculated from literature data for this fiber (=0.36).

A detailed numerical model was developed to study mass transfer with chemical reaction in the cross flow gas-liquid membrane contactor. The numerical model is solved for the detailed reaction schemes for the absorption of carbon dioxide and hydrogen sulphide in aqueous carbonate solution. The predictions of the numerical model are in good agreement with the experimental results. In case of the carbon dioxide absorption into aqueous carbonate solution, strong dependence of the absorption flux on the liquid velocity and relatively less dependence on the gas velocity indicates that mass transfer process is controlled by the liquid side mass transfer resistance. On the other hand the combined resistance of the membrane and the gas phase is dominant in the case of absorption of hydrogen sulphide in aqueous carbonate solution. The results in this work show that the detailed numerical model developed is able to predict the performance of the cross flow membrane modules. The numerical simulation can take into account complex chemical reaction schemes.

Acknowledgement

This research is part of the research program performed within the Centre for Separation Technology (CST), which is a co-operation between the Netherlands Organization for Applied Scientific Research (TNO) and the University of Twente. We thank Prof. Dr. ir. Hein Neomagus for his help in the characterization of membrane fibers. We also acknowledge Benno Knaken and Wim Leppink for the construction of the experimental set ups.

Nomenclature

A	Area	[m^2]
B_o	Viscous flow parameter	[m^2]
C	Concentration	[mol m^{-3}]
D	Diffusivity	[m^2 s^-1]
d	Diameter	[m]
F	Faraday constant = 96500	[C mol^{-1}]
Gz	Graetz number , $\frac{vd^2}{Dz}$,	[-]
J	Flux	[mol m^{-2} s^{-1}]
K	Knudsen flow parameter	[m]
K_{sub}	Reaction equilibrium constant, sub: reaction number,	
$k_{sub,1}$	Reaction rate constant, sub: reaction number, forward,	[$mol^{-1}m^3$ s^{-1}]
$k_{sub,2}$	Reaction rate constant, sub: reaction number, backward,	[$mol^{-1}m^3$ s^{-1}]
k	Mass transfer coefficient	[m s^{-1}]
L	Length	[m]
m	Distribution coefficient	[-]
P	Pressure	[kg m^{-1} s^{-2}]

Q	Flow rate	[m^{-3} s^{-1}]
r	Radius	[m]
R	Gas constant	[J mol^{-1} K^{-1}]
Re	Reynolds number, $\frac{dv\rho}{\mu}$,	[-]
Sc	Schmidt number, $\frac{\mu}{\rho D}$,	[-]
Sh	Sherwood number, $\frac{k_l d}{D}$,	[-]
t	Time	[s]
T	Temperature	[K]
v	Velocity	[m s^{-1}]
z	Length	[m]
Z	Ionic charge	[-]

Greek letters

ε	Porosity	[-]
μ	Viscosity	[kg m^{-1} s^{-1}]
ρ	Density	[kg m^{-3-}]
τ	Tortuosity	[-]
ℓ_i^∞	Ionic conductivity at infinite dilution	[m^{-2} Ω^{-1} mol^{-1}]

Subscripts

Avg	Average
e	Exit
G	Gas
i	Inlet/inner
ini	Initial
L	Liquid
o	Outer
p	Pore
w	Water
z	Local value
∞	Infinite dilution

References

Astarita, G., & Gioia, F. (1964). Hydrogen sulphide chemical absorption. *Chemical Engineering Science*, **19**, 963-971.

Astarita, G. (1967). *Mass transfer with chemical reaction*. Amsterdam: Elsevier.

Baker, G.A., & Oliphant, T.A. (1960). An implicit numerical method for solving the two dimensional heat equation. Q*uart. Appl. Math.*, **17**(4), 361-373.

Carroll, J.J., & Mather, A.E. (1989). The solubility of hydrogen sulphide in water from 0 to 90 ^{o}C and pressure to 1 MPa. *Geochim. Cosmochim. Acta*, **53**, 1163-1170.

Chun, M., & Lee, K. (1997). Analysis on a hydrophobic hollow fiber membrane absorber and experimental observations of CO_2 removal by enhanced absorption. *Separation Science and Tecnology,* **32(15)**, 2445-2466.

Diaz, D., Vega, A., & Coca, J. (1987). Correlation for the estimation of gas-liquid diffusivity. *Chemical Engineering Communication*, **52**, 271-281.

Dindore, V.Y., Brilman, D.W.F., Feron P.H.M., & Versteeg G.F. (2003). Cross flow gas-liquid membrane contactors: physical mass transfer processes. (To be published, Chapter 4 of this thesis).

Doraiswamy, L.K., & Sharma, M.M. (1984). *Heterogeneous Reactions: Analysis, Examples, and Reactor Design. Volume 2: Fluid-Fluid-Solid Reactions*. Singapore: John Wiley.

Gabelman, A., & Hwang, S. (1999). Hollow fiber membrane contactors. *Journal of Membrane Science,* **159(1)**, 61-106.

Graetz, L. (1883). Über die Wärmeleitungsfähigkeit von Flüssigkeiten, 1e Abhandlung. *Annalen der Physik und Chemie,* **18**, 79-84.

Guijt, C.S., Racz, I.G., Reith, T., & de Haan, A.B. (2000). Determination of membrane properties for use in the modeling of a membrane distillation module. *Desalination*, **132**, 255-261.

Feron, P.H.M., Jansen, A.E., Klaassen, R., Hanemaaijer, J.H., & ter Meulen, B.Ph. (1994). Membrane gas absorption processes in environmental applications *in Membrane Processes in Separation and Purification* (Edited by J.G. Crespo and K.W. Boddeker). Dordrecht: Kluwer Academic.

Feron, P.H.M., & Jansen, A.E. (1995). Capture of carbon-dioxide using membrane gas-absorption and reuse in the horticultural industry. *Energy Conversion & Management,* **36(6-9)**, 411-414.

Hanisch, C. (1999). Exploring options for CO_2 capture and management. *Environmental Science & Technology*, **33(3)**, 66A-70A.

Hikita, H., Asai, S., & Takatsuka, T. (1976). Absorption of carbon dioxide into aqueous sodium hydroxide and sodium carbonate and bicarbonate solutions. *Chemical Engineering Journal*, **11**, 131-141.

Hovarth, A.L. (1985). *Handbook of aqueous electrolytic solutions: physical properties, estimation and correlation methods*. New York: John Wiley.

Karmann, W. (1967). Pulse radiolysis of H_2S in aqueous solution. *Naturforsh*, **B22(3)**, 273.

Kreulen, H., Smolders, C.A., Versteeg, G.F., & van Swaaij, W.P.M. (1993a). Microporous hollow-fiber membrane modules as gas-liquid contactors: 1. Physical mass transfer processes - A specific application - Mass transfer in highly viscous liquids. *Journal of Membrane Science,* **78(3)**, 197-216.

Kreulen, H., Smolders, C.A., Versteeg, G.F., & van Swaaij, W.P.M. (1993b). Microporous hollow-fiber membrane modules as gas-liquid contactors: 2. Mass transfer with chemical reaction. *Journal of Membrane Science,* **78(3)**, 217-238.

Kumar, P. S. (2002). *Development and design of membrane gas absorption processes.* Ph.D. Thesis, University of Twente, the Netherlands.

Lee, Y., Noble, R. D., Yeom, B., Park, Y., & Lee, K. (2001). Analysis of CO_2 removal by hollow fiber membrane contactors. *Journal of Membrane Science,* **194**, 57-67.

Leveque, J. (1928). Les lois de la transmission de chaleur par convection. *Annls. Mines, Paris (Series 12)*, 201.

Nii, S., Takeuchi, H., & Takahashi, K. (1992). Removal of CO_2 by gas absorption across a polymeric membrane. *Journal of Chemical Engineering of Japan.,* **25(1)**, 67-71.

Nijsing, R. A. T. O., Hendriksz, R. H., & Kramers, H. (1959). Absorption of CO_2 in jets and falling films of electrolyte solutions, with and without chemical reaction. *Chemical Engineering Science*, **10**, 88-104.

Perry, R.H., & Green, D. (1984). *Perry's chemical engineer's handbook.* Singapore: McGraw-Hill.

Pohorecki, R., & Moniuk, W. (1988). Kinetics of the reaction between carbon dioxide and hydroxyl ion in aqueous electrolyte solutions. *Chemical Engineering Science*, **43**, 1677-1684.

Qi, Z., & Cussler, E.L. (1985). Microporous hollow fibers for gas absorption II. Mass transfer across the membrane. *Journal of Membrane Science*, **23**, 333-345.

Ratcliff, G.A., & Holdcroft, J.G. (1963). Diffusivities of gases in aqueous electrolyte solutions. *Transactions of Institution of Chemical Engineers*, **41**, 315-319.

Roberts, D., & Danckwerts, P. V. (1967). Kinetics of CO_2 in alkaline solution –I. *Chemical Engineering Science*, **17**, 961-969.

Sharma, M.M., & Danckwerts, P.V. (1966). The absorption of carbon dioxide into solutions of alkalis and amines (with some notes on hydrogen sulphide and carbonyl sulphide). *Chemical Engineer*, **(October)**, CE245-CE280.

Strauss, W. (1975). *Industrial gas cleaning*, *2nd Edn. In: Industrial Series in Chemical Engineering*. Oxford: Pergamon Press

Tsonopolous, C., Coulson, D.M., & Inman, L.W. (1976). Ionization constants of water pollutants. *Journal of Chemical & Engineering Data*, **21**, 190-193.

Vas Bhat, R.D., Kuipers, J.A.M., & Versteeg, G.F. (2000). Mass transfer with complex chemical reactions in gas–liquid systems: two-step reversible reactions with unit stoichiometric and kinetic orders. *Chemical Engineering Journal*, **76(2)**, 127-152.

Versteeg, G.F., & van Swaaij, W.P.M. (1988). Solubility and diffusivity of acid gases (CO_2, N_2O) in aqueous alkanolamine solutions. *Journal of Chemical & Engineering Data*, **33**, 29-34.

Vinogard, J.R., and McBain, J.W. (1941). Diffusion of electrolytes and of the ions in their mixtures, *J. Amer. Chem. Soc.*, **(63)**, 2008-2015.

Weisenberger, S., & Schumpe, A. (1996). Estimation of gas solubility in salt solutions at temperatures from 273K to 363K. *A. I .Ch. E. Journal*, **42(1)**, 298-300.

Zhang, Qi., & Cussler, E.L. (1985). Microporous hollow-fibers for gas absorption II. Mass transfer across the membrane, *Journal of Membrane Science,* **23(3)**, 333-345.

Appendix D: Physico-chemical parameters

D 1. Solubility

The distribution coefficient of CO_2 in pure water is taken from Versteeg & van Swaaij (1988).

$$m_{w,CO_2} = 3.59.10^{-7} RT.exp\left(\frac{2044}{T}\right) \quad \text{(D1)}$$

The distribution coefficient of H_2S in pure water is taken from Carroll & Mather (1989).

$$m_{w,H_2S} = 1000RT.10^{-a} \quad \text{(D2)}$$

where, $a = 2.7896 + 0.031459T - 4.81046.10^{-5}T^2 - \frac{672.791}{T} + 0.144237 \log T$

The solubility of gas in aqueous electrolytic solutions has been estimated using the method presented by Weisenberger & Schumpe (1996). The distribution coefficient for CO_2 and H_2S in aqueous solution of potassium carbonate is determined by

$$\log\left(\frac{m_{w,G}}{m_G}\right) = (0.0959 + h_G)[K^+] + (0.0839 + h_G)[OH^-] + (0.0967 + h_G)[HCO_3^-] + (0.1423 + h_G)[CO_3^{-2}] \quad \text{(D3)}$$

where the ionic concentrations are in kmol.m^{-3}. h_G is the gas specific constant and given for CO_2 and H_2S in following Eqs.

$$h_{CO_2} = -0.0172 - 3.38.10^{-4}(T - 298.15) \quad \text{(D4)}$$

$$h_{H_2S} = -0.0333 \quad \text{(D5)}$$

D 2. Diffusivity

The diffusivity of CO_2 in pure water, $D_{CO2,W}$,(m^2 s^{-1}) is taken from Versteeg & van Swaaij (1988).

$$D_{w,CO_2} = 2.35.10^{-6} RT.exp\left(\frac{-2119}{T}\right) \quad \text{(D6)}$$

The diffusivity of H_2S in pure water at 25 ^oC (2.10x10^{-9} m^{2}s^{-1}) is taken from Diaz et al. (1987). The correction for the temperature and viscosity is carried out using the modified Stokes-Einstein relation presented by Versteeg & van Swaaij (1988).

$$D\mu^{0.6} = \text{constant} \tag{D7}$$

The diffusion coefficient of gases into aqueous electrolyte solutions has been estimated by the method suggested by Ratcliff & Holdcroft (1963).

$$\frac{D}{D_w} = 1 - \left(0.154\left[K_2CO_3\right] + 0.0723\left[KHCO_3\right]\right) \tag{D8}$$

where concentrations are in kmol.m^{-3}.

In case of the carbon dioxide absorption into carbonate solutions, ionic diffusion coefficients at infinite dilution were used. The ion diffusion coefficient at infinite dilution was estimated using the Nernst equation (Horvath, 1985).

$$D_i^{\infty} = \ell_i^{\infty} \frac{RT}{z_i F^2} \tag{D9}$$

The ionic conductivity at infinite dilution of various ions, ℓ_i^{∞}, was taken from the data available in Horvath (1985). In case of the hydrogen sulphide absorption into carbonate solution, the rate absorption is determined in whole or in part by the diffusion of carbonate ions to the reaction zone. The ionic diffusion of carbonate ions is influenced by the counter diffusion of bicarbonate and HS^- ions. In this case mean effective diffusivity of ions is used for the calculation. The dependence of these diffusivities on the concentration of the carbonate solution was assumed to follow the modified Stokes-Einstein relation presented by Versteeg & van Swaaij (1988).

D 3. Kinetic rate constants

An expression for the forward rate constant, $k_{1,1,}$ as a function of co-electrolytes concentration was presented by Pohorecki & Moniuk (1988).

$$\log \frac{k_{1,1}}{k_{1,1}^{\infty}} = 0.22\left(\frac{1}{2}\left[K^+\right]Z_{K^+}^2\right) + 0.22\left(\frac{1}{2}\left[OH^-\right]Z_{OH^-}^2\right) + 0.085\left(\frac{1}{2}\left[CO_3^{-2}\right]Z_{CO_3^{-2}}^2\right) \tag{D10}$$

where $k_{1,1}^{\infty}$ (m^3 kmol^{-1} s^{-1}) is the rate constant for infinitely dilute solution and T is in kelvin.

$$\log k_{1,1}^{\infty} = 11.916 - \frac{2382}{T} \tag{D11}$$

The effect of HCO_3^- on the value of $k_{1,1}$ has not been reported, hence its influence on the forward rate constant was neglected.

Since the reactions (2) and (3) involve only proton transfer and can be considered as instantaneous, these reactions are assumed to be at equilibrium.

The reaction rate constant of the reaction of water with carbon dioxide, $k_{4,1}$, as a function of temperature is given by Sharma & Danckwerts (1966). The reaction is first order with respect to the concentration of the carbon dioxide.

$$\log k_{4,1} = 329.850 - 110.541.\log T - \frac{17265.4}{T} \qquad \text{(D12)}$$

The reaction of hydrogen sulphide with hydroxyl ion is a proton transfer reaction and can be considered as instantaneous one. The forward rate constant of reaction (11), $k_{5,1}$, is has been measured to be 10^7 m^3 $kmol^{-1}$ s^{-1} (Karmann, 1967) at 293 K. The information on the dependence of $k_{5,1}$ on the temperature was not mentioned.

D 4. Equilibrium constants

The equilibrium constant of the reaction (1), K_1 (m^3 $kmol^{-1}$), can be determined by the combination of the equilibrium for reaction (4) and reaction (3). The equilibrium constant for the reaction (2), K_2 (m^3 $kmol^{-1}$), at infinite dilution is reported by Hikita et al. (1976).

$$\log K_2^{\infty} = \frac{1568.94}{T} + 0.4134 - 0.006737T \qquad \text{(D13)}$$

The effect of the electrolyte concentration on K_2 is given by Hikita et al. (1976) and Roberts & Danckwerts (1962).

$$\log \frac{K_2}{K_2^{\infty}} = \frac{1.01\sqrt{\left[K^+\right]}}{1 + 1.49\sqrt{\left[K^+\right]}} + 0.061\left[K^+\right] \qquad \text{(D14)}$$

The solubility product, K_w ($kmol^2$ m^{-6}), has been taken from Tsonopolous et al. (1976).

$$\log K_w = -\left(\frac{5839.5}{T} + 22.4773\log T - 61.2062\right) \qquad \text{(D15)}$$

The equilibrium constant of reaction (4), K_4 ($kmol$ m^{-3}) is reported in Sharma & Danckwerts (1966).

$$\log K_4 = \frac{-3404.7}{T} + 14.843 - 0.03279T \qquad \text{(D16)}$$

The equilibrium constant of reaction (11) can be calculated from the first dissociation constant of hydrogen sulphide and ionic product of water. The first dissociation constant of hydrogen sulphide, K_a, is given by Tsonopolous et al. (1976).

$$\log K_a = \frac{-5643.83}{T} - 33.5471 \log T + 94.9363 \qquad \text{(D17)}$$

Table D1. *Parameters used for CO_2 absorption in aqueous K_2CO_3 solution at 297 K.*

Parameter	Unit	0.25 M	0.5 M
m	(-)	0.74	0.63
$k_{1,1}$	$m^3\,kmol^{-1}\,s^{-1}$	$9.84\,10^{3}$	$12.32\,10^{3}$
$k_{1,2}$	s^{-1}	$2.07\,10^{-4}$	$2.54\,10^{-4}$
$k_{4,1}$	$m^3\,kmol^{-1}\,s^{-1}$	$2.37\,10^{-2}$	$2.37\,10^{-2}$
$k_{4,2}$	s^{-1}	$5.42\,10^{4}$	$5.42\,10^{4}$
D_{CO_2}	$m^2\,s^{-1}$	$1.75\,10^{-9}$	$1.64\,10^{-9}$
$D_{CO_3^{-2}}$	$m^2\,s^{-1}$	$8.82\,10^{-10}$	$8.42\,10^{-10}$
$D_{HCO_3^-}$	$m^2\,s^{-1}$	$1.14\,10^{-9}$	$1.01\,10^{-9}$
D_{OH^-}	$m^2\,s^{-1}$	$5.40\,10^{-9}$	$5.15\,10^{-9}$

Table D2. *Parameters used for H_2S absorption in aqueous K_2CO_3 solution at 293 K.*

Parameter	Unit	0.2 M	1 M	2 M
m	(-)	2.31	1.05	0.39
$K_{5,1}$	$m^3\,kmol^{-1}\,s^{-1}$	10^{7}	10^{7}	10^{7}
$K_{5,2}$	s^{-1}	0.82	0.82	0.82
D_{H_2S}	$m^2\,s^{-1}$	$1.83\,10^{-9}$	$1.60\,10^{-9}$	$1.41\,10^{-9}$
D_{ion}	$m^2\,s^{-1}$	$1.12\,10^{-9}$	$9.78\,10^{-10}$	$8.62\,10^{-10}$

Appendix E: Characterization of the membrane for determination of the membrane mass transfer coefficient

E1. Introduction

A membrane gas contactor offers several advantages over the conventional gas-liquid contactors. Improved performance can, however, only be realized, if the larger interfacial offered by membrane contactors is not compromised by the additional mass transfer resistance of the membrane. The membrane mass transfer coefficient can be determined through its structural properties such as thickness, pore size, porosity and tortuosity (Kreulen et al. 1993a). These membrane properties can be estimated easily for the membranes with uniform cylindrical pores. However, the assumption of uniform cylindrical pores is not valid for most of membrane structures. In this appendix, these membrane properties are determined for the microporous hollow fiber Accurel Q3/2 membranes by single gas permeation method (Guijt et al. 2000).

E2. Theory

The transport of a single gas through a porous membrane can be described by the dusty gas model. In case of the Accurel Q3/2 hollow fiber membrane the maximum pore size is 0.64 μm and average pore size is 0.2 μm according to the manufacturer's specification, which are comparable to the mean free path of most of the gases at ambient conditions. Hence both Knudsen diffusion and viscous flow will contribute to the total gas flow through the membrane pores according to Eq. (E1).

$$N = -\frac{1}{RT}\left[K_o V_m + B_o \frac{P}{\mu}\right]\nabla P \qquad \text{(E1)}$$

where V_m is mean molecular velocity of the gas defined by Eq. (E2)

$$V_m = \sqrt{\frac{8RT}{\pi M}} \qquad \text{(E2)}$$

K_o and B_o are the Knudsen diffusion and viscous flow morphology parameters of the membrane. For a homogeneous membrane K_o and B_o are membrane specific constants and independent of the permeating gas as long as no other gas-membrane interaction takes place (e.g. adsorption, surface diffusion). For membranes with uniform cylindrical pores K_o and B_o are given by Eq.(E3)

$$K_o = \frac{2\varepsilon r_p}{\tau}; \qquad B_o = \frac{\varepsilon r_p^2}{8\tau}; \qquad \text{(E3)}$$

where ε and τ are membrane porosity and tortuosity respectively. Eq. (E1) can be integrated over the membrane wall to give the outlet molar permeation flux. The final equation can be rearranged to get the membrane properties K_o and B_o.

$$\frac{PQ_G \, ln\left(\frac{r_o}{r_i}\right)}{2\pi L \Delta P} = K_o V_m + \frac{B_o}{\mu} P_{avg} \qquad \text{(E4)}$$

where P is shell side pressure, Q_G is the volumetric permeation gas flux with respect to the outer membrane area, P_{avg} is the arithmetic mean of the gas pressure at the inside and at the outside of the membrane fiber, ΔP is pressure difference between the inside and the outside of the membrane fiber. According to this equation K_o and B_o can be calculated from the slope and intercept of the plot of LHS of equation (E4) versus P_{avg}.

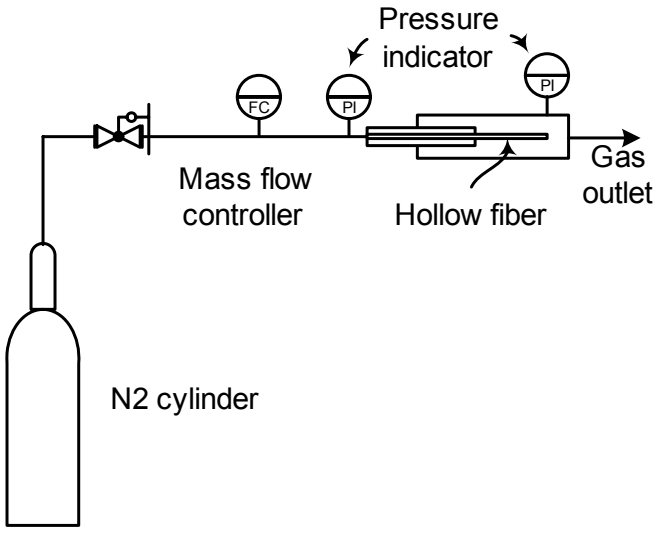

Figure E1: *Experimental set up for the single gas permeation experiments.*

E3. Experimental

The single gas permeation experiments were carried out using Accurel Q3/2 microporous hollow fiber and nitrogen as a test gas. A schematic representation of the experimental set-up is given in the Figure E1. A dead end construction is chosen so that the entire flow is forced through the fiber. To ensure the constant pressure inside the fiber, small fiber length (3.6 cm) is used for the experiments. The gas flow from the cylinder is controlled using mass flow controller. Digital pressure transducers are used to measure the pressure inside and outside of the fiber. The average of three readings was taken for each individual measurement.

E4. Results

The plot of LHS in Eq. (E4) versus P_{avg} is shown in Figure E2. A good straight line correlation is obtained for the plot. The values of the membrane constant K_o and B_o are calculated from the slope and the intercept of the plot. $K_o = 4.23.10^{-8}$ m, $B_o=2.12.10^{-15}$ m^2 and $\varepsilon/\tau = 0.42$ is obtained for Accurel Q3/2 microporous hollow fiber. The estimated ε/τ value is in good agreement with the value estimated from the literature data; $\varepsilon/\tau = 0.36$ (Guijt et al. 2000).

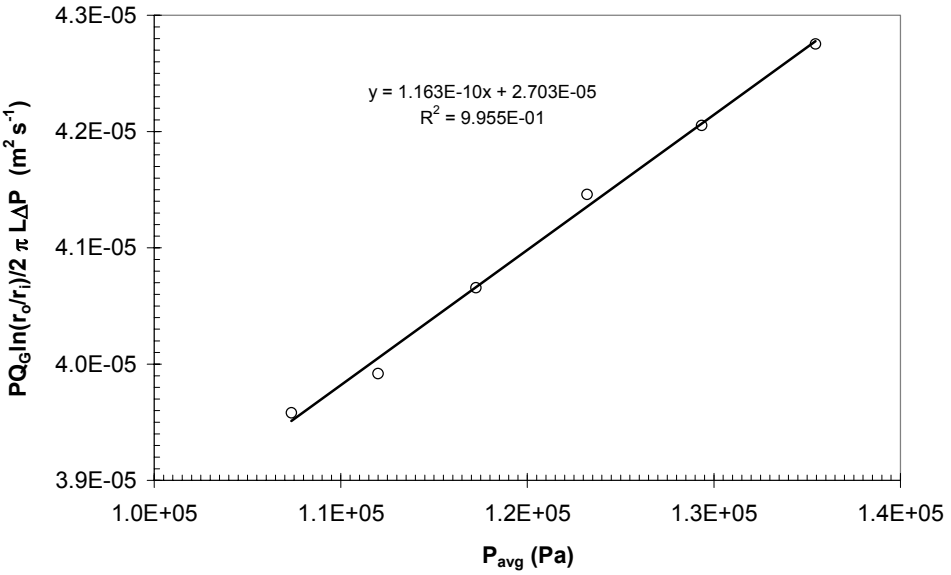

Figure E2: *Results for the single gas permeation experiments.*

Chapter 6

Hollow Fiber Membrane Contactor as a Gas–Liquid Model Contactor

Abstract:

Microporous hollow fiber gas-liquid membrane contactors have a fixed and well-defined gas-liquid interfacial area. The liquid flow through the hollow fiber is laminar, thus the liquid side hydrodynamics are well known. This allows the accurate calculation of the fiber side physical mass transfer coefficient from first principles. Moreover, in the case of gas-liquid membrane contactor, the gas-liquid exposure time can be varied easily and independently without disturbing the gas-liquid interfacial area. These features of the hollow fiber membrane contactor make it very suitable as a gas-liquid model contactor and offer numerous advantages over the conventional model contactors. The applicability and the limitations of this novel model contactor for the determination of physico-chemical properties of non-reactive and reactive gas-liquid systems are investigated in the present work. Absorption of CO_2 into water and into aqueous NaOH solutions are chosen as model systems to determine the physico-chemical properties for non-reactive and reactive conditions respectively. The experimental findings for these systems show that a hollow fiber membrane contactor can be used successfully as a model contactor for the determination of various gas-liquid physico-chemical properties. Moreover, since the membrane contactor facilitates indirect contact between the two phases, the application of hollow fiber model contactor can possibly be extended to liquid-liquid systems and/or heterogeneous catalyzed gas-liquid systems.

1.0 Introduction

A separation or production process using absorption involves transfer of one or more species from the gaseous phase to the liquid phase. In general, the absorption process can be categorized as a physical absorption or a chemical absorption. In the case of physical absorption the gaseous solute is physically dissolved in the liquid phase, whereas in the case of chemical absorption the gaseous solute reacts chemically in the liquid phase. To design an absorption system using either physical or chemical absorption, detailed information is required on the diffusivities, the solubility of the gaseous solute in the liquid bulk and the reaction rate kinetics. Various laboratory scale gas-liquid model contactors are used for acquiring this information and for discerning the controlling mechanism in the process of mass transfer accompanied by chemical reaction. In these model contactors the interfacial area is generally known so that the mass transfer coefficient can be calculated from the rate of absorption. The laboratory scale model contactors may be classified into two categories:

(1) Absorbers for which the fluid dynamics of the liquid phase are well understood.

(2) Absorbers which reproduce, on a laboratory scale, the characteristics of industrial absorbers.

Table 1: *Comparative evaluation of model contactors.*

Property	Hollow fiber	Laminar jet	Wetted wall	Stirred cell
G-L exposure time (s)	0.01-10	0.001-0.1	0.1-2	0.06-10
k_L (m s^{-1})	$1.0x10^{-4}$-$1.0x10^{-5}$	$1.6x10^{-3}$-$1.6x10^{-4}$	$1.6x10^{-4}$-$3.6x10^{-5}$	$1.6\ x10^{-5}$-$2.1\ x10^{-4}$
Interface orientation	Orientation free	Vertical	Vertical	Horizontal
Typical liquid use x 10^{-6} m^3/expt.	≈ 1000	≈5000	≈5000	≈ 500
Limitations	Wetting of membrane	Laborious	Laborious	Unknown hydrodynamics
Liquid-Liquid system	Possible	Not possible	Not possible	Possible
Operation mode w.r.t liquid phase.	Continuous	Continuous	Continuous	Batch

The first category includes model contactors like the laminar jet apparatus, the wetted wall column and the rotating drum contactor. In these types of contactors the physical mass

transfer coefficient can be estimated theoretically. The second category includes the disc tower, the multiple-sphere absorber and the stirred cell contactor. In these types of contactors, the physical mass transfer coefficient has to be determined using non-reactive systems. In general, the first category model contactors are used to determine the reaction kinetics and physical properties of gas-liquid system and second category contactors are usually used to simulate the industrial contactors. The details on these types of contactors are given in the literature (Danckwerts, 1970). A comparative evaluation of these types of contactors in terms of achievable contact time and mass transfer coefficients is given in Table 1.

Membrane gas-liquid contactors have a fixed and known mass transfer area (i.e. the physical area of the membrane). This feature of membrane contactors allows easy adaptation of membrane contactors into gas-liquid model contactors to determine the reaction kinetics and physical properties of the gas–liquid system as well as to simulate the industrial absorbers. For example, a flat sheet microporous membrane can be used in the stirred cell to fix the gas liquid interface. This allows use of higher stirring speeds in the liquid phase without disturbing the interfacial area, thus widening the operating range of the stirred cell contactor. Microporous hollow fiber membrane modules can also be conveniently converted into a model contactor. The operation of such a hollow fiber model contactor closely resembles to that of the laminar jet apparatus. The optimized hollow fiber membrane model contactor offers several advantages over the conventional model contactors. Since the liquid flow through the hollow fiber is usually laminar, the liquid side hydrodynamics are well known. This allows the accurate calculation of the physical mass transfer coefficient from first principles. In the case of conventional model contactors in which liquid phase is in continuous mode e.g. laminar jet and wetted wall column, the entrance and the exit effects affect the determination of the flow patterns and mass transfer area. This limitation is easily eliminated in the hollow fiber membrane model contactor by providing sufficient entrance length for laminar velocity profile to develop before exposing the liquid to the gaseous solute. In the case of the stirred cell apparatus, convection current set near the gas-liquid interface due to temperature variation or concentration variation (initiated if the saturated solution is denser the pure solvent) results into an unstable system. These convection currents can have significant influence on the measurement of the diffusivities and solubilities. These convection currents can be eliminated using narrow hollow fiber membranes. Stefan (1878) has successfully applied the method of absorption of a gas into a liquid contained in a narrow tube to determine the gas diffusivities. More recently, Anders Hoff (2003) has demonstrated that optimized hollow fiber membrane contactor can be used for determination of reaction kinetics.

In the present study, the general applicability of a hollow fiber membrane contactor as model contactor is explored. Initially, physical absorption of carbon dioxide into water is

carried out to study the performance of the system at shorter contact times and to optimize the system. Absorption of carbon dioxide into aqueous sodium hydroxide is chosen as a model system to test the applicability for the measurement of chemical and physical parameters for reactive systems.

2.0 Theory

The rate of absorption of a solute A into an absorbing liquid based on first principle is given by the Fick's law.

$$J_A = -D_A \left(\frac{\partial C_A}{\partial x} \right)_{G\text{-}L\ interface} \tag{1}$$

However, this procedure is not applicable in most of cases due to the laborious work required to determine the exact concentration gradient near the gas-liquid interface. Hence, a more simple approach of mass transfer coefficient is used.

$$J_A = k_L \left(C_{A,I} - C_{A,L} \right) \tag{2}$$

The mass transfer coefficient can be estimated accurately if the exact hydrodynamics near the interface is known. In the case of a liquid flowing though the hollow fiber, the liquid flow is in the laminar (for Re < 2100) region hence the hydrodynamic conditions near the interface are well known and the liquid side mass transfer coefficient can be calculated from Leveque's solution for heat transfer.

For Gz < 10, $Sh = 3.67$ (3)

For Gz > 20, $Sh = 1.62\ (Gz)^{1/3}$ (4)

Kreulen et al. (1993b) presented a fitted correlation that is valid over the intermediate range of Graetz numbers (Gz).

$$Sh = \frac{k_L d}{D_A} = \sqrt[3]{3.67^3 + 1.62^3\, Gz} \tag{5}$$

In Eq. (2), $C_{A,L}$ is the mixing cup (analogous to average bulk) concentration of A averaged over the length of the hollow fiber. For laminar flow of liquid through a hollow fiber, with a fully developed velocity profile, the mixing cup concentration of A in the liquid, at any axial distance, z from the liquid inlet side of the fiber is given as follows (Kreulen et al., 1993b):

$$C_{m,z} = C_{A,I} \left[1 - exp\left(- \frac{4 k_L z}{< v > d} \right) \right] \tag{6}$$

The average bulk concentration of A ($C_{A,L}$) in the fiber can be obtained from the integration of $C_{m,z}$ over the length of the fiber.

$$C_{A,,L} = \frac{C_{A,I}}{L}\left\{L + \frac{< v > d}{4k_L}.\left[exp\left(-\frac{4k_L\ L}{< v > d}\right) - 1\right]\right\} \tag{7}$$

The absorption flux over the length of the fiber can be calculated using Eqs. (2) and (7) if the physical properties of the system are known. Conversely, it is also possible to determine the physical properties of the non-reactive systems from experimental measurements of the absorption flux.

In the case of chemical absorption, the absorption flux is enhanced due to chemical reaction and the average absorption flux is given by

$$J_A = Ek_L\left(C_{A,I} - C_{A,L}\right) \tag{8}$$

The enhancement factor, E, describes the effect of chemical reaction on the mass transfer rate. Generally the enhancement factor (E) is defined as the ratio of absorption flux in presence of chemical reaction to the absorption flux in absence of chemical reaction for identical mass transfer driving force. Several approximate solutions to predict the enhancement factor (E), based on the different mass transfer models, are available in the literature and are applicable over a wide range of process conditions, reactions of differing complexity and chemical solute loadings. However, all the models assume the presence of a well mixed liquid bulk adjacent to the mass transfer zone (relatively large compared to the diffusion zone). This may not be the case for the gas absorption into the liquid flowing through a hollow fiber, especially for smaller diameters. In such cases, depending upon the gas-liquid contact time, the mass transfer zone in the liquid phase of the hollow fiber may actually extend up to the axis of the fiber and the centerline concentration may be disturbed. An additional feature in the gas absorption into a liquid flowing in a hollow fiber is the presence of a velocity profile in the liquid side mass transfer zone. Kumar (2002) used a modified approximate solution to predict the enhancement factor for gas absorption with second order chemical reaction in a liquid flowing through a hollow fiber. The application of the modified approximate solution was limited to relatively high values of Graetz number. However, rigorous numerical solutions are required to determine the enhancement factor at low Graetz numbers and for complex reactions. The measurement of the absorption flux in different absorption regimes and comparing it with the approximate-analytical or numerical solutions allows the determination of the chemical and physical properties for reactive systems.

3.0 Numerical model

For the reactive absorption of a gas in a liquid flowing through a microporous hollow fiber, the differential mass balance for any species 'i' present in the liquid phase is given by,

$$v_z \frac{\partial C_i}{\partial z} = D_i \left[\frac{1}{r} \frac{\partial}{\partial r} \left(r \frac{\partial C_i}{\partial r} \right) \right] - S_i \tag{9}$$

In arriving at Eq. (9), the diffusion in axial direction was neglected and axis-symmetry of the hollow fiber was assumed. 'S' is the source term due to the chemical reaction. Since the liquid flow inside the fiber is laminar, the velocity profile in the radial direction is given by,

$$v_z = 2 < v > \left[1 - \left(\frac{r}{R} \right)^2 \right] \tag{10}$$

The partial differential Eqs. (9) require the following initial and boundary conditions in the axial and radial directions respectively and the physical meaning of these boundary conditions are described in Chapter 4 (Section 3).

At z = 0; for all r; $C_i = C_{i,0}$ (11)

For z > 0; at r = 0; $$\left(\frac{\partial C_i}{\partial r} \right) = 0 \tag{12}$$

For z > 0; at r = R; $$\left(\frac{\partial C_i}{\partial r} \right)_{i \neq A} = 0 \tag{13}$$

$$- D_A \left(\frac{\partial C_A}{\partial r} \right) = k_{ext} \left(C_{A,G,bulk} - C_{A,G,I} \right) \tag{14}$$

The external mass transfer coefficient (k_{ext}) is a lumped parameter comprising of the resistances to mass transport of species 'A' due to the gas phase and the microporous membrane.

i.e., $$\frac{1}{k_{ext}} = \frac{1}{k_G} + \frac{1}{k_M} \tag{15}$$

The set of partial differential equations (the number depends on the number of chemical species involved in the reaction scheme) was solved numerically using a technique described in Chapter 4 (Section 4). The concentration profile of the absorbed gas (A) in the liquid phase was obtained from the solution of the mass balance equations. The local

absorption flux of A along the length of the fiber was subsequently calculated using Fick's law. The average absorption flux ($<J_A>$) was obtained from the integration of the local fluxes along the length of the fiber.

$$< J_A > = \frac{1}{L} \int_0^L J_A(z)\, dz \tag{16}$$

The exact numerical enhancement factor (E) is defined as the ratio of the absorption rate/flux of a gas in the liquid in the presence of a chemical reaction to the absorption rate/flux in the absence of a reaction.

$$E_{num} = \frac{< J_{A,Chem} >_{num}}{< J_{A,Phys} >_{num}} \tag{17}$$

It should be noted that the definition for the enhancement factor in Eq. (8) traditionally applies to a situation where the driving force (of A) for mass transfer is identical in the presence and absence of a chemical reaction. However, the above conditions may not be satisfied for large gas-liquid contact times in a membrane contactor (or at low Graetz numbers). In these situations, there will be a significant concentration of A in the liquid 'bulk' for the case of physical absorption. Nevertheless, this definition will be used to calculate the overall enhancement factor for a membrane contactor.

4.0 Characterization of Hollow Fiber Model Contactor

As discussed in the previous sections, because of well defined flow pattern and known mass transfer area, the hollow fiber membrane contactor can be used to determine various physico-chemical properties. In this section, the applicability of this new model contactor for the different absorption regimes is analyzed. The possibility of using simplified equations under the limiting cases is also explored.

4.1 Physical absorption

In general, diffusion coefficients of gases in inert liquids are obtained by means of the Taylor capillary method or the diaphragm cell method. However, these methods are time consuming and require considerable quantities of the liquid and the gas. A more rapid and reliable determination of the diffusivity of the gas into the solution is possible using the hollow fiber model contactor.

The Graetz number ($V_L d^2/D_A L$) is the ratio of the penetration time of the solute gas to reach the axis of the hollow fiber (from the gas-liquid interface) to the average residence time of the liquid in the fiber. At higher Graetz number, penetration of the solute is very small as compared to the internal radius of the fiber. Hence at high Graetz numbers, the average bulk

concentration of the solute in the fiber is very small. Figure 1 shows the effect of Graetz number on the average bulk concentration for initially unloaded solvent. It can be seen that at Graetz number larger than 1000, the average bulk concentration can be neglected in comparison with the gaseous solute concentration present at the gas–liquid interface. In this case the absorption process corresponds closely to that into a liquid of infinite depth and the Eq. (2) can be modified to Eq. (18).

$$J_A = k_L C_{A,i} = 1.62\left(\frac{V_L}{dL}\right)^{1/3} D^{2/3} C_{A,I} \qquad (18)$$

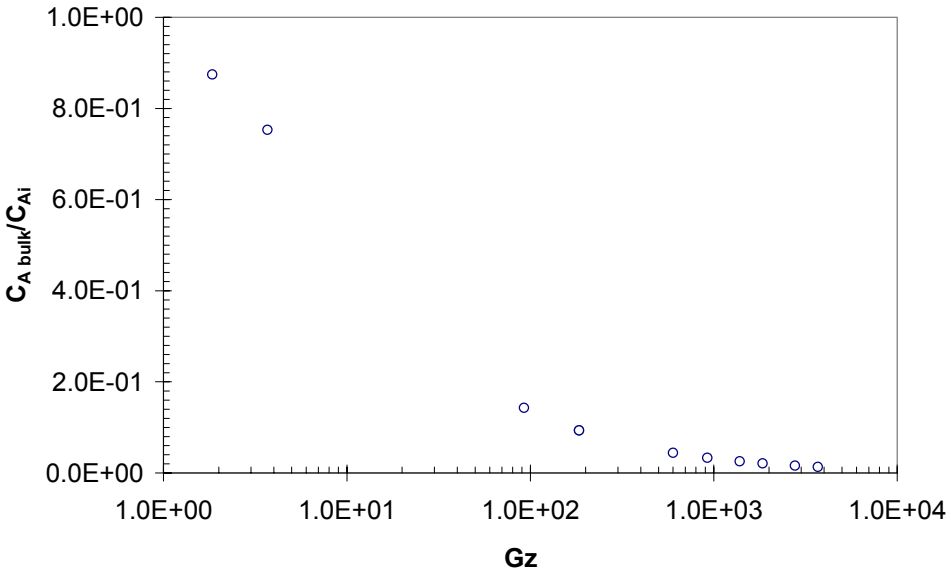

Figure 1: *Effect of Graetz number on the average bulk concentration.*

At higher Graetz numbers for the case of hollow fiber model contactor the gas absorption flux is proportional to the parameter ($D^{2/3}C_{AI}$). A plot of experimentally measured flux against $1.62(V_L/dL)^{1/3}$ should give a straight line through the origin at high Graetz numbers, having a slope of ($D^{2/3}C_{AI}$). At sufficiently high Graetz number, ($D^{2/3}C_{AI}$) can be determined from the slope of the plot using Eq. (18). However, the estimation of the Graetz number requires knowledge about the diffusivity of gas in the solution. Hence the experiments should be carried out at relatively high velocity, small fiber length and larger fiber diameter. A parametric study of the accuracy of this method is done using a theoretical analysis of carbon dioxide absorption into water. A plot of the theoretically calculated flux from Eq. (2) versus the parameter $1.62(V_L/dL)^{1/3}$ is shown in Figure 2. It can be seen from Figure 2 that at lower values of $1.62(V_L/dL)^{1/3}$ the data does not follow the straight line correlation through the origin. However, it is possible to draw a straight line passing through the origin for each data point. The slopes of thus drawn individual lines are also plotted in Figure 2 as a function of $1.62(V_L/dL)^{1/3}$. It can be seen from Figure 2 that the slopes of these

individual lines increases with $1.62(V_L/dL)^{1/3}$ and reaches a plateau at higher values of $1.62(V_L/dL)^{1/3}$. The value of this plateau should be used to calculate $(D^{2/3}C_{AI})$. Thus if any of the parameter, diffusivity or solubility, is known the other parameter can be determined easily. The comparison between the plots for two different fiber diameters indicates that this plateau is reached at somewhat lower values of $1.62(V_L/dL)^{1/3}$ for larger diameter. This is mainly because as the fiber diameter increases the average bulk concentration in the fiber decreases.

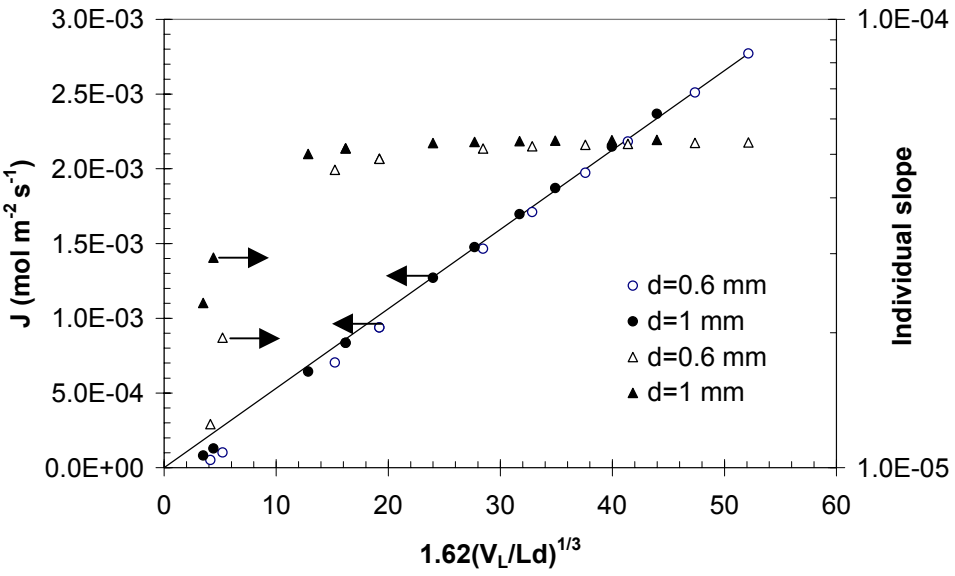

Figure 2: *Estimation of $(D^{2/3}C_{AI})$ using hollow fiber model contactor. Parameters used: L = 0.1 m; C_{AG}=40.87 mol m^{-3}; V_L=1x10^{-3}-2.0 ms^{-1}; m=0.845; T = 298 K.*

4.2 First order irreversible reaction

In the case of a first order irreversible reaction, the local reaction rate is proportional to the concentration of the dissolved gas 'A'. The rate of reaction is given by

$$R_A = -k_1 C_A \tag{19}$$

Substitution of Eq. (19) in Eq.(9) and solving with the appropriate boundary conditions gives the concentration profile of the solute in the fiber. The average absorption flux and numerical enhancement factor can be calculated using Eqs. (16) and (17) respectively. For mass transfer followed by first order irrreversible chemical reaction with infinite bulk the asymptotic approximate solution for enhancement factor in fast reaction regime (Ha >2) based on surface renewal theory is given by

$$E = Ha \tag{20}$$

where $$Ha = \frac{\sqrt{k_1 D_A}}{k_L} \qquad (21)$$

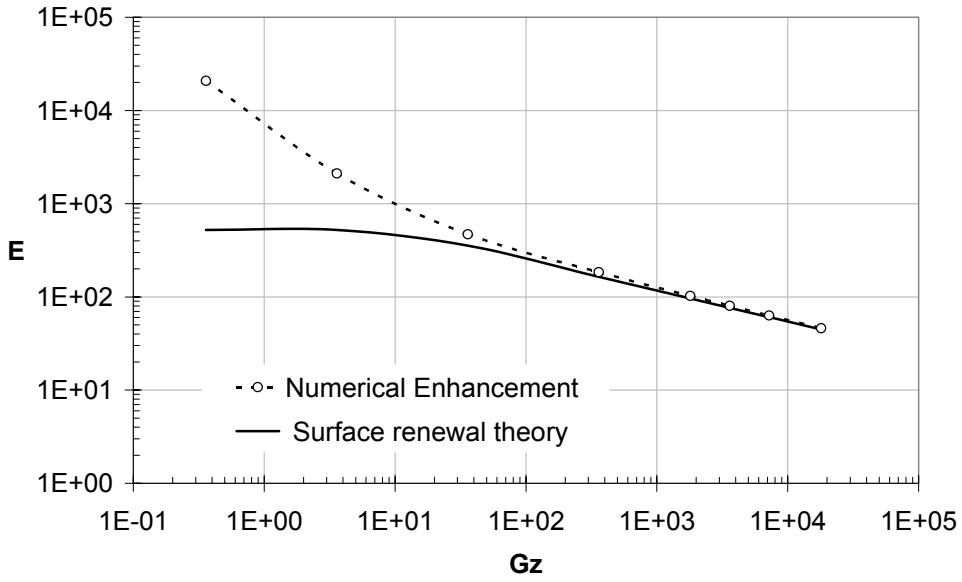

Figure 3: *Effect Graetz number on the enhancement factor for the gas absorption with first order irreversible reaction in a liquid flowing through a hollow fiber model contactor. Simulation conditions: L = 0.1m; d=600 x10^{-6}m; C_{AG}=10 mol m^{-3}; V_L=1x10^{-4}-5.0 ms^{-1}; k_1=1000 s^{-1}; D_A=1x10^{-9} m^{2}s^{-1}; m=1.0; The line indicates the E given by surface renewal theory for first order irreversible reaction (E=Ha).*

Figure 3 shows the enhancement factor predicted by the surface renewal theory as well as the exact numerical enhancement factor (Eq. 17) for reactive absorption of a gas in a liquid flowing at laminar conditions inside the hollow fiber as a function of Graetz number. The enhancement factor based on the surface renewal theory is estimated using mass transfer coefficient, $k_{L,}$ for the laminar flow conditions in the hollow fiber from Eqs. (3)-(5). It can be seen from Figure 3 that at higher Graetz numbers, the numerical enhancement E_{num} equals to the enhancement factor predicted by the surface renewal theory. At higher Graetz numbers the average bulk concentration for physical absorption is very small and can be neglected (see Figure 1). In this case the driving force for the physical and chemical absorption becomes identical. In addition, the mass transfer zone even for physical absorption is thin and restricted to the gas-liquid interface; therefore the error due to the curvature of the fiber is small and can be neglected. Hence at higher Graetz numbers (Gz >1000), the enhancement factor in the case of gas absorption in a liquid flowing through a hollow fiber can be given by traditional mass transfer theories and the average absorption flux can be calculated using Eqs. (8) and (20). In this case the average bulk concentration, C_{AL}, is zero. However, at low values of the Graetz number the numerical enhancement factor is much higher as compared to the enhancement factor predicted by the surface renewal theory. This is due to the saturation of

the liquid bulk in the corresponding case of physical absorption at lower Graetz numbers, thus substantially reducing the driving force for the corresponding case of physical absorption. In such cases rigorous numerical solutions are required to predict the enhancement factor and hence to calculate the average absorption flux.

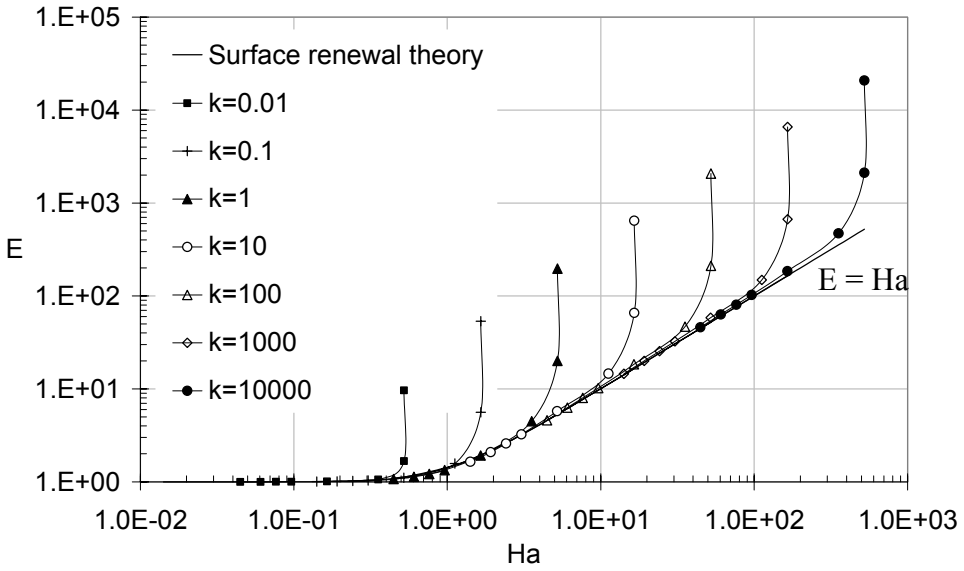

Figure 4: *E Vs Ha plot for the gas absorption with first order irreversible reaction in a liquid flowing through a hollow fiber model contactor. Simulation conditions: L = 0.1m; d=600 x10^{-6}m; C_{AG}=10 mol m^{-3}; V_L=1x10^{-4}-5.0 ms^{-1}; k_1=1x10^{-2}-1x10^4 s^{-1}; D_A=1x10^{-9} m^{2}s^{-1}; m=1.0; The line indicates the E given by surface renewal theory for first order irreversible reaction (E=Ha).*

In general the enhancement factor due to the chemical reaction is given as the E versus Ha plots. Figure 4 shows the traditional E versus Ha plot based on approximate solution for the surface renewal theory as well as the exact numerical results for the case of gas absorption in a liquid flowing through a hollow fiber accompanied by first order reaction. The Ha-number is varied by changing the first order reaction rate constant, k_1, and mass transfer coefficient, k_L, (by changing Graetz number). It can be seen from Figure 4 that there is no unique E-Ha master curve due to the saturation effects in the physical absorption case.

Figure 5 shows the effect of the liquid velocity and the parameter $C_{AI}(k_1D_A)^{1/2}$ on the average absorption flux in the fast reaction regime for different simulation conditions. It can be seen from the figure that the average absorption flux is independent of the liquid velocity and proportional to the parameter $C_{AI}(k_1D_A)^{1/2}$. Thus measurements of the experimental absorption flux in this regime, and comparing the measured absorption flux with the flux predicted by traditional mass transfer models using Eqs. (8) and (20) for higher values of

Graetz numbers or with flux predicted using exact numerical simulations, allows the estimation of $C_{AI}(k_1D_A)^{1/2}$ group.

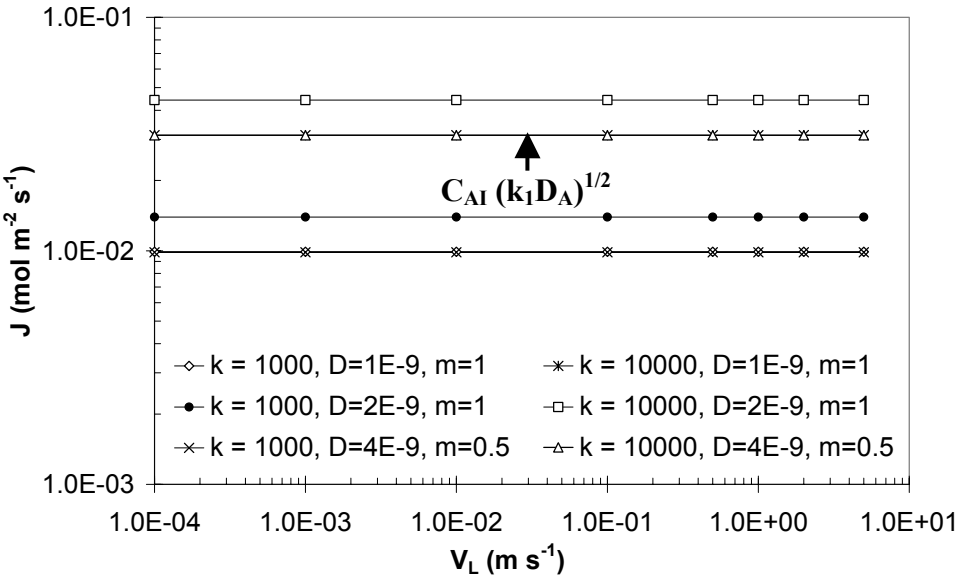

Figure 5: *Effect of liquid velocity on the average absorption flux for the gas absorption in a fast reaction regime in a liquid l flowing through a hollow fiber model contactor. Simulation conditions: L = 0.1m; d=600 x10^{-6}m; C_{AG}=10 mol m^{-3}.*

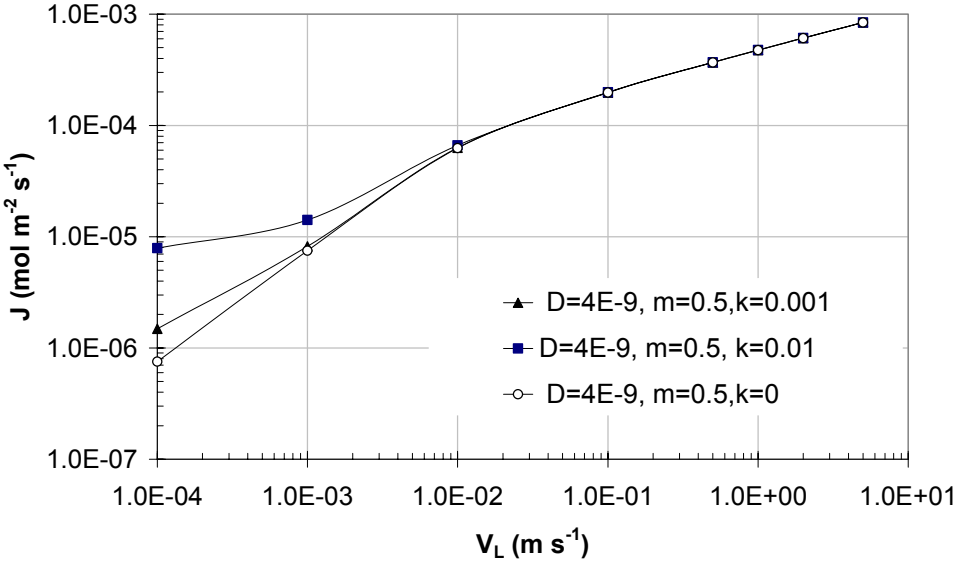

Figure 6: *Effect of liquid velocity on the average absorption flux for the gas absorption in a slow reaction regime in a liquid flowing through a hollow fiber model contactor. Simulation conditions: L = 0.1m; d=600 x10^{-6}m; C_{AG}=10 mol m^{-3}.*

In the case of the slow reaction regime, (Ha < 0.3), there is no enhancement due to chemical reaction. In this regime the absorption flux depends on the mass transfer coefficient and hence liquid velocity. Figure 6 shows the effect of liquid velocity on the average absorption flux in slow reaction regime. It can be seen from the figure than at higher values of liquid velocities (corresponds to low Ha number), the chemical absorption flux coincides with the physical absorption flux. In this regime, the absorption flux is again proportional to the parameter ($D^{2/3}C_{AI}$). Thus by measuring the absorption flux as a function of liquid velocity, the parameter ($D^{2/3}C_{AI}$) can be estimated.

4.3 Second order irreversible reaction

In the case of a second order irreversible reaction, the rate of reaction is proportional to the concentration of the dissolved gas 'A' as well as the liquid phase reactant 'B'. The rate of second order irreversible reaction is given by Eq. (22). The average absorption flux and numerical enhancement factor can be calculated by solving Eq.(9) using Eq. (22).

$$R_A = -k_{1,1}C_AC_B \qquad (22)$$

In the case of mass transfer in a liquid flowing through a hollow fiber accompanied by a second order (1,1) irreversible reaction, the saturation of species A as well as the depletion of species B in the liquid bulk is important. Under the limiting conditions of high Graetz numbers, the penetration depth of reacting species and hence the reaction zone is confined near the gas-liquid interface. Consequently, liquid far from the interface (at the axis of the fiber) is essentially undisturbed so that the depletion of species B as well as the saturation of the liquid with the solute can be neglected. This situation is analogous to the situation where a liquid bulk is assumed to be present at infinite distance, as in traditional mass transfer models. At high Graetz numbers the concentration of liquid phase reactant B at the axis of fiber is the same as the concentration of B at the inlet of the fiber. This situation is also referred as the pseudo-first order reaction regime. For this case, Kumar (2002) modified the definition of the dimensionless Hatta number and asymptotic enhancement factor based on the conditions at inlet of the fiber (z=0) and showed that, based on these definitions, it is possible to predict effect of chemical reaction on absorption flux using the approximate asymptotic solutions.

Thus when the Graetz number is relatively high and conditions for the fast reaction regime are satisfied ($2<Ha<<E_\infty$), the enhancement factor in the case of hollow fiber model contactor is equal to the modified Hatta number and the average absorption flux can be calculated using Eq. (8) with zero average bulk concentration and the enhancement factor given by Eq. (23). Similar to the irreversible first order reaction system, in this case also the average absorption flux is independent of k_L (and hence independent of the liquid velocity) and proportional to the parameter $C_{AI}(k_{1,1}D_AC_{B0})^{1/2}$. Thus from the measurement of experimental absorption flux, the parameter $C_{AI}(k_{1,1}D_A)^{1/2}$ can be estimated. However, when

the depletion of the liquid phase reactant 'B' is small but not negligible, the rigorous numerical model is required to fit the data.

Modified Hatta number: $$Ha = \frac{\sqrt{k_{1,1}\ D_A\ C_{B,0}}}{k_L} \tag{23}$$

At low Graetz numbers the penetration depth and hence the reaction zone may extend up to the axis of the fiber. Therefore the absorption regime can continuously change from the liquid entrance to the liquid exit. At the liquid inlet, there is no depletion of the species B at the gas-liquid interface and the absorption rate is influenced by the chemical reaction rate (kinetics), while the liquid velocity has no effect on the local absorption rate (Fast regime). Further, along the length of the fiber, depletion of the species B occurs at the interface. In the case of complete depletion of species B at the interface, the absorption rate is limited by the radial diffusion of the reacting species to the reaction plane and the flux is strongly influenced by the mass transfer coefficient (Instantaneous regime). At sufficiently low Graetz numbers and when $C_{B0}D_B/C_{AI}D_A << Ha$, the absorption regime over the entire fiber can be assumed as instantaneous reaction regime. In this case, the enhancement factor is given by modified asymptotic infinite enhancement factor and the average absorption flux can be calculated using Eq. (8) with zero average bulk concentration and the enhancement factor given by Eq. (24).

Modified infinite enhancement factor: $$E_\infty = \left(1 + \frac{C_{B,0}\ D_B}{\nu_B\ C_{A,,1}\ D_A}\right)\left(\frac{D_A}{D_B}\right)^n \tag{24}$$

The value of 'n' depends on the type of mass transfer model chosen. In the present case where a boundary layer flow is present in the mass transfer zone, the value of 'n' is equal to 1/3. In the instantaneous regime the average absorption flux is determined by C_{AI}, C_{B0}, D_A, D_B, ν_B and k_L. It may, therefore, be possible to infer the values of one of these quantities from the measure absorption flux if the values of other quantities are known or can be estimated.

For the general case the approximate enhancement factor, based on DeCoursey's solution, (using the definition of modified Hatta number and modified infinite enhancement factor) is given by Eq. 25;

$$E_{app} = \frac{-Ha^2}{2\left(E_\infty - 1\right)} + \sqrt{\left[\frac{Ha^4}{4\left(E_\infty - 1\right)^2} + \frac{E_\infty\ Ha^2}{\left(E_\infty - 1\right)} + 1\right]} \tag{25}$$

In the extreme case of very low Graetz number, the species 'B' is completely consumed by the reaction over a certain portion of the fiber and then species 'A' starts physically absorbing into the liquid phase containing the reaction product till it is saturated

with the species 'A'. In such cases, the enhancement due to the chemical reaction is entirely determined by the stoichiometric coefficients and the concentrations of species A and B.

Figure 7 shows the E-Ha plot for a second order reaction (with $\nu_B = 1$) . By comparing Figure 7 and Figure 4, it can be seen that this limit (here:100) is reached in case of second order reaction for all $k_{1,1}$ values, whereas in case of in the case of first order reaction no such limit is present.

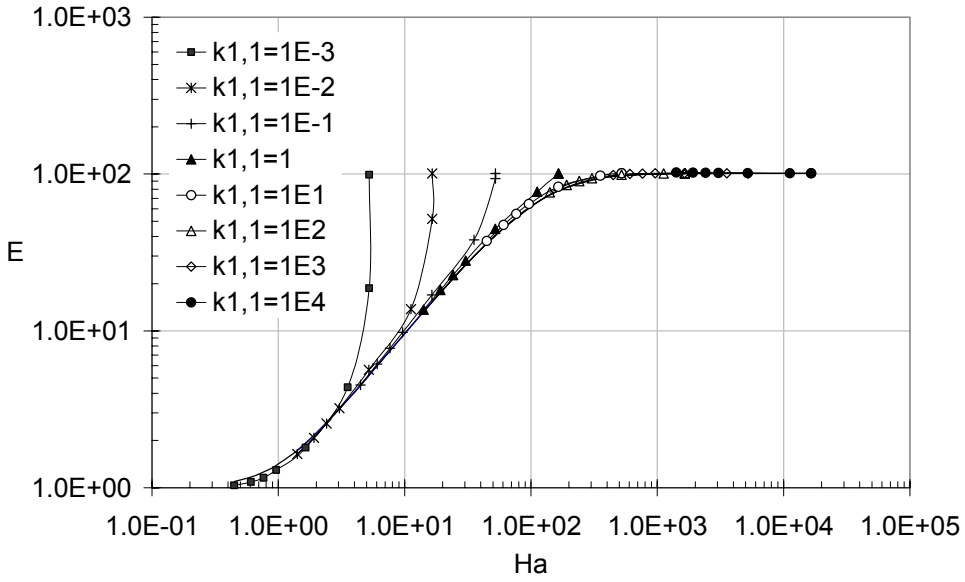

Figure 7: *E Vs Ha plot for the gas absorption with second order irreversible reaction in a liquid flowing through a hollow fiber model contactor. Simulation conditions: L = 0.1m; d=600 x10^{-6}m; C_{AG}=10 molm^{-3}; C_{B0}=1000 molm^{-3}; V_L=1x10^{-4}-5.0 ms^{-1}; k_1=1x10^{-2}-1x10^4 s^{-1}; D_B=D_A=1x10^{-9} m^{2}s^{-1}; m=1.0; The line indicates the E given by Decoursey's solution based on surface renewal theory.*

5.0 Experimental

Experiments were carried out to explore the applicability of the hollow fiber membrane device as a model contactor for the measurements of physical and chemical parameters. The absorption of carbon dioxide into water was chosen as a model system to measure the physical parameters for a non-reactive system and the absorption of carbon dioxide into aqueous NaOH solutions was chosen as a model system for the measurement of physical and chemical parameter for a reactive system. To measure the combined mass transfer coefficient of the membrane and the gas phase separate experiments of NH_3 absorption into 2M sulfuric acid were carried out.

5.1 Selection of process conditions for physical absorption

As discussed in the Section 4.1, the simplified method can be used to measure physical parameters with hollow fiber model contactor at relatively high values of Graetz

numbers. Hence experiments are carried out at very high Graetz number (Gz >1000) so that the mass transfer zone is confined to the gas-liquid interface and Eq. (18) can be used to predict the average absorption flux. The Graetz number ($V_L d^2/DL$) can be increased by increasing the fiber diameter and/or the liquid velocity through the fiber and by decreasing the fiber length. The higher values of the fiber diameter and the velocity are limited by the critical Reynolds number (2100) for laminar flow. The lower values of the fiber length are limited by the least count of the measurement technique used in the experiments. In view of these limitations, the velocity through the fiber is increased till the Reynolds number remains well below the critical limit. To increase the accuracy of the measurements, instead of a single hollow fiber, a module of five identical short hollow fibers is used in the experiments. To minimize the gas side mass transfer limitations pure carbon dioxide is used at the shell side of the module. As the hollow fiber model contactor has several advantages over the laminar jet contactor, it was tried to achieve the exposure time similar to that are possible with the laminar jet contactor.

Table 2: *Experimental conditions.*

Absorption regime	**Fiber Length (m)**	**Velocity (m s^{-1})**	**Graetz number**	**C_{NaOH} mol m^{-3}**	**$C_{CO2,G}$ mol m^{-3}**	**Temperature K**
Physical	0.015	0.1 - 1	1260-12200	-	48	298
Fast	0.015-0.017	0.8 - 1	4000-10100	250-1500	7-8	298-307
Instantaneous	0.017	0.08	800-900	250-1000	52	302

5.2 Selection of process conditions for absorption in fast reaction regime

The absorption of CO_2 in NaOH is followed by a second order (1,1) irreversible reaction of CO_2 with OH^- ions. At relatively high pH (>10) values the reaction is given by Eq. (26).

$$CO_2 + 2OH^- \rightarrow CO_3^{2-} + H_2O \qquad (26)$$

As discussed in the Section 4.2, kinetic parameters can be measured when the reaction occurs in the fast reaction regime over the entire length of the fiber with negligible depletion of OH^- ions. Hence to minimize the depletion of OH^- ions and to carry the reaction in fast absorption regime the following conditions are chosen so that the necessary condition for fast reaction regime $2< Ha< E_\infty$ is satisfied.

1. A low CO_2 partial pressure is used so as to obtain lower value of $C_{A,I}$.

2. Short exposure time. For this, short fibers with high velocity of the liquid through the fiber are used.
3. Relatively high concentrations of OH^- ions. As an additional effect $C_{A,I}$ also decreases.

The conditions chosen for the measurement of the kinetics are given in Table 2.

5.3 Selection of process conditions for absorption in instantaneous reaction regime

To measure the diffusivity ratio of OH^--ions and carbon dioxide in aqueous NaOH solutions, experiments were carried out in the instantaneous reaction regime. To satisfy the necessary condition ($Ha > E_\infty$) for the instantaneous reaction regime, experiments are carried out using high partial pressures of CO_2. Experiments are carried out at long exposure times using low velocities of the liquid through the fiber. The experimental conditions chosen for the instantaneous absorption regime are given in Table 2.

(a)

(b)

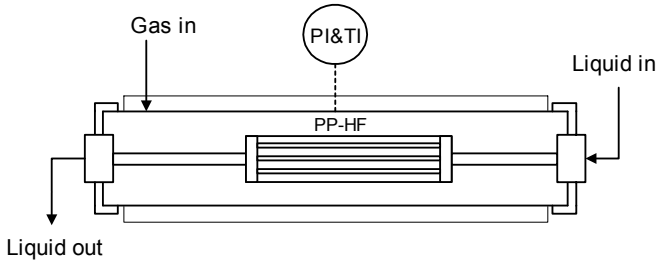

Figure 8: *Hollow fiber membrane model contactor*

5.4 Experimental procedure

Figures 8a and 8b show schematically the membrane contactor used for the absorption experiments. The details of the experimental set-up and experimental procedure are given in Chapter 2. Microporous polypropylene hollow fibers (Accurel PP: Type Q3/2; average pore diameter: 0.2 μm; inside diameter 600 μm) were used in this study. A module made up of five hollow fibers was used as a model contactor. The five hollow fibers were glued to a liquid distributor with the help of silicon glue. The length of each fiber exposed to the gas is also controlled by applying glue on the surface of the membrane. In this way, it was ensured that all five fibers have equal lengths. The glued part of the fiber provides sufficient distance for the laminar liquid flow profile inside the fiber to be fully developed before it contacts the

gas. In all the experiments the Reynolds number was maintain well below the critical value for turbulent flow (2100), generally Re < 1000.

A semi-batch mode of gas-liquid contacting operation was used during the experiments. The liquid flow through the fiber was continuous. The solvent was fed from a high pressure pump via a flow controller. The solvent used in the experiments was degassed before usage by applying vacuum in a separate apparatus. Before passing to the hollow fiber module, the solvent is passed through the heat exchanger to maintain the desired temperature. The carbon dioxide partial pressure outside the hollow fiber in the contactor was maintained constant by feeding pure carbon dioxide from a gas supply vessel, through a pressure regulator. During all the experiments the liquid side pressure was kept sufficiently higher than the shell side gas pressure to avoid the bubbling of gas. From the drop in the pressure of carbon dioxide in the gas supply vessel, the absorption rate and hence the average carbon dioxide flux across the membrane was calculated. The details of the flux calculation are given in Chapter 2.

6. Results and Discussion

6.1 Physical absorption experiments

Initial experiments are carried out to optimize the system for high liquid velocity through the fiber and for the short fiber lengths. Figure 9 shows the plot of k_L versus exposure time. From this figure it can be seen that exposure times in the order of 0.01 s are achieved. The k_L values obtained experimentally are in excellent agreement with those predicted by Leveque's equation with an average deviation of not more than 2 %. This result also confirms that the flow within hollow fiber is in the laminar region for these operating conditions.

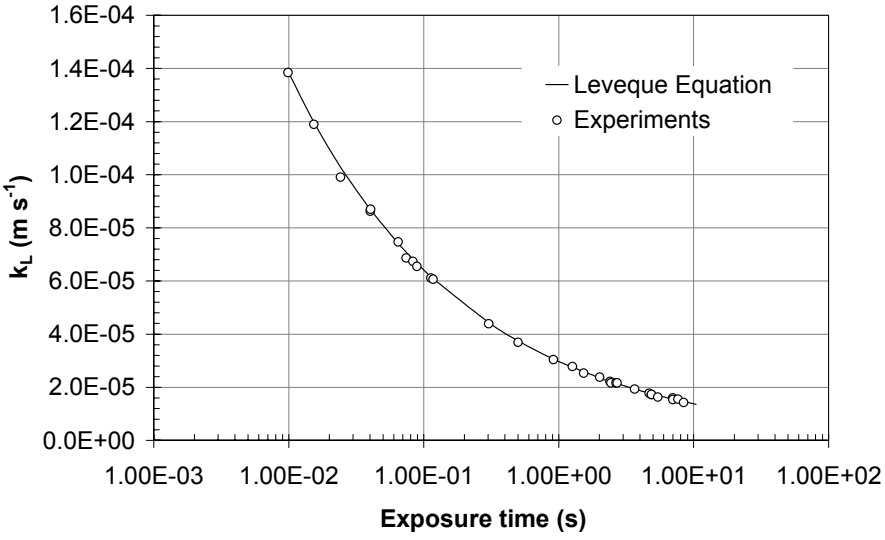

Figure 9: *Liquid side mass transfer coefficient versus exposure time for a hollow fiber model contactor; as determined by CO_2 absorption in water.*

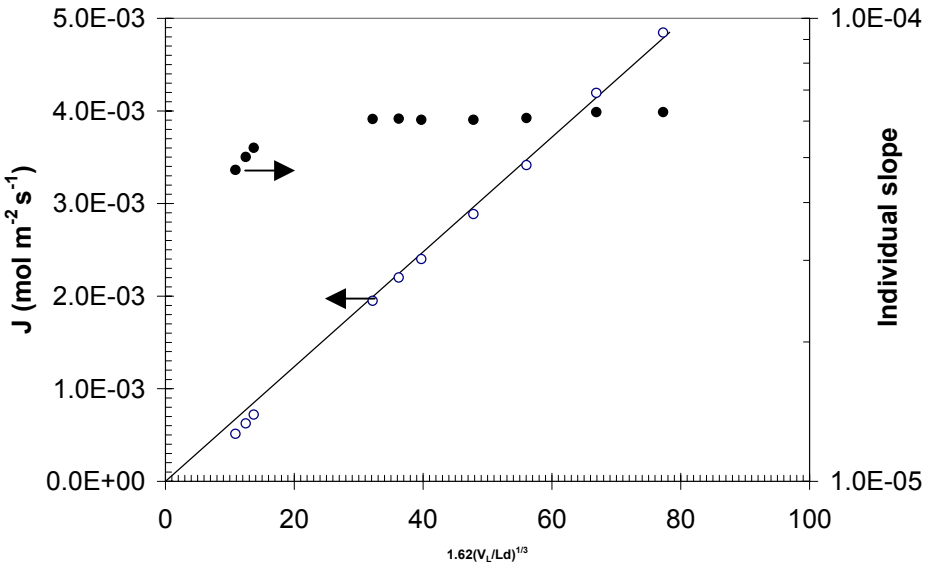

Figure 10: *Estimation of ($D^{2/3}C_{Ai}$) using a hollow fiber model contactor by CO_2 absorption in water. Experiment conditions: L = 0.015-0.33 m; C_{AG}=48.22 mol m^{-3}; V_L=0.05 -1.0 ms^{-1}; m=0.845; T = 298 K.*

The absorption of pure carbon dioxide into water is carried out at 298 K to measure the physical parameters. The plot of the experimentally obtained flux versus the parameter $1.62(V_L/dL)^{1/3}$ is shown in Figure 10. As discussed in Section 4.1, the individual slopes of the line passing through the origin and individual points are also calculated and plotted versus $1.62(V_L/dL)^{1/3}$. The individual slope reaches a constant value of 6.27x 10^{-5} at higher values of $1.62(V_L/dL)^{1/3}$. This value of slope is used to calculate the parameter ($D^{2/3}C_{AI}$). The solubility of the carbon dioxide is taken from the literature (Versteeg & van Swaaij, 1988). From the thus determined values of the parameter ($D^{2/3}C_{AI}$) and the solubility of carbon dioxide, the diffusivity of carbon dioxide into water at 298 K is calculated. This estimated value of the diffusivity (1.95 x 10^{-9} m^2 s^{-1}) is in good agreement with the literature reported data (1.92 x 10^{-9} m^2 s^{-1}).

6.2 Measurement of lumped gas and membrane mass transfer coefficient

The mass transfer coefficient of the membrane phase and the gas phase are combined to give a lumped parameter termed as external mass transfer coefficient k_{ext} in the development of the numerical model. This lumped mass transfer resistance can contribute substantially to the overall mass transfer process when inert are present in the gas phase and/or the enhancement due to the chemical reaction is considerably high. Hence detailed information on the external mass transfer coefficient is important for the accuracy of the data fitting. The membrane mass transfer coefficient can be estimated if the structural properties such as tortuosity (τ) and porosity (ε) of the membrane are known. The measurement of these properties and the estimation of the membrane mass transfer coefficient is discussed in detail

in Chapter 4 (Appendix E). The estimation of the gas side mass transfer coefficient is rather difficult due to the complex geometry of the contactor and lack of the information on the correlation to predict the gas side mass transfer coefficient for such systems. Hence it was decided to measure the lumped parameter experimentally. The absorption of NH_3 into 2 M sulfuric acid satisfies all criteria for the measurement of gas side mass transfer coefficient (Danckwerts, 1970), hence this system is used to measure the lumped mass transfer coefficient.

In these experiments, first the shell side of the contactor is filled with N_2 to about 110 kPa. A small quantity of NH_3 (8-25 kPa) was added to the shell side. The partial pressure of NH_3 was kept sufficiently small so that evaporation of the water due to the heat of reaction does not result into condensation of water in the module. The average absorption flux is calculated from the mass balance. The lumped mass transfer coefficient is calculated from the experimental absorption flux as given below.

$$k_{ext} = \frac{J_{expt}}{C_{G,NH_3}} \tag{27}$$

The thus determined value of k_{ext} was 1.01 x 10^{-2} m s^{-1}. This estimated value is used for the simulations in the next sections to fit the kinetic and physical parameters.

6.3 Absorption in fast reaction regime

The surface tension of a NaOH solution is high (due to its ionic nature), hence the liquid does not wet polyolefin microporous membranes. Considerable and accurate information is available in the literature on the physico-chemical parameters required to model the absorption process. Therefore absorption of CO_2 in aqueous NaOH is used as a model system to the study absorption in different reaction regimes and to check its ability to measure the physical and chemical properties by using a hollow fiber model contactor. In the numerical model reaction (26) was considered for the simulations. The solubility and diffusivity data used as input parameters in the model were obtained from theliterature (Schumpe & Weisenberger, 1996; Hikita et al., 1976). Electroneutrality in the liquid phase was maintained by using mean ion diffusion coefficients for the ionic species in the liquid phase.

To ensure that the absorption takes place in the fast reaction regime the experimental conditions are chosen as discussed in the experimental section. Figure 11 shows the effect of liquid velocity through the fiber on the average absorption flux. The absorption in the fast reaction regime is confirmed by the fact that flux was found to be independent of the liquid velocity through the fiber. Two different sets of experiments are carried out to study the effect of temperature and to study the effect of ionic strength on the second order reaction rate constant. For the higher accuracy and to take into account the effect of the lumped

external mass transfer coefficient, the numerical model developed in the Section 3 is used for the regression of the second order rate constant.

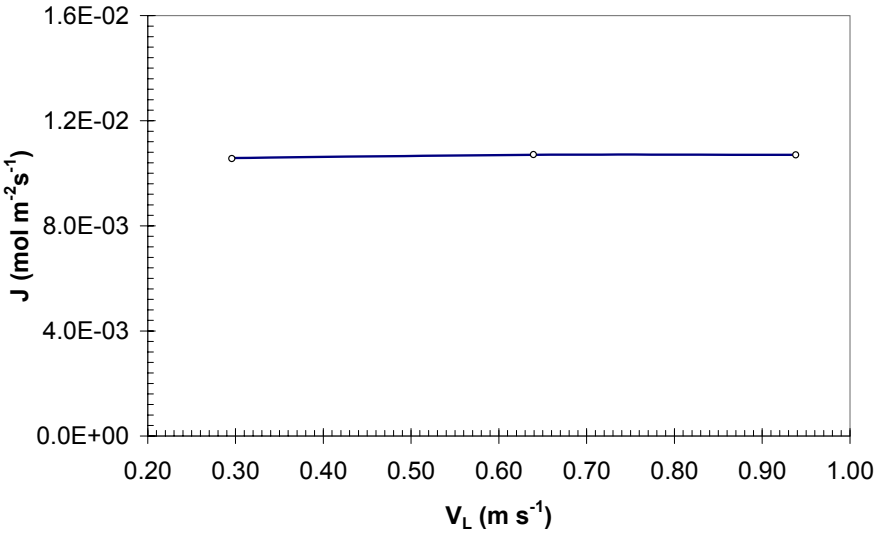

Figure 11: *Effect of liquid velocity on the average absorption flux of CO_2 in 0.5 M NaOH in a hollow fiber model contactor at 303 K.*

Figure 12 shows the Arrhenius plot for the estimated second order reaction rate constant for the absorption of CO_2 into 0.5 M NaOH solution. From the Arrhenius plot activation energy 'E_{act}' of the reaction is calculated. The estimated value of the activation energy 49.3 kJ mol^{-1} is in good agreement with the literature reported data of 44.8 kJ mol^{-1} for the ionic strength of 0.537 kmol m^{-3} (Pohorecki & Moniuk, 1988).

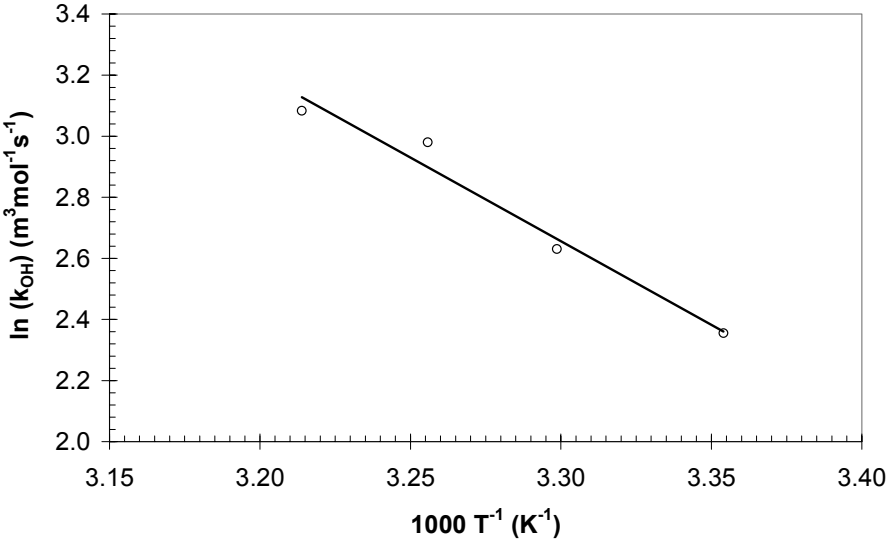

Figure 12: *Arrhenius plot for the second order reaction rate constant k_{OH}-.*

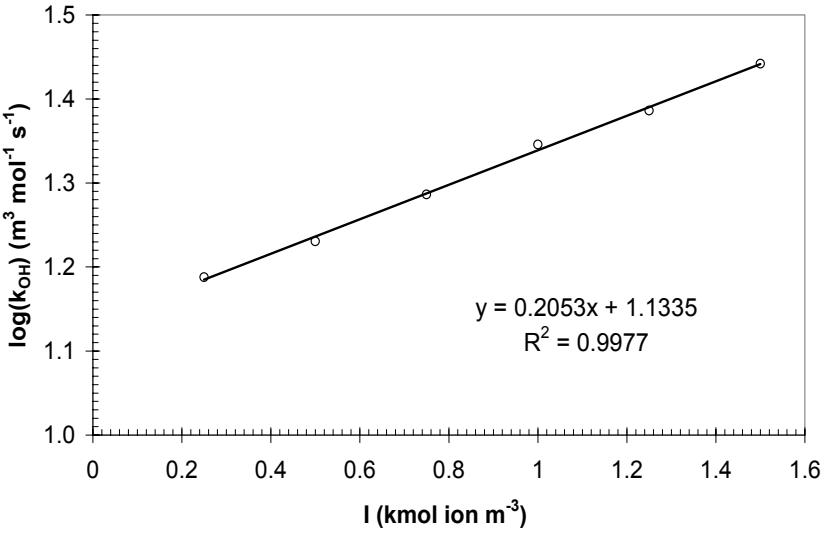

Figure 13: *Effect of ionic strength on the second order reaction rate constant k_{OH}- at 307 K.*

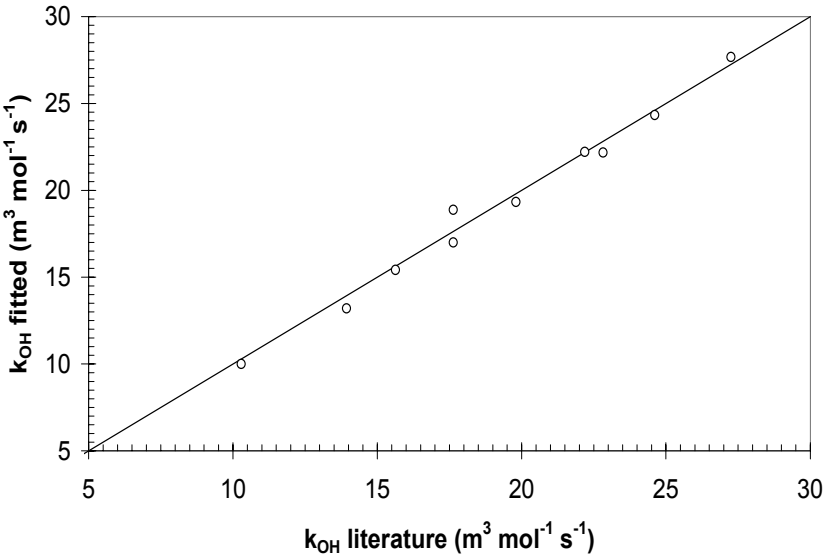

Figure 14: *Parity plot for second order reaction rate constant k_{OH}-.*

Figure 13 shows the effect of ionic strength on the estimated second order reaction rate constant at 307 K. It can be seen that inline with literature, the second order reaction rate constant increases with the ionic strength of the solution. Figure 14 shows the parity plot for the estimated second order reaction rate constant and the literature data (Pohorecki & Moniuk, 1988). It can be seen from the figure that there is good agreement between the experimentally estimated second order reaction rate constant using hollow fiber model contactor and the literature reported data.

6.4 Absorption in instantaneous reaction regime

The absorption in the instantaneous regime is governed by the diffusion process of the gaseous solute and the liquid phase reactant. As discussed in Section 4.3, the absorption flux

in the instantaneous regime is calculated using Eqs. (8) with zero average bulk concentration and using the enhancement factor given by Eq. (24). The flux equation can be simplified as given below.

$$J = k_L \left(\frac{D_A}{D_B} \right)^{\frac{1}{3}} C_{AI} + \frac{k_L C_{B0}}{\nu_B} \left(\frac{D_B}{D_A} \right)^{\frac{2}{3}} \tag{26}$$

The plot of experimentally observed flux versus the parameter $k_L C_{B0}/\nu_B$ can be used to estimate the diffusivity ratio of the liquid phase reactant to the gaseous solute into the liquid phase. To measure the diffusivity ratio, experiments were carried out in the instantaneous regime at 302 K. To ensure that the absorption take place in the instantaneous reaction regime (Ha >> E_∞) the experimental conditions are chosen as discussed in the experimental section. The parameter $k_L C_{B0}/\nu_B$ is varied by changing NaOH (i.e. C_{B0}) concentration.

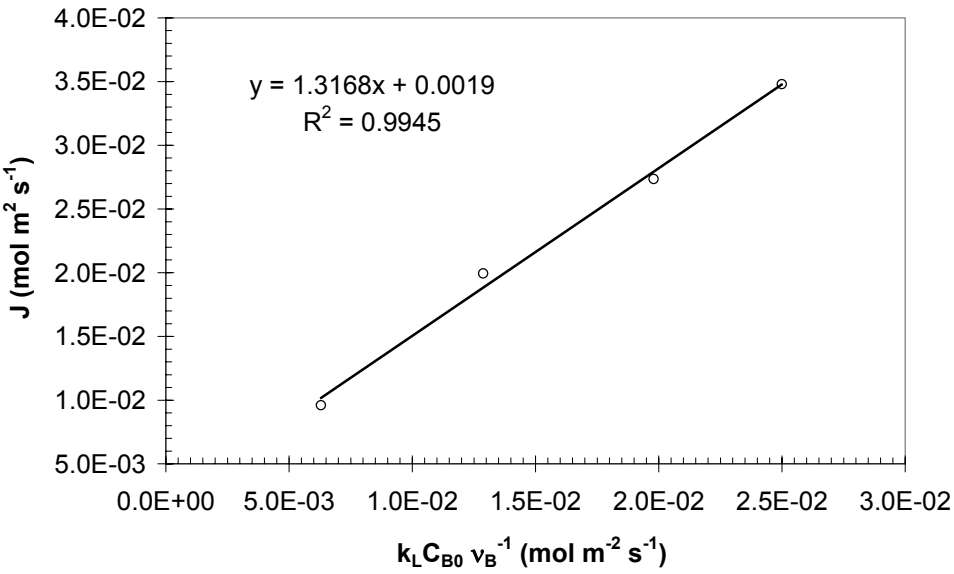

Figure 15: *Average absorption flux versus $k_L C_{B0}/\nu_B$ for absorption of CO_2 in NaOH in instantaneous regime.*

Figure 15 shows the plot of average absorption flux versus $k_L C_{B0}/\nu_B$. It can be seen from figure that as expected the average absorption flux is proportional to the parameter $k_L C_{B0}/\nu_B$. The diffusivity ratio can be calculated from the slope of the plot. Thus determined value of the ratio of diffusivity of OH^- ions to diffusivity of CO_2 in NaOH solution is 1.51 and is within 10 % of the literature reported value (Nijsing et. al. 1959).

When CO_2 reacts with OH^- ions, OH^- disappears and CO_3^{2-} ions are produced in the reaction zone. As a result the diffusion of OH^- to the reaction zone is affected by the counter

diffusion of CO_3^{2-}. Although the ionic diffusivity of OH^- ions is higher, the absorption of the CO_2 in instantaneous regime is governed by effective ionic diffusivity of OH^- ions. Hence the diffusivity ratio obtained and reported in the literature is much lower.

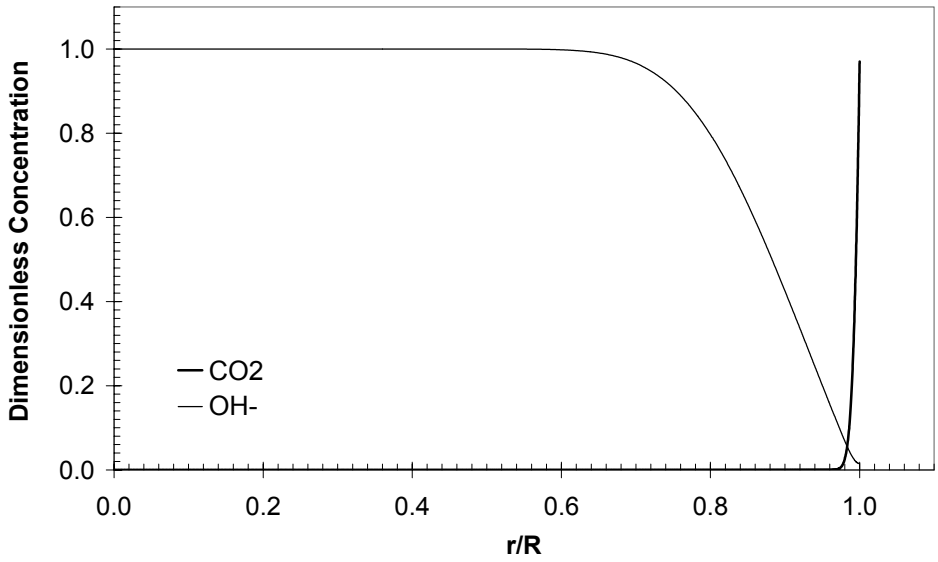

Figure 16: *The calculated radial concentration profile of CO_2 and OH^- ions in the liquid phase.*

To confirm the instantaneous regime, the radial concentration profile of CO_2 and OH^- ions at the liquid exit of the fiber is numerically calculated using the kinetics determined in the previous section and the diffusivity ratio determined in this section. This radial concentration profile for the case of absorption of pure CO_2 into 1M NaOH at 302 K is shown in Figure 16. It can be seen from figure that concentration of OH^- ions at the gas–liquid interface reaches to zero and instantaneous absorption regime is reached.

7.0 Conclusion

In present study, the use of hollow fiber membrane contactors as gas-liquid model contactor for the determination of physical and kinetic parameters for gas-liquid systems is explored. From detailed numerical simulations it was found that at relatively high Graetz numbers (>1000) the mass transfer zone in the case of gas absorption in a liquid flowing through a hollow fiber is very small and is confined near the gas-liquid interface. In such cases traditional mass transfer theories can be used to describe the mass transfer process with and without chemical reaction. Hence, at relatively high values of the Graetz number, the hollow fiber model contactor can be used to determine physical and chemical properties such as reaction rate constant, diffusivity and solubility from simplified asymptotic solutions. However, for a more complex reaction scheme and at low Graetz numbers a more detailed numerical model is required to fit these parameters.

The effect of unequal driving force, due to the saturation of liquid bulk in the case of physical absorption, in the determination of the enhancement factor for membrane hollow fiber contactors is recognized and analyzed for the cases of first order and second order reactions.

Experiments are carried out at high Graetz number to estimate the diffusivity and reaction rate constant for known systems namely absorption of CO_2 in water and in NaOH respectively. It was found that experimentally determined value of diffusivity of CO_2 in water at 298 K is in excellent agreement with the literature reported data. Effect of temperature and ionic strength on the second order reaction rate constant for the absorption of CO_2 in NaOH is studied using absorption in the fast reaction regime in the hollow fiber model contactor. The second order reaction rate constant is determined for different temperatures and ionic strengths. The ratio of effective diffusivity of OH^- ions and diffusivity of CO_2 in liquid phase is determined using absorption in the instantaneous reaction regime in the hollow fiber model contactor. The estimated values of the second order reaction rate constants and the effective diffusivity ratio are in good agreement with the literature reported data.

From the experimental validation it can be concluded that a hollow fiber membrane contactor can successfully be used as a model contactor for the determination of various gas-liquid physico-chemical properties. Moreover, since the membrane contactor facilitates indirect contact between the two phases, the application of hollow fiber model contactor can possibly be extended to liquid-liquid systems and/or heterogeneously catalyzed gas-liquid or liquid-liquid reaction systems.

Acknowledgement

This research is part of the research program performed within the Centre for Separation Technology (CST), which is a co-operation between the Netherlands Organization for Applied Scientific Research (TNO) and the University of Twente. We acknowledge Alexey Volkov for his help in experimental work. We would also like to thank Benno Knaken and Wim Leppink for the construction of the experimental set up.

Nomenclature

C	Concentration	[mol m^{-3}]
D	Diffusivity	[m^2 s-1]
d	Diameter	[m]
E	Enhancement factor	[-]
Gz	Graetz number , $\frac{vd^2}{Dz}$,	[-]
Ha	Hatta number	[-]
J	Flux	[mol m^{-2} s^{-1}]

k_1	First order forward reaction rate constant	[s^{-1}]
$k_{1,1}$	Second order forward reaction rate constant	[$mol^{-1}m^3\ s^{-1}$]
k	Mass transfer coefficient	[$m\ s^{-1}$]
L	Length	[m]
m	Distribution coefficient	[-]
r	Radius	[m]
Re	Reynolds number, $\frac{dv\rho}{\mu}$,	[-]
Sh	Sherwood number, $\frac{k_l d}{D}$,	[-]
v	Velocity	[$m\ s^{-1}$]
x	Distance	[m]
z	Length	[m]

Greek letters

ε	Porosity	[-]
τ	Tortuosity	[-]
ν	Stoichiometric coefficient	[-]

Subscripts

G	Gas
I	Interface
L	Liquid
M	Membrane
z	Local value
∞	Infinite value

References

Anders Hoff, K. (2003*). Modeling and experimental study of carbon dioxide absorption in a membrane contactor.* Ph.D. Thesis, NTNU, Norway.

Astarita, G. (1967). *Mass transfer with chemical reaction*. Amsterdam: Elsevier.

Danckwerts, P. V. (1970). *Gas liquid reactions*. New York: McGraw Hill.

Gabelman, A., & Hwang, S. (1999). Hollow fiber membrane contactors. *Journal of Membrane Science,* 159(1), 61-106.

Graetz, L. (1883). Über die Wärmeleitungsfähigkeit von Flüssigkeiten, 1e Abhandlung. *Annalen der Physik und Chemie*, 18, 79-84.

Hikita, H., Asai, S., & Takatsuka, T. (1976). Absorption of carbon dioxide into aqueous sodium hydroxide and sodium carbonate and bicarbonate solutions. *Chemical Engineering Journal*, **11**, 131-141.

Hovarth, A.L. (1985). *Handbook of aqueous electrolytic solutions: physical properties, estimation and correlation methods*. New York: John Wiley.

Kreulen, H., Smolders, C.A., Versteeg, G.F., & van Swaaij, W.P.M. (1993a). Microporous hollow-fiber membrane modules as gas-liquid contactors: 1. Physical mass transfer processes - A specific application - Mass transfer in highly viscous liquids. *Journal of Membrane Science,* 78(3), 197-216.

Kreulen, H., Smolders, C.A., Versteeg, G.F., & van Swaaij, W.P.M. (1993b). Microporous hollow-fiber membrane modules as gas-liquid contactors: 2. Mass transfer with chemical reaction. *Journal of Membrane Science,* 78(3), 217-238.

Kumar, P. S. (2002). *Development and design of membrane gas absorption processes*. Ph.D. Thesis, University of Twente, the Netherlands.

Leveque, J. (1928). Les lois de la transmission de chaleur par convection. *Annls. Mines, Paris (Series 12)*, 201.

Nijsing, R. A. T. O., Hendriksz, R. H., & Kramers, H. (1959). Absorption of CO_2 in jets and falling films of electrolyte solutions, with and without chemical reaction. *Chemical Engineering Science*, 10, 88-104.

Pohorecki, R., & Moniuk, W. (1988). Kinetics of the reaction between carbon dioxide and hydroxyl ion in aqueous electrolyte solutions. *Chemical Engineering Science*, 43, 1677-1684.

Schumpe, A., & Weisenberger, S. (1996). Estimation of gas solubility in salt solutions at temperatures from 273K to 363K. *A. I. Ch. E. Journal*, 42(1), 298-300.

Sharma, M.M., & Danckwerts, P.V. (1966). The absorption of carbon dioxide into solutions of alkalis and amines (with some notes on hydrogen sulphide and carbonyl sulphide). *Chemical Engineer*, (October), CE245-CE280.

Versteeg, G.F., & van Swaaij, W.P.M. (1988). Solubility and diffusivity of acid gases (CO_2, N_2O) in aqueous alkanolamine solutions. *Journal of Chemical & Engineering Data*, 33, 29-34.

Summary

Owing to the increasing energy demand and the abundance of low quality natural gas reservoirs containing high percentages of CO_2, considerable attention is given to the bulk removal of CO_2 and upgrading of low quality natural gas. The main goal in doing so is to increase the heating value of natural gas and to reduce the transportation cost. In addition, the large amount of CO2 emissions from anthropogenic sources is believed to contribute significantly to the green house effect and global warming. Hence, capture and storage of CO_2 from various gas streams, particularly flue or stack gas, from fossil fuel fired power plants has attracted world-wide interest. The CO_2 separation techniques in such cases may contribute significantly to the economics of the overall process. Conventional CO_2 capture technologies based on a variety of physical and chemical processes including absorption, adsorption and cryogenic separation are highly energy intensive and may not be used in these applications. Hence there is a need of energy efficient, flexible CO_2 capture technology operating over a wide range of concentrations and volumetric flow rates.

Membrane separation has emerged as an alternative to the conventional CO_2 capture processes for the upgrading of crude natural gas due to their energy efficiency and modular design. However, membrane separation processes are only economically attractive at low flow rates, high CO_2 concentrations and high feed pressures. In addition, the presence of impurities like H_2S adversely affects the process economics (Bhide & Stern, 1993). In the case of flue gas purification, the low CO_2/N_2 selectivity of commercially available gas separation membranes renders the membrane separation process less attractive (Gottlicher & Pruschek, 1997).

The benefits of the membrane separation can be combined with conventional absorption processes through a relatively new hybrid process known as 'Membrane Gas Absorption'. In this membrane gas absorption process, separation of a solute through the membrane is completely integrated with the absorption operation. Generally, membrane gas absorption processes use non-selective microporous hollow fiber membrane modules to carry out the mass transfer operation. These membrane contactors offer a flexible, modular, energy efficient gas-liquid contacting device with high specific surface area without loosing the selectivity aspect even at low concentrations of the solute. These membrane based gas absorption techniques can be adapted easily to the specific demands of an individual plant.

For economically viable processes, the pores of membrane should remain gas-filled during the operation. However, conventional absorption liquids for bulk CO_2 removal are found to wet the commercially cost-effective porous polyolefin membranes (Kreulen, 1993). The selection of a suitable membrane-absorbent combination is therefore of utmost importance in the development of membrane gas absorption process.

Previous work on the effect of the geometry on the performance of the membrane contactor has revealed that cross-flow membrane contactors offer several advantages over the conventional parallel flow contactors in terms of high shell side mass transfer coefficient, low pressure drop and reduced channeling effects. TNO Environment Energy and Process Innovation (the Netherlands) has patented and commercialized rectangular cross flow membrane contactors made of polypropylene hollow fibers (Feron & Jansen, 2002). The objective of the present study is to develop a stable membrane gas absorption process using such types of cross membrane contactors for the bulk removal of CO_2. In addition to the upgrading of low quality natural gas, its application in flue gas CO_2 capture can be foreseen.

As mentioned earlier, the selection of a proper membrane-absorbent combination is an important step in the development of membrane gas absorption processes. As no reliable guidelines are reported in literature for the selection of membrane-absorbent combinations, the governing and important criteria for the selection of membrane-absorbent combination are identified and evaluated for bulk CO_2 removal. The experimental findings of this evaluation suggested that PTFE and PP membranes can be used successfully in combination with propylene carbonate, an organic liquid, commercially applied for physical absorption of CO_2.

In membrane gas-liquid contactors usually an over pressure is applied on the liquid side to prevent bubble formation. However, long term application of such over pressures on the liquid side was found to affect the membrane morphology and resulted eventually in wetting of the membrane pores. This wetting phenomenon can be avoided successfully by reversing over-pressure and thus by retarding the liquid inside pores towards the liquid-side pore opening. In such cases the pressure drop over the fiber becomes a critical design parameter as a high pressure drop over the fiber may lead to wetting in the initial part of the fiber and/or bubbling in the end part of the fiber.

The gas absorption rates for the selected CO_2-water and CO_2-propylene carbonate in a hollow fiber absorption system (with liquid flowing through the fiber) can be described perfectly using the Graetz-Leveque equation. The single fiber membrane contactor was applied successfully at elevated partial pressures of CO_2 (up to 20 bars), which is comparable to situations in the low quality natural gas processing.

The shell-side mass transfer performance of a membrane module strongly depends on the shell-side mixing and the shell geometry. The mixing patterns on the shell side of these rectangular cross-flow hollow fiber membrane contactors are investigated in terms of three directional dispersion coefficients using dedicated gas-phase RTD measurements. A novel ultrasound based measurement technique is used to characterize the system. In general, the mixing in all direction increases with the shell side velocity. The presence of the fibers acts as a kind of packing on the shell side and thus reduces the axial mixing. The transversal

dispersion coefficient across the fiber is higher and more sensitive to the shell side velocity than the dispersion coefficient along the fiber due to the continuous splitting and remixing of shell side flow across the fibers.

In cross flow membrane contactors, the concentrations of both fluids and flow rate of the compressible fluid (gas phase) vary in both directions. Hence, unlike parallel flow contactors simple logarithmic averaging of the driving force can not be used to predict the performance of the cross flow contactors. Similar driving force changes except for the flow rate changes are observed in the cross flow heat exchangers. Hence when the volumetric flow changes are negligible, analogies developed for the cross flow heat exchangers can be applied to cross flow gas-liquid membrane contactors. The volumetric flow changes become significant at high solute concentration and at high removal fractions of the solute. In such cases a detailed mathematical model is required to predict the performance of the cross flow membrane contactor. The detailed mathematical model also provides a useful tool to optimize the cross flow contactor performance and to select the ideal operating conditions. To describe the mixing behavior on the shell side of cross flow membrane contactor, different mixing options were considered in the mathematical model. The numerical simulations showed that the effect of the shell side mixing pattern becomes important at high rates of removal and in such cases no-mixing on the shell side gives better performance.

The reactive absorption of a gas in a liquid is frequently preferred over physical absorption due to high specific rates of absorption, higher selectivity and lower solvent circulation. The effect of a chemical reaction on the absorption flux is given by traditional mass transfer theories in the form of an enhancement factor (E). However, the effects of the chemical reaction on the absorption into a liquid flowing through a hollow fiber may not be described using traditional mass transfer theories due to the lack of a well defined liquid phase bulk and the presence of the laminar velocity profile in the mass transfer zone, which is the case for cross-flow hollow fiber membrane contactors. In addition, the concentrations of both fluids, inside and outside the fiber, vary in the direction of flow as well as in direction perpendicular to the flow. These changes in concentration result into variations in the absorption regime over the entire volume of the contactor. To calculate the effect of chemical reaction on the absorption flux in a cross-flow membrane contactor, a detailed mathematical model is developed taking into account the complete reversible ionic reactions, equilibria, variation in concentrations and flow rates. The model was validated using the experimental data of absorptions of CO_2 and H_2S in aqueous carbonate solutions. An excellent match between experimental results and model predictions is obtained. The experimental observation also confirmed the fact that CO_2 absorption is controlled by the liquid side mass transfer resistance whereas H_2S absorption is controlled by the combined resistance of the membrane phase and the gas phase. The experimental study also demonstrates that aqueous

carbonate solution can be successfully used in combination with inexpensive polypropylene hollow fiber membranes for CO_2/H_2S removal.

The features like well-defined and fixed mass transfer area, well known hydrodynamics and wide range of exposure time makes the (single) hollow fiber membrane contactor ideal as a gas-liquid model contactor. It was demonstrated with model reactive as well as non-reactive systems that this novel contactor can be used to determine the physico-chemical parameters of the gas-liquid systems. Under asymptotic conditions, approximate solutions for the enhancement factor can be used to analyze the data; however, more generally a numerical model is required. Since the membrane contactor facilitates indirect contact between the two phases, the application of hollow fiber model contactor can possibly be extended to liquid-liquid systems and/or heterogeneous catalyzed gas-liquid systems.

References

Bhide, B.D., & Stern, S.A. (1993). Membrane processes for removal of acid gases from natural gas. II Effects of operating conditions, economic parameters and membrane properties. *Journal of Membrane Science*, **81**, 239-252.

Gottlicher, G., & Pruschek, R. (1997). Comparison of CO_2 removal systems for fossil fueled power plant processes. *Energy Conversion & Management*, **38**, S173-S178.

Feron, P.H.M., & Jansen, A.E. (2002). CO_2 separation with polyolefin membrane contactors and dedicated absorption liquids: performance and prospects. *Separation and Purification Technology*, **27**, 231-242.

Kreulen, H. (1993). *Microporous membranes in gas separation processes using a liquid phase*. Ph.D. Thesis, University of Twente, the Netherlands.

Samenvatting

Als gevolg van het toenemend energiegebruik en de ruime beschikbaarheid van laag-calorisch aardgas met een hoog kooldioxide gehalte wordt veel aandacht besteed aan het verwijderen van bulk hoeveelheden CO_2. Daarmee wordt de stookwaarde van het aardgas verhoogd en worden transportkosten en risico's op corrosie en koolhydraatvorming verminderd. Een andere reden voor de toenemende aandacht voor CO_2 scheidingstechnieken is de mogelijke rol van CO_2 in het vermeende broeikas-effect. Het afvangen en vervolgens opslaan van CO_2 uit diverse gasstromen, zoals stookgas van energiecentrales welke op fossiele brandstoffen gebruik, krijgt daarom wereldwijd aandacht. Het verwijderingsproces voor CO_2 uit een gasstroom is een belangrijke factor in dit geheel. Conventionele CO_2 verwijderingstechnieken zijn gebaseerd op verschillende fysische en chemische processen, waaronder absorptie, adsorptie en (cryogene) destillatie. Deze processen zijn vaak energie intensief en vormen daardoor een belangrijke kostenpost. Een energie-efficiënte, flexibele CO_2 scheidingstechniek, welke over een breed bereik van concentraties en volumetrische debieten kan opereren is derhalve zeer wenselijk.

Membraanscheiding is één van die technieken die, mede door het relatief lage energieverbruik en de modulaire opzet, wordt gezien als alternatief voor bovengenoemde conventionele processen om laag-calorisch aardgas op te werken. De membraankosten zijn echter dusdanig dat deze scheidingstechniek rendabel is bij lage gas debieten, hoge CO_2 gehaltes en een voedingsgas dat op verhoogde druk beschikbaar is. Daarbij verhoogt de mogelijke aanwezigheid van andere verontreinigingen, zoals zwavelwaterstof (H_2S), in de gasstroom de proceskosten aanzienlijk (Bhide & Stern, 1993). Voor rookgasreiniging is de lage selectiviteit voor CO_2 voor de huidige, commercieel beschikbare, membranen een belemmering (Gottlicher & Pruschek, 1997).

Belangrijke voordelen van membraanscheiding kunnen echter worden gecombineerd met de meer conventionele gas absorptie technieken in een relatief nieuw, hybride, proces, dat wordt aangeduid als 'Membrane Gas Absorption'. In dit hybride proces wordt de te verwijderen component door het membraan getransporteerd en vervolgens in een vloeistof geabsorbeerd. Voor deze scheidingstechniek wordt veelal een niet-permselectieve, microporeuze holle vezel membraanmodule voorgesteld. Deze membraancontactoren bieden flexibiliteit in ontwerp en operatie, zijn energie-efficiënt en hebben een groot specifiek uitwisselend oppervlak voor stoftransport, ongeacht variaties in debieten en concentraties van de processtromen. Door deze flexibiliteit kan een membraan gas-absorptie proces specifiek worden toegesneden op een bepaalde toepassing.

De proceseconomie hangt sterk samen met het benodigd membraan oppervlak. Om de transportflux per oppervlakte-eenheid van het membraan zo hoog mogelijk te houden is het

essentieel dat de membraan poriën gevuld zijn met gas en niet met de absorptievloeistof. De meeste conventioneel toegepaste absorptievloeistoffen voor de bulkverwijdering van CO_2 bevochtigen echter de commercieel verkrijgbare, kosten-efficiënte microporeuze polyolefine membranen (Kreulen, 1993). De juiste selectie van de combinatie van een membraan en een absorptie-vloeistof is derhalve van uitermate groot belang voor de economische doeltreffenheid van het scheidingsproces.

Uit eerdere studies naar het effect van de geometrie op de prestaties van membraan modules is naar voren gekomen dat dwars-aangestroomde membraan modules verschillende voordelen bieden boven de, meer toegepaste, parallel aangestroomde modules. Zo is de stofoverdracht aan de mantelzijde hoger, de drukval aan de mantelzijde lager en is er minder vaak sprake van voorkeursstroming. TNO-MEP (Apeldoorn) heeft dergelijke rechthoekige, dwars aangestroomde membraan modules, met polypropeen holle vezels, ontwikkeld, gepatenteerd en op de markt gebracht (Feron & Jansen, 2002).

Het doel van deze studie is de ontwikkeling van een membraan gas absorptie proces, gebruikmakend van bovengenoemde dwarsaangestroomde membraan modules, voor de verwijdering van bulk hoeveelheden CO_2. Naast het opwerken van laag-calorisch aardgas is het afvangen van CO_2 uit rookgas een voor de hand liggende toepassing van dit proces.

De selectie van een geschiktl membraan-absorptievloeistof combinatie is, zoals genoemd, een belangrijke stap in de ontwikkeling van membraan gas absorptie processen. Aangezien hiervoor geen richtlijnen voorhanden zijn in de literatuur, zijn in deze studie de belangrijkste criteria en selectie-technieken geëvalueerd en toegepast op de selectie van een geschikte combinatie voor CO_2 verwijdering. De experimentele resultaten wijzen uit dat teflon (PTFE) en polypropeen (PP) membranen met succes kunnen worden toegepast in combinatie met propyleencarbonaat, een reeds in conventionele fysische absorptie processen commercieel toegepaste, organische absorptievloeistof voor CO_2 absorptie.

In membraan gas-vloeistof contactoren wordt meestal een lichte overdruk aan de vloeistofzijde toegepast om belvorming in de vloeistof te vermijden. Na langdurige toepassing van een dergelijke overdruk bij bovengenoemd systeem van polypropyleen-propyleen carbonaat werd echter een verandering in de membraan morfologie waargenomen, welke uiteindelijk in volledige bevochtiging van de poriën resulteerde. Deze bevochtiging kon worden voorkomen cq. teruggedrongen door de lichte overdruk om te draaien en dus aan de gaszijde toe te passen. Hiermee is de drukval van de vloeistof, die door de vezel stroomt, over de lengte van de vezel een belangrijke ontwerp parameter geworden. Een te hoge drukval kan leiden to bevochtiging aan de ingangszijde van vezel of belvorming in de vloeistof nabij het einde van de vezel.

Uit de experimentele resultaten blijkt dat de gas absorptiesnelheden voor de geselecteerde CO_2-water en CO_2-propyleen carbonaat systemen voor gas absorptie in een

holle vezel contactor met vloeistof stroming door de vezel uitstekend kan worden beschreven met de Graetz-Levêque vergelijking. De holle-vezel membraanmodule is met succes toegepast bij verhoogde drukken tot CO_2 partiaalspanningen van 20 bar, overeenkomend met typische reinigingscondities voor een laag-calorisch aardgas.

De mantelzijde stofoverdracht hangt sterk samen met de menging aan de mantelzijde en de mantel geometrie. De menging aan de mantelzijde van de rechthoekige dwars-aangestroomde holle vezel membraan modules is gekarakteriseerd met behulp van metingen van de gas fase verblijftijdsspreiding. De metingen zijn geïnterpreteerd in termen van axiale en transversale dispersiecoëfficiënten in alle drie richtingen. Voor deze metingen is een op ultrasone geluidssnelheid en –demping gebaseerde meettechniek gebruikt. De menging neemt in alle richtingen toe met de gassnelheid. De aanwezige vezels zijn te beschouwen als een soort pakking en reduceren de axiale menging (dus in de hoofdstromingsrichting). De transversale dispersiecoëfficiënt voor de menging loodrecht op de vezelrichting is, door het continu opsplitsen en samenvoegen van stroomlijnen, groter en sterker afhankelijk van de gassnelheid dan de dispersiecoëfficiënt in de richting parallel aan de vezels.

In dwars-aangestroomde membraancontactoren variëren de concentraties in beide fluïda en varieert de volumetrisch gasfase debiet zowel in de gasfase hoofdstromingsrichting als in de richting parallel aan de vezels. Hierdoor is het, in tegenstelling tot parallel aangestroomde contactoren waar een logaritmische gemiddelde drijvende kracht voor stofoverdracht kan worden toegepast, niet mogelijk om op relatief eenvoudige wijze de overgedragen hoeveelheid te berekenen. Afgezien van effecten op het gasdebiet, bestaat er een vergelijkbare situatie van locaal variërende drijvende kracht bij dwars-aangestroomde warmtewisselaars. Reeds ontwikkelde analogiën voor bovengenoemde warmtewisselaars kunnen dan ook probleemloos worden toegepast voor dwars-aangestroomde gas-vloeistof membraancontactoren indien de veranderingen in het gasfase debiet verwaarloosbaar klein zijn. Dit is niet het geval voor gasstromen met een hoog CO_2 gehalte en waarbij een hoge CO_2 verwijderingsgraad wordt bereikt. In deze gevallen is een meer gedetailleerd mathematisch model vereist om de prestaties van een dwars-aangestroomde membraan module te kunnen voorspellen. Het hier ontwikkelde mathematisch model is een daarmee uitstekend middel om de membraan module prestaties te optimaliseren. Het mengpatroon aan de mantelzijde van de module is, in tegenstelling tot de vezel-zijde, niet à priori te voorspellen. Om de gevoeligheid van de resultaten voor de mate van menging aan de mantelzijde te onderzoeken zijn verschillende meng-opties geïmplementeerd. De simulaties hebben aangetoond dat het mengeffect pas belangrijk wordt bij hoge verwijderingsgraden per module. In deze situaties bleek een lagere transversale menging tot betere prestaties te leiden.

De reactieve absorptie van een gas in een vloeistof wordt vaak verkozen boven fysische absorptie vanwege de hogere specifieke absorptiesnelheid, een hogere selectiviteit en/of een lagere absorptievloeistof circulatie. Het effect van een chemische reactie op de

absorptieflux wordt in de stofoverdrachtstheorieën gewoonlijk in de vorm van een versnellingsfactor meegenomen. Bij de absorptie in een vloeistof, die door een holle vezel stroomt is geen goed gemengde vloeistof bulk aanwezig en in de vloeistof is er bovendien een laminair stromingsprofiel aanwezig nabij het gas-vloeistof grensvlak. Hierdoor kunnen bestaande stofoverdrachtstheoriëen niet zonder meer worden toegepast. Temeer daar de concentraties in beide stromen, binnen in en om de vezels, variëren in zowel de hoofdstromingsrichting als loodrecht daarop. Deze concentratieveranderingen kunnen resulteren in een variatie in het absorptie regime over het contactorvolume, waardoor de prestaties van de module niet op eenvoudige wijze kunnen worden berekend. Om deze effecten te kunnen beschrijven is een gedetailleerd mathematisch model ontwikkeld dat alle mogelijke reacties, reactie-evenwichten en variaties in concentraties en debieten verdisconteerd. Het model is gevalideerd met behulp van experimentele data voor de absorptie van CO_2 en H_2S in waterige carbonaatoplossingen. Hierbij is een goede overeenstemming van de experimentele resultaten met à priori model voorspellingen verkregen. De resultaten bevestigen dat de CO_2 absorptie wordt bepaald door de vloeistofzijde stofoverdrachts-weerstand, terwijl de H_2S absorptie wordt bepaald door de gecombineerde weerstand van de membraanfase en gasfase. De experimentele studie toont tevens aan dat een waterige carbonaatoplossing, in combinatie met de relatieve goedkope polypropeen holle vezel membranen een succesvol systeem vormt voor de verwijdering van CO_2 en H_2S.

De eigenschappen van een goed-gedefinieerd, vast oppervlak voor stofoverdracht, een bekende stromingspatroon voor de vloeistof (vezel-) zijde en de mogelijkheid tot variatie van de gas-vloeistof contacttijd over een groot bereik maken de holle vezel membraan module uitermate geschikt as gas-vloeistof modelcontactor. Door middel van experimenten met reactieve- en niet-reactieve modelsystemen is aangetoond dat deze nieuwe modelcontactor gebruikt kan worden voor de bepaling van fysisch-chemische parameters, zoals diffusiecoëfficiënten en oplosbaarheden, in gas-vloeistof systemen. Onder asymptotische condities kunnen benaderende oplossingen voor de versnellingsfactor worden gebruikt bij de analyse van de experimentele data, maar in overige situaties is een numeriek model vereist. Aangezien de membraancontactor een indirekt contact tussen de gas en vloeistoffase faciliteert, is deze contactor mogelijk ook toepasbaar voor vloeistof-vloeistof systemen en/of heterogeen gekatalyseerde gas-vloeistof systemen.

Referenties

Bhide, B.D., & Stern, S.A. (1993). Membrane processes for removal of acid gases from natural gas. II Effects of operating conditions, economic parameters and membrane properties. *Journal of Membrane Science*, **81**, 239-252.

Gottlicher, G., & Pruschek, R. (1997). Comparison of CO_2 removal systems for fossil fueled power plant processes. *Energy Conversion & Management*, **38**, S173-S178.

Feron, P.H.M., & Jansen, A.E. (2002). CO_2 separation with polyolefin membrane contactors and dedicated absorption liquids: performance and prospects. *Separation and Purification Technology*, **27**, 231-242.

Kreulen, H. (1993). *Microporous membranes in gas separation processes using a liquid phase*. Proefschrift, Universiteit Twente, Enschede (Nederland).

Acknowledgment

Four years ago I took a daring decision to venture into a relatively new area of Membrane Contactors and Natural Gas treatment without any prior background in either field. Today, four years later, I feel completely satisfied and elated. It has been a wonderful experience working on a project involving current socio-economic problems of environmental protection and the global energy crisis. The project spanned over academics as well as industrial objectives, giving enough flexibility to steer it in either direction. Culmination of this project has resulted not only in this dissertation but also in sharpening the many facets of my personal and professional development. A great number of people have contributed to the completion of this thesis, some by making direct contributions and some by making life more enjoyable at and away from the workplace. Herewith, I wish to express my gratitude to all of these wonderful people.

Foremost I would like to express my gratitude to my promoter Prof.dr.ir. G.F. Versteeg for accommodating me in the OOIP group. I appreciate very much his flexibility and openness in dealing with the specific and general needs of the project. His expertise in gas treating and heterogeneous mass transfer processes has provided new insights and elucidations to many theoretical and practical problems during the course of this research. Next, I would like to express my sincere thanks to Dr.ir. D.W.F. Brilman, my mentor, who initiated my quest to ask 'why' at each stage of learning. I acknowledge the endeavours he has put in to achieve the best possible outcome of this project. His knowledge and enthusiasm have proven an invaluable contribution to this research. I would like to extend my thanks to TNO-Environment Energy and Process Innovation, the Netherlands for funding this industrially relevant project and particularly to Dr. P.H.M Feron and Dr. F.H. Geuzebroek for providing the experimental data and membrane modules. The numerous brain storming sessions during the project meetings with TNO were very useful in the successful completion of the project.

I was fortunate enough to get excellent undergraduate, graduate as well as Ph.D. students whose valuable work is responsible for the successful realization of this project. The initial experimental work by Rogier Halvers on the flat sheet membrane experimental set-up helped me in debugging the set-up. The work by Stefan van de Riet facilitated the development of the critical entry pressure set-up. Herman Bruns laid the foundation for the single fiber membrane contactor and also assisted in the membrane-solvent characterization. In initial days, he also helped me in deciphering many Dutch documents. It was a pleasure working with the jovial Alexy Volkov, who patiently performed experiments on the hollow fiber model contactor. It was indeed a nice experience collaborating with different personalities having such diverse educational backgrounds.

The organizational tasks related to this project would not have been possible without excellent administrative support. I am indebted to Irene Gootje who acted as a panacea for every day-to-day problem with her excellent administrative skills. I also enjoyed our lively discussions on the various aspects of Asian and European cultures. I am also obliged to Nicole Haitjema and Britta Olbertz for their infinite help with the administrative work. The practical work presented in this thesis would never have been possible without the help of proficient technicians. I express my thanks to Wim Leppink who built the 'state of the art' set-ups for flat sheet and hollow fiber membrane contactors. Benno Knaken did the painstaking work of the membrane module construction and the development of the RTD set-up. He was always full of amazing ideas and provided quick-fix solutions to many experimental bugs. I am also thankful to Gerrit Schorfhaar and Henk Jan Moed for their crucial and expedient technical assistance. Thanks also goes to Robert Meijer for the instrumentation and computer related support. Last but not least, I thoroughly enjoyed the informal discussions with all of them during coffee breaks and group "borrels".

Even though there are various research groups within the Chemical Technology Faculty of Twente University, the close cooperation among these groups had a very synergistic effect in the completion of this project. I would like to mention thanks to Membrane Technology Group, especially to Prof.dr.ing. M. Wessling and to Kitty Nymeijer for supplying relevant technical information as well as membranes for this research project. I am grateful to Prof.dr.ir. J.A.M. Kuipers for lending his expertise in the numerical work. Furthermore, I would like thank Dr.ir. Bert Heesink for his guidance and help in various aspects of career development issues. It was always a fruitful consultation with Dr.ir. Kees Hogendoorn in clarifying the many mysterious phenomena in the field of mass transfer and reaction engineering. Thanks to Martin van Sint Annaland for helping me in Delphi programming and to Hein Neomagus for membrane characterization. Thanks also goes to Niels Deen for exchanging conceptual ideas about membrane contactors and to Maartje Steensma for the initial work on this research.

It was quite an adventure for me to come to Netherlands after 24 years of die-hard Indian experience and joining a totally different culture, different people and of course different weather! Cheerful colleagues and the lively ambiance at the workplace helped me in acclimatizing in this new environment with ease. Mousa joined me as an officemate, which has turned into a nice friendship. "Shukran" Mousa, for patiently tolerating me for the last four years. Senthil helped me a lot in digesting many aspects of membrane contactors and kinetics. I was always amazed by his systematic experimental skills. "Bedankt" Toine for providing a helping hand in RTD study. Pranay helped me in the initial days in settling down. It was nice talking with "beer-crazy" Peter and new buddy Jens. Thanks also to all TWAiOs and AiOs from Vlugter Lab for the marvelous coffee breaks.

One of the greatest achievements during this project is the friendship of many wonderful people who comforted me in many ways. I would like to thank all of them. I would have been starved to death without the members of "Royal Dining Club" namely Ambati, Amrish, Charudatta, Dhaneshwar, Kapil, Kiran, Jay, Makarand, Manish, Mujeeb, Parasu, Pranay, Rahul, Rama, Ranjeet, Salim, Senthil, Shankar, Srinivas and Vijay. I will never forget the exotic 'glow wine' by Uli and Ivayla. Special thanks to my (pseudo)neighbors and Indian families in and around the campus namely Pramod, Sheela, Vasughi, Jayanti-Sheshan, Kavita-Kiran, Madhavi-Ravi and Shashibabhi-Satyen who provided me "A Home away from Home".

My thirst for a research career was largely induced by distinguished faculty members, particularly Prof. Pandit, from my former alma mater, UDCT. I would like thank all of them for their continuous motivation, support and guidance. Thanks also to my long-time pals bappa, boru, dadaji, gogo, gopya, kads, kawathya, pallo, palya, patya, san and many more for their support and care over the years.

Most of all, I would like to express my deepest sense of gratitude to all my family members. Their love, care, sacrifices and encouragement have made it possible for me to come so far. I appreciate the courage, understanding and dedicated support shown by all of them despite many testing times at their end.

In closing I realize that it is impossible to mention each and everyone who crossed my path in these exciting four years. A big thank to all of you and my apologies to those I may have forgotten.

Vishwas

Résumé

Vishwas Dindore was born on April 2, 1975 in Latur, India. In 1992, after completing his higher secondary schooling at Dayanand Science College, Latur, he joined University Department of Chemical Technology (U.D.C.T.), an autonomous institution affiliated to Mumbai University, to obtain his Bachelors in Chemical Technology. During this study he worked as a trainee process engineer in Lona Industries Ltd., India.

After graduating as a Chemical Engineer in 1996, he joined Larsen and Toubro Ltd., India as a Project Engineer. As a project engineer, he was mainly involved in design and commissioning of various process plants. Subsequently, he received a Junior Research Fellowship (JRF) from the University Grants Commission, New Delhi and in August 1997, he joined his alma mater U.D.C.T. for Masters in Chemical Engineering. He worked on a dissertation titled “Mixing Time Analysis in Mechanically Agitated Contactors” under the guidance of Prof.dr. A.B. Pandit.

In September 1999, he joined a Ph.D. project in the OOIP group, University of Twente, the Netherlands, to conduct research on the design and development of membrane gas-liquid absorption processes for the removal of carbon dioxide from industrial gas streams. He was guided in his research work by Prof.dr.ir. G.F. Versteeg. From October 2003, he will be working as a research staff for NTNU, Trondheim, Norway in co-operation with Procede Twente B.V., Enschede, the Netherlands.